Title
Design and Optimization Studies as Applied to Hydrogen Production

Author
Pichardo, Patricia Aida

Publication Date
2019

Peer reviewed|Thesis/dissertation

UNIVERSITY OF CALIFORNIA

Los Angeles

Design and Optimization Studies as Applied to Hydrogen Production

A dissertation submitted in partial satisfaction of the

requirements for the degree Doctor of Philosophy

in Chemical Engineering

by

Patricia Aida Pichardo

2019

ABSTRACT OF THE DISSERTATION

Design and Optimization Studies as Applied to Hydrogen Production

by

Patricia Aida Pichardo

Doctor of Philosophy in Chemical Engineering

University of California, Los Angeles, 2019

Professor Vasilios Manousiouthakis, Chair

Stabilizing greenhouse gas emissions has become a major focus worldwide as the environmental concerns these emissions evoke continue to grow. For this reason, many countries have begun to replace fossil fuels with renewable energy sources. One such solution is hydrogen since it is an energy carrier that can be generated through a variety of methods, many of which include renewable energy sources. This work focuses on the design of novel hydrogen production methods and the optimization of pre-existing hydrogen production methods. First, a novel process intensification tool is used to optimize the steam-methane reforming process. Then, techno-economic analyses are performed on novel Integrated Gasification Combined Cycle plants. Finally, a novel intensified energetically enhanced reforming process featuring membrane reactors is presented.

The dissertation of Patricia Aida Pichardo is approved.

Jane Pei-Chen Chang

Dante A. Simonetti

Luminita Aura Vese

Vasilios Manousiouthakis, Committee Chair

University of California, Los Angeles

2019

Dedication

I dedicate this dissertation to my parents Rafael and Flor who have instilled the importance of a good education throughout my life and have supported all of my educational endeavors. This work would not have been possible without their love and support. I also dedicate this dissertation to my husband, Juan David Llanos who inspired me to pursue a doctorate degree and work under Dr. Manousiouthakis.

Table of Contents

Chapter 1: Infinite DimEnsionAl State-space as a Systematic Process Intensification Tool: Energetic Intensification of Hydrogen Production 1

1.1 Abstract 1

1.2 Introduction 1

1.3 IDEAS Mathematical Formulation of Process Flowsheeting 5

1.4 Case Study: Process Intensification of Natural Gas Reforming Based Hydrogen Production 38

1.5 Discussion-Conclusions 45

1.6 References 50

Chapter 2: On the Intensification of Natural Gas Based Hydrogen Production Utilizing Hybrid Energy Resources 57

2.1 Abstract 57

2.2 Introduction 57

2.3 IDEAS Applicability and Mathematical Formulation 62

2.3.1 Heat Exchange Network 65

2.4 IDEAS Mathematical Formulation 73

2.5 Results and Discussion 75

2.6 Conclusions 90

2.7 Notation 91

2.8 References 95

Chapter 3: Technical Economic Analysis of an Intensified Integrated Gasification Combined Cycle (IGCC) Power Plant Featuring a Sequence of Membrane Reactors 98

3.1 Abstract 98

3.2 Introduction 99

3.3 Realization of the Proposed IGCC Plant Featuring a Sequence of Membrane Reactors 101

3.4 Membrane Reactor Details 104

3.4.1 COMSOL MR Model Description and Simulations 108

3.5 Results and Discussion 118

3.5.1 Heat Integration 121

3.5.2 Technical Economic Analysis 124

3.6 Conclusions 129

3.7 Appendix 131

3.8 References 136

Chapter 4: Techno-Economic Analysis of an Intensified Integrated Gasification Combined Cycle (IGCC) Power Plant Featuring a Combined Membrane Reactor - Adsorptive Reactor (MR-AR) System 140

4.1 Abstract 140

4.2 Introduction 140

4.3 Realization of the Proposed IGCC Plant Featuring the MR-AR Design 144

4.3.1 Membrane Reactor - Adsorptive Reactor Details 146

4.3.2 COMSOL MR-AR Model Descriptions 148

4.4 Results and Discussion 151

4.4.1 Heat Integration 153

4.4.2 Techno-Economic Analysis 155

4.5 Conclusions 164

4.6 References 166

Chapter 5: Intensified Energetically Enhanced Steam Methane Reforming (IEER) Through the Use of Membrane Reactors 169

5.1 Abstract 169

5.2 Introduction 169

5.3 Gibbs Free Energy Minimization Formulation for Membrane Reactors 171

5.4 Traditional SMR Baseline Process 174

5.5 Baseline EER Process 177

5.6 Baseline SMR-MR Process 180

5.7 IEER Process 183

5.8 Results and Discussions 190

5.9 Conclusions 193

5.10 Appendix 195

5.11 References 208

List of Figures

Figure 1-1: Separator Representation 21
Figure 1-2: Representation of heat exchange network structure 28
Figure 1-3: IDEAS representation of a process flowsheet 34
Figure 1-4: Flowsheet depiction of a traditional natural gas based hydrogen production process. 40
Figure 1-5: Simplified IDEAS flowsheet for natural gas based hydrogen production (2.5:2:1 Cost Coefficient Ratio) 43
Figure 1-6: Simplified IDEAS flowsheet for natural gas based hydrogen production (1.2:1:1 Cost Coefficient Ratio, utility bounds) 43
Figure 1-7: Cost Coefficient Ratio versus the varying external hot and cold utilities 47
Figure 1-8: Total Hot Utility Cost versus the ratio of 1200K:770K utility 48
Figure 2-1: Depiction of a hot stream – cold stream heat exchanger 65
Figure 2-2: A depiction of hot stream – cold point load and cold stream – hot point load heat exchanger 69
Figure 2-3: Depiction of hot point – cold point heat exchanger 70
Figure 2-4: T-H diagram for a thermodynamically infeasible hot stream – cold stream heat exchanger 71
Figure 2-5: IDEAS depiction of a process network divided into OP and DN networks 73
Figure 2-6: Baseline Flowsheet depicting hydrogen production through traditional steam-methane reforming 76
Figure 2-7: IDEAS synthesized flowsheet for steam methane reforming with no capital cost restriction (Pichardo & Manousiouthakis, 2017). 79
Figure 2-8: Objective function as a function of heat exchange area and work of separation 84
Figure 2-9: Consumption of 1200K Utility as a function of heat exchange area and work of separation 85
Figure 2-10: Consumption of 770K Utility as a function of heat exchange area and work of separation 85
Figure 2-11: Consumption of 420K Utility as a function of heat exchange area and work of separation 86
Figure 2-12: Consumption of 298K Utility as a function of heat exchange area and work of separation 86
Figure 3-1: Baseline design of an IGCC pre-combustion CCS plant [29] 102
Figure 3-2: A schematic of our proposed IGCC plant featuring a sequence of MRs 103
Figure 3-3: A schematic of the configuration for the sequence of MRs implemented into the MR IGCC plant, where COU refers to counter-current and COC refers to co-current. 104
Figure 3-4: Depiction of the bundle module configuration inside the pressure vessel comprising an MR 105
Figure 3-5: Diagram of the membrane reactor that is being simulated 109
Figure 3-6: Results for different operational configurations of a sequence of four MRs 112
Figure 3-7: UNISIM implementation of the proposed IGCC with CCS implementing a sequence of 4 MRs operating counter-currently. 114
Figure 3-8: Simplified block diagram depicting the gas-cleanup section of the baseline IGCC design 117
Figure 3-9: Simplified block diagram depicting the gas-cleanup section of the proposed MR IGCC design 117
Figure 3-10: Heat exchange network for the baseline IGCC case depicting the Temperature-Enthalpy change diagram 122
Figure 3-11: Heat exchange network for the MR-based IGCC case depicting the Temperature-Enthalpy change diagram 123
Figure 4-1: Depiction of the combined MR-AR system operation including AR switching between adsorption/desorption 143
Figure 4-2: A schematic of our proposed MR-AR-based IGCC plant 145
Figure 4-3: UNISIM implemented flowsheet of MR-AR-proposed design 149

Figure 4-4: Block flow diagram of the baseline IGCC gas-clean-up section 150
Figure 4-5: Block flow diagram of the MR-AR-based IGCC gas-clean-up section 151
Figure 4-6: Heat exchange network for the Baseline IGCC case depicting the Temperature-Enthalpy change diagram 153
Figure 4-7: Heat exchange network for the MR-AR IGCC case depicting the Temperature-Enthalpy change diagram 154
Figure 5-1: Traditional SMR Baseline Flowsheet 175
Figure 5-2: Traditional SMR Baseline flowsheet heat integration temperature interval diagram 176
Figure 5-3: Traditional SMR Baseline flowsheet heat integration temperature-enthalpy change diagram 177
Figure 5-4: EER Baseline Flowsheet 178
Figure 5-5: EER Baseline flowsheet heat integration temperature interval diagram 179
Figure 5-6: EER Baseline flowsheet heat integration temperature-enthalpy change diagram 180
Figure 5-7: SMR-MR Baseline flowsheet 181
Figure 5-8: SMR-MR Baseline flowsheet heat integration temperature interval diagram 182
Figure 5-9: SMR-MR Baseline flowsheet heat integration temperature-enthalpy change diagram 182
Figure 5-10: IEER-MR flowsheet 183
Figure 5-11: Case study 1 flowsheet details of membrane reactor network 185
Figure 5-12: Case 1 IEER-MR flowsheet heat integration temperature interval diagram 185
Figure 5-13: Case 1 IEER-MR flowsheet heat integration temperature-enthalpy change diagram 186
Figure 5-14: Case study 2 flowsheet details of membrane reactor network 187
Figure 5-15: Case 2 IEER-MR flowsheet heat integration temperature interval diagram 187
Figure 5-16: Case 2 IEER-MR flowsheet heat integration temperature-enthalpy change diagram 188
Figure 5-17: Case study 3 flowsheet details of membrane reactor network 189
Figure 5-18: Case 3 IEER-MR flowsheet heat integration temperature interval diagram 189
Figure 5-19: Case 3 IEER-MR flowsheet heat integration temperature-enthalpy change diagram 190

List of Tables

Table 1-1: Summary Table of Natural Gas Based Hydrogen Production Case Study 42
Table 1-2: Process unit outlet temperatures 44
Table 1-3: Specifications on the inlet and exit of the reactors utilized in the baseline and IDEAS cases presented. 45
Table 1-4: Specifications on the process flows of the simplified IDEAS generated flowsheet with 1.2:1:1 cost coefficient (Figure 1-5). 49
Table 2-1: Summary table of baseline flowsheet's properties 77
Table 2-2: Summary of the heat exchange network present in the baseline 77
Table 2-3: Summary table detailing IDEAS synthesized natural gas based hydrogen production flowsheets 81
Table 2-4: Thermodynamic equilibrium reactor inlet and outlet conditions. 81
Table 2-5: Economic Analysis of IDEAS designs with heat exchange area and work of separation upper bounds 87
Table 2-6: Summary table of exothermic flowsheet's properties 88
Table 3-1: Parameters and their values utilized in the membrane reactor simulations 106
Table 3-2: Membrane permeance values used in the membrane reactor simulations 108
Table 3-3: Stream information for MR sequences depicted in Figure 3-6. 113
Table 3-4: Molar composition information for the streams featured in Figures 3-8 – 3-9 118
Table 3-5: Comparison of the baseline pre-combustion CCS IGCC plant with the IGCC plant featuring a sequence of WGS-MRs. 118
Table 3-6: Performance summary of the baseline IGCC with CCS plant compared to the proposed IGCC plant featuring WGSMRs 119
Table 3-7: Heat loads associated with the baseline IGCC and MR IGCC plants 123
Table 3-8: Summary of the assumptions used for the capital cost analysis 125
Table 3-9: Capital cost comparison between the baseline IGCC with CCS and the proposed IGCC plant featuring a sequence of WGS-MRs 125
Table 3-10: Operating cost comparison between baseline IGCC with CCS and proposed MR-based IGCC plant 127
Table 3-11: Sensitivity analysis on Membrane Reactor operating costs and Nitrogen Sale Prices 128
Table 3-12: Molar based catalyst pellet-scale model equations 131
Table 3-13: Initial and boundary conditions for catalyst pellet-scale model equations 131
Table 3-14: Molar-based reactor-scale model equations 132
Table 3-15: Initial and boundary conditions for reactor-scale model equations 133
Table 3-16: Molar-based permeation zone model equations 133
Table 3-17: Initial and boundary conditions for permeation zone model equations 134
Table 3-18: Chemical model equations. 134
Table 3-19: Flow specifications of outlet MR sequence for COMSOL simulation and corresponding UNISIM implementation 135
Table 4-1: Parametric details of membrane reactors utilized. 146
Table 4-2: Specification of species permeance for the membrane reactor simulations 147
Table 4-3: Flow information on streams featured in Figures 4-4 - 4-5 151
Table 4-4: Performance summary of Baseline IGCC design with CCS and the MR-AR-based IGCC design 152
Table 4-5: Heat loads associated with baseline IGCC and MR-AR IGCC 154
Table 4-6: Summary of cost assumptions used in TEA 157

Table 4-7: COE component breakdown for the Baseline IGCC with CCS plant and the MR-AR-based IGCC design..... 159
Table 4-8: Summary table of Shell IGCC plant with and without CCS and the MR-AR-based IGCC design..... 159
Table 4-9: Summary of capital cost for MR-AR IGCC..... 160
Table 4-10: Fixed capital cost summary for the MR-AR-based IGCC plant..... 162
Table 4-11: Variable operating cost of MR-AR-based IGCC plant..... 163
Table 4-12: Sensitivity analysis for the MR-AR-based IGCC plant..... 164
Table 5-1: Thermodynamic Gibbs Minimization equilibrium membrane reactor simulations..... 174
Table 5-2: Summary table of all case studies..... 194
Table 5-3: Traditional SMR Baseline Flowsheet material and energy stream details..... 195
Table 5-4: EER Baseline Flowsheet material and energy stream details..... 196
Table 5-5: SMR-MR Baseline Flowsheet material and energy stream details..... 198
Table 5-6: IEER-MR Case 1 Flowsheet material and energy stream details..... 199
Table 5-7: IEER-MR Case 2 Flowsheet material and energy stream details..... 202
Table 5-8: IEER-MR Case 3 Flowsheet material and energy stream details..... 204

Acknowledgements

I would like to thank UCLA for their economic support through the Eugene V. Cota Robles Fellowship and Dissertation Year Fellowship. In addition, I would also like to thank my advisor Professor Vasilios Manousiouthakis for without his help and mentorship this work would never have been accomplished.

Chapter 1: Financial support through DOE grant DE-EE0005763 “Industrial Scale Demonstration of Smart Manufacturing Achieving Transformational Energy Productivity Gains” is acknowledged. Free access to the UNISIM software by Honeywell Inc., are also acknowledged. This chapter has been published in the journal *Chemical Engineering Research and Design*. Pichardo, Patricia, and Vasilios I. Manousiouthakis. "Infinite DimEnsionAl State-space as a systematic process intensification tool: Energetic intensification of hydrogen production." *Chemical Engineering Research and Design* 120 (2017): 372-395.

Chapter 2: Financial support through NSF grant 1650574 “EAGER: Optimal Modular Process Synthesis” is acknowledged. Free access to the UNISIM software by Honeywell Inc., are also acknowledged. This chapter has been published in the journal *Smart and Sustainable Manufacturing Systems.* Pichardo, P. and Vasilios I. Manousiouthakis. "On the Intensification of Natural Gas-Based Hydrogen Production Utilizing Hybrid Energy Resources." *Smart and Sustainable Manufacturing Systems* 2, no. 2 (2018): 1-24.

Chapter 3: Financial support through US Department of Energy through grant DE-FOA-0001235 FE0026423 “A High Efficiency, Ultra-Compact Process For Pre-Combustion CO2 Capture” is gratefully acknowledged. Free access to the UNISIM software by Honeywell, Inc. is also acknowledged. This chapter has been published in the *Journal of Membrane Science.* Patricia A. Pichardo, Seçgin Karagöz, Theodore Tsotsis, Richard Ciora, Vasilios I.

Manousiouthakis. “Technical economic analysis of an intensified Integrated Gasification Combined Cycle (IGCC) power plant featuring a sequence of membrane reactors” *Journal of Membrane Science* 579 (2019): 266-282.

Chapter 4: Financial support through US Department of Energy through grant DE-FOA-0001235 FE0026423 “A High Efficiency, Ultra-Compact Process For Pre-Combustion CO2 Capture” is gratefully acknowledged. Free access to the UNISIM software by Honeywell, Inc. is also acknowledged. This chapter has been submitted for publication to the *Journal of Membrane Science.*

Chapter 5: Free access to the UNISIM software by Honeywell, Inc. is acknowledged. This chapter has been submitted for publication to the *AIChE Journal.*

VITA

2010-2014	Department of Mechanical Engineering Loyola Marymount University Bachelor of Science in Mechanical Engineering
2014-2016	Department of Chemical and Biomolecular Engineering University of California, Los Angeles Master of Science in Chemical Engineering

SELECTED PUBLICATIONS

- *Pichardo, P.*, & Manousiouthakis, V. I. (2017). Infinite DimEnsionAl State-space as a systematic process intensification tool: Energetic intensification of hydrogen production. Chemical Engineering Research and Design, 120, 372-395.
- *Pichardo, P.* & Manousiouthakis, V. (2018). On the Intensification of Natural Gas-Based Hydrogen Production Utilizing Hybrid Energy Resources. 2, (2), 1-24.
- Supowit, J. A., Baker, C. H., Zhao, B., McHale, J., Miller, R., *Pichardo*, *P.*, Zuhlke, C. A., Roth, N., Tsubaki, A., Mohammadi-Ghaleni, M., Nejati, S., Alexander, D. R. (2018). Thermal Cycle Testing of Titanium Superhydrophobic Surfaces for a Spacecraft Jumping Droplet Thermal Diode. In 2018 Joint Thermophysics and Heat Transfer Conference (p. 2946).
- *Pichardo, P.*, Karagoz, S., Tsotsis, T., Ciora, R., Manousiouthakis, V. (2019). Technical Economic Analysis of an Intensified Integrated Gasification Combined Cycle (IGCC) Power Plant Featuring a Sequence of Membrane Reactors. *Journal of Membrane Sciences* 579, 266-282.
- *Pichardo, P.*, Manousiouthakis, V. (2019). Intensified Energetically Enhanced Steam Methane Reforming (IEER) Through the Use of Membrane Reactors. Submitted to *AIChE Journal*
- *Pichardo, P.*, Karagoz, S., Tsotsis, T., Ciora, R., Manousiouthakis, V. (2019). Techno-Economic Analysis of an Intensified Integrated Gasification Combined Cycle (IGCC) Power Plant Featuring a Combined Membrane Reactor - Adsorptive Reactor (MR-AR) System. Submitted to *Journal of Membrane Science*

Chapter 1: Infinite DimEnsionAl State-space as a Systematic Process Intensification Tool: Energetic Intensification of Hydrogen Production

1.1 Abstract

In this work, process intensification is identified as a process synthesis activity seeking significant improvements over traditional designs. The Infinite-DimEnsionAl State-space (IDEAS) conceptual framework is proposed as a systematic process intensification tool, which can identify intensified process designs, and assess fundamental performance limitations of networks of technologies under consideration. The synthesis of intensified flowsheets, in an energy efficiency sense, is pursued through the simultaneous synthesis of the flowsheet and its heat exchange network. The use, for the first time in process synthesis, of atomic balance, and Gibbs free energy minimization based equilibrium reactor models, enables a broad state-space search for process intensification opportunities, even by low dimensional, feasible, linear programming, IDEAS approximations. Application of the proposed method to natural gas reforming based hydrogen production, identifies intensified process designs featuring hot utility costs that can be lower by over an order of magnitude to those of traditional designs.

1.2 Introduction

The academic development of the Chemical Engineering profession was first focused on Process Analysis. For decades, researchers developed first principle based models aiming to capture the behavior of chemical processes[1-2]. The continuous improvement of computer technology, combined with advances in model simulation methods, has enabled the repeated ad-hoc use of these process analysis methods in chemical process design. Process Synthesis methods have also begun to appear (including an early book on the subject[3]), on a variety of synthesis problems: Solvay cluster synthesis[4-5], heat integration[6-12], mass integration[13],

distillation network synthesis[14-16] and reaction attainable region based synthesis[17-23]. Roger Sargent pioneered the development of several process synthesis methods. As an example, his work with Westerberg on SPEED-UP[24], Gaminibandara on distillation[14], and Grossmann on heat exchange network synthesis[25], established algorithmic and optimization based approaches to process synthesis as a major direction in the field. In his prophetic paper[26], Sargent highlights important directions in unconstrained optimization (e.g. Davidon-Fletcher-Powell, rank-one for robust convergence, conjugate gradient Fletcher-Reeves for reduced data storage), constrained optimization with nonlinear equality or inequality constraints (generalized-reduced-gradient, variable metric projection), and problems involving discrete variables (integer programming) where he identifies branch and bound as the only practical method (at the time), albeit providing caution that "the computation and storage problems rapidly get out of hand for all but the smallest problems." Mixed integer nonlinear programs (MINLP's), and non-smooth optimization formulations, have indeed been used more recently for the synthesis of heat-integrated flowsheets (using pinch analysis)[15,27-28] and the simultaneous synthesis of flowsheets and their associated heat exchange networks[29], although Sargent's prediction prophetically remains valid. Infinite dimensional linear programming formulations to the synthesis of heat-integrated flowsheets (using pinch analysis)[30], and the simultaneous synthesis of flowsheets and their associated heat exchange networks[31], have been presented, and constitute the conceptual foundation of this work.

Process intensification is a strategy for making dramatic reductions (order 100 or more) in the size of a chemical plant that attains given production objectives[32]. These reductions can come from reducing the number of units employed in the chemical plant as well as decreasing the size of individual units. Expanding the scope of process intensification beyond size has led to

its characterization as “any chemical engineering development that leads to substantially smaller, cleaner, and more energy efficient technology”[33]. Focusing on chemical engineering developments related to process synthesis, Stankiewicz[34] refers to the methyl acetate process by Eastman Chemical[35] as “widely regarded as a textbook example of process intensification”, wherein “task analysis-based process synthesis resulted in the replacement of traditional reactors and separation units by a highly integrated reactive distillation column”. Indeed, this patented process[36] employs only three major pieces of equipment, as opposed to the traditional manufacturing process, which employs twenty-eight major pieces of equipment. This kind of reactor and separation unit replacement by highly integrated reactive distillation column equipment[33] has been pursued using such process synthesis tools as residue curve maps[37,38].

In Moulijn’s and Stankiewicz’s book on process intensification[39] process synthesis is considered to be a process intensification method worthy of a chapter (11), which “focuses on the application of *process synthesis* principles to the optimal design of integrated chemical processing plants”. In the first chapter of that same book, Stankiewicz and Drinkenburg[40] identify process synthesis as a software method that is a part of the process intensification toolbox, and state that “Process synthesis is in some sense a sister discipline of process intensification”. More recently, Moulijn et al[40] identify process systems engineering as a “chemical engineering skill” that supports process intensification, when process intensification is “considered as the technical objective.” They also state “This paper aims to … explore and activate the interface between process systems engineering (PSE) and PI.” The above combined with the statements of Stankiewicz[34] on the methyl acetate process, and Siirola[35] “process synthesis is the invention of flowsheet alternatives at conceptual design stage of the innovation process”, lead us to conclude that any process synthesis activity that attains *significant*

improvements over existing process designs can be classified as process intensification. This realization, reinforced by the suggestion of Moulijn et al[41], that "a distinction needs to be made between PI as an *objective* for process development and design and PI as a scientific *skill* area", leads us to pursue the development of systematic process intensification tools within the process synthesis toolbox through the intensification of process networks rather than just process equipment.

The Infinite DimEnsionAl State-space (IDEAS) framework is a process synthesis methodology that can serve as a systematic process intensification tool. When process synthesis is carried out, it is not known a-priori whether significant improvements can be attained over a baseline design, that would subsequently justify the characterization of the synthesized process as an intensified process over its baseline counterpart. IDEAS can serve as a process intensification tool since, unlike other synthesis methods, it does not require an a priori pre-determined network structure as a starting point for its implementation. As a result, IDEAS can arrive at truly innovative designs, since it does not encompass designer preconceptions into its methodology. IDEAS can also identify fundamental limitations to the level of performance attainable by any particular technology or combination of technologies, without any a priori commitment to any particular design. If these performance limits are close to the performance of existing known designs, then process intensification is not feasible based on the technology (technologies) under consideration, and additional/alternative technologies must be considered. If, on the other hand, IDEAS (or even low dimensional IDEAS approximations) can identify designs whose performance represents a significant improvement over the performance of known designs, then IDEAS is validated as a systematic process network intensification tool.

The remaining article is structured as follows: The IDEAS formulation to process flowsheeting is presented, including a property that enables the applicability of IDEAS to the employed reactor models. Next, an illustrative case study is presented, in which the IDEAS conceptual framework is employed as a tool in identifying intensified process flowsheets for natural gas reforming based hydrogen production. Finally, the obtained results are discussed, and conclusions are drawn.

1.3 IDEAS Mathematical Formulation of Process Flowsheeting

The IDEAS framework decomposes a process network into an operator network (OP), where the unit operations (reactors, separators, heat exchangers, etc.) occur, and a distribution network (DN), where the flow operations (mixing, splitting, recycling, and bypass) occur. IDEAS represents a paradigm shift which establishes that chemical process nonlinearities need not be manifested during flowsheet optimization, but rather can be fully accounted for prior to optimization. Within the IDEAS framework, the optimal process network synthesis problem is formulated as an infinite linear program (ILP), whose solution is approximated by finite-dimensional linear programs of ever-increasing size. It should be noted that the IDEAS infinite dimensional linear programming (ILP) formulation identifies the synthesis problem's global optimum, while the IDEAS finite dimensional linear programs represent approximations of the global optimum that can identify intensified process designs.

IDEAS has been successfully applied to numerous globally optimal process network synthesis problems, such as mass-exchange network synthesis,[42] complex distillation network synthesis,[30,43] power cycle synthesis,[31] reactor network synthesis,[44,45] reactive distillation network synthesis,[46] separation network synthesis,[47] attainable region construction,[48–51] and

batch attainable region construction[52]. More recently, the IDEAS framework has been used to incorporate efficiency considerations, which constitute one of the criteria employed in the expanded definition of process intensification[53], in reactor network synthesis, by minimizing the network's entropy generation. In particular, it has been shown that the entropy generation and energy consumption of isothermal, isobaric reactor networks only depend on the network's inlet and outlet stream compositions and flow rates, and are independent of the network structure, as long as the universe of realizable reactor/mixer units consists of either only endothermic units, interacting with a single hot reservoir, or only exothermic units interacting with a single cold reservoir, respectively[54]. It has also been shown that when the universe of realizable reactor/mixer units consists of both endothermic and exothermic units, the network's entropy generation and energy consumption depend on the network structure[54]. These results have provided the inspiration for the work presented in this manuscript. Indeed, close examination of the reactions taking place in a reformer reveals that the universe of realizable reformer units consists of both endothermic and exothermic units. In turn, this realization suggests that the energy consumption characteristics of an overall hydrogen production network (flowsheet) depend on the network structure, and can be dramatically altered, through the possible use of endothermic and/or exothermic reformer units, thus opening up dramatic opportunities for process intensification according to the latter's expanded definition[33].

In this work, the IDEAS framework is employed for process flowsheet intensification. Process flowsheets are networks that employ a variety of process units, including reactors, separators, pumps, compressors, turbines, valves, heat exchangers, and many others. As stated earlier, one way to intensify a process is to increase the efficiency of its energy use. Thus, the process intensification goal that we aim to improve in this work will be the cost of the hot and

cold utilities consumed by the process, which we will minimize. Hot and cold utilities at multiple temperature levels will be considered, reflecting the availability of both renewable and non-renewable energy resources. Possible opportunities for heat integration will also be explored by incorporating heat exchanger network (HEN) synthesis in the overall process network (PN) synthesis task, and carrying out simultaneously HEN and PN synthesis. Models for all the processes employed in this work are presented next, and the applicability of IDEAS to each such process model is ascertained. First however, Proposition 1 is proved, which is subsequently used to establish the applicability of IDEAS to the reactor model employed in this work. Proposition 1 provides a means of reducing the dimension of the state-space over which process intensification is pursued. The proposition allows for the scaling of the Gibbs free energy minimization problem, that determines the equilibrium reactor's exit compositions. Since the underlying objective function is a nonlinear homogenous function, a reduction in the dimensionality of the underlying state-space is achieved. For the considered case study, use of the equilibrium reactor models, combined with Proposition 1, enables the search for energy efficient designs to be carried out in the two-dimensional space of atomic fraction ratios, rather than the four-dimensional-space of species (CH_4, CO, CO_2, H_2O) mole fractions (H_2 mole fraction is calculated in any case).

Proposition 1

Consider the following two optimization problems, where:

$$\left\{ \begin{array}{r} \nu(a) = f(\hat{n}) \triangleq \min\limits_{n \in \mathbb{R}^k} f(n) \\ s.t.\ \ An = a \\ n \geq 0 \end{array} \right\} \text{ and } \left\{ \begin{array}{r} \nu(\lambda a) = f(\hat{n}_\lambda) \triangleq \min\limits_{n_\lambda \in \mathbb{R}^k} f(n_\lambda) \\ s.t.\ \ An_\lambda = \lambda a \\ n_\lambda \geq 0 \end{array} \right\}$$

where $\lambda > 0, A \in \mathbb{R}^{l \times k}, a \in \mathbb{R}^{l}$ and $f(\cdot)$ is a homogeneous function of degree one, i.e.

$f : \mathbb{R}^k \to \mathbb{R},\ f : n \to f(n),\ f : \lambda n \to f(\lambda n) = \lambda f(n)\ \ \forall \lambda > 0\ \ \forall n \in \mathbb{R}^k$.

Then,

a. $\nu(\lambda a) = f(\hat{n}_\lambda) = f(\lambda \hat{n}) = \lambda f(\hat{n}) = \lambda \nu(a)$.

b. If the optimization problem $\nu(a)$ has a unique global optimum $\forall a \in \mathbb{R}^l$, then

$\hat{n}_\lambda = \lambda \hat{n}\ \forall \lambda > 0$.

Proof:

a. Based on the proposition statement, $\hat{n}$ and $\hat{n}_\lambda$ are the global minima of $\nu(a)$ and $\nu(\lambda a)$ respectively.

Since $\left\{ \begin{matrix} A\hat{n} = a \\ \hat{n} \geq 0 \end{matrix} \right\} \overset{\lambda > 0}{\Leftrightarrow} \left\{ \begin{matrix} A\lambda \hat{n} = \lambda a \\ \lambda \hat{n} \geq 0 \end{matrix} \right\}$, then $\lambda \hat{n}$ is a feasible point of $\nu(\lambda a)$.

This means that $f(\lambda \hat{n}) \geq f(\hat{n}_\lambda) = \nu(\lambda a)$.

Define $\overline{n}_\lambda \triangleq \frac{1}{\lambda} \hat{n}_\lambda$.

Since $\left\{ \begin{matrix} A\hat{n}_\lambda = \lambda a \\ \hat{n}_\lambda \geq 0 \end{matrix} \right\} \overset{\lambda > 0}{\Leftrightarrow} \left\{ \begin{matrix} \frac{1}{\lambda} A\hat{n}_\lambda = \frac{1}{\lambda} \lambda a \\ \frac{1}{\lambda} \hat{n}_\lambda \geq 0 \end{matrix} \right\} \overset{\overline{n}_\lambda = \frac{1}{\lambda} \hat{n}_\lambda}{\Leftrightarrow} \left\{ \begin{matrix} A\overline{n}_\lambda = a \\ \overline{n}_\lambda \geq 0 \end{matrix} \right\}$, then, $\overline{n}_\lambda$ is a feasible point for $\nu(a)$.

This means that $f(\overline{n}_\lambda) \geq f(\hat{n}) = \nu(a)$.

In addition, since $f(\cdot)$ is a homogeneous function, it holds $f\left(\frac{1}{\lambda} \hat{n}_\lambda\right) = \frac{1}{\lambda} f(\hat{n}_\lambda)$.

It then holds,

$$\nu(a) = f(\hat{n}) \leq f(\overline{n}_\lambda) = f\left(\frac{1}{\lambda} \hat{n}_\lambda\right) = \frac{1}{\lambda} f(\hat{n}_\lambda) = \frac{1}{\lambda} \nu(\lambda a) \leq \frac{1}{\lambda} f(\lambda \hat{n}) = \frac{1}{\lambda} \lambda f(\hat{n}) = \nu(a).$$ O.E.Δ.

b. Consider, in addition that the optimization problem $\nu(a)$ has a unique global optimum $\forall a \in \mathbb{R}^I$.

Let the global optimum of $\nu(\lambda a)$, $\hat{n}_\lambda$, be such that $\hat{n}_\lambda \neq \lambda \hat{n}$. It holds however that $\lambda \hat{n}$ is a feasible point of $\nu(\lambda a)$. Then $f(\hat{n}_\lambda) < f(\lambda \hat{n})$, which in turn implies $\nu(\lambda a) = f(\hat{n}_\lambda) < f(\lambda \hat{n}) = \lambda f(\hat{n}) = \lambda \nu(a)$. This is in contradiction with $\nu(\lambda a) = \lambda \nu(a)$ which was established in part a. above. Thus, $\hat{n}_\lambda = \lambda \hat{n}$. O.E.Δ.

Having established Proposition 1, we next outline the concept of a process information map and discuss how establishing a number of properties that process information maps naturally possess, enables the development of the IDEAS conceptual framework. Historically, in the modular approach to process simulation (see for example review[46]) "each chemical processing step is represented as a separate mathematical model called a unit module … the process flow sheet is translated into an information flow sheet … process topology may be expressed directly on the FORTRAN level by use of stream (information) vectors." However, although information vectors were used to express process topology, information maps (and their properties) were not explicitly focused on. Process information maps taking inlet stream information (such as flows, component concentration, enthalpies, and so on) and transforming it to similar outlet stream information, give rise to process operators that are nonlinear, and result in nonconvex optimal network synthesis formulations. IDEAS provides a radical departure from this approach. IDEAS identifies input, and output vector decompositions and corresponding restricted input output information maps, so that three properties are satisfied, including linearity properties for these appropriately defined input output map restrictions. By then considering an

infinite cardinality universe of units, it is able to fully account for chemical process nonlinearities prior to optimization, and only employ the aforementioned linear map restrictions during optimization. Indeed, IDEAS considers that the process operator OP takes extensive inlet stream information (e.g. total flow, component flows), available at an infinite collection of appropriately defined, fixed inlet conditions (e.g. temperature, concentration, residence time, etc.) and transforms it to extensive outlet stream information (e.g. total flow) available at the corresponding outlet conditions. The resulting IDEAS process operator is linear for any chemical process, as a result of the property of chemical processes, that when their inlet flow rates increase proportionally (without altering their associated inlet conditions), their outlet flow rates also increase by the same proportion, while their associated outlet conditions remain unaltered.

Thus, having established the linearity of the IDEAS process operator OP, we are now in a position to justify the claim that the IDEAS representation gives rise to linear problem formulations. The constraints in the DN arise due to mixing and splitting operations, and are linear in the extensive (flow) variables. This fact, combined with the OP linearity, results in a linear feasible region that captures all possible process networks, by considering that the OP network inlets correspond to all possible associated conditions, and by allowing the DN network to consider all possible interconnections between external outlets (inlets)/OP inlets (outlets). In this work a novel reactor information map is provided, which utilizes a Gibbs free energy minimization model presented here for the first time for process synthesis purposes. Similarly, a novel separator information map is provided, which utilizes a minimum work of separation based model presented here for the first time for process synthesis purposes. Further, the stream creation process in the HEN operator, the mixing process preceding the distribution network, as well as the simultaneous synthesis of Heat Exchange Networks and Process Networks including

Reactors and Separators, are all presented in this work for the first time. The applicability of IDEAS to all employed process models is accomplished by establishing that each process information map satisfies the following properties:

Consider the information map $\Psi : D_1 \times D_2 \subset \mathbb{R}^{n_1} \times \mathbb{R}^{n_2} \to \mathbb{R}^{p}$,

$$\Psi : \; u = \left[u_1^{\,T} \;\; | \;\; u_2^{\,T} \right]^T \to \Psi(u) = \Psi(u_1, u_2)$$

that helps define the set D as follows: $D = \left\{ u \in D_1 \times D_2 \subset \mathbb{R}^{n_1} \times \mathbb{R}^{n_2} \; : \Psi(u_1, u_2) = 0 \right\}$

Let the considered process model have information map $\Phi : D \subset \mathbb{R}^{n_1} \times \mathbb{R}^{n_2} \to \mathbb{R}^{m_1} \times \mathbb{R}^{m_2}$,

$$\Phi : \; u = \left[u_1^{\,T} \;\; | \;\; u_2^{\,T} \right]^T \to y = \Phi(u) = \left[y_1^{\,T} \;\; | \;\; y_2^{\,T} \right]^T = \left[\left[\Phi_1(u_1, u_2) \right]^T \;\; | \;\; \left[\Phi_2(u_1, u_2) \right]^T \right]^T .$$

Having defined the maps Φ, Ψ, we can now state the properties that must hold to ensure IDEAS applicability.

Property 1:

$\exists \; \Psi_1 : \mathbb{R}^{n_1} \to \mathbb{R}^{p \times n_2}$, $\Psi_1 : u_1 \to \Psi_1(u_1)$ such that

$$\Psi(u_1, u_2) = \Psi_1(u_1) u_2 \quad \forall u = (u_1, u_2) \in D_1 \times D_2 \subset \mathbb{R}^{n_1} \times \mathbb{R}^{n_2}$$

Property 1 is best understood as follows: First, there exists a (possibly nonlinear) map (Ψ_1) that maps the unit sub-vector u_1 to a linear operator (matrix) $\Psi_1(u_1)$ that belongs to the space of matrices $\mathbb{R}^{p \times n_2}$. Then, the image of the vector (u_1, u_2) through the map Ψ is the composition of the linear operator $\Psi_1(u_1)$ with the sub-vector u_2.

Property 2:

$\exists\ \Phi_3 : \mathbb{R}^{n_1} \to \mathbb{R}^{m_1},\ \Phi_3 : u_1 \to \Phi_3(u_1)$ such that

$$y_1 = \Phi_1(u_1, u_2) = \Phi_3(u_1) \quad \forall u = (u_1, u_2) \in D \subset \mathbb{R}^{n_1} \times \mathbb{R}^{n_2}$$

Property 2 implies that $y_1 = \Phi_1(u_1, u_2)$ can be evaluated based only on knowledge of u_1, without requiring any knowledge of u_2.

Property 3:

$\exists\ \Phi_4 : \mathbb{R}^{n_1} \to \mathbb{R}^{m_2 \times n_2},\ \Phi_4 : u_1 \to \Phi_4(u_1)$ such that

$$\Phi_2(u_1, u_2) = \Phi_4(u_1) u_2 \quad \forall u = (u_1, u_2) \in D \subset \mathbb{R}^{n_1} \times \mathbb{R}^{n_2}$$

Property 3 is best understood as follows: First, there exists a (possibly nonlinear) map (Φ_4) that maps the unit sub-vector u_1 to a linear operator (matrix) $\Phi_4(u_1)$ that belongs to the space of matrices $\mathbb{R}^{m_2 \times n_2}$. Then, the image of the vector (u_1, u_2) through the map Φ is the composition of the linear operator $\Phi_4(u_1)$ with the sub-vector u_2.

A demonstration of these properties for a reactive distillation separator model is presented below for illustrative purposes. Let F^L, F^V, F^P be the liquid outlet, vapor outlet, and inlet total molar flows respectively. Let also f_i^P be the ith component's inlet molar flow rate, and x_i^L, y_i^V be the ith component's mole fractions of the liquid and vapor outlets respectively. Finally, let $R_i\left(\left\{x_j^L\right\}_1^{n-1}\right)$ be the ith component's generation rate, P_i^{sat}, γ_i be the ith component's saturation pressure, and activity coefficient respectively, P be the total pressure, and H be the liquid molar holdup.

The corresponding IDEAS information map is then defined as follows:

$$u = \left[u_1^T \quad | \quad u_2^T \right]^T = \left[x_1^L \quad \cdots \quad x_{n-1}^L \quad | \quad f_1^P \quad \cdots \quad f_n^P \quad F^L \quad F^V \quad H \right]^T$$

$$y = \left[y_1^T \quad | \quad y_2^T \right]^T = \left[x_1^L \quad \cdots \quad x_n^L \quad x_n^L \quad y_1^V \quad \cdots \quad y_n^V \quad | \quad f_1^P \quad \cdots \quad f_n^{in} \quad F^L \quad F^V \quad H \quad F^P \right]^T$$

$$u_1 \in D_1 \triangleq \left\{ u_1 = \left[x_1^L \quad \cdots \quad x_{n-1}^L \right]^T \in \mathbb{R}^{n-1} : x_i^L \geq 0 \;\; \forall i = 1, n-1; 1 - \sum_{i=1}^{n-1} x_i^L \geq 0 \right\}$$

$$u_2 \in D_2 \triangleq \begin{Bmatrix} u_2 = \left[f_1^P \quad \cdots \quad f_n^P \quad F^L \quad F^V \quad H \right]^T \in \mathbb{R}^{n+3} : \\ F^L \geq 0,\ F^V \geq 0,\ H \geq 0,\ f_k^P \geq 0 \;\; \forall k = 1, n \end{Bmatrix}$$

Property 1: the map $\Psi_1 : \mathbb{R}^{n-1} \supset D_1 \to \mathbb{R}^{n \times (n+3)}$ for the considered model is defined as follows:

$$\Psi_1 : u_1 \triangleq \left[x_1^L \quad \cdots \quad x_{n-1}^L \right] \to \Psi_1(u_1) \triangleq \begin{bmatrix} 1 & \cdots & 0 & -x_1^L & -y_1^V \left(\left\{ x_k^L \right\}_1^{n-1} \right) & R_1 \left(\left\{ x_k^L \right\}_1^{n-1} \right) \\ 0 & \ddots & 0 & \vdots & \vdots & \vdots \\ 0 & \cdots & 1 & -\left(1 - \sum_{i=1}^{n-1} x_i^L \right) & -y_n^L \left(\left\{ x_k^L \right\}_1^{n-1} \right) & R_n \left(\left\{ x_k^L \right\}_1^{n-1} \right) \end{bmatrix}^T,$$

and $\Psi_1(u_1) u_2 = \begin{bmatrix} 1 & \cdots & 0 & -x_1^L & -y_1^V \left(\left\{ x_k^L \right\}_1^{n-1} \right) & R_1 \left(\left\{ x_k^L \right\}_1^{n-1} \right) \\ 0 & \ddots & 0 & \vdots & \vdots & \vdots \\ 0 & \cdots & 1 & -\left(1 - \sum_{i=1}^{n-1} x_i^L \right) & -y_n^L \left(\left\{ x_k^L \right\}_1^{n-1} \right) & R_n \left(\left\{ x_k^L \right\}_1^{n-1} \right) \end{bmatrix}^T \begin{bmatrix} f_1^P \\ \vdots \\ f_n^P \\ F^L \\ F^V \\ H \end{bmatrix} = 0$

Property 2: the map $\Phi_3 : \mathbb{R}^{n-1} \supset D_1 \to \mathbb{R}^{2n}$ is defined as follows:

$$\Phi_3 : u_1 \to y_1 \triangleq \begin{bmatrix} x_1^L \\ \vdots \\ x_{n-1}^L \\ x_n^L \\ y_1^V \\ \vdots \\ y_n^V \end{bmatrix} = \Phi_3(u_1) \triangleq \begin{bmatrix} x_1^L \\ \vdots \\ x_{n-1}^L \\ 1-\sum_{k=1}^{n-1} x_k^L \\ \frac{P_1^{sat}\gamma_1}{P} x_1^L \\ \vdots \\ \frac{P_n^{sat}\gamma_n}{P} x_n^L \end{bmatrix}$$

Property 3: the map $\Phi_4 : \mathbb{R}^{n-1} \supset D_1 \to \mathbb{R}^{(n+4)\times(n+3)}$ is defined as follows:

$$\Phi_4 : u_1 \to \Phi_4(u_1) \triangleq \begin{bmatrix} 1 & \cdots & 0 & 0 & 0 & 0 \\ 0 & \ddots & 0 & 0 & 0 & 0 \\ 0 & \cdots & 1 & 0 & 0 & 0 \\ 0 & \cdots & 0 & 1 & 0 & 0 \\ 0 & \cdots & 0 & 0 & 1 & 0 \\ 0 & \cdots & 0 & 0 & 0 & 1 \\ 1 & \cdots & 1 & 0 & 0 & 0 \end{bmatrix} \in \mathbb{R}^{(n+4)\times(n+3)}, \text{ and}$$

$$y_2 = \begin{bmatrix} f_1^P \\ \vdots \\ f_n^P \\ F^L \\ F^V \\ H \\ F^P \end{bmatrix} = \Phi_4(u_1)u_2 = \begin{bmatrix} 1 & \cdots & 0 & 0 & 0 & 0 \\ 0 & \ddots & 0 & 0 & 0 & 0 \\ 0 & \cdots & 1 & 0 & 0 & 0 \\ 0 & \cdots & 0 & 1 & 0 & 0 \\ 0 & \cdots & 0 & 0 & 1 & 0 \\ 0 & \cdots & 0 & 0 & 0 & 1 \\ 1 & \cdots & 1 & 0 & 0 & 0 \end{bmatrix} \begin{bmatrix} f_1^P \\ \vdots \\ f_n^P \\ F^L \\ F^V \\ H \end{bmatrix}$$

Once these properties have been established, an infinite sequence $\{u_1(i)\}_{i=1}^{\infty}$ that consists of all possible values of u_1 such that the union of u_1 values considered is dense in the set where u_1

can vary, is considered. The sequences $\left\{\Psi_1\left(u_1(i)\right)\right\}_{i=1}^{\infty}, \left\{\Phi_4\left(u_1(i)\right)\right\}_{i=1}^{\infty}, \left\{\Phi_3\left(u_1(i)\right)\right\}_{i=1}^{\infty}$ of linear maps and vectors belonging to $\mathbb{R}^{p\times n_2}, \mathbb{R}^{m_2\times n_2}, \mathbb{R}^{m_1}$ respectively can then be created using the maps Ψ_1, Φ_4, Φ_3 respectively. These sequences can then be used to evaluate the infinite sequence of domains for $\left\{u_2(i)\right\}_{i=1}^{\infty}$, the infinite sequence $\left\{y_2(i)\right\}_{i=1}^{\infty} = \left\{\Phi_4\left(u_1(i)\right)\cdot u_2(i)\right\}_{i=1}^{\infty}$ and the infinite sequence $\left\{y_1(i)\right\}_{i=1}^{\infty} = \left\{\Phi_3\left(u_1(i)\right)\right\}_{i=1}^{\infty}$.

Next, utilizing these three properties the applicability of IDEAS is established for all unit operations considered in this work.

Reactors

For the considered case study, use of equilibrium reactor models is considered, since it is well known that industrial reformers operate near equilibrium (see reference 55). In addition, the use of equilibrium reactor models, combined with Proposition 1, enables the search for energy efficient designs to be carried out in the space of atomic fraction ratios, rather than the space of species mole fractions. In particular, a Gibbs free energy minimization problem is solved to identify the reactor's exit species concentrations using only temperature, pressure, and inlet atomic ratio specifications. The indices $i=1,m;\ j=1,n;\ k=1,NP$ denote the ith atom, jth species, and kth phase respectively, and the variables α, n, T, P, G denote the atomic mass flow rate (kg/s), molar flow rate (moles/s), temperature (K), pressure (bar), and Gibbs free energy (kJ) respectively. The indices NC, NE, NP are the number of components, the number of elements, and the number of phases respectively, and the variables $\mu, \nu_{i,j}$ denote the chemical potential (J/mol), the number of ith type atoms in the jth species' molecule.

$$\left\{ \begin{array}{l} \pi\left(T,P,\{\alpha_i\}_{i=1}^{m}\right) \triangleq \min\limits_{\left\{n_j^{(k)}\right\}_{(j,k)=(1,1)}^{(NC,\mathrm{NP})}} \quad G\left(T,P,\left\{n_p^{(k)}\right\}_{(p,k)=(1,1)}^{(\mathrm{n,NP})}\right) \\ \qquad\qquad s.t. \quad \alpha_i - \sum\limits_{k}^{NP}\sum\limits_{j}^{n} M_i \nu_{ij} n_j^{(k)} = 0 \qquad\qquad \forall i = 1, NE \\ \qquad\qquad\qquad n_j^{(k)} \geq 0 \qquad\qquad\qquad\qquad \forall j = 1, NC; \quad \forall k = 1, NP \end{array} \right\}, \text{ where}$$

$G\left(T,P,\left\{n_p^{(k)}\right\}_{(p,k)=(1,1)}^{(\mathrm{n,NP})}\right) = \sum\limits_{k=1}^{NP}\sum\limits_{j=1}^{n} n_j^{(k)} \mu_j^{(k)}\left(T,P,\left\{\dfrac{n_j^{(k)}}{\sum\limits_{l}^{n} n_l^{(k)}}\right\}_{j=1}^{n}\right)$. Application of the aforementioned proposition 1 to this optimization problem necessitates that the objective function be first order homogeneous. In general, $G\left(T,P,\left\{n_p^{(k)}\right\}_{(p,k)=(1,1)}^{(\mathrm{n,NP})}\right)$ is a function of $n \times NP + 2$ variables, and when treated as such it is not homogeneous. However, when T, P are fixed at $T = \bar{T}$, $P = \bar{P}$, then the restriction of G at $T = \bar{T}$, $P = \bar{P}$, $G\left(\bar{T},\bar{P},\left\{n_p^{(k)}\right\}_{(p,k)=(1,1)}^{(\mathrm{n,NP})}\right)$, is a first order homogenous function. Indeed, let $\lambda > 0$. Then

$$G\left(\bar{T},\bar{P},\left\{\lambda n_p^{(k)}\right\}_{(p,k)=(1,1)}^{(\mathrm{n,NP})}\right) = \sum_{k=1}^{NP}\sum_{j=1}^{n} \lambda n_j^{(k)} \mu_j^{(k)}\left(T,P,\left\{\frac{\lambda n_j^{(k)}}{\sum\limits_{l}^{n} \lambda n_l^{(k)}}\right\}_{j=1}^{n}\right) \Leftrightarrow$$

$$G\left(\bar{T},\bar{P},\left\{\lambda n_p^{(k)}\right\}_{(p,k)=(1,1)}^{(\mathrm{n,NP})}\right) = \lambda\left\{\sum_{k=1}^{NP}\sum_{j=1}^{n} n_j^{(k)} \mu_j^{(k)}\left(T,P,\left\{\frac{n_j^{(k)}}{\sum\limits_{l}^{n} n_l^{(k)}}\right\}_{j=1}^{n}\right)\right\} \Leftrightarrow$$

$$G\left(\bar{T},\bar{P},\left\{\lambda n_p^{(k)}\right\}_{(p,k)=(1,1)}^{(\mathrm{n,NP})}\right) = \lambda G\left(\bar{T},\bar{P},\left\{n_p^{(k)}\right\}_{(p,k)=(1,1)}^{(\mathrm{n,NP})}\right)$$

Since $G\left(\bar{T},\bar{P},\left\{n_p^{(k)}\right\}_{(p,k)=(1,1)}^{(\mathrm{n,NP})}\right)$ is a first order homogenous function, the problem constraints are linear, and the problem variables are nonnegative, and proposition 1 can be applied. Selecting $\lambda \triangleq 1\Big/\sum_i^m \alpha_i > 0$, then yields:

$$\left\{\pi\left(T,P,\left\{\frac{\alpha_i}{\sum_i^m \alpha_i}\right\}_{i=1}^{m}\right) \triangleq \min_{\left\{\frac{n_j^{(k)}}{\sum_i^m \alpha_i}\right\}_{(j,k)=(1,1)}^{(\mathrm{n,NP})}} G\left(T,P,\left\{\frac{n_p^{(k)}}{\sum_i^n \alpha_i}\right\}_{(p,k)=(1,1)}^{(\mathrm{n,NP})}\right)\right.$$

$$\left. s.t. \quad \frac{\alpha_i}{\sum_i^m \alpha_i} - \sum_k^{NP}\sum_j^n M_i \nu_{ij} \frac{n_j^{(k)}}{\sum_i^{NE} \alpha_i} = 0 \quad \forall i = 1,m \right.$$

$$\left. \frac{n_j^{(k)}}{\sum_i^m \alpha_i} \geq 0 \qquad \forall j = 1,\mathrm{n}; \quad \forall k = 1,NP \right\}$$

where $\dfrac{\alpha_i}{\sum_i^m \alpha_i}$ is the mass fraction of the ith element.

It is this optimization that will be solved to model the reactor units in this work.

The IDEAS information maps for reactors are then defined as follows. Let T^V, P^V, P^W be the outlet temperature (K), outlet pressure (bar), and inlet pressure (bar) respectively. Let also, $\left\{\dfrac{\alpha_i^W}{\sum_i^m \alpha_i^W}\right\}_{i=1}^{m}$ be the atomic mass fraction of the ith species, and $\left\{x_k^V\right\}_{k=1}^{n}$ the mass fraction of the unit's outlet kth species. Finally, let h^V, H^W, $\dot{Q}$ be the outlet stream's specific enthalpy (kJ/kg), inlet stream's heat flow (kJ/s), and unit's heat load respectively (kJ/s), and F^W, F^V, f_k^W be the

unit's inlet flow rate (kg/s), unit's outlet flow rate (kg/s), and unit inlet's kth species mass flow rate (kg/s). The subscript PR represents the Peng-Robinson equation of state model.

$$u = \left[u_1^T \quad | \quad u_2^T \right]^T = \left[T^V \quad P^V \quad \left\{ \frac{\alpha_i^W}{\sum_i^m \alpha_i^W} \right\}_{i=1}^m \quad | \quad F^W \quad f_1^W \quad \cdots \quad f_n^W \quad \dot{Q} \right]^T$$

$$y = \left[y_1^T \quad | \quad y_2^T \right]^T = \left[T^V \quad P^V \quad \left\{ \frac{\alpha_i^W}{\sum_i^m \alpha_i^W} \right\}_{i=1}^m \quad P^W \quad \left\{ x_k^V \right\}_{k=1}^n \quad h^V \quad | \quad F^W \quad \dot{Q} \quad f_1^W \quad \ldots \quad f_2^W \quad F^V \quad H^W \right]^T$$

$$\text{where } u_1 \in D_1 \triangleq \left\{ \begin{array}{l} u_1 = \left[T^V \quad P^V \quad \left\{ \frac{\alpha_i^W}{\sum_i^m \alpha_i^W} \right\}_{i=1}^m \right]^T \in \mathbb{R}^{m+2} : \\ T^V \geq 0, \; P^V \geq 0, \; \sum_{i=1}^m \frac{\alpha_i^W}{\sum_i^m \alpha_i^W} = 1, \; \frac{\alpha_i^W}{\sum_i^m \alpha_i^W} \geq 0 \; \forall i = 1, m \end{array} \right\}$$

$$u_2 \in D_2 \triangleq \left\{ \begin{array}{l} u_2 = \left[F^W \quad f_1^W \quad \cdots \quad f_n^W \quad \dot{Q} \right]^T \in \mathbb{R}^{n+2} : F^W \geq 0, \; f_k^W \geq 0 \; \forall k = 1, n \\ \left\{ \begin{array}{l} \dot{Q} \geq 0 \; \textit{if reactor is heated} \\ \dot{Q} \leq 0 \; \textit{if reactor is cooled} \end{array} \right\} \end{array} \right\}$$

The map $\Psi_1 : \mathbb{R}^{m+2} \supset D_1 \rightarrow \mathbb{R}^{m \times (n+2)}$ for the considered reactor model is defined as follows:

$$\Psi_1 : u_1 \to \Psi_1(u_1) \hat{=} \begin{bmatrix} \dfrac{\alpha_1^W}{\sum_i^m \alpha_i^W} & -R_{1,1}^W & \cdots & -R_{1,n}^W & 0 \\ \vdots & \vdots & \ddots & \vdots & \vdots \\ \dfrac{\alpha_m^W}{\sum_i^m \alpha_i^W} & -R_{m,1}^W & \cdots & -R_{m,n}^W & 0 \end{bmatrix}^T \in \mathbb{R}^{m\times(n+2)}, \text{ and}$$

$$\Psi_1(u_1)u_2 = \begin{bmatrix} \dfrac{\alpha_1^W}{\sum_i^m \alpha_i^W} & -R_{1,1}^W & \cdots & -R_{1,n}^W & 0 \\ \vdots & \vdots & \ddots & \vdots & \vdots \\ \dfrac{\alpha_m^W}{\sum_i^m \alpha_i^W} & -R_{m,1}^W & \cdots & -R_{m,n}^W & 0 \end{bmatrix}^T \begin{bmatrix} F^W \\ f_1^W \\ \vdots \\ f_n^W \\ \dot{Q} \end{bmatrix} = 0$$

Where $R_{i,k}^W = \left(ANM^{-1}\right)_{i,k}$, $\mathrm{i} = 1, m;\ k = 1, n$, where A is the diagonal matrix, $A = \begin{bmatrix} A_1 & 0 & 0 \\ 0 & \ddots & 0 \\ 0 & 0 & A_m \end{bmatrix}$,

whose entries are the molar masses of each atom or each inert molecule, N is the matrix,

$N = \begin{bmatrix} \nu_{1,1} & \cdots & \nu_{1,n} \\ \vdots & \ddots & \vdots \\ \nu_{m,1} & \cdots & \nu_{m,n} \end{bmatrix}$, of stoichiometric coefficients, $\nu_{i,k}$ that quantify the number of ith atoms

in the kth species, and M is the diagonal matrix, $M = \begin{bmatrix} M_1 & 0 & 0 \\ 0 & \ddots & 0 \\ 0 & 0 & M_n \end{bmatrix}$, whose entries are the

molar masses of each species.

The maps $\Phi_3 : \mathbb{R}^{m+2} \supset D_1 \to \mathbb{R}^{m+n+4}$ and $\Phi_4 : \mathbb{R}^{m+2} \supset D_1 \to \mathbb{R}^{(n+4)\times(n+2)}$ are defined as follows:

$$\Phi_3 : u_1 \to y_1 = \Phi_3(u_1) \triangleq \begin{bmatrix} T^V \\ P^V \\ \left\{ \dfrac{\alpha_i^W}{\sum_i^m \alpha_i^W} \right\}_{i=1}^{m} \\ P^V \\ \left\{ M_k \cdot \arg\min \pi \left(T^V, P^V, \left\{ \dfrac{\alpha_i^W}{\sum_i^m \alpha_i^W} \right\}_{i=1}^{m} \right) \right\}_{k=1}^{n} \\ h_{PR}\left(T^V, P^V, \left\{ M_k \cdot \arg\min \pi \left(T^V, P^V, \left\{ \dfrac{\alpha_i^W}{\sum_i^m \alpha_i^W} \right\}_{i=1}^{m} \right) \right\}_{k=1}^{n} \right) \end{bmatrix}$$

$$\Phi_4 : u_1 \to \Phi_4\left(u_1\right) \triangleq \begin{bmatrix} 1 & 0 & 0 & 0 & 0 \\ 0 & 0 & 0 & 0 & 1 \\ 0 & 1 & 0 & 0 & 0 \\ 0 & 0 & \ddots & 0 & 0 \\ 0 & 0 & 0 & 1 & 0 \\ 1 & 0 & 0 & 0 & 0 \\ h^V & 0 & 0 & 0 & 1 \end{bmatrix} \in \mathbb{R}^{(n+4)\times(n+2)}, \text{ and}$$

$$y_2 = \begin{bmatrix} F^W \\ \dot{Q} \\ f_1^W \\ \vdots \\ f_n^W \\ F^V \\ H^W \end{bmatrix} = \Phi_4\left(u_1\right)u_2 = \begin{bmatrix} 1 & 0 & 0 & 0 & 0 \\ 0 & 0 & 0 & 0 & 1 \\ 0 & 1 & 0 & 0 & 0 \\ 0 & 0 & \ddots & 0 & 0 \\ 0 & 0 & 0 & 1 & 0 \\ 1 & 0 & 0 & 0 & 0 \\ h^V & 0 & 0 & 0 & 1 \end{bmatrix} \begin{bmatrix} F^W \\ f_1^W \\ \vdots \\ f_n^W \\ \dot{Q} \end{bmatrix}$$

Separators

As can be seen in Figure 1-1, heat is only allowed to leave the separator at a temperature T, enter an ideal Carnot Cycle, which releases heat to the environment, and generates some work which enters the separator. That work, combined with additional work that enters the separator, so as to satisfy its energetic needs for separation, allows computation of the ideal work of separation. This separator type is similar to the separators used for the gas separation tasks typical of the considered case study (membrane separators, pressure swing adsorbers, etc.)

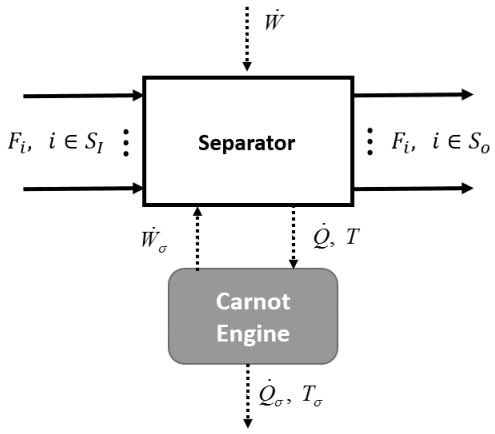

Figure 1-1: *Separator Representation*

The considered separator model is assumed to have no heat inlet ports, a single heat outlet port at a temperature T above the environmental temperature T_σ, and inlet and outlet streams with potential and kinetic energy terms that can be neglected. A Carnot engine is coupled to separator units, so as to calculate the ideal work of separation, which is later used in the IDEAS formulation for the separator units. Consider also that the separator is coupled to a power engine operating between T and T_σ. Then, the following proposition holds:

Proposition 2

Consider a separator operating at steady-state, having a single outlet heat port at $T \geq T_\sigma$, and inlet and outlet streams with potential, and kinetic energy terms that can be neglected. Let H denote the enthalpy of a stream, S denote the entropy of a stream, S_O denote the index set of

the outlet streams, and S_i denote the index set of the inlet streams. Then the ideal work of separation, and the associated ideal separator cold utility load are:

$$\dot{W} = \sum_{i\in S_O} F_i\left(H_i - T_\sigma S_i\right) - \sum_{i\in S_I} F_i\left(H_i - T_\sigma S_i\right)$$

$$\dot{Q}_\sigma = \sum_{i\in S_I} F_i T_\sigma S_i - \sum_{i\in S_O} F_i T_\sigma S_i \ .$$

Proof:

$$\left\{\begin{array}{l} 0 = \sum_{i\in S_I} F_i H_i - \sum_{i\in S_O} F_i H_i - \dot{Q} + \dot{W} + \dot{W}_\sigma \\ 0 = \sum_{i\in S_I} F_i S_i - \sum_{i\in S_O} F_i S_i - \frac{\dot{Q}}{T} + \dot{S}_G \ \wedge\ \dot{S}_G \geq 0 \\ 0 = \dot{Q} - \dot{Q}_\sigma - \dot{W}_\sigma \\ 0 = \frac{\dot{Q}}{T} - \frac{\dot{Q}_\sigma}{T_\sigma} + \dot{S}_{G,\sigma} \ \wedge\ \dot{S}_{G,\sigma} \geq 0 \end{array}\right\} \Leftrightarrow \left\{\begin{array}{l} \dot{W} + \dot{W}_\sigma = -\sum_{i\in S_I} F_i H_i + \sum_{i\in S_O} F_i H_i + \dot{Q} \\ \dot{Q} = T\sum_{i\in S_I} F_i S_i - T\sum_{i\in S_O} F_i S_i + T\dot{S}_G \ \wedge\ \dot{S}_G \geq 0 \\ \dot{W}_\sigma = \left(1 - \frac{T_\sigma}{T}\right)\dot{Q} - T_\sigma \dot{S}_{G,\sigma} \\ \dot{Q}_\sigma = \frac{T_\sigma}{T}\dot{Q} + T_\sigma \dot{S}_{G,\sigma} \ \wedge\ \dot{S}_{G,\sigma} \geq 0 \end{array}\right\} \Leftrightarrow$$

$$\left\{\begin{array}{l} \dot{W} + \dot{W}_\sigma = \sum_{i\in S_O} F_i\left(H_i - TS_i\right) - \sum_{i\in S_I} F_i\left(H_i - TS_i\right) + T\dot{S}_G \\ \dot{Q} = T\sum_{i\in S_I} F_i S_i - T\sum_{i\in S_O} F_i S_i + T\dot{S}_G \ \wedge\ \dot{S}_G \geq 0 \\ \dot{W}_\sigma = \left(T - T_\sigma\right)\left(\sum_{i\in S_I} F_i S_i - \sum_{i\in S_O} F_i S_i + \dot{S}_G\right) - T_\sigma \dot{S}_{G,\sigma} \\ \dot{Q}_\sigma = T_\sigma\left(\sum_{i\in S_I} F_i S_i - \sum_{i\in S_O} F_i S_i + \dot{S}_G\right) + T_\sigma \dot{S}_{G,\sigma} \ \wedge\ \dot{S}_{G,\sigma} \geq 0 \end{array}\right\} \Leftrightarrow$$

$$\left\{\begin{array}{l} \dot{W} = \sum_{i\in S_O} F_i\left(H_i - T_\sigma S_i\right) - \sum_{i\in S_I} F_i\left(H_i - T_\sigma S_i\right) + T_\sigma\left(\dot{S}_G + \dot{S}_{G,\sigma}\right) \\ \dot{Q} = T\sum_{i\in S_I} F_i S_i - T\sum_{i\in S_O} F_i S_i + T\dot{S}_G \ \wedge\ \dot{S}_G \geq 0 \\ \dot{W}_\sigma = \left(T - T_\sigma\right)\left(\sum_{i\in S_I} F_i S_i - \sum_{i\in S_O} F_i S_i + \dot{S}_G\right) - T_\sigma \dot{S}_{G,\sigma} \\ \dot{Q}_\sigma = \sum_{i\in S_I} F_i T_\sigma S_i - \sum_{i\in S_O} F_i T_\sigma S_i + T_\sigma\left(\dot{S}_G + \dot{S}_{G,\sigma}\right) \wedge\ \dot{S}_{G,\sigma} \geq 0 \wedge \dot{S}_G \geq 0 \end{array}\right\}$$

The ideal work of separation is obtained by considering that the separator, and the coupled power engine are both reversible (their rates of entropy generation are both zero), i.e. $\dot{S}_G = 0 \wedge \dot{S}_{G,\sigma} = 0$. Then the ideal work of separation, and the associated ideal separator cold utility load are:

$$\dot{W}_{Ideal} = \sum_{i \in S_O} F_i \left(H_i - T_\sigma S_i \right) - \sum_{i \in S_I} F_i \left(H_i - T_\sigma S_i \right)$$

$$\dot{Q}_{\sigma, Ideal} = \sum_{i \in S_I} F_i T_\sigma S_i - \sum_{i \in S_O} F_i T_\sigma S_i \text{ . O.E.}\Delta.$$

The IDEAS information maps for separators are then defined as follows. Let T_i^V, T^W, P_i^V, P^W be the unit's ith outlet temperature (K), unit's inlet temperature (K), unit's ith outlet pressure (bar), and unit's inlet pressure (bar) respectively. Let also $\left\{ x_k^V \right\}_{k=1}^n$ be the mass fraction of the unit's outlet kth species, and h_i^V, H^W, s_i^V, S^W be the ith outlet stream's specific enthalpy (kJ/kg), inlet stream's heat flow (kJ/s), unit's ith outlet specific entropy (kJ/kg K), and inlet entropy flow of the stream (kJ/s K) respectively. Finally, let F^W, f_k^W, F_i^V be the unit's inlet flow rate (kg/s), ith unit's outlet flow rate (kg/s), and unit inlet's kth species mass flow rate (kg/s) respectively, and $\dot{Q}, \dot{W}_{Ideal}$ be the reactor's heat load (kJ/s) and ideal work (kJ/s) respectively. The subscript PR represents the Peng-Robinson equation of state model.

$$u = \left[u_1^T \;\middle|\; u_2^T \right]^T = \left[T_1^V \quad P_1^V \quad \left\{ x_{1,k}^V \right\}_{k=1}^n \quad \left\{ x_{2,k}^V \right\}_{k=1}^n \;\middle|\; F_1^V \quad F_2^V \quad H^W \quad S^W \right]^T$$

$$y = \left[y_1^T \;\middle|\; y_2^T \right]^T;$$

$$y_1 = \left[T_1^V \; P_1^V \; \left\{ x_{1,k}^V \right\}_{k=1}^n \; \left\{ x_{2,k}^V \right\}_{k=1}^n \; T_2^V \; T^W \; P_2^V \; P^W \; h_1^V \; h_2^V \; s_1^V \; s_2^V \right]^T$$

$$y_2 = \left[F_1^V \; F_2^V \; f_1^W \; \ldots \; f_n^W \; H^W \; S^W \; F^W \; \dot{Q} \; \dot{W}_{Ideal} \right]^T$$

$$\text{where } u_1 \in D_1 = \left\{ \begin{array}{l} u_1 = \left[T_1^V \quad P_1^V \quad \left\{ x_{1,k}^V \right\}_{k=1}^n \quad \left\{ x_{2,k}^V \right\}_{k=1}^n \right]^T \in \mathbb{R}^{2n+2} : \\ T_1^V \geq 0,\ P_1^V \geq 0,\ \sum_{k=1}^n x_{1,k}^V = 1,\ x_{1,k}^V \geq 0,\ \forall k = 1,n \\ \sum_{k=1}^n x_{2,k}^V = 1,\ x_{2,k}^V \geq 0 \quad \forall k = 1,n \end{array} \right\}$$

$$u_2 \in D_2 \triangleq \left\{ u_2 = \left[F_1^V \quad F_2^V \quad H^W \quad S^W \right]^T \in \mathbb{R}^4 : F_1^V \geq 0,\ F_2^V \geq 0 \right\}$$

No map Ψ_1 need be defined for the considered separator model.

The maps $\Phi_3 : \mathbb{R}^{2n+2} \supset D_1 \to \mathbb{R}^{2n+10}$ and $\Phi_4 : \mathbb{R}^{2n+2} \supset D_1 \to \mathbb{R}^{(n+7)\times 4}$ are defined as follows:

$$\Phi_3 : u_1 \to y_1 = \Phi_3(u_1) \triangleq \left[\begin{array}{c} T_1^V \\ P_1^V \\ \left\{ x_{1,k}^V \right\}_{k=1}^n \\ \left\{ x_{2,k}^V \right\}_{k=1}^n \\ T_1^V \\ T_1^V \\ P_1^V \\ P_1^V \\ h_{PR}\left(T_1^V, P_1^V, \left\{ x_{1,k}^V \right\}_{k=1}^n \right) \\ h_{PR}\left(T_1^V, P_1^V, \left\{ x_{2,k}^V \right\}_{k=1}^n \right) \\ s_{PR}\left(T_1^V, P_1^V, \left\{ x_{1,k}^V \right\}_{k=1}^n \right) \\ s_{PR}\left(T_1^V, P_1^V, \left\{ x_{2,k}^V \right\}_{k=1}^n \right) \end{array} \right] \in \mathbb{R}^{2n+10} \quad ,$$

$$\Phi_4 : u_1 \to \Phi_4(u_1) \hat{=} \begin{bmatrix} 1 & 0 & 0 & 0 \\ 0 & 1 & 0 & 0 \\ 0 & 0 & 1 & 0 \\ 0 & 0 & 0 & 1 \\ x_{1,1}^V & x_{2,1}^V & 0 & 0 \\ \vdots & \vdots & \vdots & \vdots \\ x_{1,n}^V & x_{2,n}^V & 0 & 0 \\ 1 & 1 & 0 & 0 \\ -T_\sigma s_1^V & -T_\sigma s_2^V & 0 & T_\sigma \\ h_1^V - T_\sigma s_1^V & h_2^V - T_\sigma s_2^V & -1 & T_\sigma \end{bmatrix} \in \mathbb{R}^{(n+7)\times 4}$$

$$y_2 = \begin{bmatrix} F_1^V \\ F_2^V \\ H^W \\ S^W \\ f_1^W \\ \vdots \\ f_n^W \\ F^W \\ \dot{Q} \\ W \end{bmatrix} = \Phi_4(u_1)u_2 = \begin{bmatrix} 1 & 0 & 0 & 0 \\ 0 & 1 & 0 & 0 \\ 0 & 0 & 1 & 0 \\ 0 & 0 & 0 & 1 \\ x_{1,1}^V & x_{2,1}^V & 0 & 0 \\ \vdots & \vdots & \vdots & \vdots \\ x_{1,n}^V & x_{2,n}^V & 0 & 0 \\ 1 & 1 & 0 & 0 \\ -T_\sigma s_1^V & -T_\sigma s_2^V & 0 & T_\sigma \\ h_1^V - T_\sigma s_1^V & h_2^V - T_\sigma s_2^V & -1 & T_\sigma \end{bmatrix} \begin{bmatrix} F_1^V \\ F_2^V \\ H^W \\ S^W \end{bmatrix}$$

Pressure Changing Devices

The IDEAS information maps for pressure changing devices are then defined as follows. Let T^V, $T_{isentropic}^V, T^W, P^V, P^W$ be the outlet temperature (K), isentropic outlet temperature (K), inlet temperature (K), outlet pressure (bar), and inlet pressure (bar) respectively. Let also $\left\{x_k^V\right\}_{k=1}^n$, $\left\{x_k^W\right\}_{k=1}^n$ be the mass fraction of the unit's outlet kth species, and mass fraction of the unit's inlet kth species respectively, and h^V, H^W be the outlet stream's specific enthalpy (kJ/kg), and inlet stream's heat flow (kJ/s) respectively. Finally, let F^W, F^V be the unit's inlet flow rate (kg/s), and

unit's outlet flow rate (kg/s) respectively, and η the isentropic efficiency. The subscript PR represents the Peng-Robinson equation of state model.

$$u = \left[u_1^T \quad | \quad u_2^T \right]^T = \left[T^W \quad P^W \quad P^V \quad \left\{ x_k^W \right\}_{k=1}^n \quad \zeta \quad | \quad F^W \right]^T$$

$$y = \left[y_1^T \quad | \quad y_2^T \right]^T = \left[T^W \;\; P^W \;\; P^V \;\; \left\{ x_k^W \right\}_{k=1}^n \;\; \zeta \;\; \left\{ x_k^V \right\}_{k=1}^n \;\; h^W \;\; s^W \;\; T^V_{isentropic} \;\; T^V \;\; h^V \;|\; F^W \;\; F^V \;\; f_1^W \;\; \ldots \;\; f_n^W \;\; H^W \;\; W \right]^T$$

where, $\zeta = \begin{cases} 1/\eta & \textit{compressors / pumps} \\ \eta & \textit{turbines} \\ 0 & \textit{valves} \end{cases}$,

$$u_1 \in D_1 = \left\{ \begin{array}{l} u_1 = \left[T^W \quad P^W \quad P^V \quad \left\{ x_k^W \right\}_{k=1}^n \quad \zeta \right]^T \in \mathbb{R}^{n+4} : \\ T^W \geq 0, \;\; P^W \geq 0, \; \sum_{k=1}^n x_k^W = 1, \; x_k^W \geq 0 \;\; \forall k = 1, n; \; 0 \leq \zeta \leq 1 \end{array} \right\},$$

$$u_2 \in D_2 \triangleq \left\{ u_2 = \left[F^W \right]^T \in \mathbb{R} : F^W \geq 0 \right\}$$

No map Ψ_1 need be defined for the considered pressure changing device model.

The maps $\Phi_3 : \mathbb{R}^{n+4} \supset D_1 \to \mathbb{R}^{2n+9}$ and $\Phi_4 : \mathbb{R}^{n+4} \supset D_1 \to \mathbb{R}^{(n+4)\times 1}$ are defined as follows:

$$\Phi_3 : u_1 \to y_1 = \Phi_3(u_1) \triangleq \begin{bmatrix} T^W \\ P^W \\ P^V \\ \left\{x_k^W\right\}_{k=1}^n \\ \zeta \\ \left\{x_k^W\right\}_{k=1}^n \\ h_{PR}\left(T^W, P^W, \left\{x_k^W\right\}_{k=1}^n\right) \\ s_{PR}\left(T^W, P^W, \left\{x_k^W\right\}_{k=1}^n\right) \\ T_{PR}\left(s_{PR}\left(T^W, P^W, \left\{x_k^W\right\}_{k=1}^n\right),\ P^V, \left\{x_k^W\right\}_{k=1}^n\right) \\ T_{PR}\left(\begin{bmatrix} \zeta h_{PR}\left(\begin{bmatrix} T_{PR}\left(s_{PR}\left(T^W, P^W, \left\{x_k^W\right\}_{k=1}^n\right),\ P^V, \left\{x_k^W\right\}_{k=1}^n\right), \\ P^V, \left\{x_k^W\right\}_{k=1}^n \end{bmatrix}\right) + \\ h_{PR}\left(T^W, P^W, \left\{x_k^W\right\}_{k=1}^n\right)(1-\zeta) \end{bmatrix}, P^V, \left\{x_k^W\right\}_{k=1}^n\right) \\ \begin{bmatrix} \zeta h_{PR}\left(\begin{bmatrix} T_{PR}\left(\begin{bmatrix} s_{PR}\left(T^W, P^W, \left\{x_k^W\right\}_{k=1}^n\right), \\ P^V, \left\{x_k^W\right\}_{k=1}^n \end{bmatrix}\right), P^V, \left\{x_k^W\right\}_{k=1}^n \end{bmatrix}\right) + \\ h_{PR}\left(T^W, P^W, \left\{x_k^W\right\}_{k=1}^n\right)(1-\zeta) \end{bmatrix} \end{bmatrix}$$

$$\Phi_4 : u_1 \to \Phi_4\left(u_1\right) \triangleq \begin{bmatrix} 1 \\ 1 \\ x_1^W \\ \vdots \\ x_n^W \\ h^W \\ \begin{bmatrix} \zeta\left(\begin{bmatrix} h_{PR}\left(\begin{bmatrix} T_{PR}\left(s_{PR}\left(T^W, P^W, \left\{x_k^W\right\}_{k=1}^n\right),\ P^V, \left\{x_k^W\right\}_{k=1}^n\right), \\ P^V, \left\{x_k^W\right\}_{k=1}^n \end{bmatrix}\right) - \\ h_{PR}\left(T^W, P^W, \left\{x_k^W\right\}_{k=1}^n\right) \end{bmatrix}\right) \end{bmatrix} \end{bmatrix} \in \mathbb{R}^{(n+4)\times 1}$$

$$y_2 = \begin{bmatrix} F^W \\ F^V \\ f_1^W \\ \vdots \\ f_n^W \\ H^W \\ W \end{bmatrix} = \Phi_4(u_1)u_2 = \begin{bmatrix} 1 \\ 1 \\ x_1^W \\ \vdots \\ x_n^W \\ h^W \\ \left[\zeta\left(\begin{matrix} h_{PR}\left(\begin{matrix} T_{PR}\left(s_{PR}\left(T^W, P^W, \left\{x_k^W\right\}_{k=1}^n\right), P^V, \left\{x_k^W\right\}_{k=1}^n\right), \\ P^V, \left\{x_k^W\right\}_{k=1}^n \end{matrix}\right) \\ -h_{PR}\left(T^W, P^W, \left\{x_k^W\right\}_{k=1}^n\right) \end{matrix}\right)\right] \end{bmatrix} \left[F^W\right]$$

Heat Exchange Network

In this work, the heat exchanger network shown in Figure 1-2 is considered. It contains three categories of heat exchangers: hot stream - cold stream heat exchangers; stream - point load

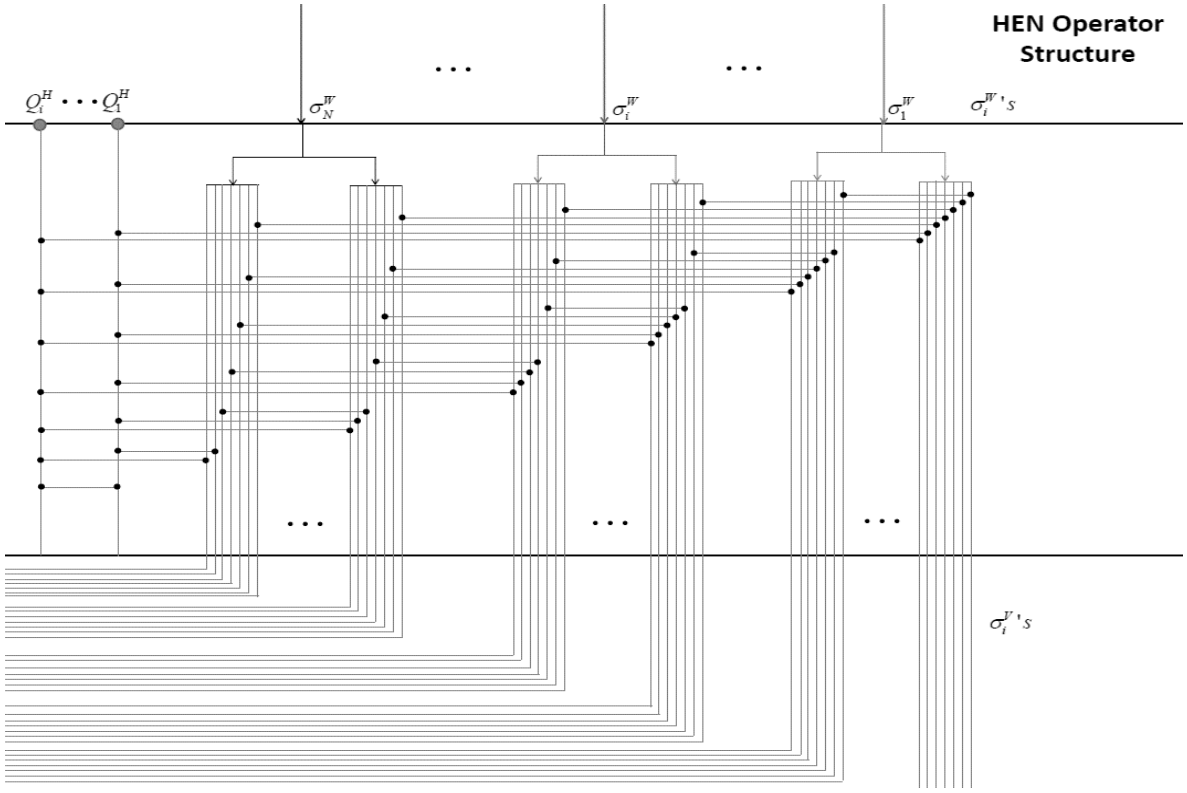

Figure 1-2: *Representation of heat exchange network structure*

heat exchangers, where a stream is cooled (heated) by a cold (hot) point load; and point load - point load heat exchangers where hot (cold) point loads and cold (hot) point loads are matched. External utilities as well as unit loads are typically considered as either hot or cold point loads. Streams are created by comparing each state with every other state, for equality of the two states' pressure and composition components. Once all streams have been created, all feasible/desirable/non-forbidden stream-stream heat exchangers, stream-point load heat exchangers, and point load-point load heat exchangers are generated. Thermodynamic feasibility of each exchanger is verified throughout its length. The objective function to be minimized in this work is the overall utility cost, for all external hot utilities.

The IDEAS information maps for stream-stream heat exchangers, whose first stream is considered to be hot, are then defined as follows. Let $T_i^V, T_i^W, P_i^V, P_i^W$ be the unit's ith outlet temperature (K), unit's ith inlet temperature (K), unit's ith outlet pressure (bar), and unit's ith inlet pressure (bar) respectively, and $\left\{x_{i,k}^V\right\}_{k=1}^n, \left\{x_{i,k}^W\right\}_{k=1}^n$ be the mass fraction of the unit's ith outlet kth species and mass fraction of the unit's ith inlet kth species respectively. Let also h_i^V, h_i^W be the ith outlet stream's specific enthalpy (kJ/kg), and ith inlet stream's heat flow (kJ/s) respectively (the subscript PR represents the Peng-Robinson equation of state model). Finally, let F_i^W, F_i^V be the ith unit's inlet flow rate (kg/s), and ith unit's outlet flow rate (kg/s) respectively, and $\dot{Q}$ be the unit's heat load (kJ/s).

$$u = \left[u_1^T \mid u_2^T\right]^T = \left[T_1^V \quad T_2^V \quad T_1^W \quad T_2^W \quad P_1^V \quad P_2^V \quad \left\{x_{1,k}^V\right\}_{k=1}^n \quad \left\{x_{2,k}^V\right\}_{k=1}^n \mid F_1^W \quad F_2^W\right]^T$$

$$\left\{ y = \left[y_1^T \mid y_2^T\right]^T = \left[T_1^V\ T_2^V\ T_1^W\ T_2^W\ P_1^V\ P_2^V\ \left\{x_{1,k}^V\right\}_{k=1}^n\ \left\{x_{2,k}^V\right\}_{k=1}^n\ P_1^W\ P_2^W\ \left\{x_{1,k}^W\right\}_{k=1}^n\ \left\{x_{2,k}^W\right\}_{k=1}^n\ h_1^W\ h_2^W\ h_1^V\ h_2^V \mid F_1^W\ F_2^W\ F_1^V\ F_2^V\ \dot{Q}\right]^T \right\}$$

where $u_1 \in D_1 = \left\{ \begin{array}{l} u_1 = \left[T_1^V \quad T_2^V \quad T_1^W \quad T_2^W \quad P_1^V \quad P_2^V \quad \left\{x_{1,k}^V\right\}_{k=1}^n \quad \left\{x_{2,k}^V\right\}_{k=1}^n \right]^T \in \mathbb{R}^{2n+6} : \\ T_1^V \geq 0,\ T_2^V \geq 0,\ T_1^W \geq 0,\ T_2^W \geq 0,\ P_1^V \geq 0,\ P_2^V \geq 0, \\ \sum_{k=1}^{n} x_{1,k}^V = 1,\ x_{1,k}^V \geq 0\ \forall k = 1,n;\ \sum_{k=1}^{n} x_{2,k}^V = 1,\ x_{2,k}^V \geq 0\ \forall k = 1,n \end{array} \right\}$

$u_2 \in D_2 \triangleq \left\{ u_2 = \left[F_1^W \quad F_2^W \right]^T \in \mathbb{R}^2 : F_1^W \geq 0,\ F_2^W \geq 0 \right\}$

The map $\Psi_1 : \mathbb{R}^{2n+6} \supset D_1 \to \mathbb{R}^{1\times 2}$ for the considered stream-stream heat exchanger model is defined as follows:

$\Psi_1 : u_1 \to \Psi_1(u_1) \triangleq \left[h_1^W - h_1^V \quad h_2^W - h_2^V \right] \in \mathbb{R}^{1\times 2}$, and $\Psi_1(u_1)u_2 = \left[h_1^W - h_1^V \quad h_2^W - h_2^V \right] \begin{bmatrix} F_1^V \\ F_2^V \end{bmatrix} = 0$

The maps $\Phi_3 : \mathbb{R}^{2n+6} \supset D_1 \to \mathbb{R}^{4n+12}$ and $\Phi_4 : \mathbb{R}^{2n+6} \supset D_1 \to \mathbb{R}^{5\times 2}$ are defined as follows:

$$\Phi_3 : u_1 \to y_1 = \Phi_3(u_1) \triangleq \begin{bmatrix} T_1^V \\ T_2^V \\ T_1^W \\ T_2^W \\ P_1^V \\ P_2^V \\ \left\{x_{1,k}^V\right\}_{k=1}^n \\ \left\{x_{2,k}^V\right\}_{k=1}^n \\ P_1^V \\ P_2^V \\ \left\{x_{1,k}^V\right\}_{k=1}^n \\ \left\{x_{2,k}^V\right\}_{k=1}^n \\ h_{PR}\left(T_1^W, P_1^V, \left\{x_{1,k}^V\right\}_{k=1}^n\right) \\ h_{PR}\left(T_2^W, P_2^V, \left\{x_{2,k}^V\right\}_{k=1}^n\right) \\ h_{PR}\left(T_1^V, P_1^V, \left\{x_{1,k}^V\right\}_{k=1}^n\right) \\ h_{PR}\left(T_2^V, P_2^V, \left\{x_{2,k}^V\right\}_{k=1}^n\right) \end{bmatrix} \in \mathbb{R}^{4n+12},$$

$$\Phi_4 : u_1 \to \Phi_4\left(u_1\right) \triangleq \begin{bmatrix} 1 & 0 \\ 0 & 1 \\ 1 & 0 \\ 0 & 1 \\ h_1^W - h_1^V & 0 \end{bmatrix} \in \mathbb{R}^{5\times 2}, \text{ and } y_2 = \begin{bmatrix} F_1^W \\ F_2^W \\ F_1^V \\ F_2^V \\ \dot{Q} \end{bmatrix} = \Phi_4\left(u_1\right)u_2 = \begin{bmatrix} 1 & 0 \\ 0 & 1 \\ 1 & 0 \\ 0 & 1 \\ h_1^W - h_1^V & 0 \end{bmatrix} \begin{bmatrix} F_1^W \\ F_2^W \end{bmatrix}$$

The IDEAS information maps for stream-point load heat exchangers, where the stream is always designated as first, are then defined as follows. Let $T_1^V, T_1^W, T_2, P_1^V, P_1^W$ be the unit's outlet stream temperature (K), unit's inlet stream temperature (K), point load's temperature (K), unit's outlet stream pressure (bar), and unit's inlet stream pressure (bar) respectively, and let $\left\{x_{1,k}^V\right\}_{k=1}^n$,

$\left\{x_{1,k}^{W}\right\}_{k=1}^{n}$ be the kth species' mass fraction of the unit's outlet stream and kth species' mass fraction of the unit's inlet stream respectively. Let also h_1^V, h_1^W be the outlet stream's specific enthalpy (kJ/kg), and inlet stream's heat flow (kJ/kg) respectively (the subscript PR represents the Peng-Robinson equation of state model). Finally, let F_1^W, F_1^V be the ith unit inlet stream's flow rate (kg/s), and ith unit outlet stream's flow rate (kg/s) respectively, and $\dot{Q}$ be the unit's heat load (kJ/s):

$$u = \left[u_1^T \;\middle|\; u_2^T \right]^T = \left[T_1^V \quad T_1^W \quad T_2 \quad P_1^V \quad \left\{x_{1,k}^V\right\}_{k=1}^n \;\middle|\; F_1^W \right]^T$$

$$y = \left[y_1^T \;\middle|\; y_2^T \right]^T = \left[T_1^V \quad T_1^W \quad T_2 \quad P_1^V \quad \left\{x_{1,k}^V\right\}_{k=1}^n \quad P_1^W \quad \left\{x_{1,k}^W\right\}_{k=1}^n \quad h_1^W \quad h_1^V \;\middle|\; F_1^W \quad F_1^V \quad \dot{Q} \right]^T$$

where $u_1 \in D_1 = \left\{ \begin{array}{l} u_1 = \left[T_1^V \quad T_1^W \quad T_2 \quad P_1^V \quad \left\{x_{1,k}^V\right\}_{k=1}^n \right]^T \in \mathbb{R}^{n+4} : \\ T_1^V \geq 0,\ T_1^W \geq 0,\ T_2 \geq 0,\ P^V \geq 0,\ \sum_{k=1}^{n} x_k^V = 1,\ x_k^V \geq 0\ \forall k = 1, n \end{array} \right\}$

$$u_2 \in D_2 \triangleq \left\{ u_2 = \left[F_1^W \right]^T \in \mathbb{R} : F_1^W \geq 0 \right\}$$

No map Ψ_1 need be defined for the considered stream-point load heat exchanger model.

The maps $\Phi_3 : \mathbb{R}^{n+4} \supset D_1 \to \mathbb{R}^{2n+7}$ and $\Phi_4 : \mathbb{R}^{n+4} \supset D_1 \to \mathbb{R}^{3\times 1}$ are defined as follows:

$$\Phi_3 : u_1 \to y_1 = \Phi_3(u_1) \triangleq \begin{bmatrix} T_1^V \\ T_1^W \\ T_2 \\ P_1^V \\ \left\{x_{1,k}^V\right\}_{k=1}^n \\ P_1^V \\ \left\{x_{1,k}^V\right\}_{k=1}^n \\ h_{PR}\left(T_1^W, P_1^V, \left\{x_{1,k}^V\right\}_{k=1}^n\right) \\ h_{PR}\left(T_1^V, P_1^V, \left\{x_{1,k}^V\right\}_{k=1}^n\right) \end{bmatrix} \in \mathbb{R}^{2n+7}$$

$$\Phi_4 : u_1 \to \Phi_4\left(u_1\right) \triangleq \begin{bmatrix} 1 \\ 1 \\ h_1^W - h_1^V \end{bmatrix} \in \mathbb{R}^{3\times 1}, \text{ and } y_2 = \begin{bmatrix} F_1^W \\ F_1^V \\ \dot{Q} \end{bmatrix} = \Phi_4\left(u_1\right)u_2 = \begin{bmatrix} 1 \\ 1 \\ h_1^W - h_1^V \end{bmatrix}\left[F_1^W\right]$$

The IDEAS information maps, for point load-point load heat exchangers with the cold point load designated with a superscript C and the hot point load with a superscript H, are then defined as follows. Let T^C, T^H be the cold point-load temperature (K), and hot point-load temperature (K) respectively, and $\dot{Q}$ be the unit's heat load (kJ/s).

$$u = \left[u_1^T \;\middle|\; u_2^T\right]^T = \left[T^C \quad T^H \;\middle|\; \dot{Q}\right]^T$$
$$y = \left[y_1^T \;\middle|\; y_2^T\right]^T = \left[T^C \quad T^H \;\middle|\; \dot{Q}\right]^T$$

where $u_1 \in D_1 \triangleq \left\{u_1 = \left[T^C \quad T^H\right]^T \in \mathbb{R}^2 : T^C \geq 0,\ T^H \geq 0\right\}$, $u_2 \in D_2 \triangleq \left\{u_2 = \left[\dot{Q}\right]^T \in \mathbb{R} : \dot{Q} \geq 0\right\}$.

No maps Ψ_1, Φ_3, or Φ_4 need be defined for the considered point load-point load heat exchanger model.

Having established the applicability of IDEAS to all considered unit operation models, the structure of the process network is discussed next. The process network is decomposed into several subnetworks as shown below in Figure 1-3. First, a distribution network (DN) where stream splitting and mixing occurs. Then, a heat exchange network (HEN) is considered as outlined in the heat exchanger section above. All unit operations (aside from heat exchangers) are included in an operator network (OP). Finally, a mixing network (MIX) is employed to account for the mixing of process unit outlet streams with identical states, as there is no benefit in allowing streams with the same state to enter the DN at different locations.

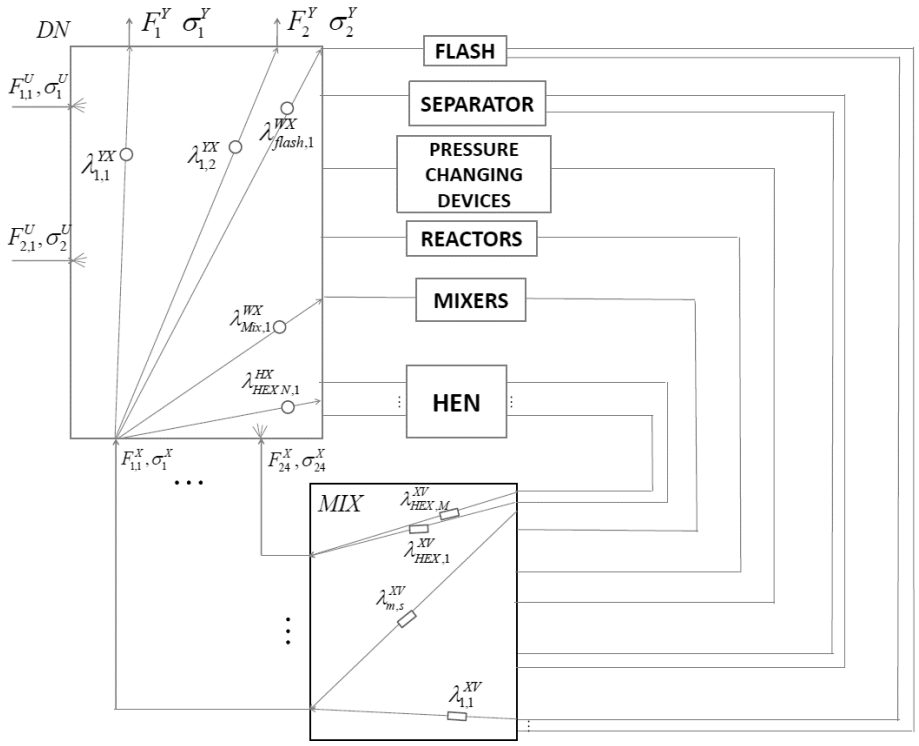

Figure 1-3: *IDEAS representation of a process flowsheet*

A linear objective is considered in the proposed IDEAS formulation, which can be generally presented as $\sum_{i=1}^{N_{HU}} C_i \dot{Q}_{HU_i}$. This objective function can be used to quantify the varying costs of the hot utilities loads ($\dot{Q}_{HU_i}$) necessary for the synthesized network through a change in the cost coefficients C.

IDEAS Mathematical Formulation

The above presented mathematical models of all considered processes (reactors, separators, etc.) are combined to yield the following IDEAS mathematical formulation. Let $F_i^U, F_s^V, F_l^W, F_i^X$, be the mass flow rates (kg/s) of the ith DN inlet, sth process unit outlet, lth process unit inlet, and ith MIX outlet respectively; let $F_p^Y, F_p^{Y,l}, F_p^{Y,u}$ be the mass flow rates (kg/s) of the pth DN outlet, pth lower limit DN outlet, and pth upper limit DN outlet respectively; let $F_{\mathrm{l},i}^{WU}, F_{l,i}^{WX}, F_{p,\mathrm{i}}^{YU}, F_{p,\mathrm{i}}^{YX}$ be the mass flow rates (kg/s) of the ith DN inlet to lth process unit inlet, ith MIX outlet to lth process unit inlet, ith DN inlet to pth DN outlet, and ith MIX outlet to pth DN outlet respectively, and $f_{l,k}^W$ be the mass flow rate of the lth OP inlet's kth species (kg/s). Let also, H^W be the total enthalpy flow of the process unit inlet (kJ/s), and $h_{\mathrm{i}}^U, h_i^V, h_i^W, h_i^X$ be the specific enthalpy (kJ/kg) of the ith DN inlet, ith process unit outlet, ith process unit inlet, and ith MIX outlet respectively; let $h_{\mathrm{p}}^Y, h_{\mathrm{p}}^{Y,l}, h_{\mathrm{p}}^{Y,u}$ be the specific enthalpy (kJ/kg) of the pth DN outlet, pth DN outlet lower limit, and pth DN outlet upper limit (kJ/kg) respectively. Let also, $N_{DN_i}, N_{DN_O}, N_{OP_i}, N_{OP_O}$ be the number of inlet streams in the DN, outlet streams in the DN, inlet streams in the OP, and outlet streams in the OP respectively; let $N_{HEN_i}, N_{HEN_O}, N_{MIX_i}, N_{MIX_O}$ be the number of inlet streams in the HEN, outlet streams in the HEN, inlet streams in the MIX, and outlet streams in the MIX respectively. Let also S^W (kJ/s K) be the total entropy flow for the process unit inlet (kJ/s K), and s_i^U, s_i^X be the specific entropy (kJ/kg K) for the process unit inlet, and process unit outlet respectively. Let also $x_{i,\mathrm{k}}^U, x_{i,k}^V, x_{i,k}^W, x_{i,k}^X$ be the kth species mass fraction of the ith DN inlet, ith process unit outlet, ith process unit inlet, and ith MIX outlet respectively;

let $x_{p,\mathrm{k}}^{Y}$, $x_{p,k}^{Y,l}$, $x_{p,k}^{Y,u}$ be the kth species mass fraction of the pth DN outlet, pth DN outlet lower limit, and pth DN outlet upper limit respectively, and $P_i^U, P_s^V, P_l^W, P_i^X, P_p^Y$ be the pressure (bar) of the ith DN inlet, sth process unit outlet, lth process unit inlet, ith MIX outlet, and pth DN outlet respectively. Finally, let $\lambda_{p,i}^{YU}, \lambda_{l,i}^{WU}, \lambda_{p,i}^{YX}, \lambda_{l,i}^{WX}$ be the flags that denote the existence of flow from the ith DN inlet to the pth DN outlet, from the ith DN inlet to the lth OP inlet, from the ith MIX outlet to the pth DN outlet, and from the ith MIX outlet to the lth OP inlet respectively; let $\lambda_{l,i}^{HU}, \lambda_{l,i}^{HX}, \lambda_{i,s}^{XV}$ be the flags that denote the flow from the ith DN inlet to the lth HEX inlet, from the ith MIX outlet to the lth HEX outlet, and from the sth process unit outlet to the ith MIX inlet respectively.

$$\nu \triangleq \inf \sum_{i=1}^{N_{HU}} C_i Q_{HU_i}$$

Subject to

$$F_i^U = \sum_{p=1}^{N_{DN_O}} \lambda_{p,i}^{YU} F_{p,i}^{YU} + \sum_{l=1}^{N_{OP_i}} \lambda_{l,i}^{WU} F_{l,i}^{WU} + \sum_{l=1}^{N_{HEN_i}} \lambda_{l,i}^{HU} F_{l,i}^{HU} \quad \forall i = 1, N_{DN_i} \tag{1}$$

$$F_i^X = \sum_{s=1}^{N_{MIX_i}} \lambda_{i,\mathrm{s}}^{XV} F_s^V = \sum_{p=1}^{N_{DN_O}} \lambda_{p,i}^{YX} F_{p,i}^{YX} + \sum_{l=1}^{N_{OP_i}} \lambda_{l,i}^{WX} F_{l,i}^{WX} + \sum_{l=1}^{N_{HEN_i}} \lambda_{l,i}^{HX} F_{l,i}^{HX} \quad \forall i = 1, N_{MIX_O} \tag{2}$$

$$F_p^{Y,l} \le \sum_{i=1}^{N_{DN_i}} \lambda_{p,\mathrm{i}}^{YU} F_{p,i}^{YX} + \sum_{i=1}^{N_{MIX_O}} \lambda_{p,\mathrm{i}}^{YX} F_{p,\mathrm{i}}^{YX} \le F_p^{Y,\mathrm{u}} \quad \forall p = 1, N_{DN_O} \tag{3}$$

$$\left[\sum_{i=1}^{N_{DN_i}} \lambda_{p,\mathrm{i}}^{YU} F_{p,\mathrm{i}}^{YU} + \sum_{i=1}^{N_{MIX_O}} \lambda_{p,\mathrm{i}}^{YX} F_{p,\mathrm{i}}^{YX} \right] x_{p,k}^{Y,l} \le \left\{ \sum_{i=1}^{N_{DN_i}} \lambda_{p,\mathrm{i}}^{YU} F_{p,\mathrm{i}}^{YU} x_{\mathrm{i,k}}^{U} + \sum_{i=1}^{N_{MIX_O}} \lambda_{p,\mathrm{i}}^{YX} F_{p,\mathrm{i}}^{YX} x_{\mathrm{i,k}}^{X} \right\} \le \left[\sum_{i=1}^{N_{DN_i}} \lambda_{p,\mathrm{i}}^{YU} F_{p,\mathrm{i}}^{YU} + \sum_{i=1}^{N_{MIX_O}} \lambda_{p,\mathrm{i}}^{YX} F_{p,\mathrm{i}}^{YX} \right] x_{p,k}^{Y,u} \quad \forall k = 1, n \ \forall p = 1, N_{DN_O} \tag{4}$$

$$\left[\sum_{i=1}^{N_{DN_i}} \lambda_{p,\mathrm{i}}^{YU} F_{p,\mathrm{i}}^{YU} + \sum_{i=1}^{N_{MIX_O}} \lambda_{p,\mathrm{i}}^{YX} F_{p,\mathrm{i}}^{YX} \right] h_p^{Y,l} \le \left\{ \sum_{i=1}^{N_{DN_i}} \lambda_{p,\mathrm{i}}^{YU} F_{p,\mathrm{i}}^{YU} h_{\mathrm{i}}^{U} + \sum_{i=1}^{N_{MIX_O}} \lambda_{p,\mathrm{i}}^{YX} F_{p,\mathrm{i}}^{YX} h_{\mathrm{i}}^{X} \right\} \le \left[\sum_{i=1}^{N_{DN_i}} \lambda_{p,\mathrm{i}}^{YU} F_{p,\mathrm{i}}^{YU} + \sum_{i=1}^{N_{MIX_O}} \lambda_{p,\mathrm{i}}^{YX} F_{p,\mathrm{i}}^{YX} \right] h_p^{Y,u} \quad \forall p = 1, N_{DN_O} \tag{5}$$

$$f_{l,k}^W = \sum_{i=1}^{N_{DN_i}} \lambda_{l,i}^{WU} F_{l,i}^{WU} x_{i,k}^U + \sum_{i=1}^{N_{MIX_O}} \lambda_{l,i}^{WX} F_{l,i}^{WX} x_{l,k}^X \quad \forall k = 1, n \ \ \forall l = 1, N_{OP_i} \tag{6}$$

$$H_l^W = \sum_{i=1}^{N_{DN_i}} \lambda_{l,i}^{WU} F_{l,i}^{WU} h_i^U + \sum_{i=1}^{N_{MIX_O}} \lambda_{l,i}^{WX} F_{l,i}^{WX} h_i^X \quad \forall l = 1, N_{OP_i} \tag{7}$$

$$S_l^W = \sum_{i=1}^{N_{DN_i}} \lambda_{l,i}^{WU} F_{l,i}^{WU} s_i^U + \sum_{i=1}^{N_{MIX_O}} \lambda_{l,i}^{WX} F_{l,i}^{WX} s_i^X \quad \forall l = N_R + 1, N_S \tag{8}$$

$$F^{U} \geq 0,\ F^{YU} \geq 0,\ F^{WU} \geq 0,\ F^{HU} \geq 0,\ F^{X} \geq 0,\ F^{YX} \geq 0,\ F^{WX} \geq 0,\ F^{HX} \geq 0 \qquad (9)$$

Where:

$$\lambda_{p,i}^{YU} = \begin{Bmatrix} 1\ if\ P_p^Y = P_i^U \\ 0\ otherwise \end{Bmatrix}, \lambda_{l,i}^{WU} = \begin{Bmatrix} 1\ if\ P_l^W = P_i^U \\ 0\ otherwise \end{Bmatrix}, \lambda_{p,i}^{YX} = \begin{Bmatrix} 1\ if\ P_p^Y = P_i^X \\ 0\ otherwise \end{Bmatrix}, \lambda_{l,i}^{WX} = \begin{Bmatrix} 1\ if\ P_l^W = P_i^X \\ 0\ otherwise \end{Bmatrix}$$

$$\lambda_{l,i}^{HU} = \begin{Bmatrix} 1\ if\ P_l^W = P_i^X, \left\{x_{l,k}^W\right\} = \left\{x_{i,k}^X\right\},\ h_l^W = h_i^X \\ 0\ otherwise \end{Bmatrix}, \lambda_{l,i}^{HX} = \begin{Bmatrix} 1\ if\ P_l^W = P_i^X, \left\{x_{l,k}^W\right\} = \left\{x_{i,k}^X\right\},\ h_l^W = h_i^X \\ 0\ otherwise \end{Bmatrix}$$

$$\lambda_{i,s}^{XV} = \begin{Bmatrix} 1\ if\ P_s^V = P_i^X, \left\{x_{s,k}^V\right\} = \left\{x_{i,k}^X\right\},\ h_s^V = h_i^X \\ 0\ otherwise \end{Bmatrix}$$

Next, the proposed IDEAS framework is illustrated on a process intensification case study for natural gas reforming based hydrogen production.

1.4 Case Study: Process Intensification of Natural Gas Reforming Based Hydrogen Production

Steam reforming of natural gas (and other light hydrocarbons) is currently the most economical process for hydrogen production[56].The commonly accepted reactions for steam reforming of methane are as follows:

$CH_4 + H_2O = CO + 3H_2$ (r1) $\Delta H_1 = 206.1 kJ/mol$ (endothermic)

$CO + H_2O = CO_2 + H_2$ (r2) $\Delta H_2 = -41.15 kJ/mol$ (exothermic)

$CH_4 + 2H_2O = CO_2 + 4H_2$ (r3) $\Delta H_3 = 164.9 kJ/mol$ (endothermic)

Hydrogen is used in refineries as raw material for the hydrocracking of oil aiming at gasoline production. In addition, hydrogen is envisioned to be an energy carrier for vehicular transportation through its use in hydrogen fuel-cell-powered cars. The steam reforming process

is typically carried out industrially at around 1100K and is highly endothermic. This large endothermic heat load is provided through the burning of natural gas and other available fuel resources in large furnaces operating at temperatures well above 1200K. Steam reforming has been the subject of process integration studies[57]. As process integration evolves into process intensification[58], steam reforming is increasingly the focus of process intensification efforts (see [59] and references therein) aiming to improve the economics of this capital and operating cost intensive process. In this case study, the IDEAS framework is applied to the process intensification of a natural gas reforming based flowsheet for hydrogen production, with an emphasis on minimizing hot utility cost. Three hot utility temperature levels are considered, with each utility having a different cost coefficient. A particular focus point of the study is to explore whether steam methane reforming based hydrogen production can be feasible, in the presence of a debilitating carbon tax for the use of methane as a fuel (and not as raw material). Separation and capital costs are only indirectly accounted for, to the extent they are reflected in the consumption of the three hot utilities, and will be the focus of a future study. Upper bounds on the use of each hot utility are imposed in some instances, to facilitate the creation of flowsheets with different energy consumption characteristics.

A baseline flowsheet is first created on the UniSim (Honeywell Inc. trademark) software, that captures a traditional design of this process. The Peng Robinson equation of state is used to capture the thermodynamic properties of the gas mixture. Natural gas (1 kmol/hr) and water (2 kmol/hr) enter the flowsheet at 298K. Subsequently, both are compressed to 5 bar through the use of a compressor and a pump. Prior to entering a reformer with outlet temperature 1100K, the water and carbon dioxide undergo heating. The reformer outlet is subsequently fed into a sequence of high temperature shift (650K outlet temperature), low temperature shift (475K outlet

temperature) reactors with cooling in between. The resultant stream is then cooled before undergoing water, carbon dioxide and hydrogen separation all at 313K. The water, unreacted methane, and carbon monoxide are recycled to the reformer, while hydrogen (4 kmol/hr) and carbon dioxide (1 kmol/hr) are the flowsheet products.

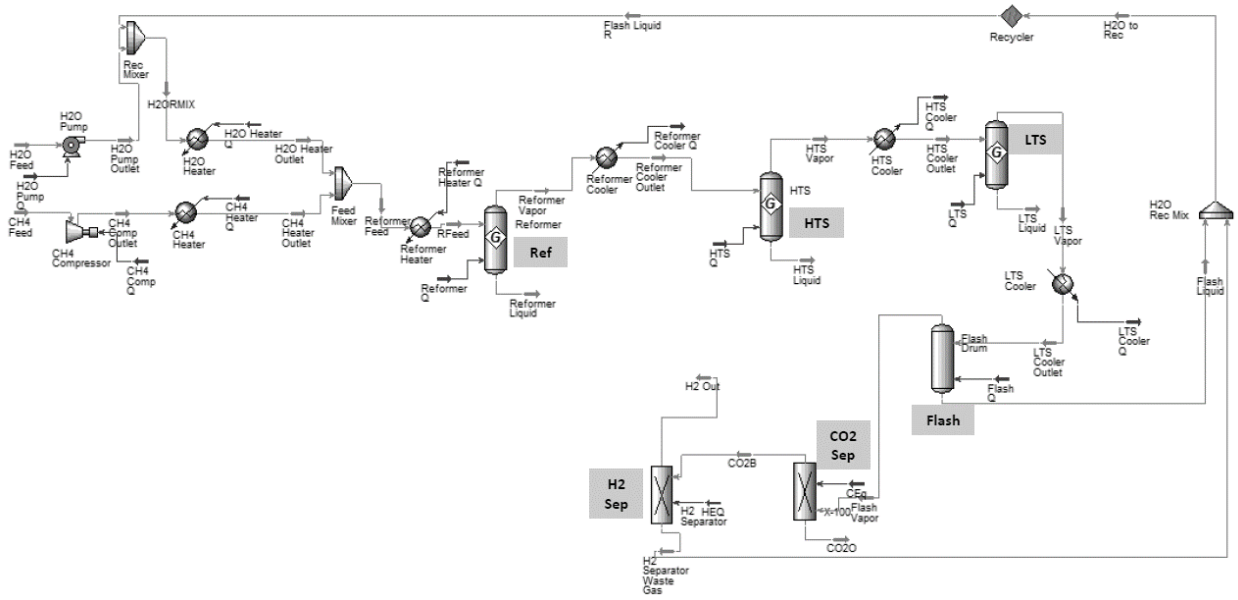

Figure 1-4: Flowsheet depiction of a traditional natural gas based hydrogen production process.

External hot utility loads of 216.8 kJ/mol of CH_4 fed, 21.78 kJ/mol of CH_4 fed, and 11.84 kJ/mol CH_4 fed are needed at 1200K, 770K and 420K respectively.

The IDEAS methodology is employed to synthesize alternative flowsheet designs to this traditional flowsheet. Given the aforementioned efficiency in searching the design space, afforded by the employed Gibbs free energy minimization based reactor modeling, low dimensional IDEAS LP approximations are employed which identify intensifying designs in the order of a few minutes. The atomic mass fraction ratios of the reformers assume values in the range of 0.33-0.38 for C/O ratio, and 0.07-0.25 for H/O ratio, which includes the atomic ratios of the aforementioned baseline design. The overall stoichiometry of the traditional flowsheet (1 kmol/hr of CH_4 in, 2 kmol/hr H_2O in, 4 H2 kmol/hr out, 1 CO_2 kmol/hr out) is imposed on all of

these IDEAS designs. Multiple optimization instances are carried out for varying cost coefficient ratios of the three hot utilities. In particular, cost coefficient ratios of 24:2:1$\left(Q_{HU_1} : Q_{HU_2} : Q_{HU_3}\right)$, 4:2:1, 3:2:1, 2.5:2:1, and 1.2:1:1 are considered, with the cost coefficient of the 420K utility being 0.00425 $/kJ. In addition, upper bounds are imposed on the use of each hot utility in some instances.

IDEAS generates several different flowsheets depending on the cost coefficient ratios of the hot utilities. When the cost coefficient ratio is 4:2:1 and 24:2:1, the resulting IDEAS flowsheet contains a reformer that has a load of -5kJ/mol of CH_4 fed. In addition, external hot utility loads of 248 kJ/mol of CH_4 and 32.01 kJ/mol of CH_4 are needed at 770K and 420K respectively. The flowsheet produces pure CO_2 as process by-product as well as 4 moles of pure H2 per mol of CH_4 fed. Removing the need for a 1200K external hot utility, allows the flowsheet's energy needs to be potentially met through use of renewable energy sources, such as solar concentrated power. As the cost coefficient ratio between the 1200K and 770K utility varies from 2.5:2 to 24:2, the amount of 1200K utility used by the IDEAS flowsheet will decrease from 26.26 kJ/s (for 2.5:2 ratio) to 0 kJ/s (for 4:2 ratios and above). These results are summarized in Table 1-1 below.

Lowering the hot utility ratio from 4:2:1 to 1.2:1:1 produces several flowsheets. Among them are the flowsheets illustrated in Figure 1-5 and 1-6, which are simplifications of IDEAS generated designs (following elimination of small flows that have minor contributions to the flowsheet characteristics). Figure 1-5 was obtained utilizing the cost coefficient of 2.5:2:1, and Figure 1-6 was obtained by utilizing a cost coefficient ratio of 1.2:1:1, and utility upper bounds of 50kJ/s (1200 K), and 15kJ/s (770 K). The Figure 1-5 flowsheet employed a reverse-gas-shift (RGS) reactor, a high-temperature swing reactor (HTS), a low-temperature swing reactor (LTS)

and three reformers operating at 1145K, 1145K, and 1100K. The Figure 1-6 flowsheet employs a reverse-gas-shift (RGS) reactor, and a steam-methane reformer operating at 1050K. Both flowsheets have 1 mol of CH_4 and 2 mols of H_2O as inputs and 1 mol of CO_2 and 4 mols of H_2 as outlets. Table 1-2 includes the exit temperature information for all process units in the IDEAS flowsheets depicted below, while Table 1-3 details the inlets to the 1145K reactor and 1100K reactors utilized in the baseline and IDEAS flowsheets, and Table 1-4 includes the details of all the process streams depicted in Figure 1-6. The IDEAS flowsheet depicted in Figure 1-6 has two reactors present, a reformer operating at 1145K and a reverse-gas-shift reactor operating at 750K. As can be seen from Table 1-1, it consumes 48.72 kJ/s, 14.56 kJ/s, and 3.00 kJ/s of 1200K, 770K, and 420K hot utilities respectively.

Table 1-1: *Summary Table of Natural Gas Based Hydrogen Production Case Study*

Metric	Baseline	IDEAS 24:2:1	IDEAS 4:2:1	IDEAS 3:2:1	IDEAS 2.5:2:1	IDEAS 1.2:1:1
Total Hot Utility Cost (24:2:1) ($/s)	6.22	0.62				
Total Hot Utility Cost (4:2:1) ($/s)	1.10		0.62			
Total Hot Utility Cost (3:2:1) ($/s)	0.83			0.64		
Total Hot Utility Cost (2.5:2:1) ($/s)	0.71				0.69	
Total Hot Utility Cost (1.2:1:1) ($/s)	0.35					0.32
HU at 1200K, (kJ/s)	60.3	0	0	3.37	26.26	48.72
HU at 770K, (kJ/s)	6.06	68.97	68.97	66.6	46.73	14.56
HU at 420K, (kJ/s)	3.29	8.9	8.9	7.64	5.14	3.00

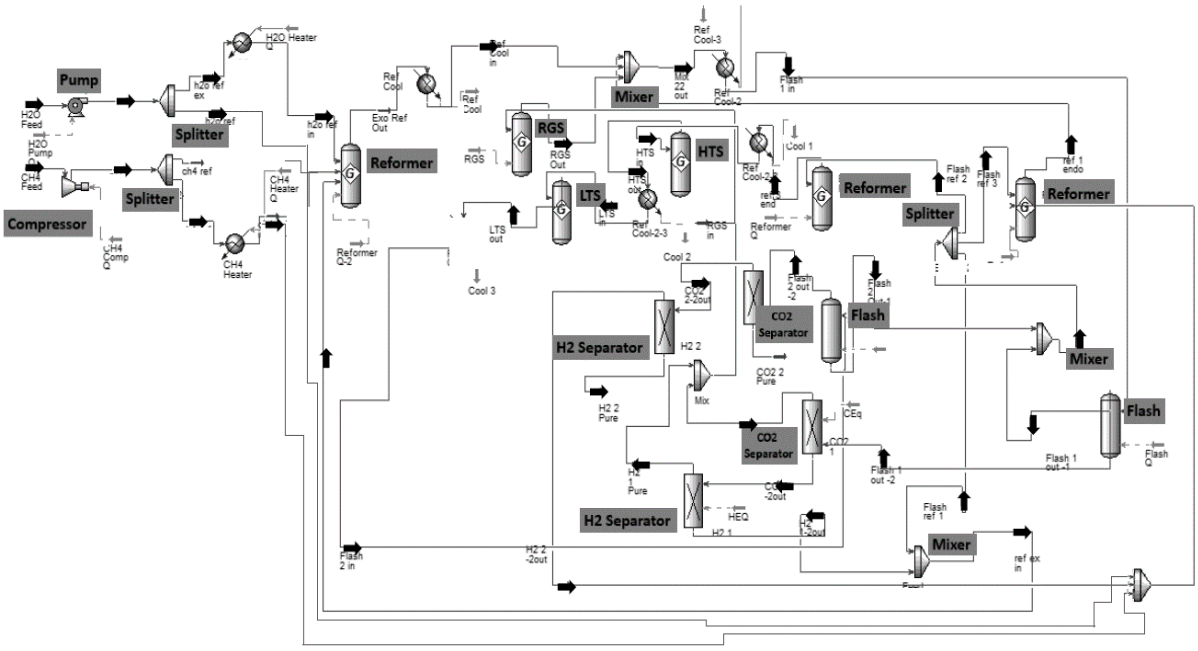

Figure 1-5: Simplified IDEAS flowsheet for natural gas based hydrogen production (2.5:2:1 Cost Coefficient Ratio)

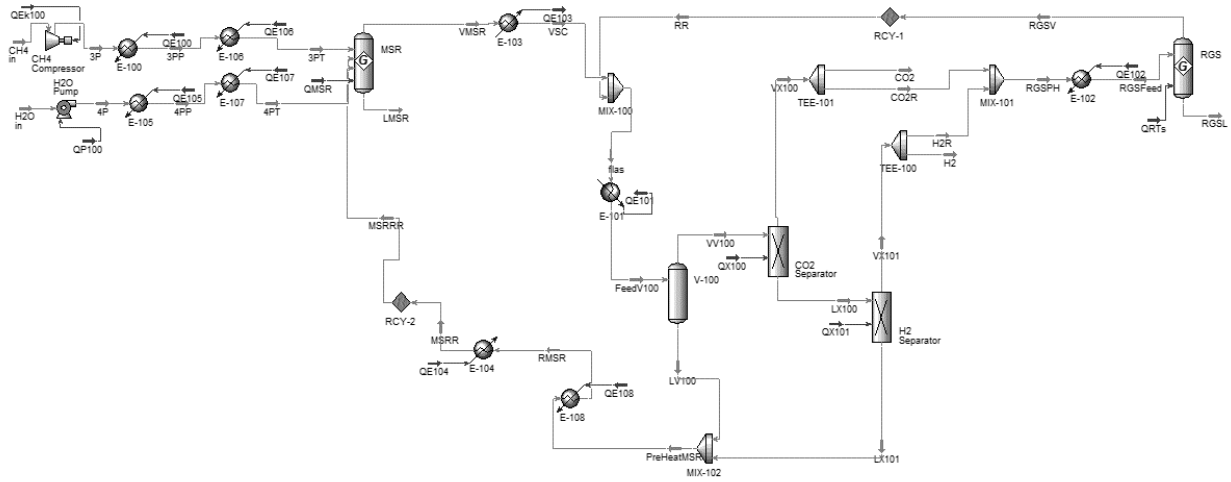

Figure 1-6: Simplified IDEAS flowsheet for natural gas based hydrogen production (1.2:1:1 Cost Coefficient Ratio, utility bounds)

The use of equilibrium reactors, modeled through the presented Gibbs free energy minimization approach, leaves each reactor's feed completely undefined in terms of species molar composition, imposing only a two dimensional restriction on the feed's atom molar ratios

(H/C, O/C). In turn this allows the employed low dimensional IDEAS representation to explore large portions of the species' state space, and to identify CO-rich reformer feeds that make the reformer exothermic (with over 95% methane conversion) and are constructed from the streams being made available from the reactor/separator universe (H_2O separators, H_2 separators, CO_2 separators, high/low temperature shift reactors, and reverse gas shift reactors) considered in the employed finite dimensional IDEAS representation. Figures 1-6, and 1-7 illustrate the dependence of the total utility cost, and the utility consumption respectively on the 1200K utility to 770K utility cost coefficient ratio, for the traditional and the IDEAS designs. At small coefficient ratios, IDEAS generates flowsheets that use a combination of 1200K and 770K utilities to reduce the total external hot utility cost.

Table 1-2: *Process unit outlet temperatures*

Temperature (K)							
Reformer (Figure 1-6)	Reformer 1 (Figure 1-5)	Reformer 2 (Figure 1-5)	Reformer 3 (Figure 1-5)	All Separators	HTS (Figure 1-5)	LTS (Figure 1-5)	RGS
1040	1145	1145	1100	313	650	475	750

At coefficient ratios of 4:2 and above, no 1200K utilities are employed in the IDEAS flowsheets. The impact on the utility cost is significant. At coefficient ratio 4:2, the IDEAS utility cost is \$0.62/s, while the baseline design is \$1.10/s. At coefficient ratio 24:2 the total utility cost discrepancy between the two designs is so pronounced (\$6.22/s to \$0.62/s) that it justifies the characterization of IDEAS as a systematic process intensification tool. Table 1-3 below specifies the molar inlets and outlets of the reactors present in the baseline case, and the IDEAS design for a hot utility coefficient ratio of 24:2.

Table 1-3: *Specifications on the inlet and exit of the reactors utilized in the baseline and IDEAS cases presented.*

Mol Inlet	Reformer Inlet (1140K) (IDEAS 24:2 utility ratio)	RGS Inlet (750K) (IDEAS 24:2 utility ratio)	HTS Inlet (650K) (Baseline)	LTS Inlet (475K) (Baseline)	Reformer Inlet (1100K) (Baseline)
CH4 (kmols/hr)	1.03	0	0.09	0.09	1.09
CO (kmols/hr)	14.64	0.14	0.82	0.33	0.07
CO2 (kmols/hr)	0.22	19.7	0.25	0.74	0
H2O (kmols/hr)	17.7	0	1	0.51	2.25
H2 (kmols/hr)	0.27	22.9	3.25	3.74	0
Mol Inlet	**Reformer Out (1145 K) (IDEAS)**	**RGS Out (750K) (IDEAS)**	**HTS Out (650K) (Baseline)**	**LTS Out (475K) (Baseline)**	**Reformer Out (1100K) (Baseline)**
CH4 (kmols/hr)	0.03	0	0.09	0.09	0.09
CO (kmols/hr)	8.69	6.08	0.33	0.08	0.82
CO2 (kmols/hr)	7.17	13.72	0.74	1	0.25
H2O (kmols/hr)	9.75	5.94	0.51	0.25	1
H2 (kmols/hr)	10.22	17	3.74	4	3.25

1.5 Discussion-Conclusions

The IDEAS conceptual framework has been put forward as a systematic tool to carry out process intensification studies for total process flowsheets. Efficient use of hot utility resources has been the driving force in this study. The introduction of a Gibbs free energy minimization model allows for the reactor inlets specification in terms of atoms, which has never been presented in process network synthesis. This has allowed the use of process models (e.g. equilibrium reactor models) that enable the systematic search of the large space of alternative process designs. The power of the IDEAS methodology as a process intensification tool is

demonstrated on a case study of natural gas reforming based hydrogen production. Minimization of the total external hot utility consumption is pursued for various cost coefficient ratios of the hot utilities considered. For large cost coefficient ratios of the hottest (1200K) available utility to the second hottest (770K) available utility, IDEAS is able to identify optimal flowsheets that do not require a heat source at 1200K, but rather only at 770K. This comes at the expense of increased separation costs, which however are not a focus of this study, since the flowsheet synthesis method is carried out without commitment to any particular separation technology. Nevertheless, it should be noted that pressure swing adsorption can be employed to separate high CO content hydrogen mixtures[60], thus avoiding cryogenic separation methods. The reduction (and often the elimination) of the 1200K utility heat load, while keeping true to the energy conservation laws of thermodynamics, necessitates that utility loads at lower temperatures be increased. Since no other material resources are allowed to enter the flowsheet, to ensure a fair comparison to the baseline case, this energy redirection is accomplished by increasing the flowrates through the flowsheet separators. Reducing (or even removing) the 1200K utility load, reduces (or removes) the need for burning natural gas or other fossil fuels to power the reformer, and introduces the possibility of using renewable energy sources, while the natural gas is only used as raw material, and not as an energy source. The HHV of natural gas is 52.2MJ/kg, and with a density of 22kg/Mcf, the HHV of natural gas is 1148.4MJ/Mcf [61]. According to the U.S. Energy Information Administration[62], the average price of natural gas for 2015 was $12.23/Mcf. Thus, the cost coefficient of natural gas used as an energy source (hot utility) is $1.064*10-5/kJ ($0.038/kWh). A potential renewable (and free on an energy input basis) energy resource that can be brought to bear as a hot utility for the above described natural gas reforming process is concentrated solar power (CSP)[63]. Solar concentration takes place typically in solar trough and

solar tower configurations. A variety of working fluids can be used, including molten salts and synthetic oils. According to the National Renewable Energy Laboratory[64], solar towers can currently deliver temperatures of 835K, and are expected to reach 920K by 2020. This is also confirmed by Poullikkas[63], who states that CSP tower plants using molten salts can deliver temperatures around 820K. Similarly, solar troughs can currently deliver 720K, and are expected to reach 773K by 2020[64].

Our future research will focus on the optimization of hydrogen producing flowsheets using alternative objective functions. Among them are total hot/cold/electric utility cost (to account for separator operating costs), and such capital cost measures as heat exchange network total heat transfer area, and reactor capital costs expressed in terms of reactor volume and catalyst weight. More realistic separator technologies will also be considered along with reaction kinetics. In addition, simultaneous reaction and separation will be explored in the future with the inclusion of process units such as membrane reactors within the IDEAS framework.

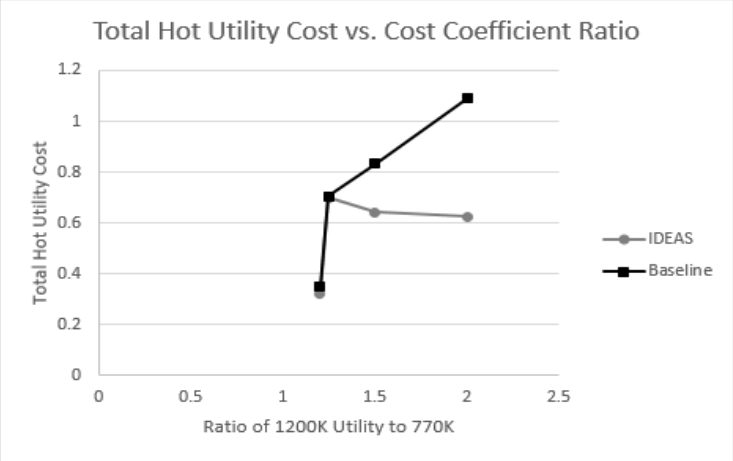

Figure 1-7: *Cost Coefficient Ratio versus the varying external hot and cold utilities*

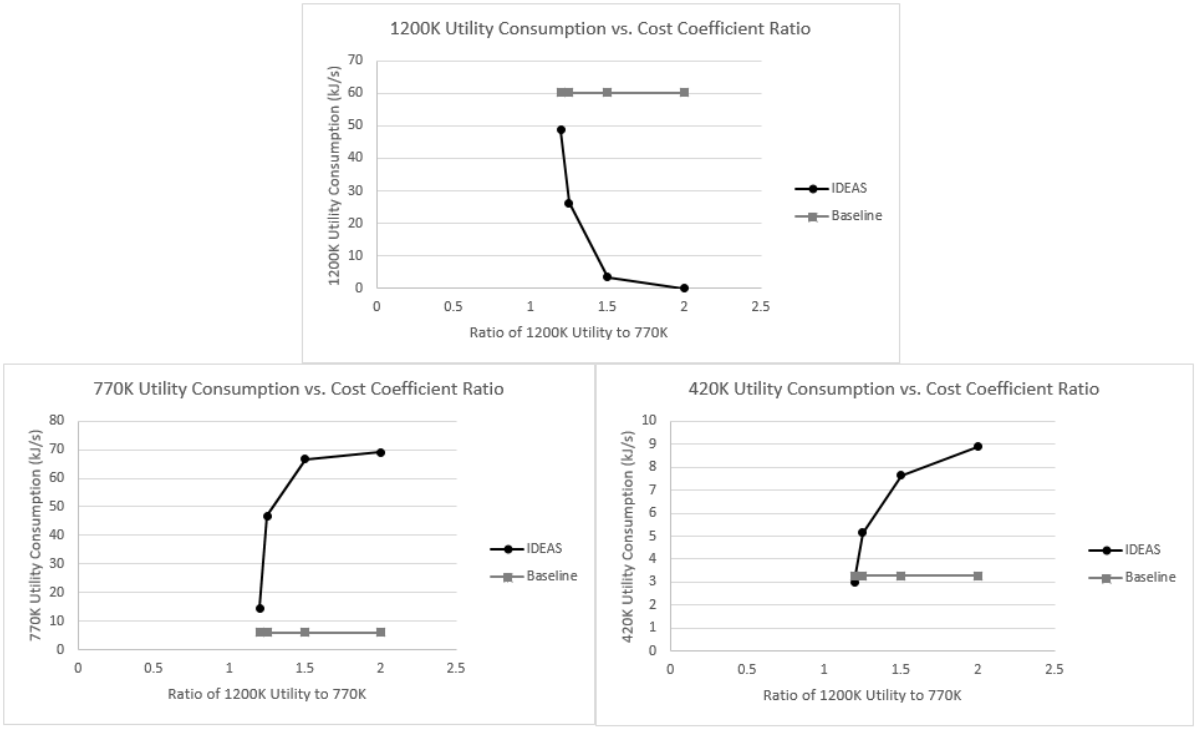

Figure 1-8: *Total Hot Utility Cost versus the ratio of 1200K:770K utility*

Table 1-4: *Specifications on the process flows of the simplified IDEAS generated flowsheet with 1.2:1:1 cost coefficient (Figure 1-5).*

Mole Fraction	VMSR	LMSR	FeedV100	VV100	LV100	LX100	VX100	VX101	LX101	PreHeatMSR	MSRR	MSRRR	CH4 in	H2O in	H2	H2R
CH4	0.0133	0.0133	0.0101	0.0129	0.0000	0.0195	0	0	0.0560	0.0253	0.0253	0.0253	1	0	0	0
CO	0.1686	0.1686	0.1540	0.1970	0.0000	0.2938	0.0059	0	0.8448	0.3821	0.3821	0.3828	0	0	0	0
CO2	0.1312	0.1312	0.2638	0.3374	0.0006	0.0051	0.9941	0	0.0146	0.0069	0.0069	0.0069	0	0	0	0
H2O	0.2703	0.2703	0.2303	0.0152	0.9994	0.0228	0	0	0.0657	0.5771	0.5771	0.5764	0	1	0	0
H2	0.4166	0.4166	0.3419	0.4375	0.0000	0.6588	0	1	0.0189	0.0086	0.0086	0.0086	0	0	1	1
	CO2	CO2R	RGSPH	RGSFeed	RGSV	RGSL	RR	3P	3PT	4P	4PT	VSC	3PP	4PP	RMSR	flas
CH4	0	0	0	0	0.0000	0.0000	0.0000	1	1	0	0	0.0133	1	0	0.0253	0.0101
CO	0.0059	0.0059	0.0046	0.0046	0.1080	0.1080	0.1078	0	0	0	0	0.1686	0	0	0.3821	0.1540
CO2	0.9941	0.9941	0.7865	0.7865	0.6832	0.6832	0.6835	0	0	0	0	0.1312	0	0	0.0069	0.2638
H2O	0	0	0	0	0.1033	0.1033	0.1033	0	0	1	1	0.2703	0	1	0.5771	0.2303
H2	0	0	0.2088	0.2088	0.1055	0.1055	0.1054	0	0	0	0	0.4166	0	0	0.0086	0.3419
	VMSR	LMSR	FeedV100	VV100	LV100	LX100	VX100	VX101	LX101	PreHeatMSR	MSRR	MSRRR	CH4 in	H2O in	H2	H2R
Vapour Fraction	1	0	0.781467	1	0	0.991973	1	1	0.948745	0.429405505	1	1	1	0	1	1
Temperature (K)	1050	1050	313	313	313	313	313	313	313	313	1040	1040	298	298	313	313
Pressure (bar)	5	5	5	5	5	5	5	5	5	5	5	5	1	1	5	5
Molar Flow (kgmole/h)	10.55	0	13.88	10.85	3.03	7.20	3.64	4.70	2.50	5.54	5.54	5.55	1	2	4	0.70
Mass Flow (kg/s)	0.0481	0	0.0807	0.0655	0.0152	0.0210	0.0445	0.0026	0.0184	0.0336	0.0336	0.0337	0.0045	0.0100	0.0022	0.0004
Heat Flow (kJ/s)	-324.3	0	-718.8	-478.6	-240.2	-82.83	-396.5	0.5511	-84.25	-324.47	-246.4	-246.7	-20.81	-159.0	0.4693	0.0819
	CO2	CO2R	RGSPH	RGSFeed	RGSV	RGSL	RR	3P	3PT	4P	4PT	VSC	3PP	4PP	RMSR	flas
Vapour Fraction	1	1	1	1	1	0	1	1	1	0	1	1	1	1	1	1
Temperature (K)	313	313	312.3	750	750	750	750	459.2	1040	298	1040	750	700	700	650	750
Pressure (bar)	5	5	5	5	5	5	5	5	5	5	5	5	5	5	5	5
Molar Flow (kgmole/h)	1	2.64	3.34	3.34	3.34	0	3.33	1	1	2	2	10.55	1	2	5.54	13.88
Mass Flow (kg/s)	0.0122	0.0323	0.0326	0.0326	0.0326	0	0.0325	0.0045	0.0045	0.0100	0.0100	0.0481	0.0045	0.0100	0.0336	0.0807
Heat Flow (kJ/s)	-108.8	-287.7	-287.62	-270.73	-267.1	0	-266.3	-19.04	-9.34	-159.01	-119	-356.5	-15.62	-126.5	-268.8	-622.8

1.6 References

1. Aris R. Introduction to the analysis of chemical reactors. Prentice-Hall; 1965.
2. Aris R., Varma A., The mathematical understanding of chemical engineering systems. Selected papers of Neal R. Amundson, Pergamon Press, Oxford, England 1980
3. Rudd D., Powers G., Siirola J., Process Synthesis. Prentice-Hall; 1973.
4. Rudd, D. F. Accessible designs in Solvay cluster synthesis. *Chemical Engineering Science* 1976; 31(8):701–703.
5. Rotstein E, Resasco D, Stephanopoulos G. Studies on the synthesis of chemical reaction paths—I: Reaction characteristics in the (ΔG, T) space and a primitive synthesis procedure. *Chemical Engineering Science*. 1982; 37(9):1337–1352.
6. Lee K., Masso A., Rudd D., Branch and Bound Synthesis of Integrated Process Designs. *Industrial Engineering Chemistry Fundamentals*, 1970; 9, 48-58
7. Georgiadis MC, Papageorgiou LG. Optimal energy and cleaning management in heat exchanger networks under fouling. *Chemical Engineering Research and Design*. 2000;78(2):168-79.
8. Holiastos K., Manousiouthakis V. Automatic Synthesis of Thermodynamically Feasible Reaction Clusters. *AIChE Journal* 1998; 44, 1, 164–173.
9. Hohmann E. C. Optimum networks for heat exchange. USC-PhD Thesis, Lockhart PhD Advisor, 1971.
10. Umeda T. A., Harada T., Shiroko K. A Thermodynamic Approach to the Synthesis of Heat-Integration Systems in Chemical Processes. *Computers and Chemical Engineering*. 1979; 3:273-282.
11. Linnhoff B, Dunford H, Smith R. Heat integration of distillation columns into overall processes. *Chemical Engineering Science*. 1983; 38(8):1175-88.

12. Holiastos K, Manousiouthakis V. Minimum hot/cold/electric utility cost for heat exchange networks. *Computers & Chemical Engineering*. 2002; 26(1):3-16.
13. El-Halwagi M. M., Manousiouthakis V. Synthesis of mass exchange networks. *AIChE Journal*. 1989; 35(8):1233-44.
14. Sargent RW. K., Gaminibandara,". Optimum Design of Plate Distillation Column," *Proceedings of the Conference on Optimization in Action held at University of Bristol*, LCW Dixon, ed., Academic Press, 1976; 267-314
15. Bagajewicz M.J., Manousiouthakis V. Mass/heat-exchange network representation of distillation networks. *AIChE Journal.* 1992;38(11):1769-800.
16. Agrawal R., Synthesis of Distillation Column Configurations for Multicomponent Separations. *Industrial Engineering Chemistry Research*, 1996; 35, 1059.
17. Horn F. Attainable and non-attainable regions in chemical reactor technique. *Proceedings of the Third European Symposium on Chemical Reaction Engineering*. London: Pergamon Press 1964: 123–138.
18. Glasser D., Hildebrandt D., Crowe C. A Geometric Approach to Steady Flow Reactors: The Attainable Region and Optimization in Concentration Space. *Ind. Eng. Chem. Res.* 1987; 26, 9, 1803–1810.
19. Feinberg M. Optimal Reactor Design from a Geometric Viewpoint. Part III: Critical CFSTRs. *Chemical Engineering Science* 2000; 55, 3553–3565.
20. Burri J., Wilson S., Manousiouthakis V. Infinite Dimensional State-Space Approach to Reactor Network Synthesis: Application to Attainable Region Construction. *Comput. Chem. Eng.* 2002; 26, 849–862.

21. Manousiouthakis V., Justanieah A., Taylor L. The Shrink-Wrap Algorithm for the Construction of the Attainable Region: Application of the IDEAS Framework. *Comput. Chem. Eng.* 2004; 28, 9, 1563–1575.
22. Cremaschi S. "A perspective on process synthesis: Challenges and prospects." *Computers & Chemical Engineering*. 2015;81:130-7.
23. Grossmann IE, Westerberg AW. "Research challenges in process systems engineering." *AIChE Journal*. 2000;46(9):1700-3.
24. Sargent R., Westerberg A.,"SPEED-UP" in chemical engineering design, *The Chemical Engineer*, 1964, 179, 190-197
25. Grossmann I.E., Sargent R.W.H. Optimum Design of Heat Exchanger Networks. *Computers and Chemical Engineering* 1978; 2, 1, 1-7
26. Sargent R., Forecasts and Trends in Systems Engineering, *The Chemical Engineer*, June 1972, 226-230
27. Duran M.A., Grossmann I.E. Simultaneous optimization and heat integration of chemical processes. *AIChE Journal*. 1986;32(1):123-38.
28. Lang Y.D., Biegler L.T., Grossmann I.E. Simultaneous optimization and heat integration with process simulators. *Computers & chemical engineering*. 1988;12(4):311-27.
29. Yee T.F., Grossmann I.E., Kravanja Z. Simultaneous optimization models for heat integration—I. Area and energy targeting and modeling of multi-stream exchangers. *Computers & chemical engineering*. 1990;14(10):1151-64.
30. Holiastos K, Manousiouthakis V.I. Infinite-dimensional state-space (IDEAS) approach to globally optimal design of distillation networks featuring heat and power integration. *Industrial & engineering chemistry research.* 2004;43(24):7826-42.

31. Martin LL, Manousiouthakis VI. Globally optimal power cycle synthesis via the Infinite-DimEnsionAl State-space (IDEAS) approach featuring minimum area with fixed utility. *Chemical engineering science*. 2003;58(18):4291-305.
32. Ramshaw, C. The incentive for process intensification. *BHR Group Conference Series Publication*, vol. 18, pp. 1-4. Mechanical Engineering Publications Limited, 1995.
33. Stankiewicz AI, Moulijn JA. Process intensification: transforming chemical engineering. *Chemical Engineering Progress*. 2000;96(1):22-34.
34. Stankiewicz A. Reactive separations for process intensification: an industrial perspective. *Chemical Engineering and Processing: Process Intensification*. 2003;42(3):137-44.
35. Siirola JJ. An industrial perspective on process synthesis. *AIChE Symposium Series* 1995 (Vol. 91, No. 304, pp. 222-234). New York, NY: American Institute of Chemical Engineers, 1971-c2002.
36. Agreda, Victor H., and Lee R. Partin. Acetic acid as reactant and extractive agent. U.S. Patent 4,435,595, issued March 6, 1984.
37. Petlyuk, Felix B. Distillation theory and its application to optimal design of separation units. Cambridge University Press, 2004.
38. Doherty, Michael F., and Michael F. Malone. Conceptual design of distillation systems. McGraw-Hill Science/Engineering/Math, 2001.
39. Stankiewicz A, Moulijn JA. Re-engineering the chemical processing plant: process intensification. CRC Press; 2003.
40. Stankiewicz A, Moulijn JA. Re-engineering the chemical processing plant: process intensification. CRC Press; 2003. p. 1-28.
41. Moulijn JA, Stankiewicz A, Grievink J, Górak A. Process intensification and process systems

engineering: a friendly symbiosis. *Computers & Chemical Engineering*. 2008;32(1):3-11.

42. Wilson S, Manousiouthakis VI. IDEAS approach to process network synthesis: Application to multicomponent MEN. *AIChE journal*. 2000;46(12):2408-16.
43. Drake JE, Manousiouthakis VI. IDEAS approach to process network synthesis: minimum utility cost for complex distillation networks. *Chemical Engineering Science.* 2002;57(15):3095-106.
44. Zhou W, Manousiouthakis VI. Non-ideal reactor network synthesis through IDEAS: Attainable region construction. *Chemical Engineering Science*. 2006;61(21):6936-45.
45. Zhou W, Manousiouthakis VI. Variable density fluid reactor network synthesis—construction of the attainable region through the IDEAS approach. *Chemical Engineering Journal.* 2007;129(1):91-103.
46. Burri JF, Manousiouthakis VI. Global optimization of reactive distillation networks using IDEAS. *Computers & chemical engineering*. 2004;28(12):2509-21.
47. Justanieah AM, Manousiouthakis VI. IDEAS approach to the synthesis of globally optimal separation networks: application to chromium recovery from wastewater. *Advances in Environmental Research.* 2003;7(2):549-62.
48. Burri JF, Wilson SD, Manousiouthakis VI. Infinite DimEnsionAl State-space approach to reactor network synthesis: application to attainable region construction. *Computers & chemical engineering*. 2002;26(6):849-62.
49. Manousiouthakis VI, Justanieah AM, Taylor LA. The Shrink–Wrap algorithm for the construction of the attainable region: an application of the IDEAS framework. *Computers & chemical engineering.* 2004;28(9):1563-75.

50. Manousiouthakis VI. On dimensionality of attainable region construction for isothermal reactor networks. *Computers & Chemical Engineering*. 2008;32(3):439-50.
51. Posada A, Manousiouthakis VI. Multi-feed attainable region construction using the Shrink–Wrap algorithm. *Chemical Engineering Science*. 2008;63(23):5571-92.
52. Davis BJ, Taylor LA, Manousiouthakis VI. Identification of the attainable region for batch reactor networks. *Industrial & Engineering Chemistry Research*. 2008;47(10):3388-400.
53. Ghougassian PG, Manousiouthakis VI. Attainable composition, energy consumption, and entropy generation properties for isothermal/isobaric reactor networks. *Industrial & Engineering Chemistry Research*. 2013;52(9):3225-38.
54. Ghougassian PG, Manousiouthakis VI. Minimum entropy generation for isothermal endothermic/exothermic reactor networks. *AIChE Journal*. 2015;61(1):103-17.
55. Hou K, Hughes R. The kinetics of methane steam reforming over a Ni/α-Al 2 O catalyst. *Chemical Engineering Journal*. 2001;82(1):311-28.
56. National Research Council, National Academy of Engineering Source: "The Hydrogen Economy: Opportunities, Costs, Barriers, and R&D Needs", *National Academies Press*, p. 39, 2004
57. Posada A, Manousiouthakis V. Heat and power integration of methane reforming based hydrogen production. *Industrial & engineering chemistry research*. 2005;44(24):9113-9.
58. Baldea M. From process integration to process intensification. *Computers & Chemical Engineering*. 2015;81:104-14.
59. Baldea M. Multum in parvo: a process intensification retrospective and outlook. *Proceedings of 8th International Conference on Foundations of Computer-Aided Process Design* 2014;34:15

60. Yang J, Lee CH, Chang JW. Separation of hydrogen mixtures by a two-bed pressure swing adsorption process using zeolite 5A. *Industrial & engineering chemistry research*. 1997;36(7):2789-98.

61. Wright, L. L. Biomass Energy Data Book: Edition 1. Oak Ridge, TN: Oak Ridge National Laboratory, 2006. Print.

62. "U.S. Price of Natural Gas Delivered to Residential Consumers (Dollars per Thousand Cubic Feet)." U.S. Price of Natural Gas Delivered to Residential Consumers (Dollars per Thousand Cubic Feet). U.S. Energy Information Administration, n.d. Web. 25 Apr. 2016.7.

63. Poullikkas A. Economic analysis of power generation from parabolic trough solar thermal plants for the Mediterranean region—A case study for the island of Cyprus. *Renewable and Sustainable Energy Reviews.* 2009; 13(9):2474-2484.

64. Turchi C, Mehos M, Ho CK, Kolb GJ. Current and future costs for parabolic trough and power tower systems in the US market. *SolarPACES* 2010.

Chapter 2: On the Intensification of Natural Gas Based Hydrogen Production Utilizing Hybrid Energy Resources

2.1 Abstract

In this work, parametric studies are carried out for natural gas based hydrogen production systems utilizing hybrid energy sources, such as natural gas and concentrated solar power (CSP). The main technologies utilized in the considered networks consist of steam methane reforming (SMR), reverse water-gas shift (RGS), high-temperature shift (HTS), and low-temperature shift (LTS) reactors; ideal hydrogen, and carbon dioxide separators; water flash separators; pressure changing devices; and a heat exchange network (HEN). A broad search of the design space is carried out, within the Infinite-DimEnsionAl State-space (IDEAS) conceptual framework, which allows for the simultaneous synthesis of the hydrogen production process and its associated HEN using linear programming (LP). The identified designs minimize the total cost of three hot utilities and one cold utility, subject to bounding constraints on the work of separation, and the HEN area. The level of exothermicity of the reforming operations, and the extent of CSP use are shown to depend on the employed utility cost ratios and on the aforementioned work and area bounds.

2.2 Introduction

In the recent international agreement in Paris (Schellnhuber, Rahmstorf, & Winkelmann, 2016), 195 nations committed to stabilize their greenhouse gas (GHG) emissions. A means of contributing to this stabilization goal is the partial (or even complete) replacement of fossil fuels with renewable energy sources (such as concentrated solar power). Hydrogen is an energy carrier that can facilitate such a replacement, since it can be generated by a variety of production methods, many of which utilize renewable energy sources. Currently, there exist three main

hydrogen production methods: thermochemical cycles, electrolysis, and steam methane reforming.

Thermochemical cycles aim to generate hydrogen from water at temperatures lower than the water's thermal decomposition temperature of about 3000 K (Lédé, et al., 1982), which is difficult to attain in an industrial environment. Each cycle accomplishes this task by employing multiple reactions, whose stoichiometric sum is equal to the water decomposition reaction, and whose operating temperatures are below 3000 K. These reactions involve intermediate species different than hydrogen, oxygen, or water, which are recycled within the cycle (Hydrogen Production: Thermochemical Water Splitting, 2017). The synthesis of thermochemical cycles has been the subject of intense research (Holiastos & Manousiouthakis, Automatic synthesis of thermodynamically feasible reaction clusters, 1998; May & Rudd, 1976; Rotstein, Resasco, & Stephanopoulos, 1982), in an effort to lower the highest operating temperature of a cycle's reactions, and thus enable the use of concentrated solar power as an energy source for hydrogen production. Nevertheless, the combination of high temperatures and chemically aggressive intermediate species continues to limit the widespread use of thermochemical cycles.

Another method of hydrogen production is electrolysis, which involves the decomposition of water into oxygen and hydrogen through the use of electricity. This electrochemical process can be divided into two reaction steps; the anode reaction (oxidation), and the cathode reaction (reduction) shown below (Von Hofmann, 1866):

Anode reaction (Oxidation):

$2\ H_2O_{(l)} \rightarrow O_{2(g)} + 4\ H^+_{(aq)} + 4e^-$ (Standard potential: -1.23 V at 25 ^oC)

Cathode reaction (Reduction):

$4\ H^{+}_{(aq)} + 4e^{-} \rightarrow 2\ H_{2(g)}$ (Standard potential: 0.00 V at 25 ^{o}C)

Overall reaction:

$2\ H_2O_{(l)} \rightarrow 2\ H_{2(g)} + O_{2(g)}$ (Standard potential: -1.23V at 25^{o}C)

There are three major electrolyzer types: Alkaline Water; Proton Exchange Membrane; and Solid Oxide; the former two of which are commercially available. Nevertheless, their large-scale use is limited by their high operating and investment costs, associated with their high levels of electricity and expensive material (e.g. platinum electrodes) use respectively. Even when ameliorated through design changes (e.g. high temperature operation, platinum honeycombs (Von Hofmann, 1866), significant operating/capital cost reductions are necessary before large scale production can be considered (Ursua, Gandia, & Sanchis, 2012).

While electrolysis and thermochemical cycles can be used to produce hydrogen, the principal industrial hydrogen production process used today is steam methane reforming (SMR) (Twigg, 1989). In fact, around 95% of all hydrogen produced in the United States comes from SMR (Udengaard, 2017). Within the SMR process, three reactions are commonly considered to occur in the presence of a metal nickel based catalyst (Leiby, 1984). They are (Twigg, 1989):

$$CH_4 + H_2O = CO + 3H_2 \quad \text{(r1)} \quad \Delta H_1 = 206.2\,kJ\ /\ mol \ \text{(endothermic)} \tag{1}$$

$$CO + H_2O = CO_2 + H_2 \quad \text{(r2)} \quad \Delta H_2 = -41.2\,kJ\ /\ mol \ \text{(exothermic)} \tag{2}$$

$$CH_4 + 2H_2O = CO_2 + 4H_2 \quad \text{(r3)} \quad \Delta H_3 = 165.0\,kJ\ /\ mol \ \text{(endothermic)} \tag{3}$$

The first step, r1, and third step, r3, are the highly endothermic reactions of methane and steam to hydrogen and carbon monoxide, and hydrogen and carbon dioxide respectively; The second step, r2, on the other hand is the exothermic water-gas shift reaction, which transforms carbon monoxide and water to carbon dioxide and hydrogen. Under typical operating conditions (700 ^{o}C

- 1000 ^{o}C, 3 bar - 25 bar, 3:1 H_2O: CH_4 feed molar ratio) (Hydrogen Production: Natural Gas Reforming, 2017), the steam methane reformer's outlet contains significant amounts of carbon monoxide. Thus, the reformer outlet is further processed in a reactor sequence within which copper oxide catalyst is used to transform carbon monoxide to carbon dioxide through the water-gas shift reaction (r2) (Twigg, 1989). The reactor sequence consists of a high temperature shift (HTS) reactor, operating at 310 ^{o}C to 450 ^{o}C, and 1 bar to 83.8 bar (Newsome, 1980), followed by a low temperature shift (LTS) reactor, operating at 200^{o}C to 250 ^{o}C, and 1 bar to 83.8 bar.

At the aforementioned operating conditions, the overall SMR process is endothermic, requiring high temperature external energy input (Udengaard, 2017). This is typically provided by carbon containing fuels, such as natural gas, diesel, biomass, coal and others. The SMR's energetic efficiency significantly contributes to a hydrogen production plant's productivity, a common metric for which is the energy consumed per unit of hydrogen produced. For this reason, numerous research efforts have been dedicated to improving the efficiency of the SMR process (Olivieri & Veglio, 2008; Zamaniyan, Ebrahimi, & Mohammadzadeh, 2008; Latham, McAuley, Peppley, & Raybold, 2011; McGreavy & Newmann, 1968), including smart manufacturing approaches aiming at efficient operation (Kumar, Baldea, Edgar, & Ezekoye, 2015). Following the recent Paris agreement, the aura of a debilitating carbon tax forbidding the use of methane as a fuel (but not as raw material), is visible. If such a circumstance came to pass, traditional steam methane reforming based hydrogen production would become infeasible. For this reason, reducing or removing the need for burning methane or other fossil fuels to power the reformer will allow for the use of natural gas only as raw material for hydrogen production, while renewable energy sources are used to satisfy the energetic needs of the hydrogen production process. As mentioned in (Pichardo & Manousiouthakis, 2017), one of these potential

energy sources is concentrated solar power (Poullikkas, 2009). Concentrated solar power (CSP) plants are typically designed in two main configurations: solar troughs and solar towers. These processes utilize a variety of working fluids, such as synthetic oils and molten salts, which can currently reach operating temperatures of 720 K, and 820 K respectively (Turchi, Mehos, Ho, & Kolb, 2010). The continued development of these technologies is projected to yield by 2020 operating temperatures of 773 K, and 920 K respectively (Turchi, Mehos, Ho, & Kolb, 2010).

The above suggest that a way to reduce the use of methane as fuel in natural gas based hydrogen production is to reduce the use of high temperature (e.g. 1200 K) hot utility associated with carbon containing fuel combustion, in favor of using medium and low temperature hot utilities (e.g. 770 K, and 420 K) associated with concentrated solar power, and possibly other renewable energy sources. In our earlier work (Pichardo & Manousiouthakis, 2017; United States Patent No. US 20,170,001,862, 2017), natural gas based hydrogen production flowsheets were identified that were intensified in the aforementioned reduced hot multi-utility consumption sense, leading to the use of the term "energetically enhanced reforming". These energetically enhanced flowsheets established the feasibility of reducing or even removing entirely the utilization of methane as fuel for the aforementioned reforming reactions, allowing for the possible use of renewable energy resources. This earlier study however did not quantify the impact of this intensification on other flowsheet metrics. Thus, this work quantifies the impact on hot/cold multi-utility cost, of upper bounds on the flowsheet's work of separation and on the associated heat exchange network's total heat transfer area. This is accomplished within the Infinite DimEnsionAl State-space (IDEAS) framework, which allows the formulation of the optimal process network synthesis problem as an infinite linear program (ILP), whose approximation by even low dimensional linear programs can carry out a broad, coarse search of

the state-space. By decomposing a process network into an operator network (OP), where unit operations (reactors, separators, pressure changing devices, and heat exchangers) ensue, and a distribution network (DN), where flow operations (splitting, mixing, recycling, and bypass) ensue, IDEAS enables the aforementioned state-space searches to be carried out without any a priori commitment to a network structure, thus identifying innovative designs, and opportunities enhancing the level of performance attainable by any particular technology or combination of technologies.

The rest of the article is structured as follows: The new components of the proposed IDEAS formulation are first presented, quantifying the overall network's heat exchanger area, and work of separation characteristics. Next, the IDEAS optimization problem is formulated taking into account these new formulation components. Finally, the obtained results are discussed, and conclusions are drawn.

2.3 IDEAS Applicability and Mathematical Formulation

The IDEAS conceptual framework has been identified as a systematic process synthesis and intensification tool with applications to reactive separator networks (da Cruz & Manousiouthakis, 2016), and process networks containing reactors, separators, pressure changing devices, and a heat exchange network (Pichardo & Manousiouthakis, 2017). IDEAS has also been employed for the globally optimal synthesis of mass-exchange networks (Wilson & Manousiouthakis, 2000), ideal distillation networks (Drake & Manousiouthakis, 2002), heat/power integrated distillation networks (Holiastos & Manousiouthakis, Infinite-dimensional state-space (IDEAS) approach to globally optimal design of distillation networks featuring heat and power integration, 2004), reactive distillation networks (Burri & Manousiouthakis, Global optimization of reactive distillation networks using IDEAS, 2004), separator networks

(Justanieah & Manousiouthakis, 2003), power cycles (Martin & Manousiouthakis, 2003), azeotropic distillation networks (Ghougassian & Manousiouthakis, Globally Optimal Networks for Multipressure Distillation of Homogeneous Azeotropic Mixtures, 2012), and reactor networks (Ghougassian & Manousiouthakis, Attainable composition, energy consumption, and entropy generation properties for isothermal/isobaric reactor networks, 2013; Ghougassian & Manousiouthakis, Minimum entropy generation for isothermal endothermic/exothermic reactor networks, 2015), and for the quantification of the attainable region for a reactor network (Burri, Wilson, & Manousiouthakis, Infinite DimEnsionAl State-space approach to reactor network synthesis: application to attainable region construction, 2002; Manousiouthakis V. , 2008; Davis, Taylor, & Manousiouthakis, 2008; Zhou & Manousiouthakis, Non-ideal reactor network synthesis through IDEAS: Attainable region construction, 2006; Zhou & Manousiouthakis, Variable density fluid reactor network synthesis—construction of the attainable region through the IDEAS approach, 2007), batch reactor network (Davis, Taylor, & Manousiouthakis, 2008), and general process network (Manousiouthakis, Justanieah, & Taylor, The Shrink–Wrap algorithm for the construction of the attainable region: an application of the IDEAS framework, 2004).

Applicability of IDEAS requires that the following three properties be satisfied by the information maps of all processes considered for participation in the network to be synthesized.

Consider the information map

$$\Psi : D_1 \times D_2 \subset \mathbb{R}^{n_1} \times \mathbb{R}^{n_2} \to \mathbb{R}^p,\ \Psi : u = (u_1, u_2) \to \Psi(u) = \Psi(u_1, u_2)$$

that helps define the set $D \triangleq \left\{ u \in D_1 \times D_2 \subset \mathbb{R}^{n_1} \times \mathbb{R}^{n_2} \ : \Psi(u_1, u_2) = 0 \right\}$.

Let the considered process model have information map $\Phi : D \subset \mathbb{R}^{n_1} \times \mathbb{R}^{n_2} \to \mathbb{R}^{m_1} \times \mathbb{R}^{m_2}$,

$$\Phi : u = (u_1, u_2) \to y = \Phi(u) = (y_1, y_2) = \left(\Phi_1(u_1, u_2), \Phi_2(u_1, u_2)\right).$$

Having defined the maps Φ, Ψ, we can now state the properties that must hold to ensure IDEAS applicability.

Property 1: $\exists\ \Psi_1 : \mathbb{R}^{n_1} \to \mathbb{R}^{p \times n_2}$, $\Psi_1 : u_1 \to \Psi_1(u_1)$ such that

$$\Psi(u_1, u_2) = \Psi_1(u_1) u_2 \quad \forall u = (u_1, u_2) \in D_1 \times D_2 \subset \mathbb{R}^{n_1} \times \mathbb{R}^{n_2}$$

Property 2: $\exists\ \Phi_3 : \mathbb{R}^{n_1} \to \mathbb{R}^{m_1}$, $\Phi_3 : u_1 \to \Phi_3(u_1)$ such that

$$y_1 = \Phi_1(u_1, u_2) = \Phi_3(u_1) \quad \forall u = (u_1, u_2) \in D \subset \mathbb{R}^{n_1} \times \mathbb{R}^{n_2}$$

Property 3: $\exists\ \Phi_4 : \mathbb{R}^{n_1} \to \mathbb{R}^{m_2 \times n_2}$, $\Phi_4 : u_1 \to \Phi_4(u_1)$ such that

$$y_2 = \Phi_2(u_1, u_2) = \Phi_4(u_1) u_2 \quad \forall u = (u_1, u_2) \in D \subset \mathbb{R}^{n_1} \times \mathbb{R}^{n_2}$$

In this work, the IDEAS framework is employed for process networks consisting of a variety of process units, such as reactors, separators, pressure changing devices, and heat exchangers. Specifically, equilibrium reactors are implemented through a Gibbs free energy minimization formulation. The use of equilibrium reactors allows for a broad search of the design space, by carrying out that search in the space of atomic fraction ratios instead of the space of species mole fractions, thus reducing the dimension of the state-space. In particular, for the steam-methane reforming synthesis problem considered here, the five-species mole fraction space is first reduced to a three-species atomic fraction space, which is then further reduced to two-dimensions by scaling the problem with respect to one of the atomic fractions. In addition to the equilibrium reactors, the separation tasks typically utilized in natural gas based hydrogen

production are modeled by separators, whose energy input is the ideal work of separation, calculated by assuming that the separator and its associated Carnot engine are reversible, leading to no entropy generation. The considered pressure changing devices include compressors, pumps, turbines, and valves, which are modeled as adiabatic processes with known isentropic efficiencies (for valves the isentropic efficiency is considered to be zero, making them isenthalpic). Finally, heat exchangers are the last processes present in the process network. They are divided into three categories: stream-stream heat exchangers, stream-point load heat exchangers, and point load-point load heat exchangers, which are detailed below. Both renewable and non-renewable energy sources are considered, through the use of hot and cold utilities at multiple temperature levels that form part of the heat exchange network (HEN). The HEN is utilized to carry out heat integration of the process flowsheet, and its formulation is presented next along with the finalized models of each heat exchanger type included in the HEN. The full mathematical models for each of the other units found in the process network, as applied in the IDEAS framework, can be found in our previous work (Pichardo & Manousiouthakis, 2017).

2.3.1 Heat Exchange Network

The HEN network presented in this work consists of three distinct types of heat exchangers, which are denoted as hot stream – cold stream heat exchangers, hot (cold) stream – cold (hot) point load heat exchangers, and hot point load – cold point load heat exchangers. Point loads are

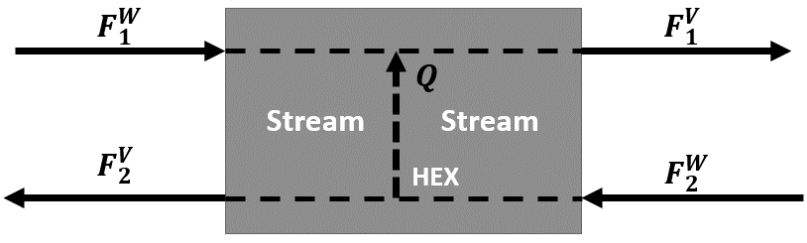

Figure 2-1: *Depiction of a hot stream – cold stream heat exchanger*

considered to be external utilities and unit heat loads associated with isothermal reactors and separators. As stated in (Pichardo & Manousiouthakis, 2017), streams are created through a comparison of states to verify that the pressure and composition of both states are identical, while their enthalpic content varies. Following the creation of all potential streams, feasibility of all hot stream – cold stream heat exchanger, hot/cold stream – cold/hot point load heat exchangers, and hot/cold point load – cold/hot point load heat exchangers is determined, and all feasible heat exchangers are then generated.

The IDEAS mathematical formulation for all process units present in the process network can be found in (Pichardo & Manousiouthakis, 2017) with the exception of the heat exchanger units. In order to account for heat exchange area as a heat exchanger capital cost surrogate, the IDEAS information map is defined below for all three heat exchanger unit types. Ensuring that these process maps satisfy the three IDEAS properties defined in (Pichardo & Manousiouthakis, 2017) will establish the applicability of IDEAS to the problem.

First, the IDEAS information map is presented for the hot stream – cold stream heat exchanger depicted in Figure 2-1, where stream 1 is hot, and stream 2 is cold.

$$u = \left[{u_1}^T \;\middle|\; {u_2}^T \right]^T = \left[h_1^V \quad h_2^V \quad h_1^W \quad h_2^W \quad P_1^V \quad P_2^V \quad \left\{ x_{1,k}^V \right\}_{k=1}^n \quad \left\{ x_{2,k}^V \right\}_{k=1}^n \;\middle|\; F_1^W \quad F_2^W \right]^T$$

$$\left\{ \begin{array}{l} y = \left[{y_1}^T \;\middle|\; {y_2}^T \right]^T = \\ \left[h_1^V \; h_2^V \; h_1^W \; h_2^W \; P_1^V \; P_2^V \; \left\{ x_{1,k}^V \right\}_{k=1}^n \left\{ x_{2,k}^V \right\}_{k=1}^n \; P_1^W \; P_2^W \; \left\{ x_{1,k}^W \right\}_{k=1}^n \left\{ x_{2,k}^W \right\}_{k=1}^n \; T_1^W \; T_2^W \; T_1^V \; T_2^V \; \Delta T^{lm} \mid F_1^W \; F_2^W \; F_1^V \; F_2^V \; \dot{Q} \; A \right]^T \end{array} \right\}$$

$$\text{where } u_1 \in D_1 = \left\{ \begin{array}{l} u_1 = \left[h_1^V \quad h_2^V \quad h_1^W \quad h_2^W \quad P_1^V \quad P_2^V \quad \left\{ x_{1,k}^V \right\}_{k=1}^n \quad \left\{ x_{2,k}^V \right\}_{k=1}^n \right]^T \in \mathbb{R}^{2n+6} : \\ P_1^V \geq 0, \;\; P_2^V \geq 0, \; \sum_{k=1}^n x_{1,k}^V = 1, \; \sum_{k=1}^n x_{2,k}^V = 1, \; x_{1,k}^V \geq 0 \wedge x_{2,k}^V \geq 0 \;\; \forall k = 1, n \end{array} \right\}$$

$$u_2 \in D_2 \triangleq \left\{ u_2 = \left[F_1^W \quad F_2^W \right]^T \in \mathbb{R}^2 : F_1^W \geq 0, \; F_2^W \geq 0 \right\}$$

The map $\Psi_1 : \mathbb{R}^{2n+6} \supset D_1 \to \mathbb{R}^{1\times 2}$ for the considered stream-stream heat exchanger model is defined as follows:

$$\Psi_1 : u_1 \to \Psi_1(u_1) \triangleq \begin{bmatrix} h_1^W - h_1^V & h_2^W - h_2^V \end{bmatrix} \in \mathbb{R}^{1\times 2}, \text{ and } \Psi_1(u_1)u_2 = \begin{bmatrix} h_1^W - h_1^V & h_2^W - h_2^V \end{bmatrix} \begin{bmatrix} F_1^W \\ F_2^W \end{bmatrix} = 0$$

The maps $\Phi_3 : \mathbb{R}^{2n+6} \supset D_1 \to \mathbb{R}^{4n+13}$ and $\Phi_4 : \mathbb{R}^{2n+6} \supset D_1 \to \mathbb{R}^{6\times 2}$ are defined as follows:

$$\Phi_3 : u_1 \to y_1 = \begin{bmatrix} h_1^V \\ h_2^V \\ h_1^W \\ h_2^W \\ P_1^V \\ P_2^V \\ \left\{x_{1,k}^V\right\}_{k=1}^n \\ \left\{x_{2,k}^V\right\}_{k=1}^n \\ P_1^W \\ P_2^W \\ \left\{x_{1,k}^W\right\}_{k=1}^n \\ \left\{x_{2,k}^W\right\}_{k=1}^n \\ T_1^W \\ T_2^W \\ T_1^V \\ T_2^V \\ \Delta T^{lm} \end{bmatrix} = \Phi_3(u_1) \triangleq \begin{bmatrix} h_1^V \\ h_2^V \\ h_1^W \\ h_2^W \\ P_1^V \\ P_2^V \\ \left\{x_{1,k}^V\right\}_{k=1}^n \\ \left\{x_{2,k}^V\right\}_{k=1}^n \\ P_1^V \\ P_2^V \\ \left\{x_{1,k}^V\right\}_{k=1}^n \\ \left\{x_{2,k}^V\right\}_{k=1}^n \\ T_{PR}\left(h_1^W, P_1^V, \left\{x_{1,k}^V\right\}_{k=1}^n\right) \\ T_{PR}\left(h_2^W, P_2^V, \left\{x_{2,k}^V\right\}_{k=1}^n\right) \\ T_{PR}\left(h_1^V, P_1^V, \left\{x_{1,k}^V\right\}_{k=1}^n\right) \\ T_{PR}\left(h_2^V, P_2^V, \left\{x_{2,k}^V\right\}_{k=1}^n\right) \\ \dfrac{\left\{\left[T_{PR}\left(h_1^W, P_1^V, \left\{x_{1,k}^V\right\}_{k=1}^n\right) - T_{PR}\left(h_2^V, P_2^V, \left\{x_{2,k}^V\right\}_{k=1}^n\right)\right] - \left[T_{PR}\left(h_2^W, P_2^V, \left\{x_{2,k}^V\right\}_{k=1}^n\right) - T_{PR}\left(h_1^V, P_1^V, \left\{x_{1,k}^V\right\}_{k=1}^n\right)\right]\right\}}{\ln\left(\dfrac{T_{PR}\left(h_1^W, P_1^V, \left\{x_{1,k}^V\right\}_{k=1}^n\right) - T_{PR}\left(h_2^V, P_2^V, \left\{x_{2,k}^V\right\}_{k=1}^n\right)}{T_{PR}\left(h_2^W, P_2^V, \left\{x_{2,k}^V\right\}_{k=1}^n\right) - T_{PR}\left(h_1^V, P_1^V, \left\{x_{1,k}^V\right\}_{k=1}^n\right)}\right)} \end{bmatrix} \in \mathbb{R}^{4n+13}$$

,

$$\Phi_4 : u_1 \to \Phi_4(u_1) \triangleq \begin{bmatrix} 1 & 0 \\ 0 & 1 \\ 1 & 0 \\ 0 & 1 \\ h_1^W - h_1^V & 0 \\ \dfrac{h_1^W - h_1^V}{U \cdot \Delta T^{lm}} & 0 \end{bmatrix} \in \mathbb{R}^{6\times 2}, \text{ and } y_2 = \begin{bmatrix} F_1^W \\ F_2^W \\ F_1^V \\ F_2^V \\ \dot{Q} \\ A \end{bmatrix} = \Phi_4(u_1)u_2 = \begin{bmatrix} 1 & 0 \\ 0 & 1 \\ 1 & 0 \\ 0 & 1 \\ h_1^W - h_1^V & 0 \\ \dfrac{h_1^W - h_1^V}{U \cdot \Delta T^{lm}} & 0 \end{bmatrix} \begin{bmatrix} F_1^W \\ F_2^W \end{bmatrix}$$

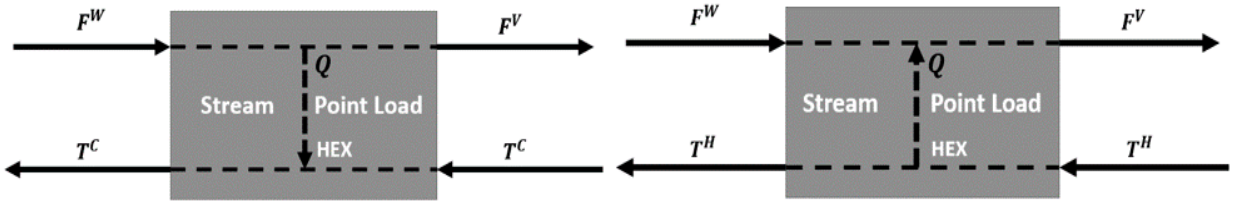

Figure 2-2: *A depiction of hot stream – cold point load and cold stream – hot point load heat exchanger*

Next, the IDEAS information map is presented for the hot (cold) stream – cold (hot) point load heat exchanger depicted in Figure 2-2.

$$u = \left[u_1^T \;\middle|\; u_2^T \right]^T = \left[h_1^V \quad h_1^W \quad T_2 \quad P_1^V \quad \left\{ x_{1,k}^V \right\}_{k=1}^n \;\middle|\; F_1^W \right]^T$$

$$y = \left[y_1^T \;\middle|\; y_2^T \right]^T = \left[h_1^V \quad h_1^W \quad T_2 \quad P_1^V \quad \left\{ x_{1,k}^V \right\}_{k=1}^n \quad P_1^W \quad \left\{ x_{1,k}^W \right\}_{k=1}^n \quad T_1^W \quad T_1^V \quad \Delta T^{lm} \;\middle|\; F_1^W \quad F_1^V \quad \dot{Q} \quad A \right]^T$$

where

$$u_1 \in D_1 = \left\{ u_1 = \left[h_1^V \quad h_1^W \quad T_2 \quad P_1^V \quad \left\{ x_{1,k}^V \right\}_{k=1}^n \right]^T \in \mathbb{R}^{n+4} : T_2 \geq 0,\ P_1^V \geq 0,\ \sum_{k=1}^n x_{1,k}^V = 1,\ x_{1,k}^V \geq 0\ \forall k = 1, n \right\}$$

$$u_2 \in D_2 \triangleq \left\{ u_2 = \left[F_1^W \right]^T \in \mathbb{R} : F_1^W \geq 0 \right\}$$

No map Ψ_1 need be defined for the considered stream-point load heat exchanger model.

The maps $\Phi_3 : \mathbb{R}^{n+4} \supset D_1 \to \mathbb{R}^{2n+8}$ and $\Phi_4 : \mathbb{R}^{n+4} \supset D_1 \to \mathbb{R}^{4\times 1}$ are defined as follows:

$$\Phi_3 : u_1 \to y_1 = \begin{bmatrix} h_1^V \\ h_1^W \\ T_2 \\ P_1^V \\ \left\{x_{1,k}^V\right\}_{k=1}^n \\ P_1^W \\ \left\{x_{1,k}^W\right\}_{k=1}^n \\ T_1^W \\ T_1^V \\ \Delta T^{lm} \end{bmatrix} = \Phi_3(u_1) \triangleq \begin{bmatrix} h_1^V \\ h_1^W \\ T_2 \\ P_1^V \\ \left\{x_{1,k}^V\right\}_{k=1}^n \\ P_1^V \\ \left\{x_{1,k}^V\right\}_{k=1}^n \\ T_{PR}\left(h_1^W, P_1^V, \left\{x_{1,k}^V\right\}_{k=1}^n\right) \\ T_{PR}\left(h_1^V, P_1^V, \left\{x_{1,k}^V\right\}_{k=1}^n\right) \\ \dfrac{\left|T_{PR}\left(h_1^W, P_1^V, \left\{x_{1,k}^V\right\}_{k=1}^n\right) - T_2\right| - \left|T_{PR}\left(h_1^V, P_1^V, \left\{x_{1,k}^V\right\}_{k=1}^n\right) - T_2\right|}{\ln\left(\dfrac{\left|T_{PR}\left(h_1^W, P_1^V, \left\{x_{1,k}^V\right\}_{k=1}^n\right) - T_2\right|}{\left|T_{PR}\left(h_1^V, P_1^V, \left\{x_{1,k}^V\right\}_{k=1}^n\right) - T_2\right|}\right)} \end{bmatrix} \in \mathbb{R}^{2n+8}$$

$$\Phi_4 : u_1 \to \Phi_4\left(u_1\right) \triangleq \begin{bmatrix} 1 \\ 1 \\ h_1^W - h_1^V \\ \dfrac{h_1^W - h_1^V}{U \cdot \Delta T^{lm}} \end{bmatrix} \in \mathbb{R}^{4\times 1}, \text{ and } y_2 = \begin{bmatrix} F_1^W \\ F_1^V \\ \dot{Q} \\ A \end{bmatrix} = \Phi_4\left(u_1\right) u_2 = \begin{bmatrix} 1 \\ 1 \\ h_1^W - h_1^V \\ \dfrac{h_1^W - h_1^V}{U \cdot \Delta T^{lm}} \end{bmatrix} \begin{bmatrix} F_1^W \end{bmatrix}$$

Finally, the IDEAS information map is presented for the hot point load (designated with a superscript H) – cold point load (designated with a superscript C) heat exchanger depicted in Figure 2-3.

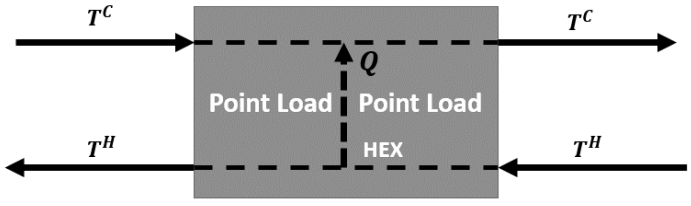

Figure 2-3: *Depiction of hot point – cold point heat exchanger*

$$u = \left[u_1^T \;\middle|\; u_2^T \right]^T = \left[T^C \quad T^H \;\middle|\; \dot{Q} \right]^T$$
$$y = \left[y_1^T \;\middle|\; y_2^T \right]^T = \left[T^C \quad T^H \quad \Delta T^{lm} \;\middle|\; \dot{Q} \quad A \right]^T$$

where $u_1 \in D_1 \triangleq \left\{ u_1 = \left[T^C \quad T^H \right]^T \in \mathbb{R}^2 : T^C \geq 0,\ T^H \geq 0 \right\}$, $u_2 \in D_2 \triangleq \left\{ u_2 = \left[\dot{Q} \right]^T \in \mathbb{R} : \dot{Q} \geq 0 \right\}$.

No map Ψ_1 need be defined for the considered hot point load - cold point load heat exchanger.

The maps $\Phi_3 : \mathbb{R}^2 \supset D_1 \to \mathbb{R}^3$ and $\Phi_4 : \mathbb{R}^2 \supset D_1 \to \mathbb{R}^{2\times 1}$ are defined as follows:

$$\Phi_3 : u_1 \to y_1 = \begin{bmatrix} T^C \\ T^H \\ \Delta T^{lm} \end{bmatrix} = \Phi_3(u_1) \triangleq \begin{bmatrix} T^C \\ T^H \\ T^H - T^C \end{bmatrix} \in \mathbb{R}^3,$$

$$\Phi_4 : u_1 \to \Phi_4(u_1) \triangleq \begin{bmatrix} 1 \\ \dfrac{1}{U \cdot \Delta T^{lm}} \end{bmatrix} \in \mathbb{R}^{2\times 1}, \text{ and } y_2 = \begin{bmatrix} \dot{Q} \\ A \end{bmatrix} = \Phi_4(u_1) u_2 = \begin{bmatrix} 1 \\ \dfrac{1}{U \cdot \Delta T^{lm}} \end{bmatrix} \left[\dot{Q} \right]$$

These properties ensure the linearity of process units employed within IDEAS, and are used to develop the aforementioned heat exchangers' information maps. The thermodynamic feasibility of these heat exchangers is determined through the analysis of T-H diagrams for the considered streams. One such diagram is shown in Figure 2-4; This T-H diagram indicates that the hot and cold stream heat loads are equal, and the countercurrent heat

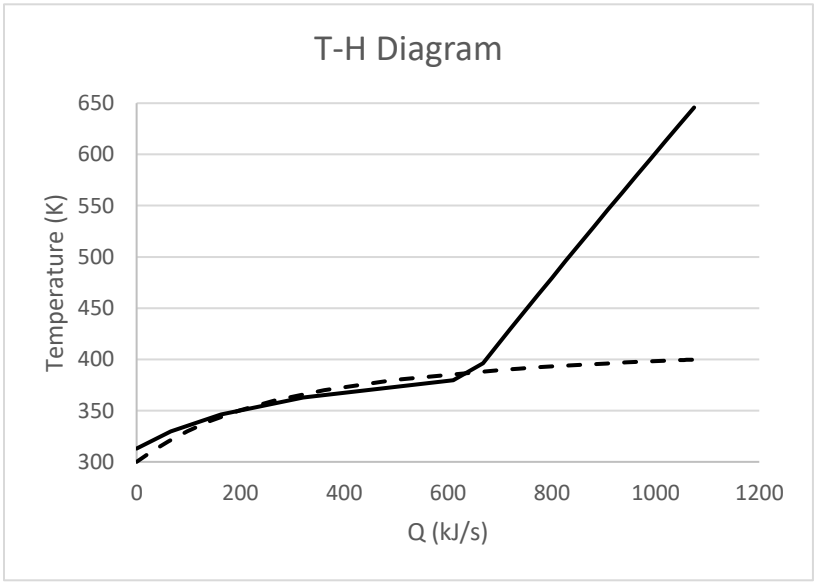

Figure 2-4: *T-H diagram for a thermodynamically infeasible hot stream – cold stream heat exchanger*

exchanger's hot stream inlet and outlet temperatures are above the corresponding cold stream inlet and outlet temperatures. These conditions would normally characterize this unit as thermodynamically feasible, although this is not the case here due to a temperature crossover, possibly attributable to a phase change within the heat exchanger, leading to a violation of thermodynamic feasibility.

Following the generation of all heat exchangers in the HEN operator, the associated HEN heat transfer area is quantified and subjected to an upper bound limit, giving rise to a linear constraint within the linear programming IDEAS formulation. The hydrogen and carbon dioxide separators are next considered. These are considered to be pressure swing adsorption based separators, whose energy consumption is largely compression work related. To properly account for the impact that these separations have on the obtained process designs, the ideal work of separation for these processes is quantified and subjected to an upper bound limit, thus giving rise to an additional linear constraint within the linear programming IDEAS formulation, which otherwise describes the remaining process operations in the same manner as in (Pichardo & Manousiouthakis, 2017). For this study, a hot/cold, multi-utility cost, linear objective function is considered that can be stated as $\sum_{i=1}^{N_{HU}} C_i \dot{Q}_{HU_i} + \sum_{i=1}^{N_{CU}} C_i \dot{Q}_{CU_i}$. This enables parametric studies on the impact of heat transfer area and work of separation upper bounds on the optimum objective function value. In our previous study (Pichardo & Manousiouthakis, 2017), only the hot utility was considered in the objective function, whereas in this study all utilities are considered, since they all contribute to the hot/cold utility cost of the process. Aside from the work of separation, which is separately and explicitly accounted for during the optimization, compressor work is

considered to be the same for all synthesized flowsheets, since all processes are assumed to be isobaric at 5 bar.

2.4 IDEAS Mathematical Formulation

The employed IDEAS process network is depicted in Figure 2-5, and the resulting finite dimensional IDEAS mathematical formulation is presented below.

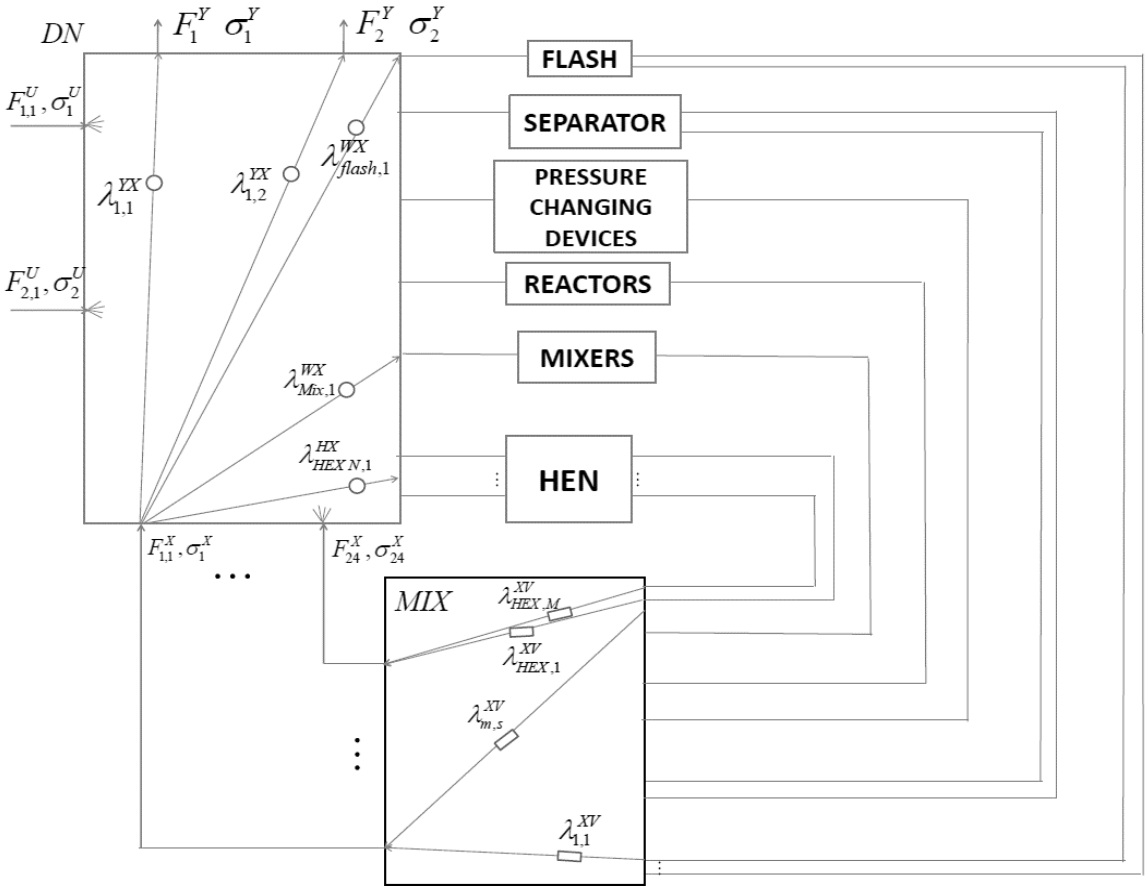

Figure 2-5: *IDEAS depiction of a process network divided into OP and DN networks*

$$\nu \triangleq \inf\left(\sum_{i=1}^{N_{HU}} C_i \dot{Q}_{HU_i} + \sum_{i=1}^{N_{CU}} C_i \dot{Q}_{CU_i}\right)$$

Subject to

$$\sum_{i=1}^{N_{H_2}+N_{CO_2}} W_i \le W^{\max} \tag{1}$$

$$\sum_{i=1}^{N_{HEN}} A_i \le A^{\max} \tag{2}$$

$$F_i^U = \sum_{p=1}^{N_{DN_O}} \lambda_{p,i}^{YU} F_{p,i}^{YU} + \sum_{l=1}^{N_{OP_i}} \lambda_{l,i}^{WU} F_{l,i}^{WU} + \sum_{l=1}^{N_{HEN_i}} \lambda_{l,i}^{HU} F_{l,i}^{HU} \quad \forall i = 1, N_{DN_i} \tag{3}$$

$$F_i^X = \sum_{s=1}^{N_{MIX_i}} \lambda_{i,\mathrm{s}}^{XV} F_s^V = \sum_{p=1}^{N_{DN_O}} \lambda_{p,i}^{YX} F_{p,i}^{YX} + \sum_{l=1}^{N_{OP_i}} \lambda_{l,i}^{WX} F_{l,i}^{WX} + \sum_{l=1}^{N_{HEN_i}} \lambda_{l,i}^{HX} F_{l,i}^{HX} \quad \forall i = 1, N_{MIX_O} \tag{4}$$

$$F_p^{Y,l} \le \sum_{i=1}^{N_{DN_i}} \lambda_{p,\mathrm{i}}^{YU} F_{p,i}^{YX} + \sum_{i=1}^{N_{MIX_O}} \lambda_{p,\mathrm{i}}^{YX} F_{p,\mathrm{i}}^{YX} \le F_p^{Y,\mathrm{u}} \quad \forall p = 1, N_{DN_O} \tag{5}$$

$$\left[\sum_{i=1}^{N_{DN_i}} \lambda_{p,\mathrm{i}}^{YU} F_{p,\mathrm{i}}^{YU} + \sum_{i=1}^{N_{MIX_O}} \lambda_{p,\mathrm{i}}^{YX} F_{p,\mathrm{i}}^{YX}\right] x_{p,k}^{Y,l} \le \left\{\sum_{i=1}^{N_{DN_i}} \lambda_{p,\mathrm{i}}^{YU} F_{p,\mathrm{i}}^{YU} x_{\mathrm{i,k}}^{U} + \sum_{i=1}^{N_{MIX_O}} \lambda_{p,\mathrm{i}}^{YX} F_{p,\mathrm{i}}^{YX} x_{\mathrm{i,k}}^{X}\right\} \le \left[\sum_{i=1}^{N_{DN_i}} \lambda_{p,\mathrm{i}}^{YU} F_{p,\mathrm{i}}^{YU} + \sum_{i=1}^{N_{MIX_O}} \lambda_{p,\mathrm{i}}^{YX} F_{p,\mathrm{i}}^{YX}\right] x_{p,k}^{Y,u} \quad \forall k = 1, n \ \forall p = 1, N_{DN_O} \tag{6}$$

$$\left[\sum_{i=1}^{N_{DN_i}} \lambda_{p,\mathrm{i}}^{YU} F_{p,\mathrm{i}}^{YU} + \sum_{i=1}^{N_{MIX_O}} \lambda_{p,\mathrm{i}}^{YX} F_{p,\mathrm{i}}^{YX}\right] h_p^{Y,l} \le \left\{\sum_{i=1}^{N_{DN_i}} \lambda_{p,\mathrm{i}}^{YU} F_{p,\mathrm{i}}^{YU} h_{\mathrm{i}}^{U} + \sum_{i=1}^{N_{MIX_O}} \lambda_{p,\mathrm{i}}^{YX} F_{p,\mathrm{i}}^{YX} h_{\mathrm{i}}^{X}\right\} \le \left[\sum_{i=1}^{N_{DN_i}} \lambda_{p,\mathrm{i}}^{YU} F_{p,\mathrm{i}}^{YU} + \sum_{i=1}^{N_{MIX_O}} \lambda_{p,\mathrm{i}}^{YX} F_{p,\mathrm{i}}^{YX}\right] h_p^{Y,u} \quad \forall p = 1, N_{DN_O} \tag{7}$$

$$f_{l,k}^{W} = \sum_{i=1}^{N_{DN_i}} \lambda_{l,i}^{WU} F_{l,i}^{WU} x_{i,k}^{U} + \sum_{i=1}^{N_{MIX_O}} \lambda_{l,i}^{WX} F_{l,i}^{WX} x_{l,k}^{X} \quad \forall k = 1, n \ \ \forall l = 1, N_{OP_i} \tag{8}$$

$$H_l^W = \sum_{i=1}^{N_{DN_i}} \lambda_{l,i}^{WU} F_{l,i}^{WU} h_i^U + \sum_{i=1}^{N_{MIX_O}} \lambda_{l,i}^{WX} F_{l,i}^{WX} h_i^X \quad \forall l = 1, N_{OP_i} \tag{9}$$

$$S_l^W = \sum_{i=1}^{N_{DN_i}} \lambda_{l,i}^{WU} F_{l,i}^{WU} s_i^U + \sum_{i=1}^{N_{MIX_O}} \lambda_{l,i}^{WX} F_{l,i}^{WX} s_i^X \quad \forall l = N_R + 1, N_S \tag{10}$$

$$F^U \geq 0,\ F^{YU} \geq 0,\ F^{WU} \geq 0,\ F^{HU} \geq 0,\ F^X \geq 0,\ F^{YX} \geq 0,\ F^{WX} \geq 0,\ F^{HX} \geq 0 \tag{11}$$

Where:

$$\lambda_{p,i}^{YU} = \begin{Bmatrix} 1 \text{ if } P_p^Y = P_i^U \\ 0 \text{ otherwise} \end{Bmatrix}, \lambda_{l,i}^{WU} = \begin{Bmatrix} 1 \text{ if } P_l^W = P_i^U \\ 0 \text{ otherwise} \end{Bmatrix}, \lambda_{p,i}^{YX} = \begin{Bmatrix} 1 \text{ if } P_p^Y = P_i^X \\ 0 \text{ otherwise} \end{Bmatrix}, \lambda_{l,i}^{WX} = \begin{Bmatrix} 1 \text{ if } P_l^W = P_i^X \\ 0 \text{ otherwise} \end{Bmatrix}$$

$$\lambda_{l,i}^{HU} = \begin{Bmatrix} 1 \text{ if } P_l^W = P_i^U, \left\{x_{l,k}^W\right\} = \left\{x_{i,k}^U\right\},\ h_l^W = h_i^U \\ 0 \text{ otherwise} \end{Bmatrix}, \lambda_{l,i}^{HX} = \begin{Bmatrix} 1 \text{ if } P_l^W = P_i^X, \left\{x_{l,k}^W\right\} = \left\{x_{i,k}^X\right\},\ h_l^W = h_i^X \\ 0 \text{ otherwise} \end{Bmatrix}$$

$$\lambda_{i,s}^{XV} = \begin{Bmatrix} 1 \text{ if } P_s^V = P_i^X, \left\{x_{s,k}^V\right\} = \left\{x_{i,k}^X\right\},\ h_s^V = h_i^X \\ 0 \text{ otherwise} \end{Bmatrix}$$

Next, the results obtained from the solution of the above IDEAS formulation are presented.

2.5 Results and Discussion

Prior to discussing the results obtained through the IDEAS methodology, a traditional natural gas reforming based hydrogen production flowsheet is first presented, to provide a baseline design that can serve as a means of comparison with the IDEAS derived designs. This baseline flowsheet consists of a 1100 K reformer, as well as a 650 K high temperature shift (HTS) reactor and a 475 K low temperature shift (LTS) reactor. The inlets of the flowsheet include one kmol/hr of CH_4 and two kmols/hr of H_2O, which are compressed before being fed into the 1100 K reformer.

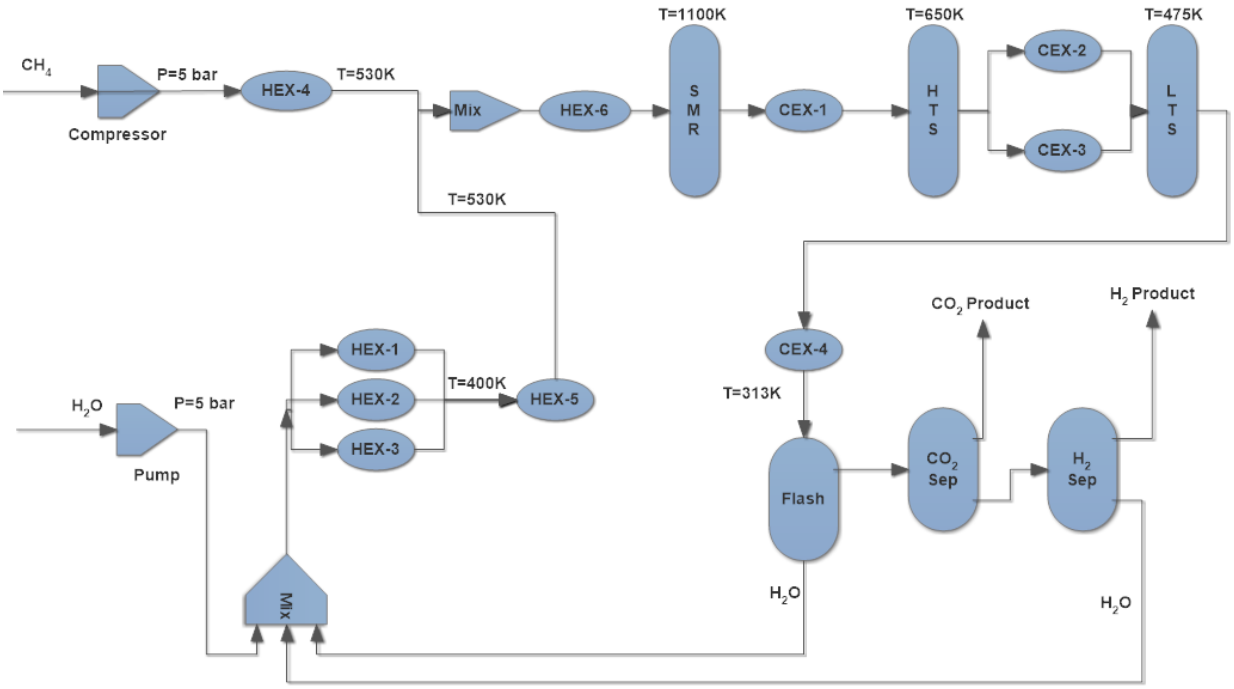

Figure 2-6: *Baseline Flowsheet depicting hydrogen production through traditional steam-methane reforming*

Subsequently, the outlet of the reformer is cooled and fed into a series of water-gas-shift reactors, whose outlet first undergoes water flash separation, and subsequently, hydrogen, and carbon dioxide separation. The flowsheet outlets consist of 4 kmols/hr of H_2 and 1 kmol/hr of CO_2, and the associated heat exchange network's hot/cold utility use consists of 62.34 kJ/s (224.5 kJ/mol CH_4 fed) of 1200K hot utility, 3.09 kJ/s (11.1 kJ/mol CH_4 fed) of 770 K hot utility, 4.16 kJ/s (15.0 kJ/mol CH_4 fed) of 420K hot utility, and 4.63 kJ/s (16.7 kJ/mol CH_4 fed) of 298 K cold utility. Finally, the work of separation (ideal) required by the baseline flowsheet to produce pure hydrogen and carbon dioxide streams is 4.60 kJ/s (15.6 kJ/mol CH_4 fed), while the area of the associated heat exchange network is 10.7 m^2.

Table 2-1 summarizes several of the key characteristics of the baseline design, and Figure 2-6 includes a process design drawing of the baseline. These characteristics will be used to establish a comparison basis of the baseline and IDEAS derived designs. The heat exchange network in

the baseline design flowsheet depicted in Figure 2-6 visually depicts all stream – stream heat exchangers and stream – point load heat exchangers. Point load – point load heat exchangers are not visually depicted in the flowsheet, but can be found in Table 2-2 along with the details of the stream – stream and stream – point load exchangers. The heat exchange network consists of four stream – stream heat exchangers, four stream – point load heat exchangers, and three point load – point load heat exchangers. Table 2-2 shows all of the details regarding the heat exchangers present in Figure 2-6 as well as the point load – point load exchangers.

Table 2-1: *Summary table of baseline flowsheet's properties*

Baseline Case	
CH4 inlet (kmols/hr)	1
H2O inlet (kmols/hr)	2
H2 outlet (kmols/hr)	4
CO2 outlet (kmols/hr)	1
1200K Hot Utility (kJ/s)	62.34
770K Hot Utility (kJ/s)	3.09
420K Hot Utility (kJ/s)	4.16
298K Cold Utility (kJ/s)	4.63
Work of Separation (kJ/s)	4.60
Area of HEN (m^2)	10.7
Reformer Temperature (K)	1100
HTS Temperature (K)	650
LTS Temperature (K)	475

The four stream – stream exchangers' details in Table 2-2 depict the stream matches based on the heat exchangers found in Figure 2-6. The four stream – point load heat exchangers are depicted in the baseline design as HEX-3, which consists of two stream – point load exchangers where water is heated from 301K to 400K by the LTS reactor and the 420K hot utility, and HEX-5, which consist of two stream – point load exchangers where water is heated from 400K to 530K by the HTS reactor and the 770K hot utility. The design also includes three point load – point load heat exchangers; the reformer and 1200K hot utility, the hydrogen separator and 298K cold utility, and the carbon dioxide separator and 298K cold utility. The details including all heat exchangers present in the flowsheet are summarized in Table 2-2 below.

Table 2-2: *Summary of the heat exchange network present in the baseline*

Heat Exchanger Name	Heat Exchanger Type	Cold Stream/Point	Cold Stream/Point	Hot Stream/Point	Hot Stream/Point	Cold Stream/Point Source	Hot Stream/Point Source

		Temperature In	Temperature Out	Temperature In	Temperature Out		
HEX-1 CEX-2	Stream – Stream	301	400	650	475	HEX-1	CEX-2
HEX-2 CEX-3	Stream – Stream	434	530	650	475	HEX-4	CEX-3
HEX-3 CEX-1	Stream – Stream	530	1050	1100	642	HEX-6	CEX-1
HEX-4 CEX-4	Stream - Stream	301	400	475	313	HEX-2	CEX-4
HEX-3	Stream - Point	301	400	475	475	HEX-3	LTS
	Stream - Point	301	400	420	420	HEX-3	Hot Utility
HEX-5	Stream - Point	400	530	650	650	HEX-5	HTS
	Stream - Point	400	530	770	770	HEX-5	Hot Utility
N/A	Point - Point	298	298	313	313	Cold Utility	H2 Separator
N/A	Point - Point	298	298	313	313	Cold Utility	CO2 Separator
N/A	Point - Point	1050	1050	1200	1200	Hot Utility	Reformer

The IDEAS methodology was utilized to identify alternative designs to traditional natural gas based hydrogen production that are capable of using hybrid energy sources. These hybrid energy sources are represented as the 770K utility, whose source is solar energy, while the 1200K utility's source is a methane burning furnace. Upper bound restrictions have been imposed on the total heat exchange network area, and the work of separation, which act as capital cost, and electricity cost surrogates. In the considered cases, both the total heat exchange area utilized and the total work of separation are varied from one to three times the amount used by the baseline design. The considered cost coefficients for the 1200K hot utility, 770K hot utility, 420K hot utility, and 298K cold utility are assumed to have an 8:4:2:1 ratio. Currently, the average cost of methane in the United States is 0.408$/kg (EIA, 2017), while methane's heat of combustion is 55700 kJ/kg (Commerce, 2016), which then yields to a 1200 K hot utility cost coefficient of 0.00733$/MJ. A high carbon tax on fuel case is also considered, in which the

aforementioned cost coefficient ratios are altered to 40:4:2:1. All IDEAS generated flowsheets are required to have the same inlet and outlet flowrates as the aforementioned baseline design, namely 1 kmol/hr of CH_4 and 2 kmol/hr of H_2O inlets, and 4 kmols/hr of H_2 and 1 kmol/hr of CO_2 outlets. A summary of important characteristics of these IDEAS generated flowsheets can be found in Table 2-3.

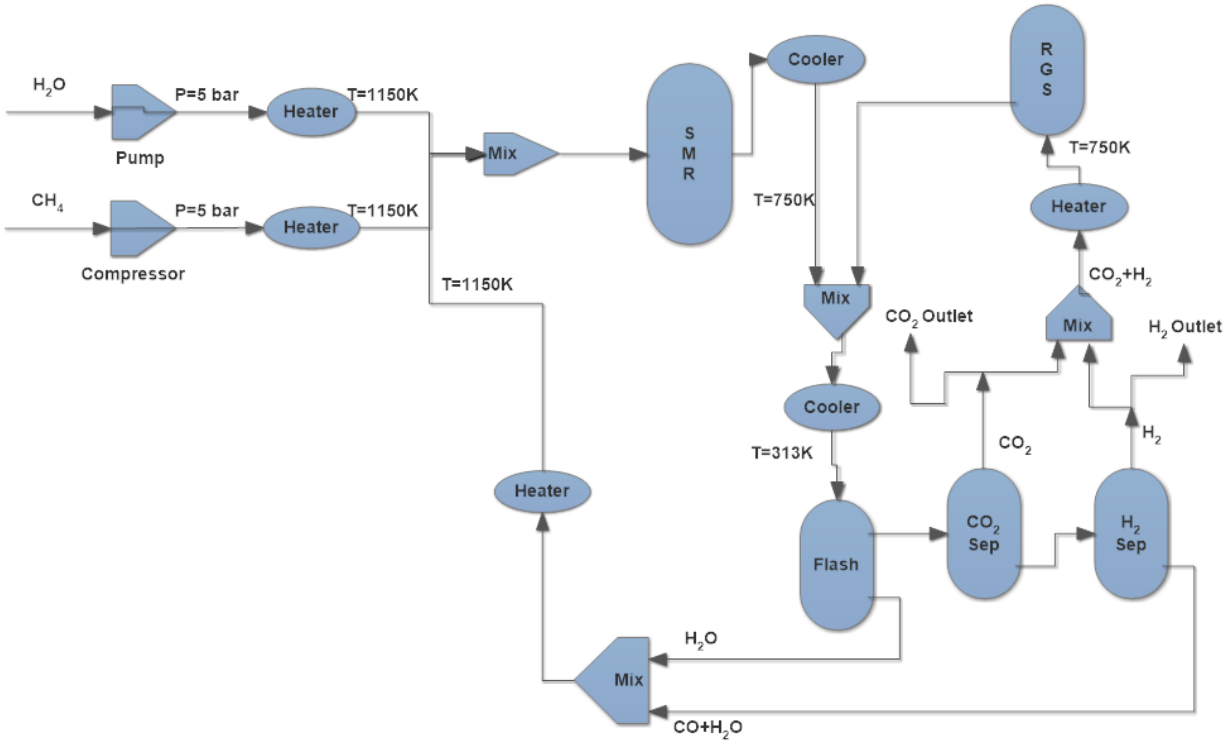

Figure 2-7: *IDEAS synthesized flowsheet for steam methane reforming with no capital cost restriction (Pichardo & Manousiouthakis, 2017).*

Energetically enhanced reforming pursues the reduction of the highly endothermic load of a traditional SMR (steam-methane reformer) through introduction of CO into the reformer feed. The effects of CO in the reformer feed can be seen below in Table 2-4, which demonstrates that as the CO SMR inlet feed increases, the total heat load of the reactor decreases. These calculations are performed utilizing Gibbs Free Energy formulation for equilibrium reactors. It can be seen that even when the CO inlet is increased slightly (from 0 kmol/h to 0.5 kmol/h) the

heat load of the reformer can be reduced up to 6%. For exothermicity to be reached, the CO content has to be greater than 10 kmol/h with significant amounts of water (>12 kmol/h), but even a CO inlet of 2 kmol/h with a CH_4 inlet of 1 kmol/h and H_2O inlet of 3 kmol/h can decrease the reactor heat load from 59.33 kmol/h to 48.10 kmol/h, which results in a 20% decrease in the energetic requirements of reforming when compared to a reformer with no CO in the inlet. A CO inlet of 5 kmol/h with a CH_4 inlet of 1 kmol/h and H_2O inlet of 10 kmol/h can decrease the reactor heat load from 56.76 kmol/h to 35.59 kmol/h, which results in a 37% decrease in the energetic requirements of reforming, when compared to a reformer with no CO in the inlet. As long as the H2O feed is large enough, the CH4 conversion remains well over 95% even with CO input.

In addition to reformers with significant CO feed content, reverse-gas-shift (RGS) reactors are also considered to generate the CO utilized in the feed of the reformer. All reformer temperatures range between 1040 K-1145 K, and reach over 85% methane conversion. It should be noted that all IDEAS flowsheets have the same amount of compression work as the baseline design, and that all reactors and separators employed operate at 5 bar for both the baseline design and IDEAS designs. In our previous work (Pichardo & Manousiouthakis, 2017), IDEAS found alternative flowsheets that utilized reformers with a CO feed as high as 15 kmols/hr, H_2O feed of 18 kmols/hr, and a CH_4 feed of 1 kmol/hr. These IDEAS generated flowsheets were able to produce entirely exothermic reformers that required no 1200 K utility, and an example of such a flowsheet is shown in Figure 2-7 above. The exothermicity was achieved through the recycling of carbon monoxide that was produced utilizing a reverse-gas-shift reactor. This makes reaction r2 to be the prevalent steam-methane reforming reaction. In this work, the synthesized hybrid steam-methane reforming flowsheets generated by IDEAS account for the work of separation

and heat exchange area required to attain reduced reforming endothermicity.

Table 2-3*: Summary table detailing IDEAS synthesized natural gas based hydrogen production flowsheets*

Work U.B. (kJ/s)	**4.70**	**4.70**	**4.70**	**20**	**20**	**20**	**30**	**30**	**30**
Area U.B. (m^2)	10.7	21.4	32.1	10.7	21.4	32.1	10.7	21.4	32.1
HU 1200K (kJ/s)	61.5	35.0	13.5	59.6	41.9	20.0	58.0	34.3	16.6
HU 770K (kJ/s)	5.0	39.2	64.4	0.0	19.8	46.3	0.0	11.9	39.0
HU 420K (kJ/s)	0.00	3.17	0.87	1.41	4.99	0.00	0.00	9.71	1.45
CU 298K (kJ/s)	5.0	13.3	14.9	12.4	18.4	17.7	17.6	17.3	18.3
Work of Separation (kJ/s)	4.36	4.70	4.70	20	20	20	28	30	30
HEX Area (m^2)	10.7	21.4	32.1	10.7	21.4	32.1	10.7	21.4	32.1
Total Utility Cost ($/h)	1.71	1.50	1.26	1.62	1.46	1.20	1.59	1.18	1.02

Table 2-4: *Thermodynamic equilibrium reactor inlet and outlet conditions.*

Reactor Inlet (kmol/hr)			Reactor Outlet (kmol/hr)					T=1150 K P= 5 bar
CH_4	*CO*	*H_2O*	*CH_4*	*CO*	*CO_2*	*H_2O*	*H_2*	*Heat Load (kJ/s)*
1	0	2.5	0.02	0.73	0.25	1.27	3.19	59.37
1	0.1	2.5	0.02	0.81	0.27	1.25	3.20	59.05
1	0.2	2.5	0.02	0.89	0.29	1.23	3.22	58.74
1	0.5	2.5	0.03	1.12	0.35	1.18	3.26	57.83
1	1	2.5	0.04	1.53	0.43	1.11	3.32	56.42
1	2	2.5	0.06	2.37	0.58	0.98	3.41	53.98
1	5	2.5	0.10	5.03	0.87	0.73	3.58	48.72
1	15	2.5	0.16	14.57	1.27	0.39	3.79	40.84

1	0	3	0.01	0.68	0.30	1.71	3.27	59.33
1	0.1	3	0.01	0.76	0.33	1.68	3.29	59.00
1	0.2	3	0.02	1.06	0.42	1.59	3.37	57.75
1	0.5	3	0.03	1.44	0.53	1.50	3.45	56.31
1	1	3	0.04	2.25	0.71	1.33	3.59	53.77
1	2	3	0.08	4.85	1.07	1.00	3.85	48.10
1	5	3	0.12	9.48	1.41	0.71	4.06	42.42
1	15	3	0.14	14.26	1.59	0.55	4.17	39.04
1	0	5	0.00	0.53	0.46	3.54	3.45	58.42
1	0.1	5	0.00	0.59	0.50	3.50	3.49	58.02
1	0.2	5	0.00	0.65	0.54	3.46	3.53	57.62
1	0.5	5	0.01	0.84	0.66	3.35	3.64	56.47
1	1	5	0.01	1.16	0.83	3.18	3.80	54.68
1	2	5	0.01	1.86	1.12	2.89	4.08	51.51
1	5	5	0.04	4.21	1.76	2.28	4.65	44.19
1	15	5	0.10	13.15	2.75	1.34	5.46	30.82
1	0	10	0.00	0.34	0.66	8.34	3.66	56.76
1	0.1	10	0.00	0.38	0.72	8.28	3.72	56.19
1	0.2	10	0.00	0.42	0.78	8.22	3.78	55.63
1	0.5	10	0.00	0.55	0.95	8.05	3.95	54.00
1	1	10	0.00	0.78	1.22	7.78	4.22	51.42
1	2	10	0.00	1.29	1.71	7.30	4.70	46.76
1	5	10	0.01	3.15	2.84	6.17	5.81	35.59
1	15	10	0.05	11.01	4.94	4.11	7.78	13.12
1	0	20	0.00	0.20	0.80	18.20	3.80	55.44
1	0.1	20	0.00	0.22	0.88	18.12	3.88	54.72
1	0.2	20	0.00	0.25	0.95	18.05	3.95	54.01
1	0.5	20	0.00	0.32	1.18	17.82	4.18	51.92
1	1	20	0.00	0.47	1.53	17.47	4.53	48.56
1	2	20	0.00	0.80	2.20	16.80	5.20	42.27
1	5	20	0.00	2.10	3.90	15.10	6.90	26.13
1	15	20	0.02	8.35	7.64	11.38	10.58	-10.17

Overall, as expected, the minimum utility cost of the synthesized flowsheets decreases as the heat exchange area (work of separation) upper bound increases, while the work of separation (heat exchange area) upper bound is kept constant. In particular, if the work of separation is identical to the baseline flowsheet work of separation, a threefold increase to the baseline design's HEN area yields 26% decrease in optimal utility cost. The above trends are illustrated in Figure 2-8, where it can also be seen that as the work of separation is allowed to increase from 20kJ/s to 30kJ/s the decrease in optimum total utility cost is much more significant than when the work of separation is increased from 4.7kJ/s to 20kJ/s. In addition, as shown in Table 2-3 and in Figures 2-9 and 2-10, as the total heat exchange network area is allowed to increase, while the work of separation upper bound is kept constant, the 1200 K (770 K) hot utility consumption is reduced (increased). Further examination of Figure 2-9 demonstrates that even as the work of separation is kept constant at a value of approximately 4.7 kJ/s, the 1200 K hot utility use can be reduced dramatically (approximately 78%) by increasing total heat exchange network area. These results demonstrate that as the heat exchange area is allowed to increase, the 770 K utility increasingly replaces the use of the 1200 K utility. The use of the 420 K utility does not exhibit these monotonous trends. As illustrated in Figure 2-11, the use of the 420 K utility initially increases and subsequently decreases, as the HEN area is allowed to increase. On the other hand, cold utility use increases as the HEN area is allowed to increase, as can be seen in Figure 2-12.

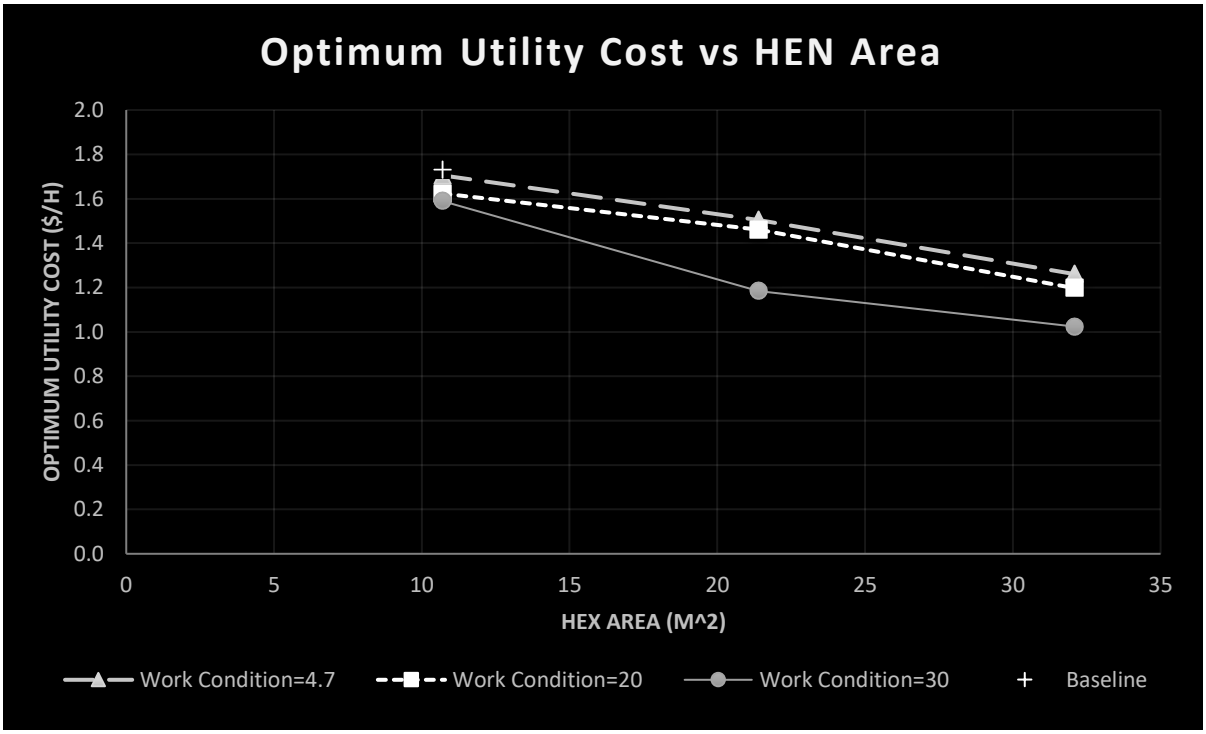

Figure 2-8: *Objective function as a function of heat exchange area and work of separation*

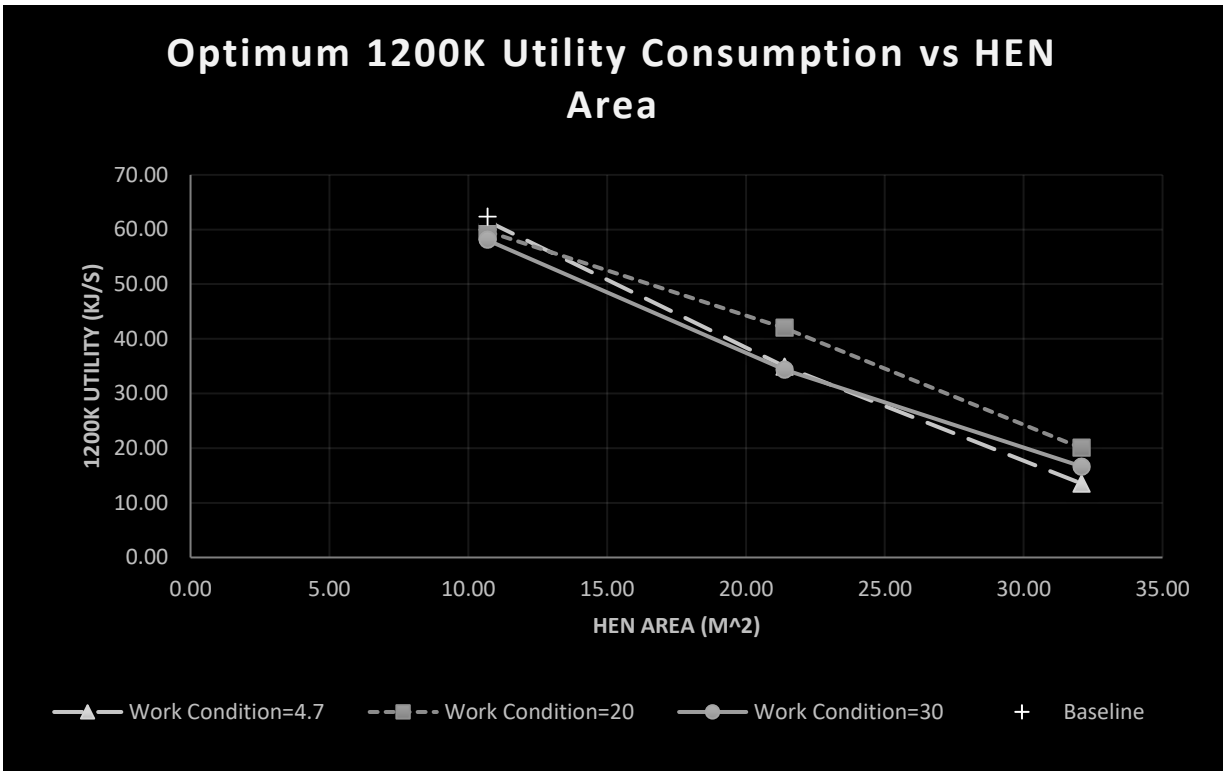

Figure 2-9*: Consumption of 1200K Utility as a function of heat exchange area and work of separation*

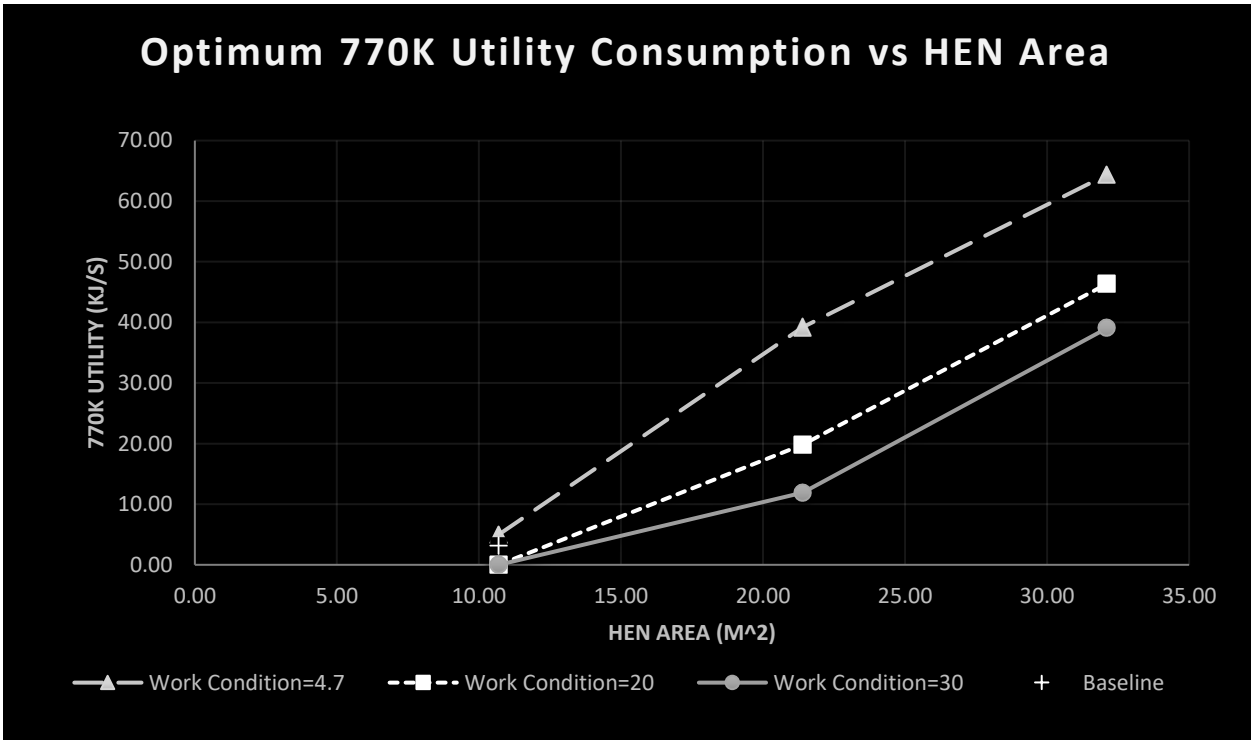

Figure 2-10*: Consumption of 770K Utility as a function of heat exchange area and work of separation*

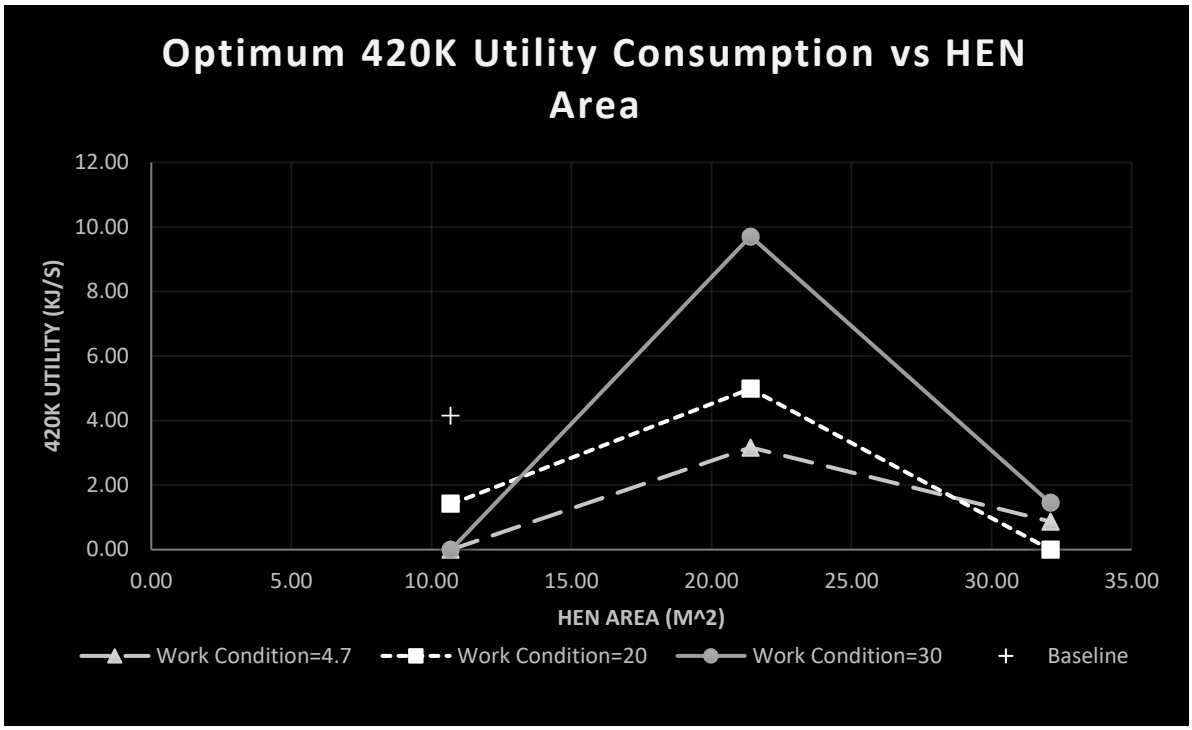

Figure 2-11*: Consumption of 420K Utility as a function of heat exchange area and work of separation*

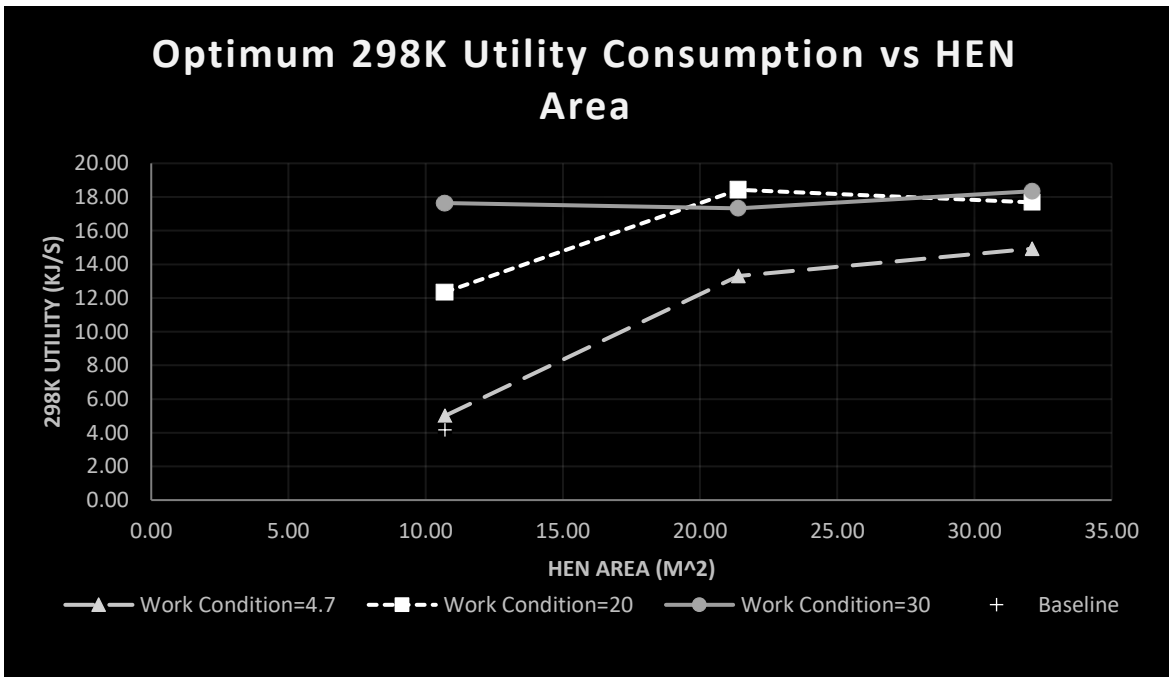

Figure 2-12: *Consumption of 298K Utility as a function of heat exchange area and work of separation*

As discussed earlier, the 1200 K hot utility cost coefficient is 0.00733$/MJ. In addition, a total heat exchange network area of 10.7m^2 costs approximately $13,000 (Peters, Timmerhaus, & West, 2003), which can be scaled up using the equation:

$$Cost\ of\ Equipment\ A = (Cost\ of\ Equipment\ B)\left(\frac{Capacity\ of\ A}{Capacity\ of\ B}\right)^{0.44}$$ (Peters, Timmerhaus, & West, 2003)

This yields a cost of $17,636 and $21,080 for a total heat exchange network area of 21.4 m^2 and 32.1m^2 respectively. Further, using an interest rate of 3% over a 10-year period, the amortized cost of a heat exchange network of 10.7m^2, 21.4 m^2, and 32.1 m^2, would be approximately 0.15$/h, 0.21$/h, and $0.25/h respectively. As can be seen in Table 2-5, the total utility cost of the IDEAS designs, when the work of separation upper bound is fixed at 4.7 kJ/s and the heat exchange area is allowed to increase from 10.7m^2 to 32.1m^2, decreases from 1.71$/h to 1.23$/h (a 26% decrease). For a work of separation upper bound of 20 (30), the total utility cost decreases from 1.62$/h to 1.20$/h (1.50$/h to 1.02$/h), which represents a 26% (36%) decrease. For all of these cases, the cost of increasing the HEN area is only 0.10$/h, which allows the flowsheets with higher area to be more economical than ones with a lower area. The cost coefficients of the 1200 K hot utility, 770 K hot utility, 420 K hot utility, and 298 K cold utility are 0.00733$/MJ, 0.003665$/MJ, 0.0018325$/MJ, and 0.00091625$/MJ.

Table 2-5: *Economic Analysis of IDEAS designs with heat exchange area and work of separation upper bounds*

Work U.B. (kJ/s)	**4.70**	**4.70**	**4.70**	**20**	**20**	**20**	**30**	**30**	**30**
Area U.B. (m^2)	10.7	21.4	32.1	10.7	21.4	32.1	10.7	21.4	32.1
Cost of HEN Area ($/h)	0.15	0.21	0.25	0.15	0.21	0.25	0.15	0.21	0.25

Cost HU 1200K ($/h)	1.62	0.92	0.36	1.57	1.11	0.53	1.53	0.91	0.44
Cost HU 770K ($/h)	0.07	0.52	0.85	0.00	0.26	0.61	0.00	0.16	0.51
Cost HU 420K ($/h)	0.00	0.02	0.01	0.01	0.03	0.00	0.00	0.06	0.01
Cost CU 298K ($/h)	0.02	0.04	0.05	0.04	0.06	0.06	0.06	0.06	0.06
Total Utility Cost ($/h)	1.71	1.50	1.26	1.62	1.46	1.20	1.59	1.18	1.02

The imposition of a debilitating carbon tax on the use of methane as fuel can have a significant impact on the structure of the IDEAS generated designs. For example, if the cost of burning methane is 10x the cost of a renewable solar powered (770K) utility, yielding a cost coefficient ratio of 40:4:2:1, the IDEAS generated design (for work of separation and total heat exchange area upper bounds of 30 kJ/s and 42.1m^2 respectively) features fully exothermic reforming. Associated characteristics of this design can be found in Table 2-6.

Table 2-6: *Summary table of exothermic flowsheet's properties*

Exothermic Case	
CH4 inlet (kmols/hr)	1
H2O inlet (kmols/hr)	2
H2 outlet (kmols/hr)	4
CO2 outlet (kmols/hr)	1
1200K Hot Utility (kJ/s)	0
770K Hot Utility (kJ/s)	60.75
420K Hot Utility (kJ/s)	0
298K Cold Utility (kJ/s)	22.10
Work of Separation (kJ/s)	30
Area of HEN (m^2)	42.1
Total Utility (kJ/s)	82.85

For these cost coefficients, the baseline utility cost is 16.62$/h, while the IDEAS exothermic case utility cost is 1.75$/h (an 89% decrease). This cost reduction can be further amplified by the elimination of the need for a methane burning furnace for exothermic reformer designs, which can thus require lower capital investments for their realization. The potential removal of the methane burning furnace is a demonstration of the intensification, in regard to a methane fuel consumption metric, of the proposed process as this would vastly decrease the size of the reforming reactor. As has been

mentioned in our previous work (Albassam, Conner, & Manousiouthakis, 2018), carbon taxes on the use of methane as fuel has already been implemented by several countries including Japan, which has imposed a carbon tax, as of 2012, of $2.89/ton of CO2 on fossil fuels, such as natural gas, burned within a chemical process. As these taxes increase, the exothermic case presented above becomes increasingly compelling. This energetically enhanced reforming process is especially useful because it is able to replace energy loads at high temperature (1200K), resulting from the burning of methane as fuel, with energy loads at lower temperatures (770K), resulting from the use of concentrated solar power, albeit at the potential increase in the total energy loads required. Significantly reducing the temperature at which the flowsheet's energy requirements are delivered can yield many benefits, which for the SMR process include the capital cost of the furnace, material resources by allowing the CH4 to be used only as raw material, and any additional costs created through carbon taxes. The flowsheet's energy consumption makeup becomes increasingly renewable due to the allowed increase in heat exchange area and work of separation.

An emerging technology that can provide 770 K hot utility needed by the IDEAS designs is concentrated solar power (CSP). Indeed, solar energy is freely available, and solar concentration technologies, such as troughs and towers, are currently able to deliver hot utility at 720 K and 835 K respectively, while they are expected to reach 773K and 920K by 2020 (Turchi, Mehos, Ho, & Kolb, 2010). Therefore, the proposed IDEAS designs are hybrid energy users that combine CSP with fossil fuel use, to generate hydrogen from natural gas.

2.6 Conclusions

The IDEAS methodology is employed as a process intensification tool to the synthesis of novel natural gas based hydrogen production designs utilizing hybrid energy sources. The considered intensification metric is the process network's total hot/cold multi-utility cost, which is minimized subject to upper bounds on the total heat exchange network area and work of separation, which act as capital cost and electricity operating cost surrogates. The IDEAS obtained intensified designs can significantly reduce the use of methane as a fuel source, enabling the use of concentrated solar power based renewable energy for hydrogen production. Parametric studies are performed to determine the effect of increasing heat exchange network area and work of separation upper bounds on the total hot/cold multi-utility cost. It was found that as the heat exchange network area and work of separation upper bounds are allowed to increase the total hot/cold multi-utility cost decreases. Increasing the heat exchange area alone can yield a 26% decrease in optimal utility cost.

2.7 Notation

A Area of heat exchanger (m^2)

$A^{\max}$ Maximum area constraint (m^2)

C_i Cost coefficient of ith external hot utility (\$/kJ/s)

F_i^U, $i = 1, N_{DN_i}$, mass flow rate of ith DN network inlet (kg/s)

F_s^V, $s = 1, N_{OP_O} + N_{HEN_O}$, mass flow rate of the sth OP and HEN unit outlet (kg/s)

F_l^W, $l = 1, N_{OP_i} + N_{HEN_i}$, mass flow rate of the lth OP and HEN inlet (kg/s)

$f_{l,k}^W$, $l = 1, N_{OP_i}$, $k = 1, n$, mass flow rate of the lth OP inlet's kth species (kg/s)

F_i^X, $i = 1, N_{MIX_O}$, mass flow rate of the ith MIX outlet (kg/s)

F_p^Y, $p = 1, N_{DN_O}$, mass flow rate of the pth DN outlet (kg/s)

$F_p^{Y,l}$, $p = 1, N_{DN_O}$, lower limit of the mass flow rate of the pth DN outlet (kg/s)

$F_p^{Y,u}$, $p = 1, N_{DN_O}$, upper limit of the mass flow rate of the pth DN outlet (kg/s)

$F_{l,i}^{WU}$, $l = 1, N_{OP_i} + \mathrm{N}_{HEN_i}$, $i = 1, N_{DN_i}$, mass flow rate from the ith DN inlet to the lth OP and HEN inlet (kg/s)

$F_{l,i}^{WX}$, $l = 1, N_{OP_i} + \mathrm{N}_{HEN_i}$, $i = 1, N_{MIX_O}$, mass flow rate from the ith MIX outlet to the lth OP and HEN inlet (kg/s)

$F_{p,i}^{YU}$, $p = 1, N_{DN_O}$, $i = 1, N_{DN_i}$, mass flow rate from the ith DN inlet to the pth DN outlet (kg/s)

$F_{p,\mathrm{i}}^{YX}$, $p = 1, N_{DN_O}$, $i = 1, N_{MIX_O}$, mass flow rate of the ith MIX outlet to the pth DN outlet (kg/s)

H^W, total enthalpy flow of the process unit inlet (J/s)

h_{i}^U, $i = 1, N_{DN_i}$, total specific enthalpy of the ith DN inlet (J/kg)

h^V, total specific enthalpy of the process unit outlet (J/kg)

h^W, total specific enthalpy of the process unit inlet (J/kg)

h_i^X, $i = 1, N_{MIX_O}$, total specific enthalpy of the ith MIX outlet (J/kg)

h_{p}^Y, $p = 1, N_{DN_O}$, total specific enthalpy of the pth DN outlet(J/kg)

$h_{\mathrm{p}}^{Y,l}$, $p = 1, N_{DN_O}$, lower limit of total specific enthalpy of the pth DN outlet(J/kg)

$h_{\mathrm{p}}^{Y,u}$, $p = 1, N_{DN_O}$, upper limit of total specific enthalpy of the pth DN outlet(J/kg)

N_{DN_i} Number of inlet streams in the DN

N_{DN_O} Number of outlet streams in the DN

N_{OP_i} Number of inlet streams in the OP

N_{OP_O} Number of outlet streams in the OP

P_i^U, $i = 1, N_{DN_i}$, pressure of the ith DN inlet (J/kg)

P^V, pressure of the process unit outlet (bar)

P^W, pressure of the process unit inlet (bar)

P_i^X, $i = 1, N_{MIX_O}$, pressure of the ith MIX outlet (bar)

P_p^Y, $p = 1, N_{DN_O}$, pressure of the pth DN outlet (bar)

$\dot{Q}$ heat load (J/s)

Q_{HU_i} external ith hot utility load (J/s)

Q_{CU_i} external ith cold utility load (J/s)

S^W, total entropy flow for the process unit inlet (J/K)

s_{i}^U, $i = 1, N_{DN_i}$, total specific entropy of the ith DN inlet (J/kg K)

s_i^X, $i = 1, N_{MIX_O}$, total specific entropy of the ith MIX outlet (J/kg K)

T_{Pr} temperature calculated through the Peng-Robinson equation of state (K)

ΔT^{lm} logarithmic mean temperature difference (K)

T^V temperature of process unit outlet (K)

T^W temperature of process unit inlet (K)

T^C temperature of process unit cold point load (K)

T^H temperature of process hot point load (K)

$W^{\max}$ Maximum ideal work constraint (kJ/s)

$x_{\mathrm{i,k}}^U$, $i = 1, N_{DN_i}$, $k = 1, n$, mass fraction of the ith DN inlet's kth species.

x_k^V, $k=1,n$, mass fraction of the process unit's outlet kth species

x_k^W, $k=1,n$, mass fraction of the lth process unit's inlet kth species

$x_{i,k}^X$, $i=1,N_{MIX_O}$, $k=1,n$, mass fraction of the ith MIX outlet's kth species

$x_{p,k}^Y$, $p=1,N_{DN_O}$, $k=1,n$, mass fraction of the pth DN outlet's kth species

$x_{p,k}^{Y,l}$, $p=1,N_{DN_O}$, $k=1,n$, lower limit of the mass fraction of the pth DN outlet's kth species

$x_{p,k}^{Y,u}$, $p=1,N_{DN_O}$, $k=1,n$, upper limit of the mass fraction of the pth DN outlet's kth species.

$\lambda_{p,i}^{YU}$ Flag that denotes the existence of flow from the ith DN inlet to the pth DN outlet

$\lambda_{l,i}^{WU}$ Flag that denotes the existence of flor from the ith DN inlet to the lth OP inlet

$\lambda_{p,i}^{YX}$ Flag that denotes the existence of flor from the ith MIX outlet to the pth DN outlet

$\lambda_{l,i}^{WX}$ Flag that denotes the existence of flor from the ith MIX outlet to the lth OP inlet

$\lambda_{l,i}^{HU}$ Flag that denotes the existence of flor from the ith DN inlet to the lth HEX inlet

$\lambda_{l,i}^{HX}$ Flag that denotes the existence of flor from the ith MIX outlet to the lth HEX inlet

$\lambda_{i,s}^{XV}$ Flag that denotes the existence of flor from the sth process unit outlet to the ith MIX inlet

2.8 References

Albassam, A., Conner, J., & Manousiouthakis, V. (2018). Natural gas derived hydrogen in the presence of carbon fuel taxes and concentrated solar power. *ACS Sustainable Chem. Eng.*

Burri, J., & Manousiouthakis, V. (2004). Global optimization of reactive distillation networks using IDEAS. *Computers & chemical engineering*, 2509-2521.

Burri, J., Wilson, S., & Manousiouthakis, V. (2002). Infinite DimEnsionAl State-space approach to reactor network synthesis: application to attainable region construction. *Computers & chemical engineering*, 849-862.

Commerce, T. U. (2016). *National Institute of Standards and Technology*. Retrieved May 17, 2017, from https://perma.cc/B8C9-GCTX

da Cruz, F., & Manousiouthakis, V. (2016). Process Intensification of Reactive Separator Networks through the IDEAS Conceptual Framework. *Computers & Chemical Engineering.*

Davis, B., Taylor, L., & Manousiouthakis, V. (2008). Identification of the attainable region for batch reactor networks. *Industrial & Engineering Chemistry Research*, 3388-3400.

Drake, J., & Manousiouthakis, V. (2002). IDEAS approach to process network synthesis: minimum utility cost for complex distillation networks. *Chemical Engineering Science*, 3095-3106.

EIA. (2017). *Natural Gas*. Retrieved May 19, 2017, from https://perma.cc/3NW4-PCNZ

Ghougassian, P., & Manousiouthakis, V. (2012). Globally Optimal Networks for Multipressure Distillation of Homogeneous Azeotropic Mixtures. *Industrial & Engineering Chemistry Research*, 11183-11200.

Ghougassian, P., & Manousiouthakis, V. (2013). Attainable composition, energy consumption, and entropy generation properties for isothermal/isobaric reactor networks. *Industrial & Engineering Chemistry Research*, 3225-3238.

Ghougassian, P., & Manousiouthakis, V. (2015). Minimum entropy generation for isothermal endothermic/exothermic reactor networks. *AIChE Journal*, 103-117.

Holiastos, K., & Manousiouthakis, V. (1998). Automatic synthesis of thermodynamically feasible reaction clusters. *AIChE Journal*, 164-173.

Holiastos, K., & Manousiouthakis, V. (2004). Infinite-dimensional state-space (IDEAS) approach to globally optimal design of distillation networks featuring heat and power integration. *Industrial & engineering chemistry research*, 7826-7842.

Hydrogen Production: Natural Gas Reforming. (2017, January 12). Retrieved from Office of Energy Efficiency & Renewable Energy: https://perma.cc/Y8MH-DRRP

Hydrogen Production: Thermochemical Water Splitting. (2017, Fenruary 10). Retrieved from Office of Energy Efficiency & Renewable Energy: https://perma.cc/SA7G-BQTN

Justanieah, A., & Manousiouthakis, V. (2003). IDEAS approach to the synthesis of globally optimal separation networks: application to chromium recovery from wastewater. *Advances in Environmental Research*, 549-562.

Kumar, A., Baldea, M., Edgar, T., & Ezekoye, O. (2015). Smart manufacturing approach for efficient operation of industrial steam-methane reformers. *Industrial & Engineering Chemistry Research*, 4360-4370.

Latham, D. A., McAuley, K. B., Peppley, B. A., & Raybold, T. M. (2011). Mathematical modeling of an industrial steam-methane reformer for on-line deployment. Fuel Process. *Fuel Process. Technol*, 1574-1586.

Lédé, J., Lapicque, F., Villermaux, J., Cales, B., Ounalli, A., Baumard, J., & Anthony, A. (1982). Production of hydrogen by direct thermal decomposition of water: preliminary investigations. *International Journal of Hydrogen Energy*, 939-950.

Leiby, S. (1984). Options for refinery hydrogen PEP report no. 212, process economic program. *SRI International*.

Manousiouthakis, V. (2008). On dimensionality of attainable region construction for isothermal reactor networks. *Computers & Chemical Engineering*, 439-450.

Manousiouthakis, V., Albassam, A., & Conner, J. (2017). *United States Patent No. US 20,170,001,862.*

Manousiouthakis, V., Justanieah, A., & Taylor, L. (2004). The Shrink–Wrap algorithm for the construction of the attainable region: an application of the IDEAS framework. *Computers & chemical engineering*, 1563-1575.

Martin, L., & Manousiouthakis, V. (2003). Globally optimal power cycle synthesis via the Infinite-DimEnsionAl State-space (IDEAS) approach featuring minimum area with fixed utility. *Chemical engineering science*, 4291-4305.

May, D., & Rudd, D. (1976). Development of solvay clusters of chemical reactions. *Chemical Engineering Science*, 59-69.

McGreavy, C., & Newmann, M. W. (1968). Development of a mathematical model of a steam methane reformer. *Conference on the Industrial Applications of Dynamic Modelling.* Durham, NC.

Newsome, D. S. (1980). The Water-Gas Shift Reaction. *Catalysis Reviews: Science and Engineering*, 275-318.

Olivieri, A., & Veglio, F. (2008). Process simulation of natural gas steam reforming: Fuel distribution optimization in the furnace. *Fuel Process.Technol*, 622-632.

Peters, M. S., Timmerhaus, D. K., & West, R. E. (2003). *Plant Design and Economics for Chemical Engineers* (Fifth ed.). New York: McGraw-Hill.

Pichardo, P., & Manousiouthakis, V. (2017). Infinite DimEnsionAl State-space as a systematic process intensification tool: Energetic intensification of hydrogen production. *Chemical Engineering Research and Design*, 372-395.

Poullikkas, A. (2009). Economic analysis of power generation from parabolic trough solar thermal plants for the Mediterranean region—A case study for the island of Cyprus. *Renewable and Sustainable Energy Reviews*, 2474-2484.

Rotstein, D., Resasco, E., & Stephanopoulos, G. (1982). Studies on the synthesis of chemical reaction paths—I: Reaction characteristics in the (ΔG, T) space and a primitive synthesis procedure. *Chemical Engineering Science*, 1337-1352.

Schellnhuber, H. J., Rahmstorf, S., & Winkelmann, R. (2016). Why the right climate target was agreed in Paris. *Nature Climate Change*, 649-653.

Turchi, C., Mehos, M., Ho, C., & Kolb, G. (2010). Current and future costs for parabolic trough and power tower systems in the US market. *SolarPACES*.

Twigg, M. (1989). *Catalyst handbook.* England: Wolfe Publishing Ltd.

Udengaard, N. R. (2017, May 18). Hydrogen Production by Steam Reforming of Hydrocarbons. *49*, 906-907. Retrieved from Argonne National Lab: https://web.anl.gov/PCS/acsfuel/preprint%20archive/Files/49_2_Philadelphia_10-04_1205.pdf

Ursua, A., Gandia, L., & Sanchis, P. (2012). Hydrogen production from water electrolysis: current status and future trends. *Proceedings of the IEEE*, 410-426.

Von Hofmann, A. W. (1866). *Introduction to Modern Chemistry: Experimental and Theoretic; Embodying Twelve Lectures Delivered in the Royal College of Chemistry, London.* . London: Walton and Maberly.

Wilson, S., & Manousiouthakis, V. (2000). IDEAS approach to process network synthesis: Application to multicomponent MEN. *AIChE Journal*, 2408-2416.

Zamaniyan, A., Ebrahimi, H., & Mohammadzadeh, J. S. (2008). A unified model for top fired methane steam reformers using three-dimensional zonal analysis. *Chem. Eng. Process*, 946-956.

Zhou, W., & Manousiouthakis, V. (2006). Non-ideal reactor network synthesis through IDEAS: Attainable region construction. *Chemical Engineering Science*, 6936-6945.

Zhou, W., & Manousiouthakis, V. (2007). Variable density fluid reactor network synthesis—construction of the attainable region through the IDEAS approach. *Chemical Engineering Journal*, 91-103.

Chapter 3: Technical Economic Analysis of an Intensified Integrated Gasification Combined Cycle (IGCC) Power Plant Featuring a Sequence of Membrane Reactors

3.1 Abstract

In this work, a technical economic analysis (TEA) is carried-out for the design of an Integrated Gasification Combined Cycle (IGCC) power plant featuring a sequence of hydrogen-permeable ceramic membrane reactors (MRs). The proposed design features membrane reactors that generate hydrogen of higher purity than conventional reactor-separator systems used in IGCC plants, and enable over 90% carbon capture in the Dual-Stage Selexol unit. A multi-scale model is used to simulate the proposed MR sequence, and a commercial process flowsheet simulator is used to create the proposed intensified MR IGCC plant flowsheet, which is subsequently heat integrated. The TEA developed for the MR IGCC power plant allows for the economic characteristics of its design to be compared with those of a traditional IGCC plant equipped with carbon capture storage (CCS) technology.

3.2 Introduction

Currently (2016), over 60% of energy production in the United States (US) employs fossil fuels, such as coal, petroleum, and natural gas [1]. Each year, approximately 6,870 million metric tons (MMT) of greenhouse gases are emitted into the atmosphere, over 80% of which is in the form of CO_2 [2]. As a result, the United States Environmental Protection Agency (EPA) has begun planning environmental policies that may eventually penalize companies generating substantial amounts of CO_2. The current standard in the USA for CO_2 emissions is a maximum of 1,000 lbs of CO_2/MWh of electricity produced in new natural gas power plants, and 1,400 lbs of CO_2/MWh of electricity produced in new coal power plants, according to the recently proposed Affordable Clean Energy (ACE) Rule [3,4]. These limits on emissions will make it necessary in the future for all new US coal power plants to include CCS technology.

CCS involves capturing the CO_2 emitted from the burning of fossil fuels, safely transporting it and storing it underground. Several of these CCS technologies have already been integrated into power plants to capture at minimum 90% of the emitted carbon, including the world's largest post-combustion carbon capture project (the Petra Nova coal-fueled power plant in Texas [5]). The CO_2 captured in this plant is supplied for enhanced oil recovery (EOR), which serves as an additional revenue source for the power plant. There currently exist three different methods for carbon capture: pre-combustion, oxyfuel combustion, and post-combustion CO_2 capture. Pre-combustion CO_2 capture involves gasifying coal to produce syngas, which is a mixture of mostly hydrogen (H_2), carbon monoxide (CO), and CO_2, which then undergoes the water-gas-shift (WGS) reaction that uses H_2O to convert the CO into H_2 and CO_2, which is then separated from the syngas for storage underground or sold as raw material, while the H_2 is used to produce electricity in fuel cells or turbines [6]. Oxy-fuel combustion utilizes an Air Separation

Unit (ASU) to remove N_2 from air, and then utilizes the O_2 in the combustion of coal to produce electricity. The flue-gas generated contains mostly CO_2 and water vapor, from which the CO_2 can be readily separated to be stored underground [7]. The last CCS method, i.e., post-combustion CO_2 capture, involves the direct removal of the CO_2 from the flue-gas after the fossil fuel has been burned to produce electricity [8,9].

Previous research on the implementation and economics of conventional and reactive membrane technology in coal-fired power plants has been carried-out for all three different CCS methods [10–12]. While membrane-based oxy-fuel combustion and pre-combustion CO_2 capture power plants were found favorable compared to the post-combustion route, the conclusion of all prior studies was that membrane-based processes are not, as yet, suitable for commercial implementation, and they still require extensive research and development before their commercial implementation [10]. Our team has extensive experience with the use of MRs [13–24], including a recent experimental study on their use in power generation for pre-combustion CO_2 capture. The MRs make use of hydrogen-selective carbon molecular sieve (CMS) membranes, and of a sulfur-tolerant catalyst for carrying-out the WGS reaction [15]. The present study focuses on the implementation of such MRs for pre-combustion CCS in an IGCC plant. The proposed design features a sequence of MRs, using H_2-permeable CMS membranes, that is used to produce a high-purity H_2 stream (known as the permeate stream) as well as a stream consisting mostly of CO_2, unreacted CO, H_2O, and H_2 (known as the reject stream) that is further processed through a Dual-Stage Selexol unit to generate clean syngas for power generation, and pure CO_2 for sequestration.

Both multi-scale single system models and process flowsheet models, widely used in the chemical reactor field [25–28], will be implemented in the proposed design.

The rest of the paper is structured as follows: the proposed MR IGCC plant is presented, and the MRs utilized in the design are described in detail, including the governing equations utilized in the MR model. Next, a flowsheet implementation of the proposed design in a commercial simulator is presented. Subsequently, the economic and technical analysis of the presented flowsheet is described. Finally, the obtained results are discussed, and conclusions are drawn.

3.3 Realization of the Proposed IGCC Plant Featuring a Sequence of Membrane Reactors

The standard IGCC plant with pre-combustion CCS is depicted in Figure 3-1 [29]. Coal is mixed with water to create a slurry which is fed into a gasifier to generate syngas. Steam is mixed with this syngas to obtain the desired H_2O:CO molar ratio, and the mixture is then fed into a WGS reactor. The reactor's outlet stream, which consists mostly of H_2 and CO_2 together with small amounts of unreacted CO and of impurities like mercury and various sulfur compounds, then

undergoes clean-up to remove the mercury and sulfur impurities, and gas separation, to generate a H_2-rich syngas stream, and a relatively pure CO_2 stream for sequestration and/or EOR.

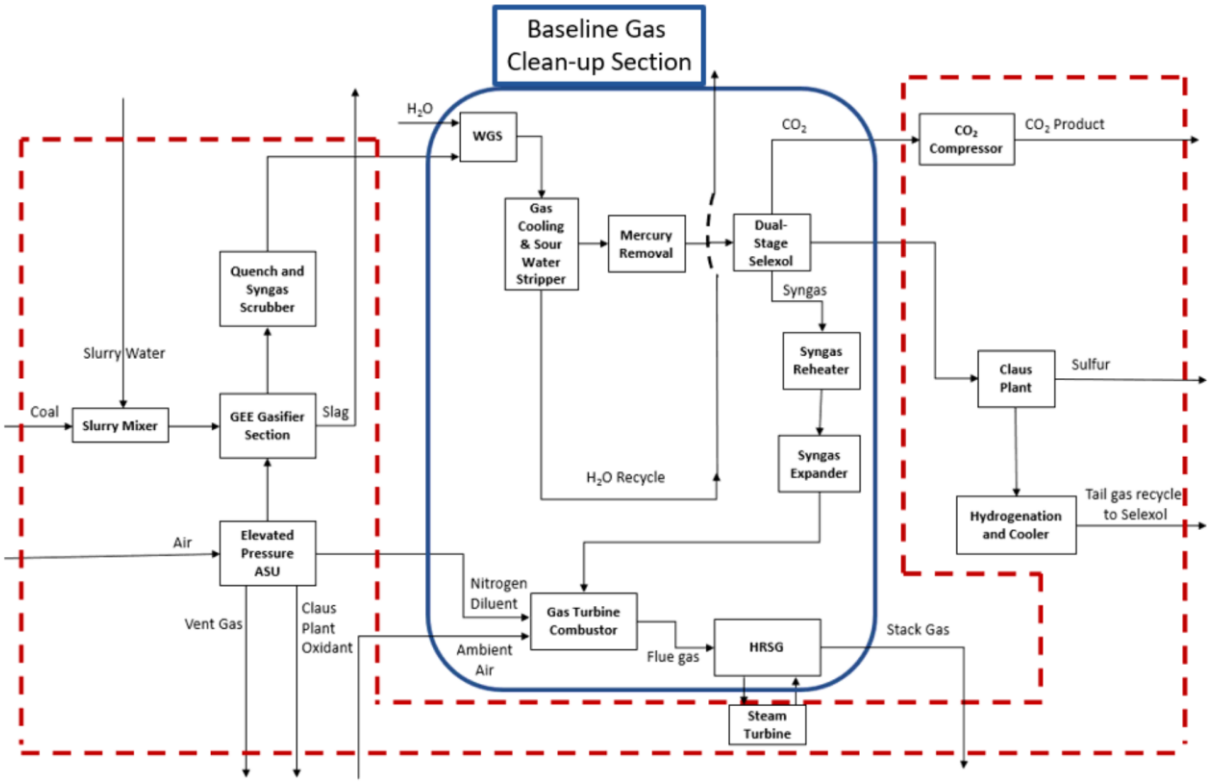

Figure 3-1: *Baseline design of an IGCC pre-combustion CCS plant [29]*

The H_2-rich syngas is heated, in preparation for expansion, before it is fed into the Gas Turbine Combustor to produce power. This design is used as the baseline to which our proposed MR-based power plant will be compared. A schematic of the latter plant can be seen in Figure 3-2. In this design, the WGS reactor section of the baseline plant (within the blue block in Figure 3-1) is replaced with a WGS-MR section (blue block in Figure 3-2). The red dashed box in both Figures 3-1 and 3-2 encompasses the sections of the plant with identical inlet and outlet streams for both designs.

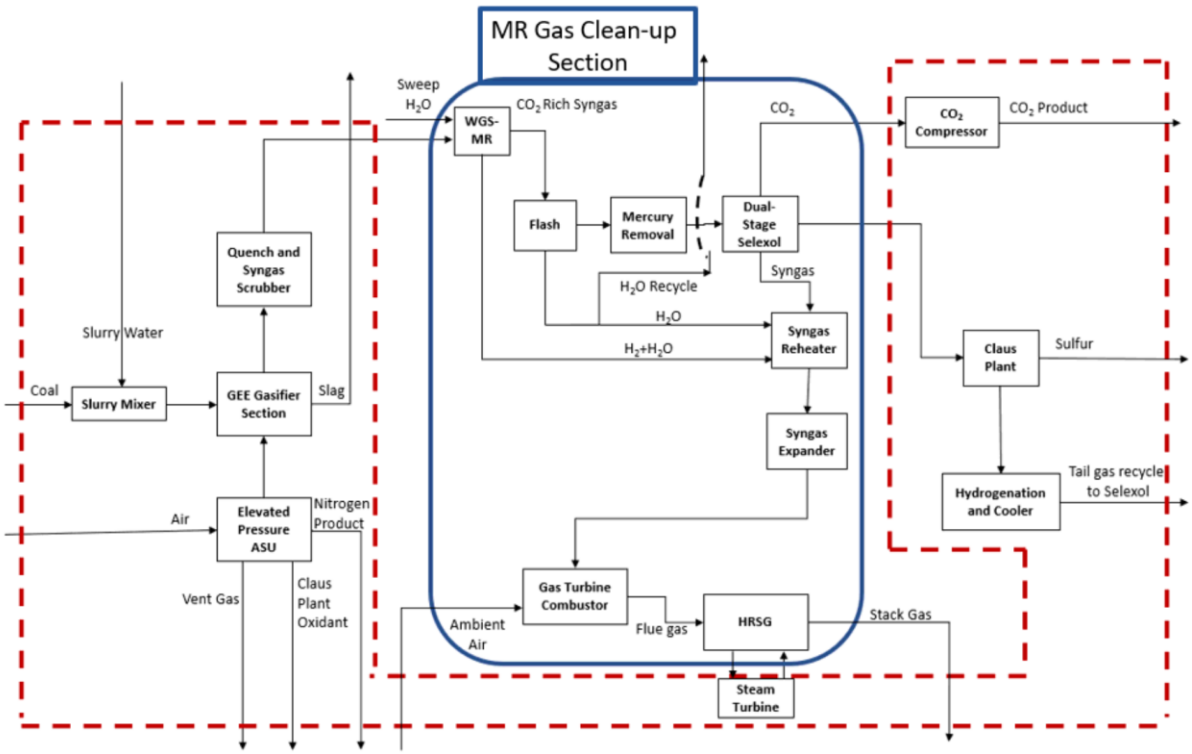

Figure 3-2: *A schematic of our proposed IGCC plant featuring a sequence of MRs*

The retentate stream of the WGS-MR is cooled to undergo a knock-out step, with the water recovered from the flash unit being sent to the Gas Turbine Combustor as hydrogen diluent, while the remainder stream is sent to a Dual-Stage Selexol unit to generate a H_2-rich syngas stream, and a relatively pure CO_2 stream for sequestration and/or EOR. The syngas stream is then mixed with the WGS-MR permeate stream that consists primarily of hydrogen and steam, and is then used once again in power generation. This process schematic is implemented into the commercial simulator UNISIM (Honeywell^{TM}) to create a process flowsheet.

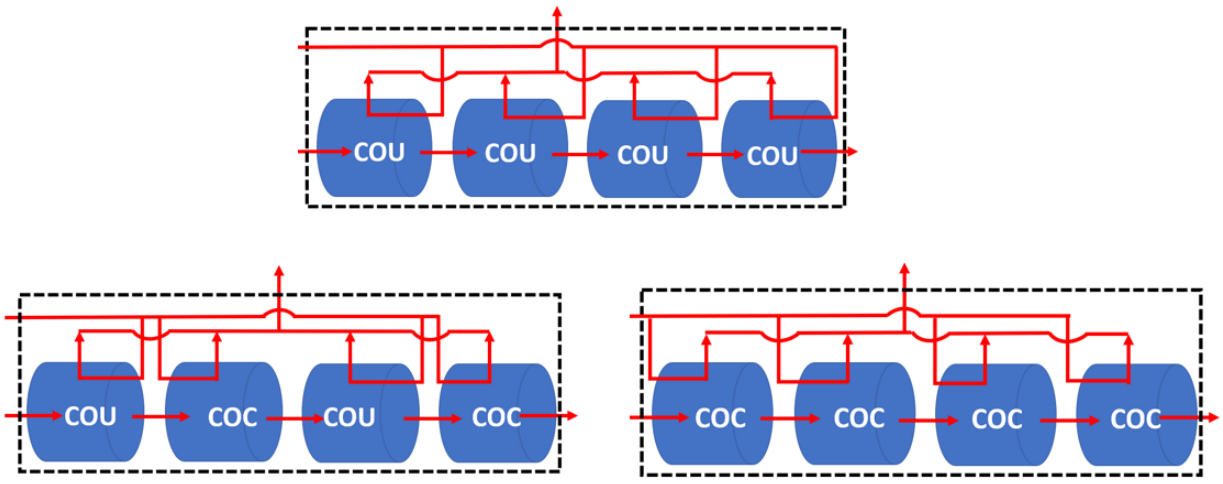

Figure 3-3: *A schematic of the configuration for the sequence of MRs implemented into the MR IGCC plant, where COU refers to counter-current and COC refers to co-current.*

In this work, three different configurations of the WGS-MR's sequence of MRs are considered (Figure 3-3): a sequence of four counter-current (COU) reactors; a sequence of four co-current (COC) reactors; and a sequence of four counter-current/co-current reactors alternating in order. The MR sequence inlets are syngas (bottom left), and steam (top left) used as sweep in the permeate side, while its outlets are the combined permeate stream from all MRs (top), and the retentate stream of the last MR (right).

3.4 Membrane Reactor Details

The membrane reactor consists of a pressure vessel that houses several membrane bundles, each bundle consisting of multiple CMS membrane tubes. The bundles can be configured in either a candle-filter design or in an open-ended design. These bundles, typically, consist of 85-100 CMS membrane tubes, with inner and outer diameters of 3.5 mm and 5.7 mm, respectively, and a length of 1 m. The open-ended design has both membrane tube ends open, thus allowing permeate side sweep, while the candle-filter design has one membrane tube end closed and is, typically, used

under no sweep conditions. Each membrane tube bundle is encased in its own individual stainless-steel module. In the MR design employed here a number of these aforementioned modules are encased in a large pressure vessel, which can withstand the high pressures of the off-gas exiting the coal gasifier. In this work, the configuration of bundle modules inside the pressure vessel can be seen in Figure 3-4. The bundles are arranged so that there are 900 bundle series across the pressure vessel's cross-section, each of which contains 6 bundles along its length. Bundles operating in a series allow the retentate stream exiting one bundle to enter the next bundle in the series, while each bundle series is fed by the pressure vessel's inlet stream, which is split equally amongst all parallel bundle series. The permeate streams of all bundles are mixed together to form the pressure vessel's (MR's) permeate stream.

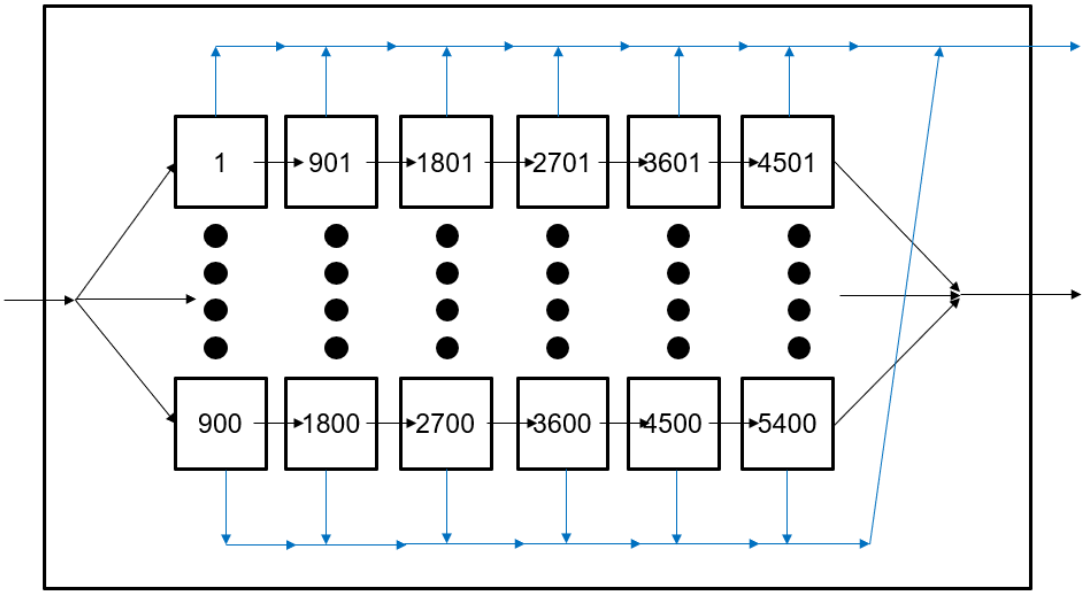

Figure 3-4: *Depiction of the bundle module configuration inside the pressure vessel comprising an MR*

Table 3-1 shows the details of the MRs utilized in the proposed IGCC design, where D_{Ti} is the CMS membrane tube inner diameter (m), D_{To} is the membrane tube outer diameter (m), L_T is the length of the membrane tube (m), D_{Bi} is the bundle module's inner diameter (m), D_{Bo} is the bundle module's outer diameter (m), L_B is the length of the bundle module (m), D_{Vi} is the pressure vessel's inner tube diameter (m), D_{Vo} is the pressure vessel's outer tube diameter (m), L_V is the length of the pressure vessel (m), N_T is the number of the membrane tubes in a bundle, and N_{bv}^c, N_{bv}^l are the numbers of bundle module series and the number of bundle modules in a series, along the length of the pressure vessel, respectively. The outer diameter of the membrane is utilized in the calculation of the surface area available to transport since the catalyst bed is packed in the annular space in between the membranes and the reactor wall. In addition, for these membranes the selective CMS layer lies on their outer surface.

Table 3-1: *Parameters and their values utilized in the membrane reactor simulations*

D_{Ti}	3.5 mm
D_{To}	5.7 mm
L_T	1 m
D_{Bi}	98.55 mm
D_{Bo}	101.6 mm
L_B	1 m
D_{Vi}	4.27 m
D_{Vo}	4.28 m
L_V	6 m
N_T	85
N_{bv}^c	900
N_{bv}^l	6

Based on the above parameter values, the following MR characteristics can then be evaluated:

$$\text{Total Membrane Surface Area} = N_{bv}^{c} \cdot N_{bv}^{l} \cdot N_T \left(\pi D_{To} L_T \right) \quad (1)$$

$$\text{Pressure Vessel Volume} = \frac{\pi}{4} D_{Vi}^2 L_V \quad (2)$$

$$L_V = N_{bv}^{l} L_B \quad (3)$$

The packing density, defined as (total membrane surface area)/(pressure vessel volume), of 94.5 m^2/m^3 is assumed for our simulations. The current membrane bundles produced by Media Process and Technology (MP&T) have a packing density of 31.5 m^2/m^3, while their ideal packing density is 500 m^2/m^3. Thus, the current MR configuration leaves a significant amount of empty space. For this reason, an increased packing density value of 94.5 m^2/m^3 was chosen as a realistic alternative, between the current and the ideal packing densities. This proposed packing density is approximately 3 times that of the current packing density, which is achievable by using an 8" membrane bundle and a face seal versus the currently used radial seal.

In addition, it is considered that each bundle contains catalyst pellets packed around the ceramic membrane tubes. The employed catalyst is KATALCOJM™ K8-11HA, which has a density of 40 lb/ft^3 (640.7 kg/m^3) and costs \$700/ft^3 (\$24,720/m^3). The membrane tube manufacturer MP&T prices their membrane tube bundles on the basis of membrane surface area at \$1,200/m^2. Table 3-2 lists the membrane permeances for the CMS tubes used in the simulataions. These permeance values were taken directly from our previous experimental work studying the MR in the production of hydrogen from coal-derived syngas [15], and are also typical of the values M&PT reports for these membranes.

Table 3-2: *Membrane permeance values used in the membrane reactor simulations*

H_2	H_2O	CO	CO_2	CH_4
$1\ \frac{m^3(STP)}{m^2\ h\ bar}$	$0.333\ \frac{m^3(STP)}{m^2\ h\ bar}$	$0.0027\frac{m^3(STP)}{m^2\ h\ bar}$	$0.0018\frac{m^3(STP)}{m^2\ h\ bar}$	$0.0027\frac{m^3(STP)}{m^2\ h\ bar}$
$44.64\frac{mol}{m^2\ h\ bar}$	$14.87\frac{mol}{m^2\ h\ bar}$	$0.1205\frac{mol}{m^2\ h\ bar}$	$0.0804\frac{mol}{m^2\ h\ bar}$	$0.1205\frac{mol}{m^2\ h\ bar}$
370.3 GPU	*123.3* GPU	*1* GPU	*0.6667* GPU	*1* GPU

$$*1\ \text{GPU} = 0.0027\frac{m^3(STP)}{m^2\ h\ bar} = 0.1206\frac{mol}{m^2\ h\ bar}$$

The flow inside each ceramic tube (permeate stream) can be either cocurrent (COU) or countercurrent (COC) to the flow outside the tube (retentate stream). When the flow configuration is cocurrent (countercurrent), the permeate flow follows in the same (in the opposite) direction as the retentate flow of the reactor.

3.4.1 COMSOL MR Model Description and Simulations

In this study, we model the MR shown in Figure 3-5 as a multi-scale [30], multiphase system that performs different process functions in its various zones. From a physical standpoint, the reaction zone in the MR is modeled at two different scales: the so-called microscale, which considers pellet-scale features, including average pore size, reaction rates, pellet material properties, and pellet shape; and the macroscale, which considers reactor-scale features, including membrane module dimensions, membrane tube characteristics, and catalyst packing void fraction.

The permeation zone is modeled at the macroscale level only, since it contains no catalyst and/or

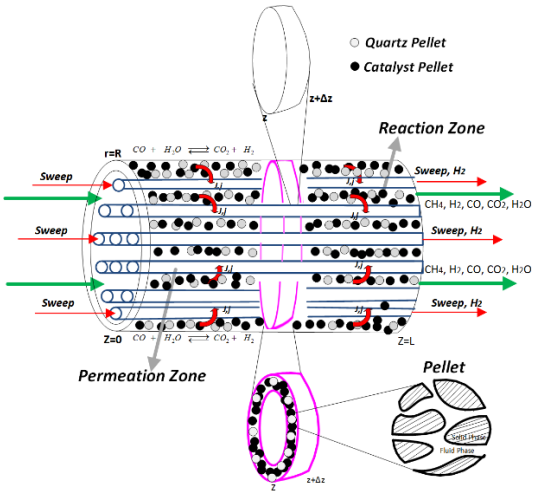

Figure 3-5: *Diagram of the membrane reactor that is being simulated*

adsorbent pellets. In the model, these MR regions are modeled as individual domains, so that one can properly assess the contribution of each of their parameters to the overall system performance. Regardless of the length scale, phase, or region of the system, conservation laws must hold. Thus, in the derivation of the MR model equations, the Reynolds transport theorem (RTT) is applied separately to each of the MR domains: the pellet domain, the reactor domain, and the permeation zone domain.

Computations in the three domains (catalyst pellet, reactor, and permeation zones) are coupled, e.g., information regarding gas pressure, temperature, velocity, and species' concentrations in the reactor domain is provided to the pellet and permeation domains, while temperature and effectiveness factor information in the catalyst pellet domain and temperature of the inert pellet domain are provided to the reactor domain. The conservation equations are simultaneously solved for each domain by COMSOL Multiphysics®. The full model description and equations can be found in [31]. The full set of equations can also be found in the Appendix of this paper.

The membrane reactor model detailed in the previous section is used to simulate in COMSOL six membrane bundles operating in series, where the first bundle's feed has the same composition as that of the stream entering the MR from the IGCC, while the retentate exit of each bundle is the retentate feed to the next bundle. (It should be noted, that in the simulations it is assumed that no H_2S permeation occurs. The H_2S permeance values we measure with these membranes are, typically, at or below the values for methane [15, 24]; in the laboratory but also in the field-testing of these membranes [32], the H_2S concentrations in the permeate-side stream are below the threshold of concern for power generation in a turbine). As detailed above, a single MR vessel contains 900 bundle series across its cross-section operating in parallel, with each series having 6 bundles along its length. For this reason, in the simulations the total flow rate of the IGCC plant is split evenly amongst the bundle series operating in parallel allowing for the MR to be modeled as 6 bundles operating in series. It is reasonable to consider that the other bundle series operating in parallel across the MR vessel's cross-section will behave in exactly the same way as the simulated single 6-bundle series. The exit (retentate) of the WGS-MR (i.e., the 6 bundles in series) is then cooled to a temperature for which the mixture remains a gas (see further discussion below), before being fed into the next WGS-MR (i.e., the next series of 6 bundles). This is done throughout the MR reactor vessel sequence, regardless of the sweep configuration used.

Prior to the UNISIM implementation, several WGS-MR simulations were run utilizing COMSOL for different MR operating modes. Three modes (with all implementing inter-stage cooling in between each MR) were investigated: a sequence of four WGS-MRs operating co-currently; a sequence of four WGS-MRs operating counter-currently; and a sequence of four WGS-MRs alternating counter-currently, co-currently, counter-currently, and co-currently. Since the baseline design [29] features four WGS reactors in series with inter-stage cooling, a

configuration of four WGS-MRs in series with inter-stage cooling was chosen, that ensures an MR inlet temperature of 500K, the lowest potential temperature that still ensures that the water component in the syngas mixture remains in the gas phase as steam. In addition, the inlet conditions for all MR sequences were taken from the baseline IGCC design [29], whose WGS reactor inlet has a flow rate of 29,284 kmol/hr, with a feed composition of CO, CO_2, H_2O, H_2 = 0.2823, 0.1089, 0.3190, 0.2689, with the remaining components being a mixture of inert species. NETL's baseline design also inputs additional steam to reach a H_2O:CO ratio of 2:1, while the MR design does not require this additional steam in the retentate. These results are summarized below in Figure 3-6 and Table 3-3, where the total reactor conversion of the sequence is depicted, as well as the

conversion of each individual MR, and the percent of the total outlet that comes out of the permeate side of each MR.

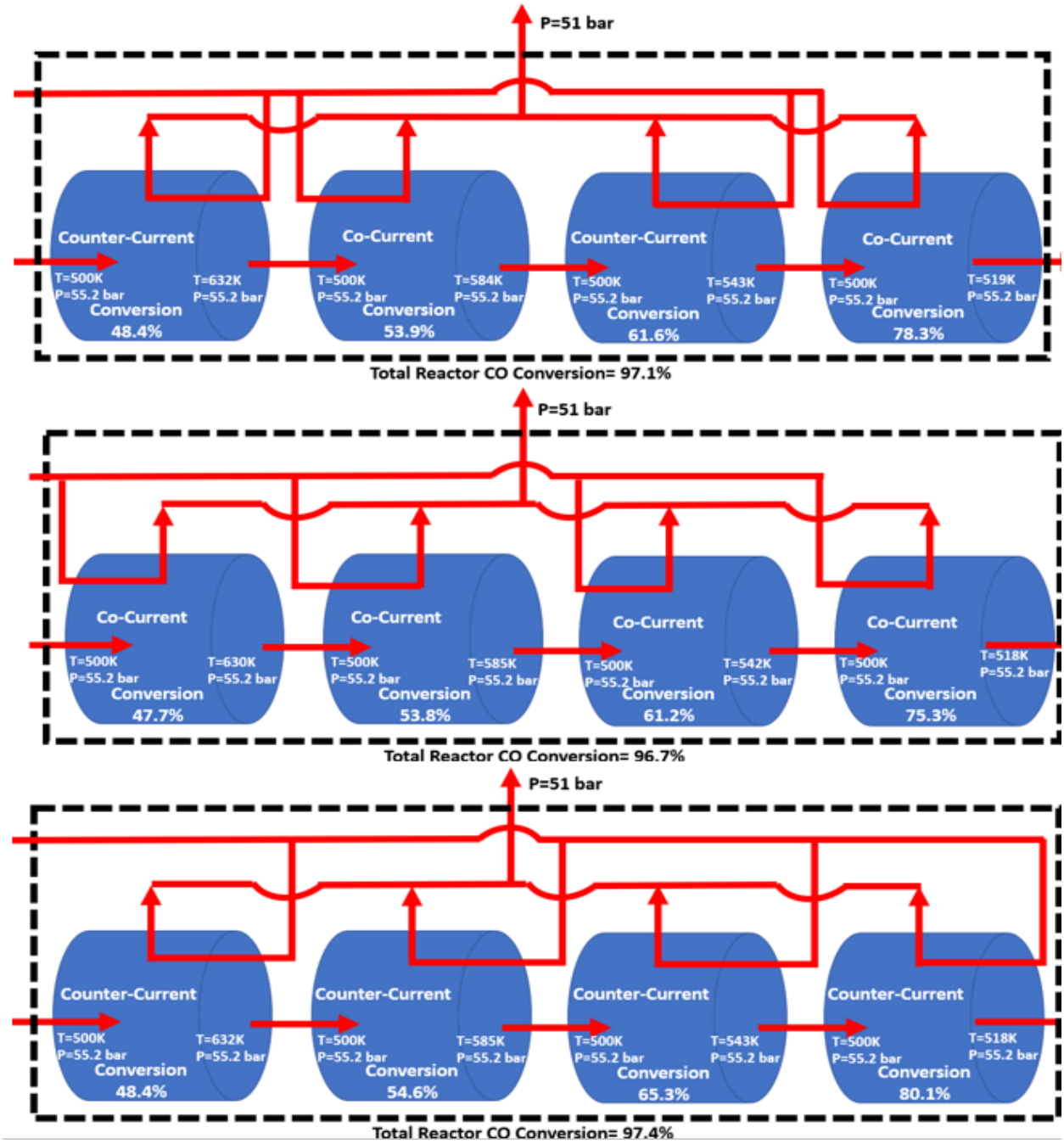

Figure 3-6: *Results for different operational configurations of a sequence of four MRs*

As can be seen from Figure 3-6 and Table 3-3, the best configuration is a sequence of four MRs operating counter-currently, since it yields the highest total conversion (97.4%), with a permeate stream consisting of 54.1% of the total H_2 exiting, 45.3% of the total H_2O exiting, 2.15% CO_2 exiting, and 39.9% of the total CO exiting. The amount of carbon (CO and CO_2) leaked to the permeate stream accounts for approximately 2.85% of the total carbon, allowing for a >90% carbon capture scenario to be possible. The result of the sequence of 4 MRs operating counter-currently was implemented into a process flowsheet utilizing Honeywell's UNISIM software.

Table 3-3: *Stream information for MR sequences depicted in Figure 3-6*

	Inlet Flow to each configuration		**Co-Current / Counter-Current**		**Co-Current**		**Counter-Current**	
	Inlet-gas	Steam-Sweep	Permeate	Retentate	Permeate	Retentate	Permeate	Retentate
CO	0.2823	0.0000	0.0044	0.0049	0.0046	0.0059	0.0044	0.0041
CO2	0.1089	0.0000	0.0155	0.3451	0.0129	0.3469	0.0125	0.3488
H2	0.2689	0.0000	0.4444	0.2329	0.4419	0.2325	0.4460	0.2320
H2O	0.3190	1.0000	0.5351	0.3982	0.5401	0.3957	0.5365	0.3961
Inert	0.0209	0.0000	0.0006	0.0190	0.0006	0.0191	0.0006	0.0190
Flow Rate (kgmol /h)	29284	21559	19201	31642	19324	31519	19310	31533

The depiction of the UNISIM developed flowsheet can be seen in Figure 3-7. In order to simulate a MR accurately, the results from the COMSOL WGS-MR simulations are used to produce a process unit in UNISIM that takes in the same process flow stream as the simulated MR, and produces an identical outlet process flow stream. This is done in the UNISIM simulation environment using a combination of a conversion reactor and an ideal separator, essentially acting

as a black-box unit that can reproduce the modeled WGS-MR. This reactor/separator combination can be seen encased in a black-box labeled membrane reactor in Figure 3-7. This combination of a conversion reactor and ideal separator to simulate an MR has identical inlet and outlet flowrates as the MR COMSOL simulation. In addition, the inlet to the sequence of MRs is identical to the inlet of the traditional IGCC pre-combustion CCS plant shown in Figure 3-1 [29].

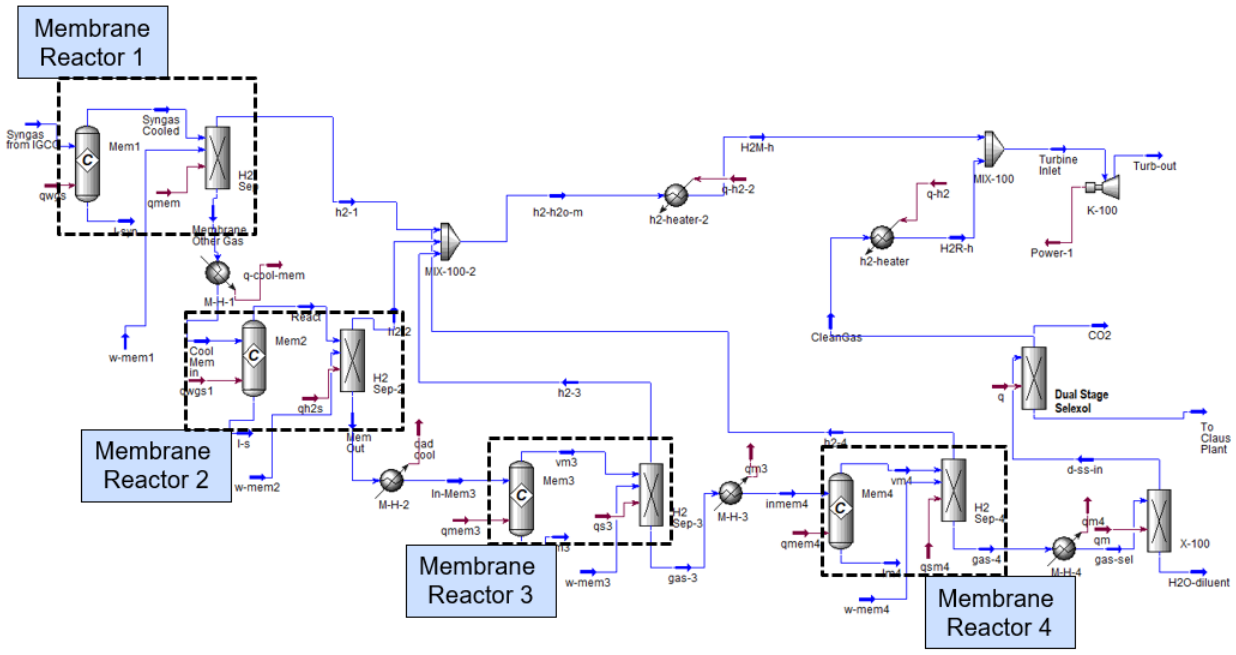

Figure 3-7: *UNISIM implementation of the proposed IGCC with CCS implementing a sequence of 4 MRs operating counter-currently.*

The exothermicity of the WGS reaction, combined with the requirement that the inlet temperature of each MR in the sequence is at (or below) 500K, necessitate that inter-stage cooling must be employed. The outlet of the 4-MR sequence is then cooled once more, before undergoing a series of separation steps. The first of these separators is a flash unit that removes the excess water from the system, which is then recycled to the WGS-MRs. The vapor outlet of the flash

separator is fed into a Dual-Stage Selexol unit that removes first the sulfur (which is sent to a Claus Plant for post-processing), and then removes a pure CO_2 stream (which is sent for sequestration). The remaining hydrogen-rich gas mixture is then mixed with the high-purity hydrogen from the permeate side of the MR sequence that has also been cooled and passed through a flash separator. The resulting mixture, containing 93.3% hydrogen, is heated and then combusted/expanded for power generation purposes. Figures 3-8 and 3-9 depict, in a stream input-output block diagram form, the hatched sections of the IGCC plant in Figures 3-1 and 3-2, where the proposed MR modifications are implemented.

An important feature to be noted in the MR-based IGCC plant is the excess steam to be used as sweep for the sequence of counter-current MRs and to subsequently be used as diluent for the gas turbine combustor. The use of water as diluent allows for all of the N_2 produced in the IGCC's Air Separation Unit (ASU) to be sold as product. Table 3-4 shows the associated molar compositions of the streams displayed in Figures 3-8 and 3-9. The units prior to the Gas-Cleanup Section have identical inlet and outlet streams for both the baseline and MR design, while the units following the Gas-Cleanup Section have streams that are similar but not identical. This is illustrated in Figure 3-1 and 3-2 with the red dashed box identifying all units that have identical inlet and outlet streams. Since these units are unchanged between the baseline and MR design, then the capital cost of these units is identical in both designs. The pure CO_2 stream produced by the MR plant and baseline design are both approximately 90% of the total carbon in the plant with identical pressure and temperature conditions. Therefore, considering the conditions and flow rate are the same, it is assumed that the subsequent sequestration units for the baseline and MR plants are identical. Similarly, the inlet of the Claus Plant contains the same amount of sulfur for both the baseline and MR plants with only a slight variation in the amount of CO_2 present in the inlet stream.

This difference is miniscule and, therefore, the Claus Plant is also assumed to be identical for both cases.

The Gas Turbine Combustor is the only post Gas-Cleanup plant component with significant inlet stream differences. Both the baseline and MR designs have the same amount of H_2 in the inlet stream, which is the source of the power generation, but differ in the diluents used to maintain the temperature below any level that may cause turbine corrosion. The overall process stream inlet flow to the Gas Turbine Combustor is equal, with the only major difference lying in the water and nitrogen concentrations. Due to the excess water required by the MRs for sweep operation, the MR plant has a significant amount of water that can be used as diluent to prevent excessive turbine temperatures. Utilizing the water as diluent allows for all of the N_2 produced via the ASU to be sold as product. The amount of diluent water fed to the Gas Turbine Combustor is thermodynamically analyzed through an equilibrium reactor, thus ensuring the water diluent works as effectively as the N_2. To account for the excess water used as diluent a maximum inlet rotor temperature of 1300°C is enforced to prevent turbine corrosion [29]. It is assumed that the power generation systems following the Gas-Cleanup Section are economically and energetically equal for the baseline and MR designs since the flow rate of the MR design is smaller than that of the baseline due to the larger specific heat of water when compared to nitrogen. Steam as diluent in hydrogen/oxygen combustion has been previously implemented by Mitsubishi Motors, where the turbine temperature is allowed to reach 1700°C, with an inlet steam mole fraction of 0.15 [33]. By contrast in the hydrogen/air/steam combustion proposed here, the maximum temperature of the proposed MR design is 1300°C, with an inlet steam mole fraction of 0.07. These assumptions are utilized in the following sections for both the heat integration and techno-economic analysis that is carried-out.

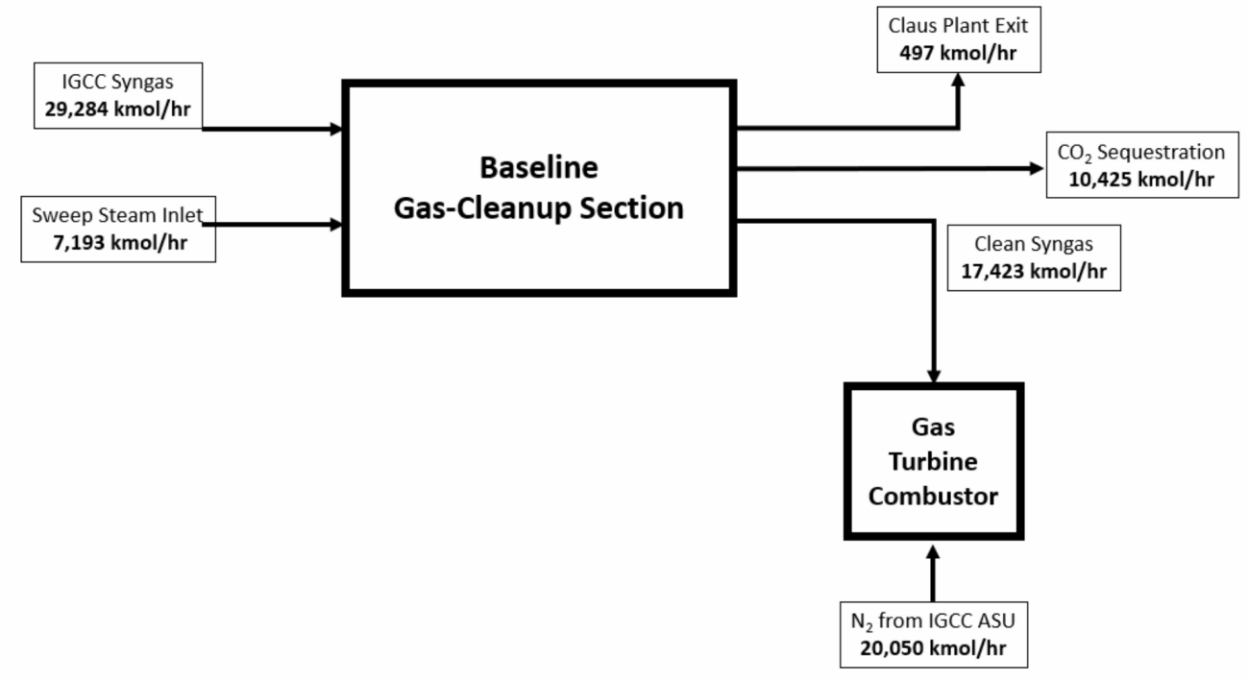

Figure 3-8: *Simplified block diagram depicting the gas-cleanup section of the baseline IGCC design*

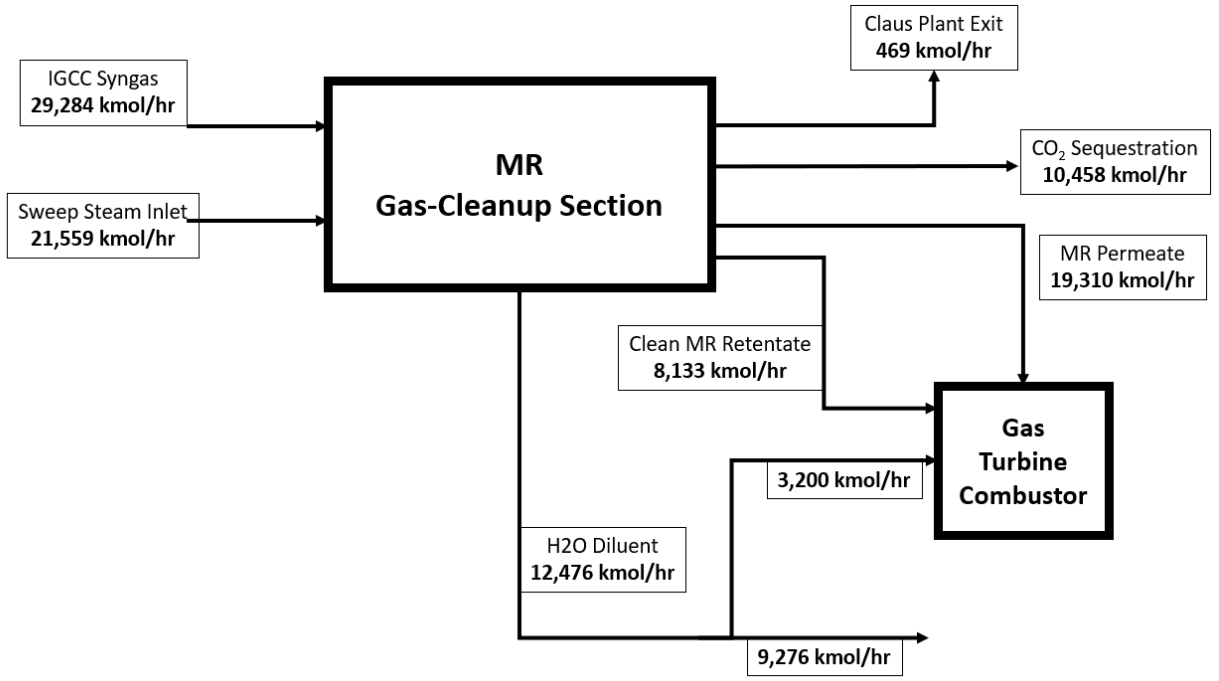

Figure 3-9: *Simplified block diagram depicting the gas-cleanup section of the proposed MR IGCC design*

Table 3-4: *Molar composition information for the streams featured in Figures 3-8 – 3-9*

Baseline Gas-Cleanup Section (Molar Composition)							
Stream Name	**IGCC Syngas**	**Sweep Steam Inlet**	**Claus Plant Exit**	**CO_2 Sequestration**	**Clean Syngas**	**N_2 from IGCC ASU**	
Temp (K)	479	561	321	324	514	366	
Pressure (bar)	55.2	55.2	1.6	1	51	26.5	
CO	0.28	0	0.01	0	0.01	0	
CO_2	0.11	0	0.52	0.99	0.02	0	
H_2O	0.32	1	0.02	0	0	0	
H_2	0.27	0	0.1	0.01	0.95	0	
N_2	0.006	0	0	0	0.01	0.99	
H_2S	0.006	0	0.35	0	0	0	
Ar	0.008	0	0	0	0.01	0	
O_2	0	0	0	0	0	0.01	

MR Gas-Cleanup Section (Molar Composition)							
Stream Name	**IGCC Syngas**	**Sweep Steam Inlet**	**Claus Plant Exit**	**CO_2 Sequestration**	**MR Permeate**	**Clean MR Retentate**	**H_2O Diluent**
Temp (K)	479	479	321	324	514	514	308
Pressure (bar)	55.2	55.2	1.6	1	51	51	55
CO	0.28	0	0.01	0	0	0.02	0
CO_2	0.11	0	0.53	1	0.01	0.043	0
H_2O	0.32	1	0.01	0	0.53	0	1
H_2	0.27	0	0.05	0	0.46	0.89	0
N_2	0.006	0	0.01	0	0	0.02	0
H_2S	0.006	0	0.38	0	0	0	0
Ar	0.008	0	0.01	0	0	0.027	0
O_2	0	0	0	0	0	0	0

3.5 Results and Discussion

The developed IGCC plant featuring WGS-MRs is able to capture >90% of the carbon entering the plant, maintaining the same CO conversion, H_2 recovery, and CO_2 purity and recovery numbers with the baseline design, as shown in Table 3-5 below.

Table 3-5: *Comparison of the baseline pre-combustion CCS IGCC plant with the IGCC plant featuring a sequence of WGS-MRs*

	% CO Conversion	**% H_2 Recovery**	**% CO_2 Purity**	**% CO_2 Recovery**

Baseline IGCC Plant with CCS [29]	97	98	99	90
MR IGCC Plant	97	98	99	90

However, due to the high-purity hydrogen produced in the permeate side of the WGS-MR sequence, the hydrogen content in the resultant fuel mixture employed for power generation is higher than that in the standard IGCC plant with CCS. Thus, the implementation of WGS-MRs into the IGCC plant is able to either meet or exceed the performance of the standard IGCC power plant with pre-combustion CCS. Table 3-6 shows the performance summary of both the baseline design, and the proposed IGCC plant featuring a sequence of WGS-MRs. The gross power produced via the Combustion Turbine and Steam Turbine by the MR-based IGCC plant is the same as for the traditional IGCC power plant, since the streams have the same quantity of H_2 and residual fuels, whereas the Sweet Gas Expander power is higher for the MR-based IGCC plant (The sweet gas expander step is the clean syngas expansion that takes place prior to the Gas Turbine Combustor). This is due to the significant amount of water that the MR permeate stream contains, which means that the flow rate of gas passing through the Sweet Gas Expander is significantly larger than the clean gas product of the baseline Dual-Stage Selexol unit. This, then, accounts for the difference in power generation between the baseline and MR-based IGCC designs.

Table 3-6: *Performance summary of the baseline IGCC with CCS plant compared to the proposed IGCC plant featuring WGSMRs*

Performance Summary	**Baseline IGCC** [29]	**MR IGCC**
Combustion Turbine Power, MWe	464	464
Sweet Gas Expander Power, MWe	7	11
Steam Turbine Power, MWe	264	264
Total Gross Power, MWe	**734**	**738**
Air Separation Unit Main Air Compressor, kWe	67,330	67,330

Oxygen Compressor, kWe	10,640	10,640
Nitrogen Compressors, kWe	35,640	35,640
CO_2 Compression, kWe	31,160	30,960
Acid Gas Removal, kWe	19,230	11,678
Balance of Plant, kWe	26,870	26,870
Total Auxiliaries, MWe	**191**	**183**
Net Power, MWe	**543**	**555**

As can be seen in Table 3-6, the MR-based IGCC plant has a slightly higher gross power and net power production than the baseline plant. Specifically, the MR IGCC plant produces 2.21% more net power than the baseline IGCC plant, because of the reduced power consumption in the CO_2 compression and acid gas removal steps (in addition to the increased power produced by the Sweet Gas Expander step) This decrease in power required for the removal of acid gas is due to the decreased flow rate processed by the Dual-Stage Selexol unit that only processes the reject-side stream, since in the sequence of MRs approximately 54% of the H_2 produced ends-up in the permeate stream that requires no further treatment. This reduction in power consumption was determined by first calculating the ideal work of separation of the Dual-Stage Selexol unit of the baseline IGCC plant and comparing it with that for the MR-based IGCC plant. The ideal work of separation (Eq. 4 [34] below) is utilized in this calculation, where $\dot{W}_{Ideal}$ is the ideal work of separation (kWe), F is the molar flow rate (mol/s), H is the molar enthalpy (kJ/mol), S is the molar entropy (kJ/mol K), T_σ is the environmental temperature (K), $i \in S_O$ denote the outlet flows, and $i \in S_i$ denote the inlet flows. The change in ideal work of separation from the proposed MR-based IGCC plant and the baseline IGCC plant is then used as an efficiency measure to reduce the

actual energy consumption of the baseline IGCC plant to determine the energy consumption of the proposed MR-based IGCC plant.

$$\dot{W}_{Ideal} = \sum_{i \in S_O} F_i \left(H_i - T_\sigma S_i \right) - \sum_{i \in S_I} F_i \left(H_i - T_\sigma S_i \right) \qquad (4)$$

All other auxiliary processes are thought to consume the same amount of power, since they are assumed to be identical for the baseline IGCC and the MR-based IGCC plants, because the rest of the plant is identical for both cases.

3.5.1 Heat Integration

Heat integration analyses were also carried-out for the baseline and MR-based IGCC cases. These analyses focused on the modified IGCC sections, depicted in the line-encircled boxes in Figures 3-1, 3-2, 3-8, and 3-9, and the results can be seen below in Figures 3-10 and 3-11. No hot utility is made available to the flowsheets, while two cold utilities are made available to the flowsheets where one of the cold utilities (steam at 470K) generates income, while the other (cooling water at 298K) generates expenses. The heat loads used in the heat integration are summarized in Table 3-7.

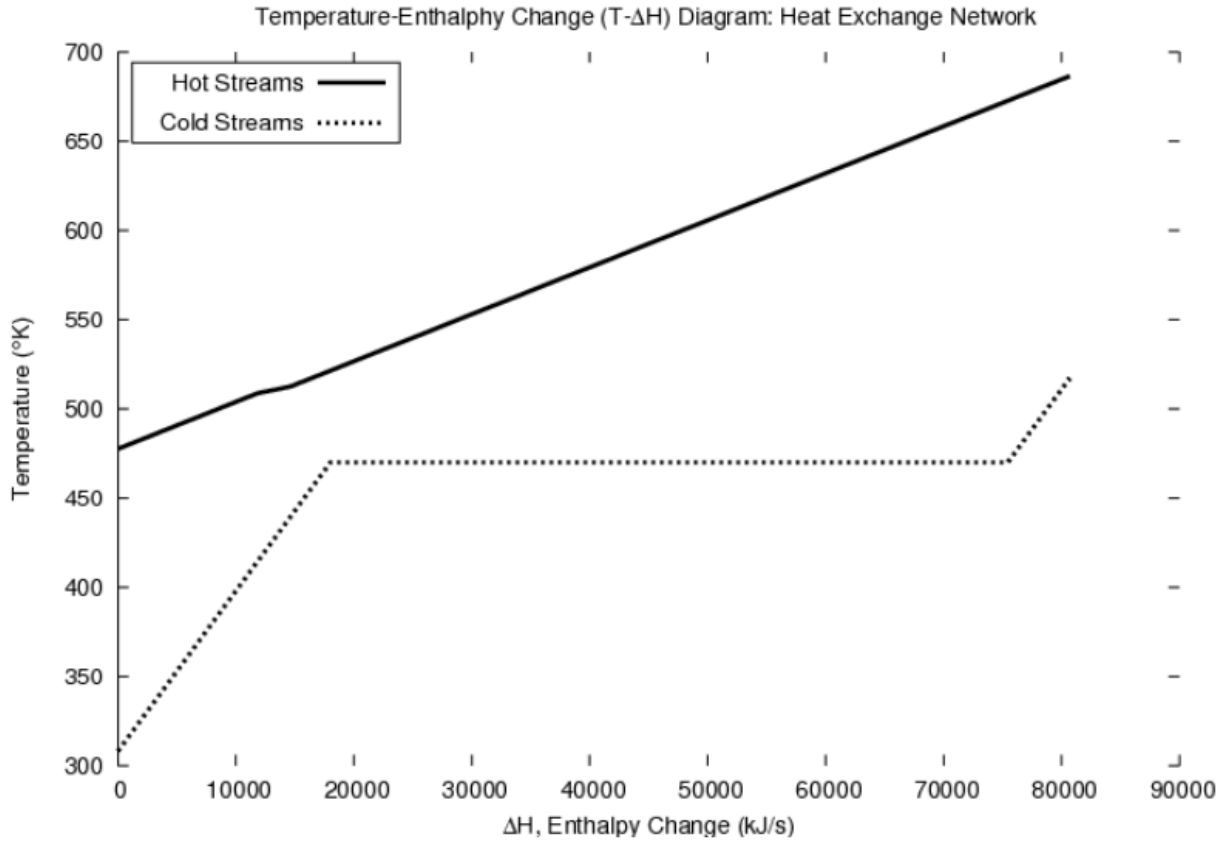

Figure 3-10: *Heat exchange network for the baseline IGCC case depicting the Temperature-Enthalpy change diagram*

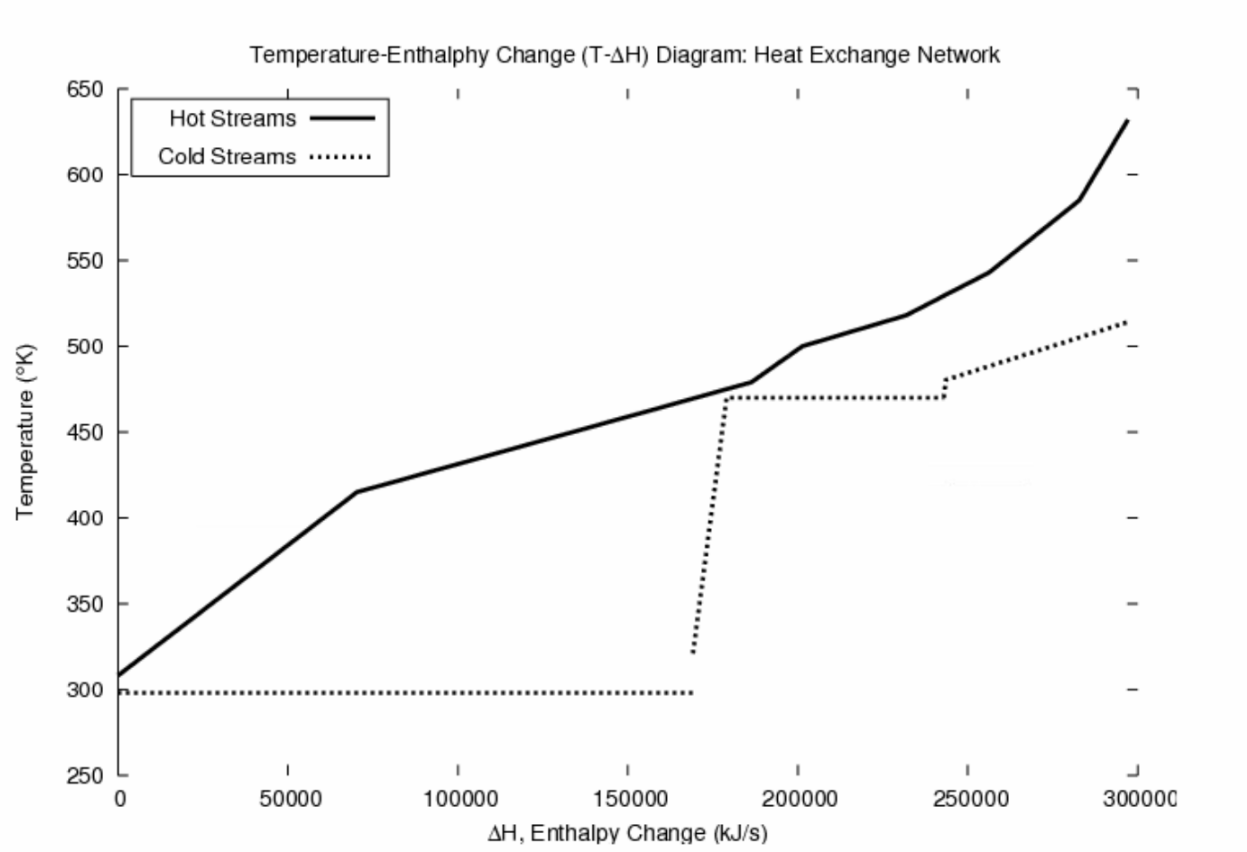

Figure 3-11: *Heat exchange network for the MR-based IGCC case depicting the Temperature-Enthalpy change diagram*

Table 3-7: *Heat loads associated with the baseline IGCC and MR IGCC plants*

Baseline IGCC				**MR IGCC**			
Unit	**T in**	**T out**	**Heat Load (kJ/s)**	**Unit**	**T in**	**T out**	**Heat Load (kJ/s)**
Gas Cooling	686	478	264840	**WGSMR-1**	632	500	40227
Gas Cooling	513	509	184119	**WGSMR-2**	585	500	27878
Syngas Reheater	308	517	-102001	**WGSMR-3**	544	500	15173
				WGSMR-4	518	479	13334
				WGSMR-4	479	415	127097
				WGSMR-4	415	308	23782
				Syngas Reheater	307	525	-114848
				Syngas Reheater	525	534	-25907
				Syngas Reheater	534	538	-136479
				Syngas Reheater	538	540	-17677
				Syngas Reheater	314	514	-27796

The heat integration method utilized in this paper was developed in [35], and the results show that 63.8 MJ/s of heat are utilized to produce approximately 31 kg/s of steam for the MR-based IGCC plant versus the 57.4 MJ/s of heat utilized to produce approximately 28 kg/s of steam for the baseline IGCC plant. In addition, 169 MJ/s of excess cooling are required for the MR-based IGCC plant, since the excess steam used as sweep in the operation of the counter-current MRs is then cooled to act as diluent for the gas turbine combustor, which requires excess cooling in order to ensure the gas turbine temperature remains under 1,300°C to prevent corrosion. This extra steam can be seen in the simplified box diagram mentioned above (Figure 3-9). The amount of steam fed into the MR-based IGCC plant is approximately 3 times that of the baseline IGCC plant, and the costs can be seen in the next section. Utilizing the heat exchange area targeting scheme presented in [36,37], and assuming a heat transfer coefficient of 0.8 kW/(m^2 K) yields a 10,483 m^2 higher heat exchange area for the proposed MR IGCC plant versus the baseline design. This area is then accounted for in the techno-economic analysis presented below, where the cost methodology for heat exchangers developed by [38] is used.

3.5.2 Technical Economic Analysis

The capital and operating costs of the hatched sections for both the baseline IGCC and the 4 COU-MR-based IGCC plants were evaluated and the associated computations are elaborated below for the Gas-Cleanup Sections. Table 3-8 summarizes the capital cost assumptions used in the economic analysis and Table 3-9 shows the capital costs of the baseline IGCC plant and the 4-COU-MR-based IGCC plant.

Table 3-8: *Summary of the assumptions used for the capital cost analysis*

Unit	Cost Assumptions
Double Stage Selexol	The cost is adjusted using the aforementioned NETL scaling equation with corresponding NETL scaling parameters with the volumetric flow rate serving as the scaling parameters
Elemental Sulfur Plant	The cost is assumed to be the same due to NETL scaling parameters. The amount of sulfur is identical between the two cases
Mercury Removal	The cost is assumed to be the same due to NETL scaling parameters. The amount of mercury is identical between the two cases
Shift Reactors	The cost is different since the baseline uses PBRs and the proposed design uses MRs
Fuel Gas Piping	The cost is assumed to be the same due to NETL scaling parameters
Heat Exchange Network	The increase in heat exchanger areas required detailed by the heat integration in the previous section are reflected in this section
Combustion Turbine & Accessories	The cost is assumed to be the same since the nitrogen diluent is replaced by water and the hydrogen content is equal between the two cases
HRSG, Ducting & Stack	The cost is assumed to be the same since the nitrogen diluent is replaced by water and the hydrogen content is equal between the two cases

Table 3-9: *Capital cost comparison between the baseline IGCC with CCS and the proposed IGCC plant featuring a sequence of WGS-MRs*

	Baseline IGCC Plant ($/1000) [29]					**MR IGCC Plant ($/1000)**				
Description	**Equipment Cost**	**Material Cost**	**Labor**		**Bare Erected Cost**	**Equipment Cost**	**Material Cost**	**Labor**		**Bare Erected Cost**
			Direct	**Indirect**				**Direct**	**Indirect**	
Double Stage Selexol	$160,990	$0	w/equip.	$0	$160,990	$79,932	$0	w/equip.	$0	$79,932
Elemental Sulfur Plant	$12,451	$2,427	$15,954	$0	$30,833	$12,451	$2,427	$15,954	$0	$30,833
Mercury Removal	$1,973	$0	$1,491	$0	$3,464	$1,973	$0	$1,491	$0	$3,464
Shift Reactors	$11,566	$0	$4,624	$0	$16,190	$39,472	$0	w/ equip	$0	$39,472
Fuel Gas Piping	$0	$812	$531	$0	$1,344	$0	$812	$531	$0	$1,344
Heat Exchange Network	N/A	N/A	N/A	N/A	N/A	$2,999	$0	w/equip	$0	$2,999
Combustion Turbine & Accessories	$117,901	$1,016	$9,975	$0	$128,892	$117,901	$1,016	$9,975	$0	$128,892
HRSG, Ducting & Stack	$33,630	$2,884	$9,498	$0	$46,012	$33,630	$2,884	$9,498	$0	$46,012
Total	**$387,725**					**$332,948**				

The MRs used in the MR-based IGCC plant result in a higher capital cost expenditure, as compared to the shift reactors utilized in the baseline IGCC plant. However, the bare-erected cost for the Gas-Cleanup Section of the MR-based IGCC plant is 14.1% lower than that of the corresponding

section of the Baseline IGCC plant, due to the significant decrease in the inlet flow to the Dual-Stage Selexol unit, a 59% volumetric flow rate reduction when compared to the baseline IGCC plant. The equipment and material costs were calculated utilizing the following equipment cost by scaling Eq. 5 utilized by NETL [39]:

$$SC = RC * \left(\frac{SP}{RP} \right)^{Exp} \quad (5)$$

where Exp=exponent, RC=reference cost, RP=reference parameter, SC=scaled cost, and SP=scaling parameter. The labor for all cleanup units is assumed to be the same even with the reduction in cost in the process flowsheet, as a conservative estimate. For the cost of the MR shift reactors, the equipment cost was divided into the pressure vessel cost [40], and the membrane cost, \$1200/m^2 of required membrane surface area (per MP&T estimate). As mentioned earlier, the heat exchange network cost was calculated based on [38]. The results show that the bare-erected cost for the MR IGCC plant is 14.1% less than that of the baseline IGCC plant for the reactor/cleanup sections of the plant (the black-box section in Figure 3-1 – 3-2), and this reduction in capital cost translates to a 3% reduction in the total capital cost for the plant, assuming the rest of the sections' cost are identical between the baseline and MR-based IGCC plants.

Along with the capital costs, operating costs were also calculated for the sections that are different between the MR-based IGCC and Baseline IGCC plants. These results are summarized below in Table 3-10. The catalyst used in all of the simulations is the KATALCOJM™ K8-11HA, which has a minimum lifespan of 3-5 years, a cost of \$17.5/lb, and a density of 40 lb/ft^3. The amount of Selexol solution is assumed to decrease in cost by the same factor used to scale the capital cost portion contributed by the Dual-Stage Selexol. The membrane lifespan is assumed to

be 10 years, with a membrane packing cost of $650/m^2, where it is considered that there are 85 tubes inside a bundle, 5400 bundles inside a pressure vessel, 4 pressure vessels, and each tube has about 1.5 m^2 of surface area. These numbers are justified in [41], which includes extensive information on the testing of the proposed MRs.

Table 3-10: *Operating cost comparison between baseline IGCC with CCS and proposed MR-based IGCC plant*

Operating Costs					
Baseline IGCC Plant					
Consumables					
	Consumption				**Cost ($)**
	Initial Fill	**Per Day**	**Per Unit**	**Initial Fill**	Annual Cost
Water (/1000 gallons):	0	4,201	$1.67	$0	$2,053,253
Carbon (Mercury Removal) (lb)	135,182	231	$5.50	$743,501	$371,751
Shift Catalyst (ft^3)	6,246	4.28	$771.99	$4,822,025	$964,405
Selexol Solution (gal)	298,498	95	$36.79	$10,982,126	$1,020,094
Claus Catalyst (ft^3)	w/equip	2.01	$203.15	$0	$119,487
Makeup and Waste Water Treatment Chemicals	0	25,026	$0.27	$0	$1,957,230
Total:				**$16,547,652**	**$6,486,220**
MR-based IGCC Plant					
Consumables					
	Consumption				**Cost ($)**
	Initial Fill	**Per Day**	**Per Unit**	**Initial Fill**	Annual Cost
Water (/1000 gallons):	0	6,670	$1.67	$0	$3,259,985
Carbon (Mercury Removal) (lb)	67,118	231	$5.50	$743,501	$371,751
Membrane Packs (m^2)	w/equip	n/a	$650	$0	$2,138,046
Shift Catalyst (ft^3)	4,112	2.82	$699.33	$3,878,296	$575,674
Selexol Solution (gal)	148,205	63	$36.79	$5,452,638	$506,478
Claus Catalyst (ft^3)	w/equip	2.01	$203.15	$0	$119,487
Makeup and Waste Water Treatment Chemicals	0	25,026	$0.27	$0	$3,107,628
Total:				**$10,074,435**	**$10,079,049**
Products					
Nitrogen Sold (ton)	**0**	**14,591**	**-$30**	**$0**	**-$111,228,000**

As can be seen from Table 3-10, the WGS-MRs utilize 34% less catalyst in the reactor sequence than the standard sequence of WGS reactors employed in conventional pre-combustion IGCC plants. This is an expected result, and a benefit of MRs, since the continuous removal of product moves the reaction forward, thus requiring less catalyst, typically, than a standard reactor. While the WGS-MRs do not require excess steam for the reaction to occur, steam is utilized as

sweep for the counter-current MRs in the proposed design. In addition, as shown by the heat integration studies performed in the previous section, additional cooling water is also required for the MR-based IGCC plant. These water requirements have been accounted for in the operating costs, thus increasing the water costs by approximately 59%. These costs are ameliorated since the water is used as diluent in the gas combustion turbine, removing the need for pure Nitrogen, which can then be sold for approximately $30/ton [42]. The cost of semi-pure (99%) bulk Nitrogen including transportation and delivery costs has been quoted at approximately $414/ton, by several companies such as Praxair and West Air Gas. To account for Nitrogen transportation/storage/delivery costs, the above mentioned $30/ton will be used in the operating cost analysis. This cost of $30/ton was taken from a TEA of an ASU plant where the Nitrogen product could be sold on site disregarding transportation and storage costs. These changes result in an operating cost increase of approximately 55% over the baseline design without considering the Nitrogen sold by the MR-based IGCC plant (which utilizes all such Nitrogen for dilution of the gas entering the turbine).

Table 3-11: *Sensitivity analysis on Membrane Reactor operating costs and Nitrogen Sale Prices*

Sensitivity Analysis					
	Consumption				**Cost ($)**
	Initial Fill	**Per Day**	**Per Unit**	**Initial Fill**	**Annual Cost**
10 Year MR Lifespan					
Membrane Packs (m^2)	w/equip	n/a	$650	$0	$2,138,046
Total:				**$10,074,435**	**$10,079,049**
5 Year MR Lifespan					
Membrane Packs (m^2)	w/equip	n/a	$650	$0	$4,276,092
Total:				**$10,074,435**	**$12,217,095**
2 Year MR Lifespan					
Membrane Packs (m^2)	w/equip	n/a	$650	$0	$10,690,230
Total:				**$10,074,435**	**$18,631,233**
Sensitivity Analysis					
	Consumption				**Cost ($)**
	Initial Fill	**Per Day**	**Per Unit**	**Initial Fill**	**Annual Cost**
$30/ton Nitrogen Price					
Nitrogen (tons)	0	14,591	$30	$0	$111,228,000
$1/ton Nitrogen Price					
Nitrogen (tons)	0	14,591	$1	$0	$3,707,600

$414/ton Nitrogen Price					
Nitrogen (tons)	0	14,591	$414	$0	$1,534,946,400

The Nitrogen sold generates $111,228,000/year for the plant, which can easily take care of all variable operating costs and still produce $101,148,951/year of profit. Table 3-11 illustrates a sensitivity analysis performed on the operating costs of replacing the membranes in the MR. The sensitivity analysis includes the cost of membrane replacements over 10-year, 5-year, and 2-year lifespans. It shows that the total variable operating costs would increase by 21%, if the lifespan is 5-years versus 10-years, and by 85% if the membrane lifespan is 2-years versus 10 years. The initial fill operating costs remain the same for all membrane lifespans since the one time initial fill cost of the membrane is accounted for in the capital costs in the $1200/$m^2$. The sale of nitrogen would still be able to take care of these increased costs, while generating additional profit every year. In addition, it includes the total profit produced through the sale of Nitrogen produced via the plant by varying the sale price from $1/ton - $414/ton. At the current selling price of $30/ton the Nitrogen generates $111,228,000/year, which can vary from $3,707,500/year to $1,534,946,400/year with a sale price of $1/ton and $414/ton respectively. Overall, the capital costs and operating costs are reduced and the MR-based IGCC plant is able to generate more power than the traditional IGCC plant with CCS.

3.6 Conclusions

An IGCC plant featuring a sequence of membrane reactors was proposed as a pre-combustion CCS method and compared to a standard pre-combustion CCS NETL IGCC plant. The MR sequence operation was studied to determine optimal operating conditions between counter-current, co-current, and a mix of counter/co-current MRs, and it was determined that the counter-current MR sequence produced the highest conversion and hydrogen separation. These

simulations were then utilized to develop a process flowsheet using Honeywell's UNISIM software. A technical economic analysis (TEA) was developed, and heat integration studies were done on the developed UNISIM flowsheet. It was found that the MR-based IGCC case produces 2.21% more power than the baseline IGCC design, has a lower bare-erected cost than that of the baseline IGCC plant for the pre-combustion CCS section with an increase in operating cost, primarily due to the cost of replacing the membrane packs and the additional water that it uses. It is expected that as membrane reactor use proliferates, their capital/operating costs will be further reduced due to a reduction in the membrane costs.

3.7 Appendix

Table 3-12: *Molar based catalyst pellet-scale model equations*

Constitutive laws

Continuity Equation:

$$\sum_{i=1}^{\nu} R_{f,i}^{p} r^2 = \frac{d}{dr}\left(\varepsilon_{f,A}^{p} r^2 c_f^{p} \overrightarrow{v_f^{p}}\right) \tag{6}$$

Component mass conservation:

$$R_{f,i}^{p} r^2 = \frac{d}{dr}\left[\varepsilon_{f,A}^{p} r^2 \left(x_{f,i}^{p} c_f^{p} \overrightarrow{v_f^{p}} + \overrightarrow{j_{f,i}^{p}}\right)\right] \tag{7}$$

Diffusion model (DGM):

$$-\frac{1}{\sum_{j=1}^{\nu} c_{f,j}^{p}} \sum_{\substack{j=1 \\ j\neq i,p}}^{\nu}\left(\frac{c_{f,j}^{p}}{D_{ij}^{eff}} \overrightarrow{J_{f,i}^{p}} - \frac{c_{f,i}^{p}}{D_{ij}^{eff}} \overrightarrow{J_{f,j}^{p}}\right) - \frac{\overrightarrow{J_{f,i}^{p}}}{D_{iK}^{eff}} = \frac{d}{dr} c_{f,i}^{p} - x_{f,i}^{p} \frac{d}{dr} c_{f,tot}^{p} + \frac{c_{f,i}^{p}}{\sum_{i=1}^{\nu} c_{f,i}^{p} RT^{p}}\left(1 + \frac{p^{p}}{D_{iK}^{eff}} \frac{B_O}{\mu_f^{p}}\right) \frac{d}{dr} p^{p} \tag{8}$$

Energy conservation:

$$\varepsilon_{s,V}^{p} \rho_s^{p}\left[\sum_{i=1}^{\upsilon}\left(\tilde{H}_i^{0} + \int_{T^0}^{T^{p}} C_{P,i}^{p}(T')dT'\right)\bar{R}_{f,i}^{p}\right] = \left(\sum_{i=1}^{\nu} \varepsilon_{f,A}^{p} x_{f,i}^{p} c_f^{p} C_{f,i}^{p}\right)\overrightarrow{v_f^{p}} \frac{dT^{p}}{dr} + \frac{dT^{p}}{dr}\left(\lambda^{p} \frac{dT^{p}}{dr}\right) \tag{9}$$

Table 3-13: *Initial and boundary conditions for catalyst pellet-scale model equations*

Initial Conditions: ***Boundary Conditions:***

$$\left.\begin{aligned} x_{f,i}^{p} &= \left(x_{f,i}^{p}\right)_{in} \\ T^{p} &= T^{r} = T_{in} \\ p^{p} &= \left(p^{p}\right)_{in} \\ Q_r &= -\lambda^{p}\vec{\nabla}T^{p} = 0 \\ \vec{\nabla}p^{p} &= 0 \end{aligned}\right\} \text{for } t=0,\ \forall r \quad (10) \qquad \left.\begin{aligned} \overrightarrow{J_{f,i}^{p}} &= 0 \\ Q_r &= -\lambda^{p}\vec{\nabla}T^{p} = 0 \\ \vec{\nabla}p^{p} &= 0 \end{aligned}\right\} \text{for } r=0$$

$$\left.\begin{aligned} R_{f,i}^{r} &= \overrightarrow{j_{f,i}^{p}} + x_{f,i}^{p}c_f^{p}\overrightarrow{v_f^{p}} \\ -h^{p}\left(T^{r}-T^{p}\right) &= Q_r + \left(\sum_{j=1}^{n_s} x_{f,i}^{p}c_f^{p}C_{f,i}^{p}\right)\overrightarrow{v_f^{p}}T^{p} \\ x_{f,i}^{p} &= x_{f,i}^{r} \\ p^{p} &= p^{r} \end{aligned}\right\} \text{for } r=r^{p} \qquad (10)$$

Table 3-14: *Molar-based reactor-scale model equations*

Bulk-Gas Constitutive laws

Continuity Equation:

$$\varepsilon_{p-s,V}^{r}\frac{A^{p}}{\varepsilon_{s,V}^{p}V^{p}}\sum_{i=1}^{v}\left[\left(\varepsilon_{f,A}^{p}\overrightarrow{J_{f,i}^{p}}\right)\Big|^{z,r^{p}}\right] - N_T\frac{A^{per}}{V^{r}}\sum_{i=1}^{v}\left[\overrightarrow{J_{f,i}^{per}}\Big|^{z}\right] = \frac{d}{dz}\left(\varepsilon_{f,A}^{r}c_f^{r}\overrightarrow{v_f^{r}}\right) \qquad (11)$$

Component mass conservation:

$$\varepsilon_{p-s,V}^{r}\frac{A^{p}}{\varepsilon_{s,V}^{p}V^{p}}\left[\left(\varepsilon_{f,A}^{p}\overrightarrow{J_{f,i}^{p}}\right)\Big|^{z,r^{p}}\right] - N_T\frac{A^{per}}{V^{r}}\overrightarrow{J_{f,i}^{per}}\Big|^{z} = \frac{d}{dz}\left(\varepsilon_{f,A}^{r}x_{f,i}^{r}c_f^{r}\overrightarrow{v_f^{r}}\right) + \frac{d}{dz}\left(\varepsilon_{f,A}^{r}\overrightarrow{j_j^{r}}\right) \qquad (12)$$

Diffusion Model (Stefan-Maxwell):

$$\left\{\begin{aligned} &\sum_{j=1}^{\upsilon}\left[\frac{x_{f,i}^{r}x_{f,j}^{r}}{D_{ij}}\left(\frac{1}{\rho_{f,j}^{r}}\overrightarrow{J_{f,j}^{r}} - \frac{1}{\rho_{f,i}^{r}}\overrightarrow{J_{f,i}^{r}}\right)\right] = \\ &\qquad \frac{d}{dz}x_{f,i}^{r} + \left(\frac{x_{f,i}^{r}-w_{f,i}^{r}}{p_f^{r}}\right)\frac{d}{dz}p_f^{r} + \sum_{j=1}^{\upsilon}\left[\frac{x_{f,i}^{r}x_{f,j}^{r}}{\rho_f^{r}D_{ij}^{r}}\left(\frac{\tilde{D}_i^{r}}{w_{f,i}^{r}} - \frac{\tilde{D}_j^{r}}{w_{f,j}^{r}}\right)\right]\frac{1}{T_f^{r}}\frac{d}{dz}T_f^{r} \end{aligned}\right\} \qquad (13)$$

Table 3-15: *Initial and boundary conditions for reactor-scale model equations*

Initial Conditions: ***Boundary Conditions:***

$$\left.\begin{aligned} x_{f,i}^{r} &= \left(x_{f,i}^{r}\right)_{in} \\ T_{f}^{r} &= \left(T_{f}^{r}\right)_{in} \\ p_{f}^{r} &= \left(p_{f}^{r}\right)_{in} \end{aligned}\right\} \text{for } t=0,\ \forall z \quad (14)$$

$$\left.\begin{aligned} \overrightarrow{v_{f}^{r}} &= \left(\overrightarrow{v_{f}^{r}}\right)_{in} \\ p_{f}^{r} &= \left(p_{f}^{r}\right)_{in} \\ x_{f,i}^{r} &= \left(x_{f,i}^{r}\right)_{in} \\ T_{f}^{r} &= \left(T_{f}^{r}\right)_{in} \end{aligned}\right\} \text{for } z=0 \quad (15)$$

$$\left.\begin{aligned} \vec{\nabla} T_{f}^{r} &= 0 \\ \overrightarrow{J_{j}^{r}} &= 0 \\ \vec{\nabla} p_{f}^{r} &= 0 \end{aligned}\right\} \text{for } z=L \quad (16)$$

Table 3-16: *Molar-based permeation zone model equations*

Bulk-Gas Constitutive laws

Continuity Equation:

$$N_T \frac{A^{per}}{V^{r}} \sum_{i=1}^{v} \left[\overrightarrow{J_{f,i}^{per}} \Big|^{z} \right] = \frac{d}{dz}\left(c_{f}^{per} \overrightarrow{v_{f}^{per}} \right) \quad (17)$$

Component mass conservation:

$$N_T \frac{A^{per}}{V^{r}} \overrightarrow{J_{f,i}^{per}} \Big|^{z} = \frac{d}{dz}\left(x_{f,i}^{per} c_{f}^{per} \overrightarrow{v_{f}^{per}} \right) \quad (18)$$

Momentum conservation:

$$\frac{d}{dz}\left(\rho_f^{per}\overrightarrow{v_f^{per}}\overrightarrow{v_f^{per}}\right)=-\frac{dp_f^{per}}{dz}+\mu_f^{per}\frac{d^2\overrightarrow{v_f^{per}}}{dz^2} \quad (19)$$

Energy conservation:

$$\left\{\begin{array}{l}\frac{d}{dz}\left(\lambda^{per}\frac{d}{dz}T_f^{per}\right)+\frac{A^{per}U^{per}}{V^r}\left(T_f^r-T_f^{per}\right)+\\ \left(\frac{A^{per}}{V^r}\right)\sum_{i=1}^{v}\left(\overrightarrow{J_i^{per}}\left(\tilde{h}_{f,i}^r-\tilde{h}_{f,i}^{per}\right)\right)\Big|^z\end{array}\right\}=\left(\sum_{i=1}^{v}x_{f,i}^{per}c_f^{per}C_{P,i}^{per}\right)\overrightarrow{v_f^{per}}\cdot\left(\frac{dT_f^{per}}{dz}\right) \quad (20)$$

Table 3-17: *Initial and boundary conditions for permeation zone model equations*

Initial Conditions:

$$\left.\begin{array}{l}x_{f,i}^{per}=0\\ T_f^{per}=\left(T_f^{per}\right)_{in}\\ p_f^{per}=\left(p_f^{per}\right)_{in}\end{array}\right\}\ for\ t=0,\ \forall z \quad (21)$$

Boundary Conditions:

$$\left.\begin{array}{l}\overrightarrow{v_f^{per}}=\overrightarrow{\left(v_f^{per}\right)_{in}}\\ p_f^{per}=\left(p_f^{per}\right)_{in}\\ x_{f,i}^{per}=\left(x_{f,i}^{per}\right)_{in}\\ T_f^{per}=\left(T_f^{per}\right)_{in}\end{array}\right\}\ for\ z=0 \quad (22)$$

$$\left.\begin{array}{l}\vec{\nabla}T_f^{per}=0\\ \vec{\nabla}p_f^{per}=0\end{array}\right\}\ for\ z=L \quad (23)$$

Table 3-18: *Chemical model equations*

Reaction Rate:
$$R_{f,i}^p=k_0 exp\left(-\frac{E_a}{RT_f^p}\right)p_{CO}^l p_{H_2O}^m p_{CO_2}^n p_{H_2}^q\left(1-\frac{1}{K_{eq}}\frac{p_{CO_2}\cdot p_{H_2}}{p_{CO}\cdot p_{H_2O}}\right) \quad (24)$$

$$K_{eq}=exp\left(\frac{4577.8}{T_f^p}-4.33\right) \quad (25)$$

Table 3-19: *Flow specifications of outlet MR sequence for COMSOL simulation and corresponding UNISIM implementation*

COMSOL				
	Inlet (kmol/h)	Water Inlet (kmol/h)	Permeate (kmol/h)	Retentate (kmol/h)
CO	8267	0	86	129
CO2	3189	0	242	10999
H2	7874	0	8611	7315
H2O	9342	21559	10360	12489
Inert	609	0	0	609
Total	29281	21559	19299	31542
	UNISIM			
	Inlet (kmol/h)	Water Inlet (kmol/h)	Permeate (kmol/h)	Retentate (kmol/h)
CO	8267	0	86	129
CO2	3189	0	243	10998
H2	7874	0	8612	7314
H2O	9342	21560	10361	12488
Inert	609	0	0	609
Total	29281	21560	19302	31538

3.8 References

[1] U.S. Energy Facts - Energy Explained, Your Guide To Understanding Energy - Energy Information Administration, (n.d.). https://www.eia.gov/energyexplained/?page=us_energy_home (accessed October 4, 2017).

[2] O. US EPA, U.S. Greenhouse Gas Inventory Report: 1990-2014, US EPA. (2016). https://www.epa.gov/ghgemissions/us-greenhouse-gas-inventory-report-1990-2014 (accessed October 4, 2017).

[3] EPA Regulation of Greenhouse Gas Emissions from New Power Plants | Center for Climate and Energy Solutions, (n.d.). https://www.c2es.org/federal/executive/epa/ghg-standards-for-new-power-plants (accessed October 4, 2017).

[4] O. US EPA, EPA Proposes Affordable Clean Energy (ACE) Rule, US EPA. (2018). https://www.epa.gov/newsreleases/epa-proposes-affordable-clean-energy-ace-rule (accessed October 8, 2018).

[5] 01/10/2017 | Aaron Larson, World's Largest Post-Combustion Carbon Capture Project Completed, POWER Mag. (2017). http://www.powermag.com/worlds-largest-post-combustion-carbon-capture-project-completed/ (accessed March 27, 2018).

[6] Pre-Combustion Carbon Capture Research | Department of Energy, (n.d.). https://energy.gov/fe/science-innovation/carbon-capture-and-storage-research/carbon-capture-rd/pre-combustion-carbon (accessed October 4, 2017).

[7] Oxy-fuel combustion systems – The Carbon Capture & Storage Association (CCSA), (n.d.). http://www.ccsassociation.org/what-is-ccs/capture/oxy-fuel-combustion-systems/ (accessed October 4, 2017).

[8] What is Post-Combustion Capture? - Fossil Transition Project, (n.d.). http://www.fossiltransition.org/pages/post_combustion_capture_/128.php (accessed October 4, 2017).

[9] K. Ramasubramanian, Y. Zhao, W.S.W. Ho, CO2 capture and H2 purification: Prospects for CO2-selective membrane processes, AIChE J. 59 (2013) 1033–1045. doi:10.1002/aic.14078.

[10] P. Maas, N. Nauels, L. Zhao, P. Markewitz, V. Scherer, M. Modigell, D. Stolten, J.-F. Hake, Energetic and economic evaluation of membrane-based carbon capture routes for power plant processes, Int. J. Greenh. Gas Control. 44 (2016) 124–139. doi:10.1016/j.ijggc.2015.11.018.

[11] J. Franz, P. Maas, V. Scherer, Economic evaluation of pre-combustion CO2-capture in IGCC power plants by porous ceramic membranes, Appl. Energy. 130 (2014) 532–542. doi:10.1016/j.apenergy.2014.02.021.

[12] S. Troy, A. Schreiber, P. Zapp, Life cycle assessment of membrane-based carbon capture and storage, Clean Technol. Environ. Policy. 18 (2016) 1641–1654. doi:10.1007/s10098-016-1208-x.

[13] Z. Ziaka, V. Manousiouthakis, Best Achievable Isomerization Reaction Conversion in a Membrane Reactor, Ind. Eng. Chem. Res. 37 (1998) 3551–3560. doi:10.1021/ie970764w.

[14] R.J. Ciora, B. Fayyaz, P.K.T. Liu, V. Suwanmethanond, R. Mallada, M. Sahimi, T.T. Tsotsis, Preparation and reactive applications of nanoporous silicon carbide membranes, Chem. Eng. Sci. 59 (2004) 4957–4965. doi:10.1016/j.ces.2004.07.015.

[15] M. Abdollahi, J. Yu, P.K.T. Liu, R. Ciora, M. Sahimi, T.T. Tsotsis, Hydrogen production from coal-derived syngas using a catalytic membrane reactor based process, J. Membr. Sci. 363 (2010) 160–169. doi:10.1016/j.memsci.2010.07.023.

[16] R.G. Minet, T.T. Tsotsis, Catalytic ceramic membrane steam-hydrocarbon reformer, US5229102 A, 1993. http://www.google.com/patents/US5229102 (accessed October 4, 2017).

[17] J.G. Sanchez Marcano, T.T. Tsotsis, Pervaporation Membrane Reactors, in: Catal. Membr. Membr. React., Wiley-VCH Verlag GmbH & Co. KGaA, 2002: pp. 97–132. doi:10.1002/3527601988.ch3.

[18] R.G. Minet, T.T. Tsotsis, Catalytic ceramic membrane steam/hydrocarbon reformer, US4981676 A, 1991. http://www.google.com/patents/US4981676 (accessed October 4, 2017).

[19] A. Garshasbi, H. Chen, M. Cao, S. Karagöz, R.J. Ciora, P.K.T. Liu, V.I. Manousiouthakis, T.T. Tsotsis, Membrane-based reactive separations for process intensification during power generation, Catal. Today. (2017). doi:10.1016/j.cattod.2017.10.039.

[20] J. Yu, M. Tan, P.K.T. Liu, M. Sahimi, T.T. Tsotsis, Hydrogen Production from Biomass-Derived Syngas Using a Membrane Reactor Based Process, Ind. Eng. Chem. Res. 53 (2014) 819–827. doi:10.1021/ie402603c.

[21] M.M. Yousef Motamedhashemi, M. Monji, F. Egolfopoulos, T. Tsotsis, A hybrid catalytic membrane reactor for destruction of a chemical warfare simulant, J. Membr. Sci. 473 (2015) 1–7. doi:10.1016/j.memsci.2014.08.043.

[22] P.K. Liu, M. Sahimi, T.T. Tsotsis, Process intensification in hydrogen production from coal and biomass via the use of membrane-based reactive separations, Curr. Opin. Chem. Eng. 1 (2012) 342–351. doi:10.1016/j.coche.2012.06.001.

[23] M. Abdollahi, J. Yu, P.K.T. Liu, R. Ciora, M. Sahimi, T.T. Tsotsis, Ultra-pure hydrogen production from reformate mixtures using a palladium membrane reactor system, J. Membr. Sci. 390–391 (2012) 32–42. doi:10.1016/j.memsci.2011.10.053.

[24] Abdollahi, M., Yu, J., Hwang, H.T., Liu, P.K.T., Ciora, R., Sahimi, M., Tsotsis, T.T., Membrane Reactor-Based Hydrogen Production Process from Biomass" Abstracts ACS, 241, 120-PETR, 2011., in: Abstracts ACS, 2011: pp. 120-PETR.

[25] I.H. Moskowitz, W.D. Seider, M. Soroush, U.G. Oktem, J.E. Arbogast, Chemical Process Simulation for Dynamic Risk Analysis: A Steam–Methane Reformer Case Study, Ind. Eng. Chem. Res. 54 (2015) 4347–4359. doi:10.1021/ie5038769.

[26] K. Zygourakis, Transient operation of monolith catalytic converters: a two-dimensional reactor model and the effects of radially nonuniform flow distributions, Chem. Eng. Sci. 44 (1989) 2075–2086. doi:10.1016/0009-2509(89)85143-7.

[27] J. Huang, L. El-Azzami, W.S.W. Ho, Modeling of CO2-selective water gas shift membrane reactor for fuel cell, J. Membr. Sci. 261 (2005) 67–75. doi:10.1016/j.memsci.2005.03.033.

[28] K. Ramasubramanian, H. Verweij, W.S. Winston Ho, Membrane processes for carbon capture from coal-fired power plant flue gas: A modeling and cost study, J. Membr. Sci. 421–422 (2012) 299–310. doi:10.1016/j.memsci.2012.07.029.

[29] Department of Energy/National Energy Technology Laboratory. Cost and Performance Baseline for Fossil Energy Plants Volume 1b: Bituminous Coal (IGCC) to Electricity Revision 2b – Year Dollar Update. Document Number: DOE/NETL- 2015/1727., (n.d.).

[30] D. Maroudas, Multiscale modeling of hard materials: Challenges and opportunities for chemical engineering, AIChE J. 46 (2000) 878–882. doi:10.1002/aic.690460502.

[31] S. Karagöz, F.E. da Cruz, T.T. Tsotsis, V.I. Manousiouthakis, Multi-scale membrane reactor (MR) modeling and simulation for the water gas shift reaction, Chem. Eng. Process. - Process Intensif. (2018). doi:10.1016/j.cep.2018.09.012.

[32] D. Parsley, R.J. Ciora, D.L. Flowers, J. Laukaitaus, A. Chen, P.K.T. Liu, J. Yu, M. Sahimi, A. Bonsu, T.T. Tsotsis, Field evaluation of carbon molecular sieve membranes for the separation and purification of hydrogen from coal- and biomass-derived syngas, J. Membr. Sci. 450 (2014) 81–92. doi:10.1016/j.memsci.2013.08.008.

[33] H. Sugishita, H. Mori, K. Uematsu, A Study of Advanced Hydrogen/Oxygen Combustion Turbines, in: T.O. Saetre (Ed.), Hydrog. Power Theor. Eng. Solut., Springer Netherlands, 1998: pp. 511–516.

[34] P. Pichardo, V.I. Manousiouthakis, Infinite DimEnsionAl State-space as a systematic process intensification tool: Energetic intensification of hydrogen production, Chem. Eng. Res. Des. 120 (2017) 372–395. doi:10.1016/j.cherd.2017.01.026.

[35] K. Holiastos, V. Manousiouthakis, Minimum hot/cold/electric utility cost for heat exchange networks, Comput. Chem. Eng. 26 (2002) 3–16. doi:10.1016/S0098-1354(01)00726-8.

[36] V. Manousiouthakis, L.L. Martin, A minimum area (MA) targeting scheme for single component MEN and HEN synthesis, Comput. Chem. Eng. 28 (2004) 1237–1247. doi:10.1016/j.compchemeng.2003.08.012.

[37] B. Linnhoff, S. Ahmad, Cost optimum heat exchanger networks—1. Minimum energy and capital using simple models for capital cost, Comput. Chem. Eng. 14 (1990) 729–750. doi:10.1016/0098-1354(90)87083-2.

[38] S.G. Hall, S. Ahmad, R. Smith, Capital cost targets for heat exchanger networks comprising mixed materials of construction, pressure ratings and exchanger types, Comput. Chem. Eng. 14 (1990) 319–335. doi:10.1016/0098-1354(90)87069-2.

[39] Department of Energy/National Energy Technology Laboratory, Quality Guidelines For Energy System Studies – Capital Cost Scaling Methodology, n.d.

[40] M.S. Peters, K.D. Timmerhaus, R.E. West, Plant design and economics for chemical engineers, in: Plant Des. Econ. Chem. Eng., 5th ed., Mc Graw Hill, 1968.

[41] P.K.T. Liu, Robust and energy efficient dual-stage membrane-based process for enhanced CO2 recovery, Media and Process Technology Inc., Pittsburgh, PA (United States), 2017. doi:10.2172/1411212.

[42] S. Schmidt, R. Clayton, Dynamic Design of a Cryogenic Air Separation Unit, (2013) 41.

Chapter 4: Techno-Economic Analysis of an Intensified Integrated Gasification Combined Cycle (IGCC) Power Plant Featuring a Combined Membrane Reactor - Adsorptive Reactor (MR-AR) System

4.1 Abstract

In this work, the novel concept of a combined membrane-adsorptive reactor sequence (MR-AR) is developed and implemented in an Integrated Gasification Combined Cycle (IGCC) plant. This novel MR-AR IGCC plant is subsequently analyzed from an economic viewpoint through a techno-economic analysis (TEA) of the proposed plant. This novel design can achieve over 90% carbon capture without the use of a Dual-Stage Selexol unit. The resultant intensified design is more efficient from both an economic and power production perspective than the traditional IGCC plants with pre-combustion Carbon-Capture Storage (CCS) technology. The COMSOL software package is utilized to simulate the MR-AR sequence proposed in this work, and the UNISIM software (Honeywell^{TM}) is used to create an intensified process flowsheet of the proposed MR-AR IGCC plant, which is subsequently heat-integrated. The TEA developed for the MR-AR IGCC power plant will be used to identify the extent of process intensification the proposed design has over the traditional IGCC plants with pre-combustion CCS. The results demonstrate a reduction in both the cost-of-electricity (COE) and in the capital cost of the proposed design over the baseline case.

4.2 Introduction

Integrated Gasification Combined Cycle (IGCC) power generation plants convert coal into syngas (containing $CO/H_2/CO_2$ with small amounts of CH_4 and various impurities) via a high-pressure gasifier in the presence of steam and oxygen (1). In standard pre-combustion IGCC plants, this syngas is further processed in a packed-bed water-gas-shift reactor (WGSR) sequence consisting of two High/Low Temperature shift reactors with inter-stage cooling that can deliver CO conversions of over 95% (2–4) with pre/post-processing for contaminant removal.

Subsequently, the CO_2 is removed from the stream usually through an absorber with amine-based solvents prior to undergoing compression for transport and sequestration. The resultant stream is hydrogen-rich and is mixed with nitrogen as diluent before entering an F-class gas-turbine to produce power (4).

The projected energy and capital costs associated with this carbon capture and storage (CCS) IGCC technology are considered prohibitive for near-term market deployment since this pre-combustion CCS technology is more expensive and inefficient than a standard IGCC plant with no CCS. In fact, according to the U.S. National Energy Technology Laboratory (NETL), the efficiency of an IGCC power plant with CO_2 capture decreases approximately 15-20% compared to an IGCC power plant without CO_2 capture (5). In the United States, coal-based power will continue to be relevant in the foreseeable future; and while current technology has significantly reduced SO_2, NO_x, and particulate emissions, CO_2 emissions continue to be a problem. For this reason, CCS has become a major research focus in recent years as the primary process for the reduction of domestic and global CO_2 emissions from coal power plants. The current CCS systems require additional energy compared to projects without CCS, and are currently not economic for near-term market deployment, unless further legislation requiring the CCS technology is implemented (6).

For this reason, a novel hybrid MR-AR process is proposed here as a more efficient and realizable alternative to standard pre-combustion CCS technology. It consolidates two novel process units (i.e., MR and AR) into a single operation, and is a transformational technology with clear potential for application in the IGCC process. Multifunctional reactors, such as membrane reactors (MR), have been used in the past for simultaneous production, separation, and purification of hydrogen from syngas mixtures (7–11). In these reactors, hydrogen-selective membranes are

used to enhance the rate of reaction in the WGSR by overcoming thermodynamic equilibrium conversion limitations through the in situ removal of the hydrogen product from the reaction mixture. The potential advantages of the MR technology include lower operating temperatures, lower steam requirements, reduced catalyst cost, and a high-purity hydrogen product stream (3,7,9,12–19). Typically, Pd and Pd-alloy (dense) membranes, and silica, zeolite, and carbon molecular sieve (microporous) membranes (3,20) are utilized. The authors have extensive experience in the study of MRs for hydrogen production, including lab-scale testing and simulations (3,10,13,21–24).

In addition to the MR, the AR is also a most promising multifunctional reactor. The AR removes the other WGSR product (CO_2) via an adsorbent, thus again shifting the reaction equilibrium toward the products, which then allows for higher conversions of CO with simultaneous CO_2 capture. Along with these advantages, the AR system can also operate at lower reaction temperatures, with reduced material costs, increased operational safety, reduced need for excess steam in the reaction, and catalyst amount required, and with no need for downstream CO_2 separation. Consequently, a number of research efforts to date have been dedicated to the study of this AR system (3,12,13,21).

In essence, the proposed novel process for use in intensified IGCC with pre-combustion CCS employs a unique adsorption-enhanced WGS membrane reactor (MR-AR) concept. This concept has undergone extensive simulation and lab-scale testing by the authors (22). The proposed process will combine an MR followed by an AR producing a high-purity hydrogen stream until adsorbent saturation is reached. Once the adsorbent is saturated, the AR unit will be taken off -line for desorption, and another AR unit fresh from desorption will replace the unit taken off-line. During desorption, the AR unit will undergo regeneration via a combined pressure-swing-

adsorption/temperature-swing-adsorption (PSA/TSA) operation. Figure 4-1 below depicts the steps of the combined MR-AR process illustrating the switching that occurs when the adsorbent is saturated.

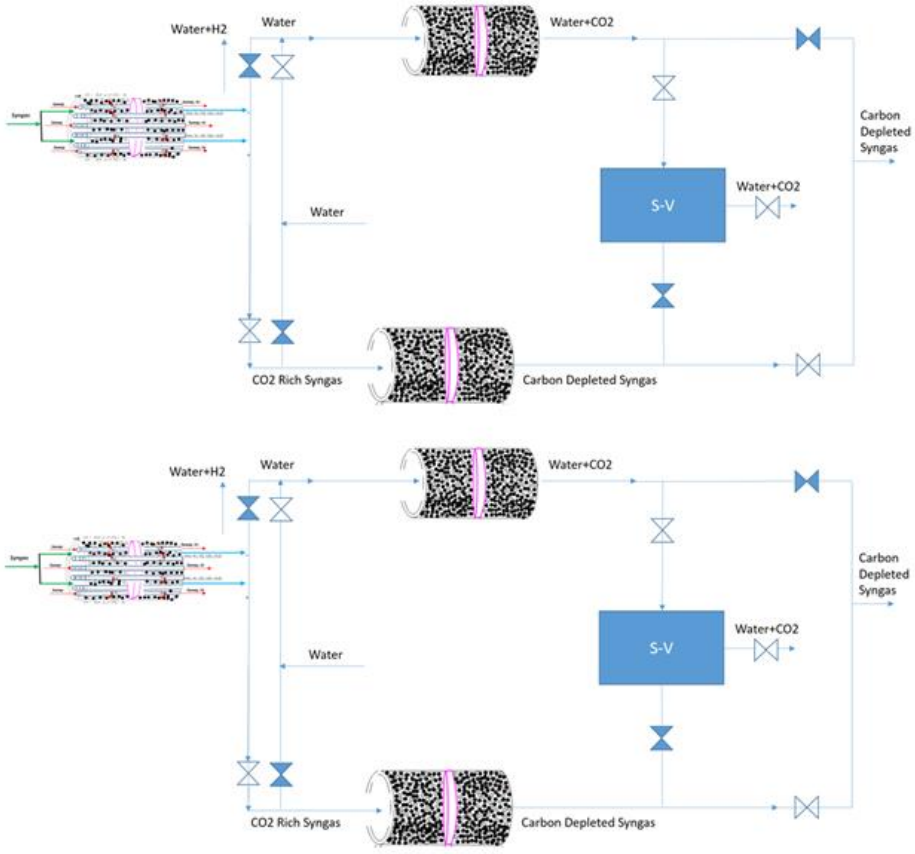

Figure 4-1: *Depiction of the combined MR-AR system operation including AR switching between adsorption/desorption*

The benefit of the combined MR-AR system is that it allows for both of the ultimate reaction products (H_2 and CO_2) to be removed, whereas the stand-alone MR (25), and sorption-enhanced, PSA-based AR technologies (26,27) for hydrogen production found in the literature only allow H_2 or CO_2 separation, respectively. In the combined system, performance is improved due to the significant interaction and synergy that is present between the two individual units. When considering a solitary MR system, for example, trying to maximize CO conversion while

simultaneously trying to meet high H_2 recovery and purity conditions can create process challenges. To improve the H_2 purity, a highly permselective membrane is preferred, which per its Robeson plot will result in a smaller permeance, but this will reduce the CO conversion as well as the H_2 recovery. Similarly, for the stand-alone AR system trying to meet simultaneous CO_2/H_2 recovery/purity along with CO conversion targets is a difficult task to accomplish (26). For this reason, the novel combined MR-AR system is proposed since the use of the MR preceding the AR system makes the possiblity of attaining these targets a reality. For example, in the combined system the MR component can be designed to achieve high H_2 purity without one worrying about simultaneously meeting the CO conversion and H_2 recovery targets, since the AR following the MR can carry-out these goals. Consequently, the proposed system has the potential to improve upon both the stand-alone MR and AR systems currently in place as well as the traditional WGSR design. This work is a continuation of our previous work (28), which focused on a TEA of an MR IGCC plant.

The remaining article is structured as follows: the proposed novel MR-AR IGCC plant is first presented, and the MR-AR system utilized in the design is described in detail, including the governing equations utilized in the MR-AR models. Next, the UNISIM flowsheet implementation of the proposed design is presented, and discussed prior to carrying-out a full TEA. Finally, the obtained TEA results are discussed, and conclusions are drawn.

4.3 Realization of the Proposed IGCC Plant Featuring the MR-AR Design

As mentioned above, the standard IGCC plant with pre-combustion CCS takes the product from the gasification of a coal slurry and utilizes a WGSR reactor along with steam to produce a syngas mixture containing mostly H_2 and CO_2. This mixture then undergoes clean-up via a Dual-Stage Selexol unit in order to remove all impurities and to separate out the CO_2. After the

impurities and CO_2 are removed, the clean carbon-depleted syngas is heated and burned in an F-Class Gas Turbine to produce power. In this study, this design will serve as the baseline to which the proposed MR-AR system will be compared. The proposed MR-AR-based system can be seen in Figure 4-2, where a blue box is utilized to depict the sections of the IGCC plant that will be modified to account for the MR-AR system. It should be noted that due to the AR's ability for CO_2 separation, a Dual-Stage Selexol unit is no longer required in the proposed plant and has, therefore, been replaced by a Single-Stage Selexol unit for impurities removal. The remaining structure of the plant is identical to the baseline IGCC plant described above, whose technical details can also be found in NETL's Bituminous Coal Report (Case B5B) (4).

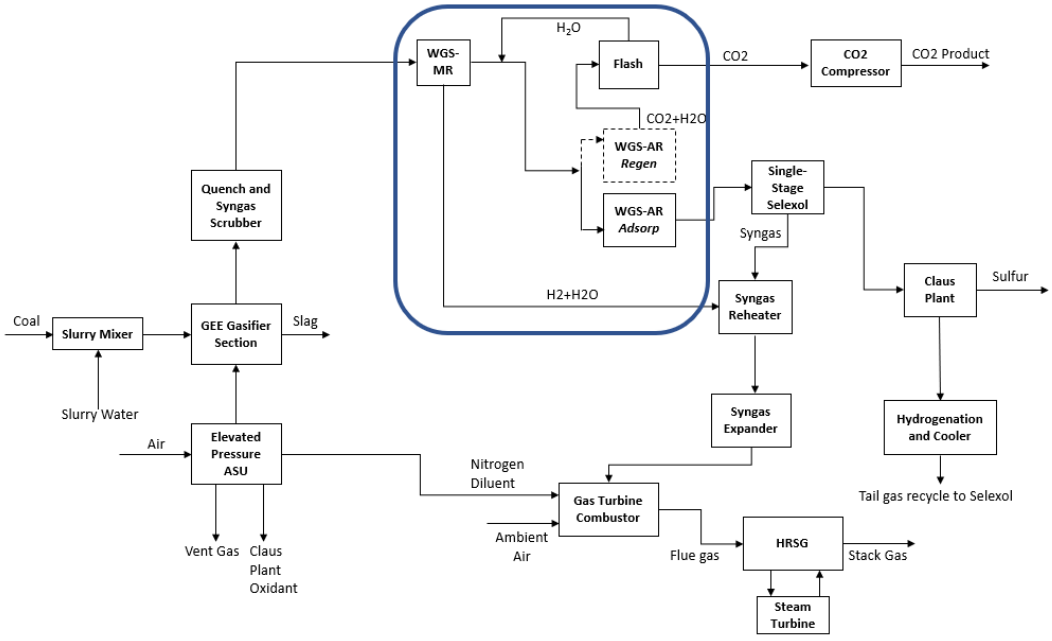

Figure 4-2: *A schematic of our proposed MR-AR-based IGCC plant*

The proposed MR-AR-based IGCC plant also gasifies a coal/water/oxygen mixture into syngas. This syngas is then fed into the WGS-MR, whose permeate stream, consisting of H_2/H_2O, is fed into the syngas reheater, while the retentate stream acts as the feed to the AR undergoing

adsorption and reaction until the adsorbent reaches saturation. The carbon-depleted stream that the AR generates then undergoes clean-up to remove all impurities via a Single-Stage Selexol unit. As the AR undergoes adsorption/reaction, another AR simultaneously undergoes regeneration, whereby steam is used as sweep to desorb the CO_2 thus producing a stream consisting of CO_2/H_2O. This CO_2/H_2O mixture undergoes flash separation to produce a stream of pure CO_2 that is further compressed for transport/sequestration. The carbon-depleted, hydrogen-rich syngas stream exiting the Single-Stage Selexol unit is then mixed with the H_2/H_2O from the MR permeate side before undergoing heating. Subsequently, this H_2-rich stream undergoes expansion and combustion via an F-Class Gas Turbine to produce power. The gas turbine is used along with a steam turbine to maximize power production. All steps downstream of the Single-Stage Selexol unit are identical to the above described baseline IGCC plant with CCS, since in this work the intensification is solely focused on the WGSR and CO_2 purification steps for CCS.

4.3.1 Membrane Reactor - Adsorptive Reactor Details

The MR is divided into three parts: the pressure vessel, the membrane modules (bundles), and the ceramic membrane tubes. The pressure vessel contains several membrane bundles, each consisting of 85-100 membrane tubes. Table 4-1 below, shows all the parameters utilized in the MR-AR simulations for the combined MR-AR system.

Table 4-1: *Parametric details of membrane reactors utilized*

D_{Ti} (Membrane tube inner diameter)	3.5 mm
D_{To} (Membrane tube outer diameter)	5.7 mm
L_T (Membrane tube length)	1 m
D_{Bi} (Bundle inner diameter)	98.55 mm
D_{Bo} (Bundle outer diameter)	101.6 mm
L_B (Bundle length)	1 m
D_{Vi} (Vessel inner diameter)	4.27 m
D_{Vo} (Vessel outer diameter)	4.28 m

L_V (Length of vessel)	6 m
N_{tb} (Number of tubes in bundle)	85
N_{bv}^{c} (Number of bundles in vessel cross-section)	900
N_{bv}^{l} (Number of bundles in vessel length)	6

$$\text{Bundle Cross Section Area} = \frac{\pi}{4} D_{Bi}^2 \quad (11)$$

$$\text{Reactive Region Cross Section Area} = \frac{\pi}{4} D_{Bi}^2 - N_{tb} \frac{\pi}{4} D_{To}^2 \quad (12)$$

$$\text{Solid Membrane Tube Cross Section Area} = \frac{\pi}{4} N_{tb} \left(D_{To}^2 - D_{Ti}^2 \right) \quad (13)$$

$$\text{Membrane Tube Permeation Cross Section Area} = \frac{\pi}{4} N_t D_{Ti}^2 \quad (14)$$

$$\text{Total Membrane Surface Area} = N_{bv}^{c} \cdot N_{bv}^{l} \cdot N_t \left(\pi D_{To} L \right) \quad (15)$$

$$\text{Pressure Vessel Volume} = \frac{\pi}{4} D_{Vi}^2 L_V \quad (16)$$

Table 4-2: *Specification of species permeance for the membrane reactor simulations*

H_2	H_2O	CO	CO_2	CH_4
1 $\frac{\mathrm{m}^3(\mathrm{STP})}{\mathrm{m}^2\ \mathrm{h\ bar}}$	*0.333* $\frac{\mathrm{m}^3(\mathrm{STP})}{\mathrm{m}^2\ \mathrm{h\ bar}}$	*0.0027* $\frac{\mathrm{m}^3(\mathrm{STP})}{\mathrm{m}^2\ \mathrm{h\ bar}}$	*0.0018* $\frac{\mathrm{m}^3(\mathrm{STP})}{\mathrm{m}^2\ \mathrm{h\ bar}}$	*0.0027* $\frac{\mathrm{m}^3(\mathrm{STP})}{\mathrm{m}^2\ \mathrm{h\ bar}}$
44.64 $\frac{\mathrm{mol}}{\mathrm{m}^2\ \mathrm{h\ bar}}$	*14.87* $\frac{\mathrm{mol}}{\mathrm{m}^2\ \mathrm{h\ bar}}$	*0.1205* $\frac{\mathrm{mol}}{\mathrm{m}^2\ \mathrm{h\ bar}}$	*0.0804* $\frac{\mathrm{mol}}{\mathrm{m}^2\ \mathrm{h\ bar}}$	*0.1205* $\frac{\mathrm{mol}}{\mathrm{m}^2\ \mathrm{h\ bar}}$
370.3 GPU	*123.3* GPU	*1* GPU	*0.6667* GPU	*1* GPU

$$*1\ \mathrm{GPU} = 0.0027 \frac{\mathrm{m}^3(\mathrm{STP})}{\mathrm{m}^2\ \mathrm{h\ bar}} = 0.1206 \frac{\mathrm{mol}}{\mathrm{m}^2\ \mathrm{h\ bar}}$$

The MR species permeances for the membrane reactor simulations can be found in Table 4-2, and are taken from (22). The catalyst used in the simulation is the KATALCOJM™ K8-11HA, which has a density of 40 lb/ft^3 (640.7 kg/m^3) and a cost of \$700/ft^3 (\$24,720/m^3). As for the membrane costs, Media Process and Technology, Inc. (M&PT) currently prices their membrane bundles based on the membrane surface area they contain, for a cost of \$1200/m^2.

4.3.2 COMSOL MR-AR Model Descriptions

In the modeling of the MR-AR system, we develop comprehensive, multi-scale (microscale and macroscale levels), multiphase, computational fluid dynamics (CFD) models quantifying the many complex physicochemical phenomena occurring in each unit, and thus providing the basis to better understand, and intensify the overall reaction/separation, steady-state/cyclic processes. A MR consists of the catalyst pellet, the reactor (bulk gas phase) and the permeation domains, while an AR consists of the catalyst pellet, adsorbent pellet and reactor (bulk gas phase) domains. These regions are modeled as independent domains, so one can properly assess the contribution of each parameter to the overall system. Regardless of the length scale, phase, or region of the system, conservation laws must hold. Thus, in the derivation of the model equations, the Reynolds Transport Theorem (RTT) is applied separately to each of these domains. At the micro-level, i.e., the pellet scale, we account for all catalyst/adsorbent pellet features, including average pore size, reaction/adsorption kinetic rates, pellet material properties, and pellet shapes. At the macro level, i.e., the reactor scale, we consider all the MR/AR features, such as reactor dimensions, catalyst/adsorbent packing, void fraction, and others.

The coupled, non-isothermal, steady-state/dynamic model equations in the aforementioned three domains are solved simultaneously along the MR/AR reactor length. An information network on gas pressure, temperature, velocity, and species concentrations and effectiveness factors is built between the catalyst-reactor, reactor-permeation and adsorbent-reactor domains via a multi-scale modeling approach. The conservation equations are simultaneously solved for each domain by COMSOL Multiphysics®. The full details of the MR/AR reactor models can be found in prior papers by the Group (29–31). This multiscale model enables the quantification of catalyst and adsorbent effectiveness factors within the reactor environments, thus eliminating the need to employ the commonly used assumption that these factors are constant.

Flowsheet Implementation into the UNISIM Simulation Platform

The MR-AR IGCC plant illustrated in Figure 4-2 was subsequently implemented into the UNISIM design platform where the simulations described above were used to design a flowsheet of the proposed process.

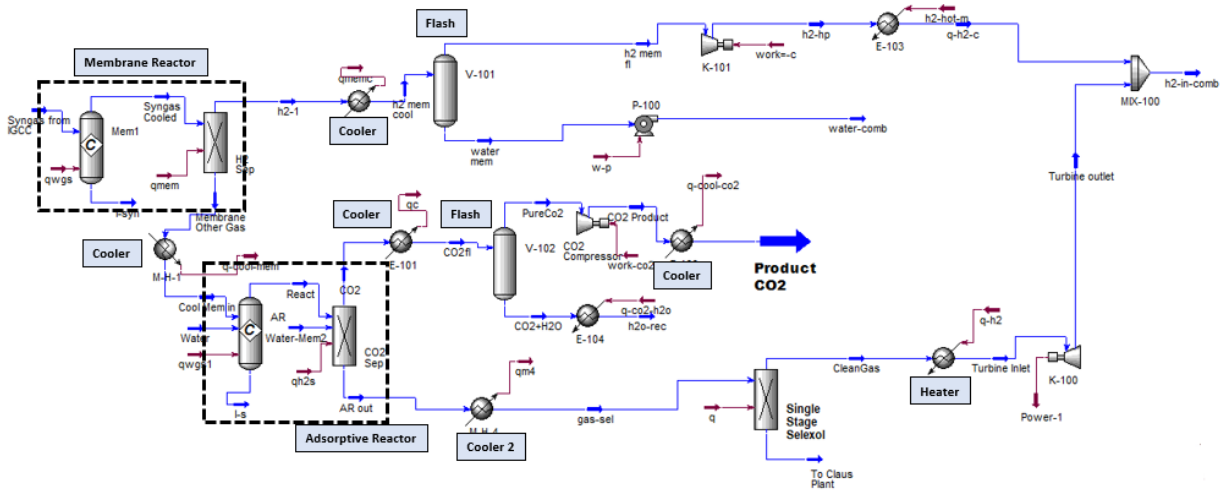

Figure 4-3: *UNISIM implemented flowsheet of MR-AR-proposed design*

In the UNISIM-implemented design flowsheet, the cooled syngas is fed into the MR first at 55.2 bar, where reaction occurs in the retentate side and H_2/H_2O permeate through the membrane (membrane permeances shown in Table 4-2) with additional steam acting as sweep and exit at 51 bar. The permeate stream is expanded to 31.7 bar and cooled before being mixed with the clean-gas outlet from the Single-Stage Selexol unit. The permeate stream exists at 51 bar to produce excess power through the expansion of the hydrogen/steam mixture. The retentate from the MR is then cooled before being fed into the AR where adsorption/reaction occurs. The stream that exits the AR is then processed by a Single-Stage Selexol unit to remove impurities before it undergoes expansion to 31.7 bar and mixed with the MR permeate stream. Subsequently, the H_2/H_2O stream is diluted with excess H_2O from the IGCC plant and fed into a Gas Turbine Combustor, at which

point the MR-AR IGCC plant and the baseline IGCC with CCS are then identical. During the AR reneneration (desorption) step, CO_2 is swept with H_2O producing a stream that is cooled before undergoing flash separation to produce a stream of pure CO_2. This pure CO_2 is produced at 55.2 bar and is subsequently compressed to 152.7 bar for transport/sequestration. Figure 4-3 depicts the UNISIM implementation of the proposed process, where both the MR and AR units are modeled using a conversion reactor followed by an ideal separator that identically reproduces the inlet and outlet conditions derived through the COMSOL simulations for the combined MR-AR system.

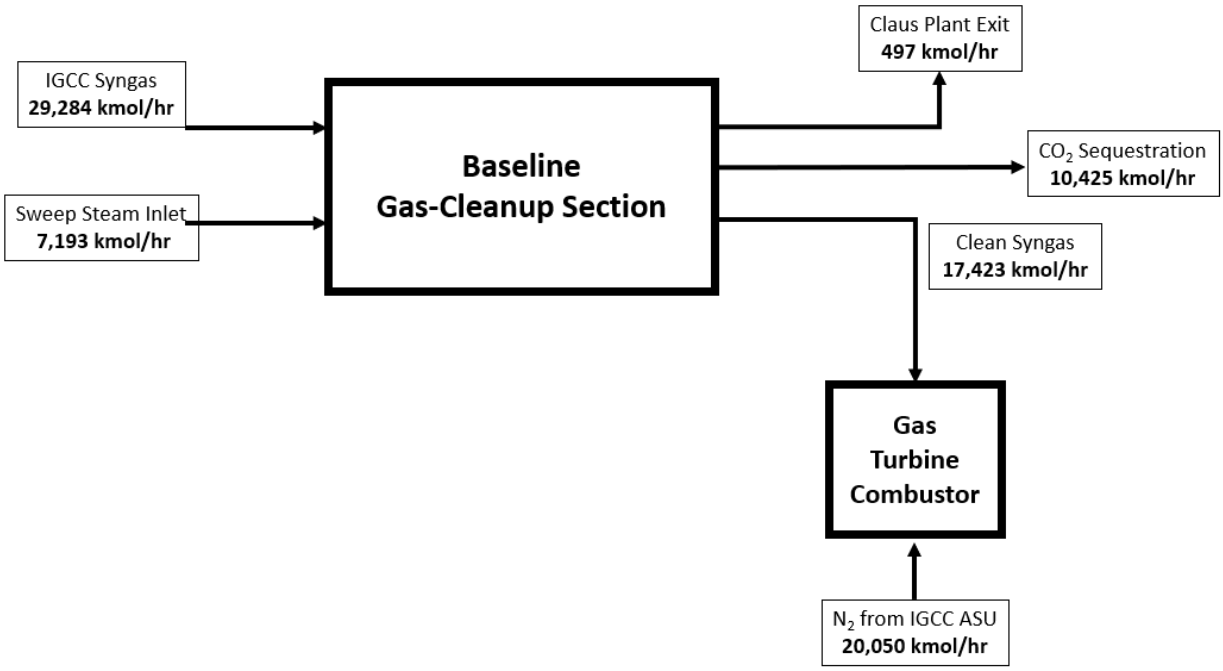

Figure 4-4: *Block flow diagram of the baseline IGCC gas-clean-up section*

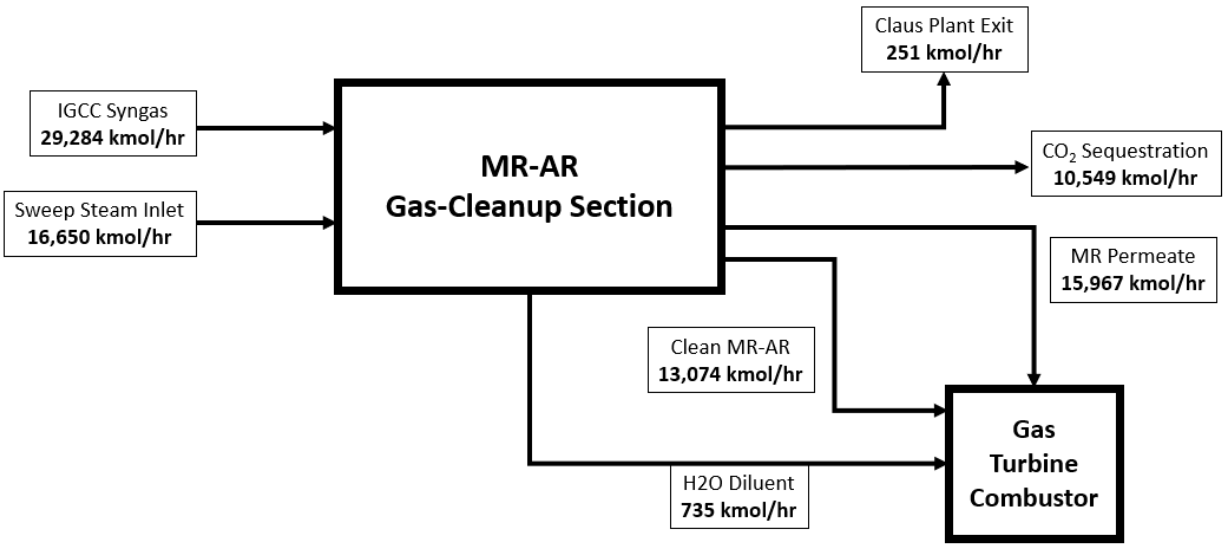

Figure 4-5: *Block flow diagram of the MR-AR-based IGCC gas-clean-up section*

Table 4-3: *Flow information on streams featured in Figures 4-4 - 4-5*

Gas-Clean-up Section of Baseline Plant (Molar Composition)								
Stream Name	IGCC Syngas	Sweep Steam Inlet	Claus Plant Exit	CO_2 Sequestration	Clean Syngas			N_2 from IGCC ASU
CO	0.28	0	0.01	0	0.01			0
CO_2	0.11	0	0.52	0.99	0.02			0
H_2O	0.32	1	0	0	0			0
H_2	0.27	0	0.1	0.01	0.95			0
N_2	0.01	0	0	0	0.01			0.99
H_2S	0.01	0	0.35	0	0			0
Gas-Clean-up Section of MR-AR-Based Plant (Molar Composition)								
Stream Name	IGCC Syngas	Sweep Steam Inlet	Claus Plant Exit	CO_2 Sequestration	MR Permeate	Clean MR-AR	H_2O Diluent	N_2 from IGCC ASU
CO	0.28	0	0	0	0.01	0	0	0
CO_2	0.11	0	0	1	0.01	0	0	0
H_2O	0.32	1	0.03	0	0.77	0.01	1	0
H_2	0.27	0	0	0	0.21	0.97	0	0
N_2	0.01	0	0.31	0	0	0.02	0	0.99
H_2S	0.01	0	0.66	0	0	0	0	0

4.4 Results and Discussion

The above developed UNISIM flowsheet for the MR-AR-based IGCC plant was utilized to develop the performance summary shown in Table 4-3, that includes the power production and

consumption breakdown of the proposed MR-AR-based design and its comparison to the Baseline case. The following differences exist between the Baseline (Case B5B) and the MR-AR-based design. The "sweet-gas" expander power is slightly higher in the MR-AR case since the MR permeate-side stream contains a significant quantity of water most of which, as steam, is used as sweep during MR operation; this increase in water in the "sweet-gas" accounts for the increase in expander power production. Along with a slightly higher "sweet-gas" expander power, the CO_2 compression of the MR-AR-based design is significantly lower than in the Baseline, since the CO_2 produced through the AR is at a much higher pressure (55.2 bar compared to 1 bar). In addition, the hydrogen/water mixture from the membrane permeate is expanded to reach 31.7 bar, and subsequently mixed with the expanded clean gas from the Single-Stage Selexol unit prior to being fed into the hydrogen combustion turbine, where it is assumed that the same total gross power is produced since the total hydrogen produced is equivalent in both cases.

Table 4-4: *Performance summary of Baseline IGCC design with CCS and the MR-AR-based IGCC design*

Performance Summary	Baseline IGCC with CCS (Case B5B)	MR-AR IGCC
Combustion Turbine Power, MWe	464	464
Sweet Gas Expander Power, MWe	7	11
Steam Turbine Power, MWe	264	264
Total Gross Power, MWe	**734**	**739**
Air Separation Unit Main Air Compressor, kWe	67,330	67,330
Oxygen Compressor, kWe	10,640	10,640
Nitrogen Compressors, kWe	35,640	35,640
CO_2 Compression, kWe	31,160	2,997
Acid Gas Removal, kWe	19,230	2,590
Balance of Plant, kWe	26,870	26,870
Total Auxiliaries, MWe	**191**	**146**
Net Power, MWe	**543**	**593**

4.4.1 Heat Integration

Heat integration analysis for the MR-AR-based process was carried out for the Baseline and MR-AR-based IGCC cases (only for the modified IGCC sections, which is depicted in blue-lined box in Figure 4-2), and the results can be seen below in Figures 4-6 – 4-7.

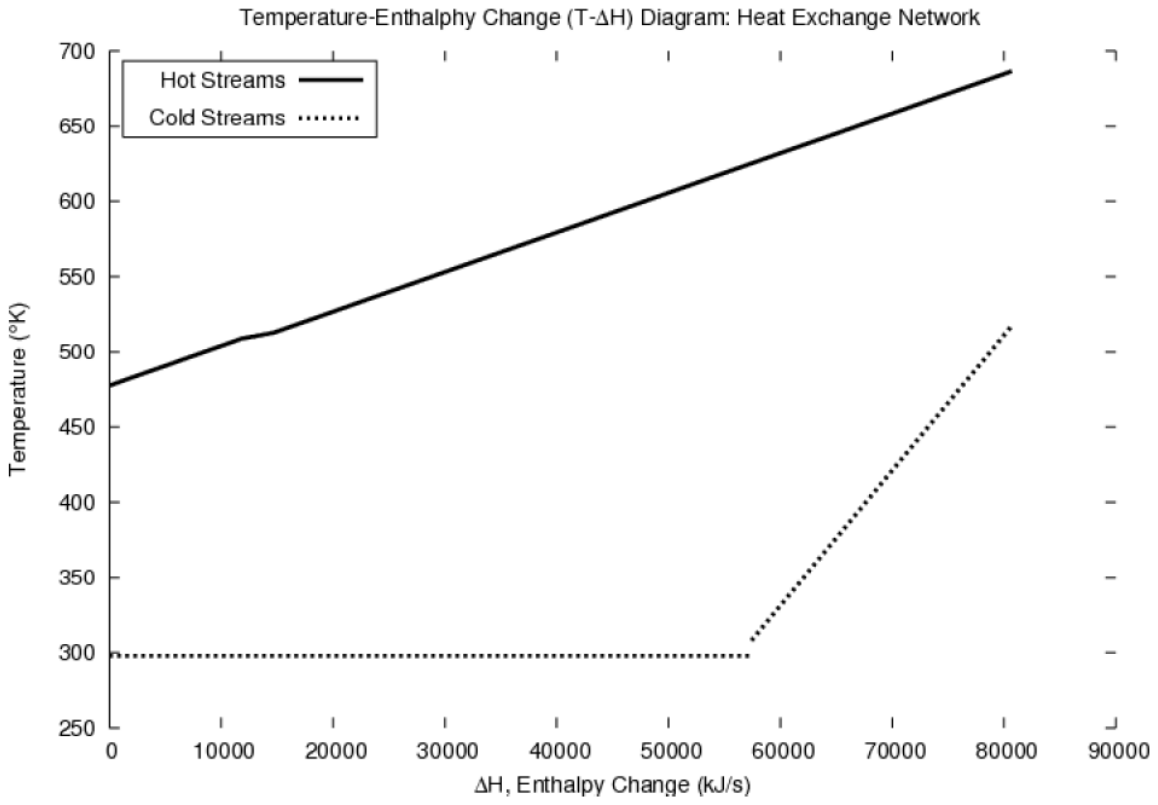

Figure 4-6: *Heat exchange network for the Baseline IGCC case depicting the Temperature-Enthalpy change diagram*

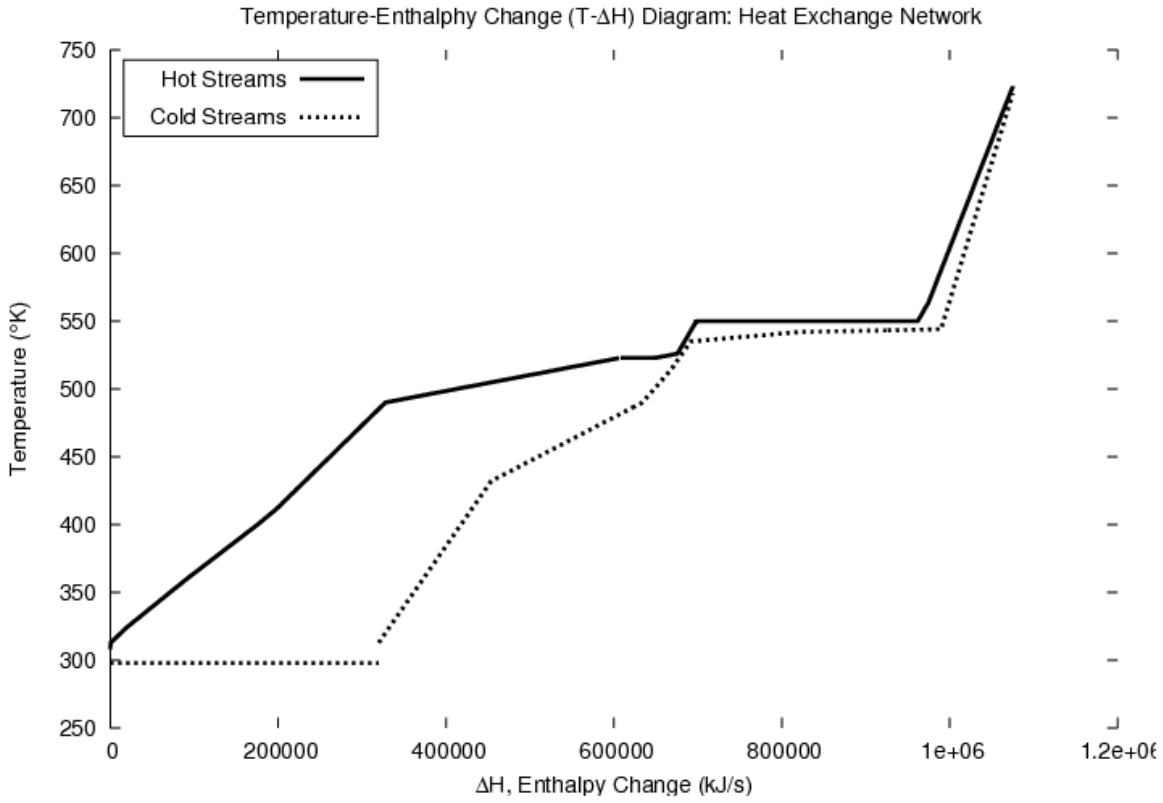

Figure 4-7: *Heat exchange network for the MR-AR IGCC case depicting the Temperature-Enthalpy change diagram*

Table 4-5: *Heat loads associated with baseline IGCC and MR-AR IGCC*

Baseline IGCC				MR-AR-Based IGCC			
Unit	**T in (K)**	**T out (K)**	**Heat Load (kJ/s)**	**Unit**	**T in (K)**	**T out (K)**	**Heat Load (kJ/s)**
Gas Cooling	686	478	264840	**MR-Ret**	563	523	-12503
Gas Cooling	513	509	184119	**AR-out**	523	400	-14294
Syngas Reheater	308	517	-102001	**AR-out**	400	360	-10669
				AR-out	360	308	-8335
				CO_2	723	526	-124267
				CO_2	526	490	-301620
				CO_2	490	313	-271867
				CO_2-Comp	412	324	-26448
				H_2O-rec	313	544	249943
				H_2O-rec	544	542	129247
				H_2O-rec	542	535	169105

	H_2O-rec	535	723	87894
	Clean gas	432	490	114593
	Clean gas	490	514	6964
	AR	523	523	-41548

The heat integration method utilized in this paper was previously developed in ref. (32), and its results show that 406 MJ/s of exothermic heat in the 500K – 300K temperature range are available for pre-heating any other streams in the plant for the MR-AR-based IGCC plant versus the 57.4 MJ/s of exothermic heat in the 600K – 470K temperature range that are available for the Baseline IGCC plant. In addition, the MR-AR-based design requires approximately 201 MJ/s of heat at 560K to evaporate the sweep steam required for AR operation. The amount of steam fed into the MR-AR-based IGCC plant is approximately 2.3 times that of the Baseline IGCC plant, and the costs can be seen in the next section. Utilizing the heat exchange area targeting scheme presented in (33,34), and assuming a heat transfer coefficient of 0.8 kW/(m^2 K) yields a higher heat exchange area of 64,650 m^2 for the proposed MR-AR-based IGCC plant versus the Baseline design. This area is then accounted for in the techno-economic analysis presented below, where the cost methodology for heat exchangers developed in ref. (35) is used.

4.4.2 Techno-Economic Analysis

A techno-economic analysis was performed on the MR-AR-based IGCC plant pictured in Figure 4-3 with the results tabulated in Tables 4-7 – 4-11, and the capital cost analysis summary Table 4-9 being shown at the end of this section. Equipment scaling was done according to the following NETL-provided equipment cost-scaling equation (36), with corresponding scaling parameters.

$$SC = RC * \left(\frac{SP}{RP} \right)^{Exp}$$, where

Exp – Exponent; RC – Reference Cost; RP – Reference Parameter; SC – Scaled Cost; SP – Scaling Parameter

The two major units that have undergone equipment scaling are the Single-Stage Selexol unit and the CO_2 compression and drying system. The rest of the units present in both the MR-AR-based IGCC and the Baseline IGCC design are identical and do not require any scaling. As mentioned above in the description of the MR, the membrane reactors were priced based on the membrane surface area that the bundles contain, currently valued at \$1200/m^2 according to M&PT. The cost components of the outer pressure vessels for the MR was taken from Timmerhouse (37), and this assumption was also utilized for the AR, and the flash separators. All other capital cost metric assumptions were taken from the NETL report (38) "Performing Techno-economic Analysis for Power Generation Plants", including the Contingency costs, where a 22% cost of equipment BEC was used, a value taken from NETL BBS case B5B (4).

The details of the operating cost analysis for the variable operating costs is presented at the end of this section (Table 4-11); the shift catalyst used in the proposed design is KATALCOJM™ K8-11HA, which costs \$17.5/lb, and the adsorbent used costs \$1/lb (these prices were provided by M&PT). The membrane life-span is assumed to be 10 years (sensitivity analysis of the impact on costs of membrane life-span is presented at the end of this section), with a membrane pack cost of \$650/m^2. The membrane replacement cost of \$650/m^2 is lower than the cost of a full membrane (\$1200/m^2) because the only part of the MR replaced is the membrane tube and the price \$1200/m^2 includes all of the steel house piping within the bundles that do not need to be replaced every 10

years along with the membrane tubes. All other variable costs are assumed to be the same as the Baseline IGCC with CCS plant, with the exception of the Selexol solution cost, which is scaled from NETL information on Single-Stage Selexol units in the same manner as the capital cost scaling. This assumption is used since a Single-Stage Selexol unit is implemented in the proposed MR-AR design instead of the Dual-Stage Selexol unit employed in the Baseline case. All cost assumptions utilized are summarized in Table 4-6.

Table 4-6: *Summary of cost assumptions used in TEA*

Unit	Cost Assumptions
Single-Stage Selexol	The cost is adjusted using the aforementioned NETL scaling equation with corresponding NETL scaling parameters, with the volumetric flow rate serving as the scaling parameters
Elemental Sulfur Plant	The cost is assumed to be the same due to NETL scaling parameters. The amount of sulfur is identical between the two cases
Mercury Removal	The cost is assumed to be the same due to NETL scaling parameters. The amount of mercury is identical between the two cases
Shift Reactors	The cost is different since the Baseline case uses PBRs and the proposed design uses MR-ARs
Fuel Gas Piping	The cost is assumed to be the same due to NETL scaling parameters
Heat Exchange Network	The increase in the heat exchanger areas required detailed by the heat integration in the previous section are reflected in this section
Combustion Turbine & Accessories	The cost is assumed to be the same since the nitrogen diluent is replaced by water and the hydrogen content is equal between the two cases
HRSG, Ducting & Stack	The cost is assumed to be the same since the nitrogen diluent is replaced by water and the hydrogen content is equal between the two cases
CO_2 compression	The cost is adjusted using the aforementioned NETL scaling equation with corresponding NETL scaling parameters with the power required for compression serving as the scaling parameters

The Cost of Electricity (COE) breakdown for the Baseline IGCC with CCS plant and our proposed MR-AR-based IGCC design is shown below in Table 4-7. The fixed operating cost, and fuel cost is assumed to be the same for the Baseline IGCC with CCS, and the MR-AR design. Finally, in the proposed MR-AR-based design, water is used as diluent in the Gas Turbine, and to account for the excess water used as diluent a maximum inlet rotor temperature of 1300°C is enforced to prevent turbine corrosion (4). The ASU produces 619 ton/h of pure N_2, which can therefore be sold for approximately $30/ton (39). The cost of semi-pure (99%) bulk Nitrogen have

been quoted at approximately $414/ton by different Nitrogen providers such as Praxair and West Air Gas. This value includes transportation, storage, and delivery costs, therefore, to account for these added costs, a $30/ton of N_2 will be the cost metric implemented in the TEA as the on site Nitrogen sale price. This could reduce the total COE by approximately 26.7. Table 4-8 summarizes the results and demonstrates that the MR-AR-based IGCC system is a transformational technology, since the CO_2 purity exceeds 95%, and the COE is significantly reduced compared to the COE of the Baseline IGCC with CCS design (Case B5B), including a net power production increase of more than 9%.

The detailed TEA for the MR-AR-based IGCC system that is used to calculate all the COE values can be found in Table 4-9 – 4-11 below. From these results, it is apparent that the MR-AR-based IGCC plant is a more efficient alternative for CCS than the traditional IGCC technologies currently proposed for CCS. Analysis of the capital costs of the MR-AR-based IGCC plant against the Baseline IGCC with CCS design shows a 16% capital cost reduction. By contrast, analysis of the variable operating costs of the MR-AR-based IGCC plant against the Baseline IGCC with CCS case indicates an increase of 2% in cost. The sale of Nitrogen provides $111,228,000/year in profit for the plant, which not only offsets any increase in operating costs it also produces added profit for the plant. The MR-AR-based IGCC system has unique intensification features that allow for significant decreases in the capital and operating costs of the IGCC plant. This is accomplished through the removal of the costly Dual-Stage Selexol unit, the production of higher-pressure CO_2 (55.2 bar), and the reduction of the amount of catalyst required for the WGSR step. The proposed plant not only produces 9.2% more power, but it is also less expensive from a capital-cost perspective while producing a valuable commodity product (Nitrogen) for sale. In addition, a sensitivity analysis was performed on the critical technology parameters for the MR-AR

technology (MR life-span and Nitrogen Sale Price). The results of this analysis are shown in Table 4-9. Reducing the membrane life-span from a 10 years, to 5 years, and then 2 years, increases the total COE by 0.2% and 0.6% respectively. Decreasing the sale price of Nitrogen to $1/ton, increases the total COE by 30%, whereas increasing the sale price of nitrogen to $414/ton would pay for all plant expenditures. These results illustrate that the intensification of the pre-combustion CCS of traditional IGCC plants via the proposed MR-AR design can improve the efficiency of CCS technologies and help reduce the time it takes for these technologies to be implemented in the USA and around the world.

Table 4-7: *COE component breakdown for the Baseline IGCC with CCS plant and the MR-AR-based IGCC design*

Baseline IGCC with CCS Plant (Case B5B)		**MR-AR-Based IGCC Plant**	
COE Component	**Value, $/MWh**	**COE Component**	**Value, $/MWh**
Capital Cost	74.2	Capital Cost	56.9
Fixed Operating Cost	18.2	Fixed Operating Cost	16.7
Variable Operating Cost	12.2	Variable Operating Cost	11.4
Fuel Cost	30.7	Fuel Cost	28.1
Total COE	135.4	Total COE (No N_2 sale / N_2 sale)	113.1/ 86.3

Table 4-8: *Summary table of Shell IGCC plant with and without CCS and the MR-AR-based IGCC design*

Designs	**Net Power Production (MWe)**	**CO_2 Capture (%)**	**CO_2 Purity**	**COE ($/MWh)**
Shell IGCC w/ CCS– Dual-Stage Selexol (Case B5B)	543	90	99	135.4
MR-AR-Based IGCC Plant	593	92	99	86.3

Table 4-9: *Summary of capital cost for MR-AR IGCC*

Case:		B5B – GEE Radiant IGCC w/ CO_2					Estimate Type:			Conceptual	
Plant Size (MW,net):		543					Cost Base:			Jun 2011	
Item No.	Description	Equipment Cost	Material Cost	Labor		Bare Erected Cost	Eng'g CM H.O.& Fee	Contingencies		Total Plant Cost	
				Direct	Indirect			Process	Project	$/1,000	$/kW
1		Coal & Sorbent Handling									
Subtotal		$17,335	$3,040	$13,259	$0	$33,633	$3,363	$0	$7,399	$44,396	$75
2		Coal & Sorbent Prep & Feed									
Subtotal		$29,564	$5,170	$17,541	$0	$52,275	$5,227	$1,906	$11,882	$71,290	$120
3		Feedwater & Miscellaneous BOP Systems									
Subtotal		$29,677	$9,494	$12,243	$0	$51,415	$5,142	$0	$12,479	$69,035	$116
4		Gasifier & Accessories									
Subtotal		$384,551	$14,421	$91,949	$0	$490,920	$49,092	$30,249	$76,387	$646,648	$1,090
5A		Gas Cleanup & Piping									
5A.1	Single Stage Selexol	$3,970	$0	$3,346	0	$7,316	$732	$0	$1,610	$9,658	$16
5A.2	Elemental Sulfur Plant	$12,451	$2,427	$15,954	$0	$30,833	$3,083	$0	$6,783	$40,699	$69
5A.3	Mercury Removal	$1,973	$0	$1,491	$0	$3,464	$346	$173	$797	$4,780	$8
5A.4	Reactor Vessels (MR+AR)	$2,415	$0	$966	$0	$3,381	$338	$0	$744	$4,463	$8
5A.5	Membrane Pack	$9,892	$0	w/equip	$0	$9,892	$989	$0	$2,176	$13,057	$22
5A.6	Flash Separators	$690	$0	$276	$0	$966	$97	$0	$212	$1,275	$2
5A.7	Fuel Gas Piping	$0	$812	$531	$0	$1,343	$134	$0	$296	$1,774	$3
5A.9	HGCU Foundations	$0	$735	$495	$0	$1,230	$123	$0	$406	$1,760	$3
5A.10	Heat Exchange Network	$12,987	$0	w/equip	$0	$12,987	$1,299	$0	$2,857	$17,143	$29
Subtotal		$44,378	$3,974	$23,059	$0	$71,411	$7,141	$173	$15,881	$94,609	$160
5B		CO_2 Compression									
5B.2	CO_2 Compression & Drying	$5,126	$769	$2220	0	$8,115	$811	0	$1,785	$10,711	$18
Subtotal		$5,126	$769	$2220	0	$8,115	$811	0	$1,785	$10,711	$18
6		Combustion Turbine & Accessories									
Subtotal		$117,901	$1,016	$9,975	$0	$128,892	$12,889	$11,909	$16,270	$169,960	$286
7		HRSG, Ducting, & Stack									
Subtotal		$33,630	$2,884	$9,498	$0	$46,012	$4,601	$0	$5,797	$56,411	$95
8		Steam Turbine Generator									
Subtotal		$55,693	$1,108	$16,654	$0	$73,456	$7,346	$0	$12,319	$93,121	$157
9		Cooling Water System									
Subtotal		$8,296	$12,271	$9,900	$0	$30,467	$3,047	$0	$7,077	$40,591	$68

10	Ash & Spent Sorbent Handling Systems									
Subtotal	$17,787	$9,928	$17,885	$0	$45,600	$4,560	$0	$5,403	$55,563	$94
11	Accessory Electric Plant									
Subtotal	$36,715	$16,126	$29,455	$0	$82,297	$8,230	$0	$17,319	$107,845	$182
12	Instrumentation & Control									
Subtotal	$13,381	$2,713	$8,797	$0	$24,891	$2,489	$1,245	$4,807	$33,431	$56
13	Instrumentation & Control									
Subtotal	$3,923	$2,312	$10,297	$0	$16,532	$1,653	$0	$5,456	$23,641	$40
14	Instrumentation & Control									
Subtotal	$0	$8,248	$9,382	$0	$17,630	$1,763	$0	$3,175	$22,568	$38
Total	$819,238	$93,474	$302,270	$0	$1,214,986	$121,497	$45,482	$212,551	$1,539,820	$2,597

Table 4-10: *Fixed capital cost summary for the MR-AR-based IGCC plant*

Description	$/1,000
Pre-Production Costs	
6 Months All Labor	$16,298
1 Month Maintenance Materials	$3,682
1 Month Non-fuel Consumables	$676
1 Month Waste Disposal	$494
25% of 1 Months Fuel Cost at 100% CF	$3,046
2% of TPC	$36,802
Total	**$60,998**
Inventory Capital	
60-day supply of fuel and consumables at 100% CF	$25,290
0.5% of TPC (spare parts)	$9,201
Total	**$34,491**
Other Costs	
Initial Cost for Catalyst and Chemicals	$16,548
Land	$900
Other Owner's Costs	$276,017
Financing Costs	$49,683
Total Overnight Costs (TOC)	**$2,278,752**
TASC Multiplier (IOU, high-risk, 35 year)	1.140
Total As-Spent Cost (TASC)	**$2,597,777**

Table 4-11: *Variable operating cost of MR-AR-based IGCC plant*

Case:	B5B – GEE Radiant IGCC w/ CO_2				Cost Base:	Jun 2011
Plant Size (MW,net):	579	Heat Rate-net (Btu/kWh):		10,459	Capacity Factor (%):	80
Operating & Maintenance Labor						
Operating Labor				**Operating Labor Requirements per Shift**		
Operating Labor Rate (base):	39.70	**$/hour**		Skilled Operator:	2.0	
Operating Labor Burden:	30.00	**% of base**		Operator:	10.0	
Labor O-H Charge Rate:	25.00	**% of labor**		Foreman:	1.0	
				Lab Tech's, etc.:	3.0	
				Total:	**16.0**	
Fixed Operating Costs						
					Annual Cost	
					($)	
Annual Operating Labor:					$7,233,658	
Maintenance Labor:					$18,843,231	
Administrative & Support Labor:					$6,519,222	
Property Taxes and Insurance:					$36,802,296	
Total:					**$69,398,406**	
Variable Operating Costs						
					($)	
Maintenance Material:					$35,348,580	
Consumables						
	Consumption				**Cost ($)**	
	Initial Fill	**Per Day**	**Per Unit**	**Initial Fill**		
Water (/1000 gallons):	0	6,108	$1.67	$0	$2,985,305	
Makeup and Waste Water Treatment Chemicals (lbs)	0	25,026	$0.27	$0	$2,845,681	
Carbon (Mercury Removal) (lb):	135,182	231	$5.50	$743,501	$371,751	
Shift Catalyst (ft^3):	2,553	3.39	$700	$2,844,744	$568,949	
Adsorbent (lb)	303,456	0.81	$1	$606,912	$121,382	
Membrane Packs (m^2)	w/equip	n/a	$650	$0	$535,780	
Selexol Solution (gal):	19,038	3	$36.79	$700,421	$30,340	
Claus Catalyst (ft^3):	w/equip	2.01	$203.15	$0	$119,487	
Subtotal:				**$4,895,578**	**$7,578,675**	
Waste Disposal						
Spent Mercury Catalyst (lb.):	0	231	$0.65	$0	$43,941	
Flyash (ton):	0	0	$0.00	$0	$0	
Slag (ton):	0	641	$25.11	$0	$4,701,292	
Subtotal:				**$0**	**$4,745,232**	
By-Products						
Sulfur (tons):	0	146	$0.00	$0	$0	
Subtotal:				**$0**	**$0**	
Variable Operating Costs Total:				**$16,547,652**	**$47,672,487**	
Fuel Cost						
Illinois Number 6 (ton):	0	5,844	$68.54	$0	$116,961,258	
Total:				**$0**	**$116,961,258**	

Table 4-12: *Sensitivity analysis for the MR-AR-based IGCC plant*

Sensitivity Analysis – Membrane Reactor Lifespan					
	Consumption				Cost ($)
	Initial Fill	Per Day	Per Unit	Initial Fill	Annual Cost
10 Year MR Lifespan					
Membrane Packs (m^2)	w/equip	n/a	$650	$0	$535,780
Total Variable Cost:				$16,547,652	$47,672,487
Total COE:					86.3
5 Year MR Lifespan					
Membrane Packs (m^2)	w/equip	n/a	$650	$0	$1,071,560
Total Variable Cost:				$10,074,435	$48,208,277
Total COE:					86.5
2 Year MR Lifespan					
Membrane Packs (m^2)	w/equip	n/a	$650	$0	$2,678,900
Total Variable Cost:				$10,074,435	$49,815,607
Total COE:					86.8
Sensitivity Analysis – Nitrogen Sale Price					
	Consumption				Cost ($)
	Initial Fill	Per Day	Per Unit	Initial Fill	Annual Profit
$30/ton Nitrogen Price					
Nitrogen (tons)	0	14,591	$30	$0	$111,228,000
Total COE ($/MWe)					86.3
$1/ton Nitrogen Price					
Nitrogen (tons)	w/equip	n/a	$1	$0	$3,707,600
Total COE ($/MWe)					112.2
$414/ton Nitrogen Price					
Nitrogen (tons)	w/equip	n/a	$414	$0	$1,534,946,400
Total COE ($/MWe)					-255.8

4.5 Conclusions

The intensification of an IGCC plant with pre-combustion CCS technology was explored through the implementation of a combined MR-AR reactor system. This MR-AR reactor system was simulated through the COMSOL software and implemented into the IGCC structure via a flowsheet developed through Honeywell's flowsheet simulator UNISIM™ with corresponding heat integration studies. A TEA of the proposed MR-AR-based IGCC plant was developed, and the MR-AR-based IGCC plant produced more than 9% additional power than the Baseline IGCC with CCS design. In addition, the MR-AR-based IGCC plant had a more than 16% reduction in capital cost and a significant reduction in the COE of the plant when compared to the Baseline pre-

combustion CCS technology. Finally, the proposed plant's COE reduction over the Baseline case demonstrates that the MR-AR reactor system can help bridge the cost-gap that is currently rendering CCS prohibitive for near-term market deployment.

4.6 References

1. Liu PK, Sahimi M, Tsotsis TT. Process intensification in hydrogen production from coal and biomass via the use of membrane-based reactive separations. Curr Opin Chem Eng. 2012 Aug 1;1(3):342–51.

2. Yu J, Tan M, Liu PKT, Sahimi M, Tsotsis TT. Hydrogen Production from Biomass-Derived Syngas Using a Membrane Reactor Based Process. Ind Eng Chem Res. 2014 Jan 15;53(2):819–27.

3. Abdollahi M, Yu J, Liu PKT, Ciora R, Sahimi M, Tsotsis TT. Hydrogen production from coal-derived syngas using a catalytic membrane reactor based process. J Membr Sci. 2010 Nov 1;363(1):160–9.

4. Department of Energy/National Energy Technology Laboratory. Cost and Performance Baseline for Fossil Energy Plants Volume 1b: Bituminous Coal (IGCC) to Electricity Revision 2b – Year Dollar Update.

5. Urech J, Tock L, Harkin T, Hoadley A, Maréchal F. An assessment of different solvent-based capture technologies within an IGCC–CCS power plant. Energy. 2014 Jan 1;64:268–76.

6. Gibbins J, Chalmers H. Carbon capture and storage. Energy Policy. 2008 Dec 1;36(12):4317–22.

7. De Falco M, Marrelli L, Iaquaniello G, editors. Membrane reactors for hydrogen production processes. London ; New York: Springer; 2011. 235 p.

8. Dixon AG. Recent Research in Catalytic Inorganic Membrane Reactors. Int J Chem React Eng [Internet]. 2003 [cited 2018 Jul 23];1(1). Available from: https://www.degruyter.com/view/j/ijcre.2002.1.1/ijcre.2002.1.1.1123/ijcre.2002.1.1.1123.xml

9. TSAI C-Y, MA YH, MOSER WR, DIXON AG. Modeling and Simulation of a Nonisothermal Catalytic Membrane Reactor. Chem Eng Commun. 1995 May 1;134(1):107–32.

10. Harale A, Hwang HT, Liu PKT, Sahimi M, Tsotsis TT. Experimental studies of a hybrid adsorbent-membrane reactor (HAMR) system for hydrogen production. Chem Eng Sci. 2007 Aug 1;62(15):4126–37.

11. Mendes D, Mendes A, Madeira LM, Iulianelli A, Sousa JM, Basile A. The water-gas shift reaction: from conventional catalytic systems to Pd-based membrane reactors—a review. Asia-Pac J Chem Eng. 5(1):111–37.

12. Adrover ME, López E, Borio DO, Pedernera MN. Simulation of a membrane reactor for the WGS reaction: Pressure and thermal effects. Chem Eng J. 2009 Nov 15;154(1):196–202.

13. Fayyaz B, Harale A, Park B-G, Liu PKT, Sahimi M, Tsotsis TT. Design Aspects of Hybrid Adsorbent−Membrane Reactors for Hydrogen Production. Ind Eng Chem Res. 2005 Dec 1;44(25):9398–408.

14. Lund CRF. WATER-GAS SHIFT KINETICS OVER IRON OXIDE CATALYSTS AT MEMBRANE REACTOR CONDITIONS [Internet]. National Energy Technology Lab., Pittsburgh, PA (US); National Energy Technology Lab., Morgantown, WV (US); 2002 Aug [cited 2018 Jul 23]. Report No.: FG26-99FT40590-03. Available from: https://www.osti.gov/biblio/803841

15. Morreale BD, Ciocco MV, Enick RM, Morsi BI, Howard BH, Cugini AV, et al. The permeability of hydrogen in bulk palladium at elevated temperatures and pressures. J Membr Sci. 2003 Feb 15;212(1):87–97.

16. Halabi MH, de Croon MHJM, van der Schaaf J, Cobden PD, Schouten JC. Reactor modeling of sorption-enhanced autothermal reforming of methane. Part I: Performance study of hydrotalcite and lithium zirconate-based processes. Chem Eng J. 2011 Apr 1;168(2):872–82.

17. Tosti S, Bettinali L, Violante V. Rolled thin Pd and Pd–Ag membranes for hydrogen separation and production. Int J Hydrog Energy. 2000 Apr 1;25(4):319–25.

18. Criscuoli A, Basile A, Drioli E. An analysis of the performance of membrane reactors for the water–gas shift reaction using gas feed mixtures. Catal Today. 2000 Feb 25;56(1):53–64.

19. Li X, Liu TM, Fan YQ, Xu NP. Preparation of composite palladium-silver alloy membranes by photocatalytic deposition. Thin Solid Films. 2008 Sep 1;516(21):7282–5.

20. Park B-G. A hybrid adsorbent-membrane reactor (HAMR) system for hydrogen production. Korean J Chem Eng. 2004 Jul 1;21(4):782–92.

21. Harale A, Hwang HT, Liu PKT, Sahimi M, Tsotsis TT. Design aspects of the cyclic hybrid adsorbent-membrane reactor (HAMR) system for hydrogen production. Chem Eng Sci. 2010 Jan 1;65(1):427–35.

22. Garshasbi A, Chen H, Cao M, Karagöz S, Ciora RJ, Liu PKT, et al. Membrane-based reactive separations for process intensification during power generation. Catal Today [Internet]. 2017 Oct 26 [cited 2017 Dec 1]; Available from: http://www.sciencedirect.com/science/article/pii/S0920586117307368

23. Ziaka Z, Manousiouthakis V. Best Achievable Isomerization Reaction Conversion in a Membrane Reactor. Ind Eng Chem Res. 1998 Sep 1;37(9):3551–60.

24. Chmielewski D, Ziaka Z, Manousiouthakis V. Conversion targets for plug flow membrane reactors. Chem Eng Sci. 1999 Jul 1;54(13):2979–84.

25. Soltani S, Sahimi M, Tsotsis T. Catalytic Membrane Reactors. In: Encyclopedia of Membrane Science and Technology [Internet]. American Cancer Society; 2013 [cited 2018 Jul 23]. p. 1–39. Available from: https://onlinelibrary.wiley.com/doi/abs/10.1002/9781118522318.emst110

26. Sorption-Enhanced Hydrogen Production: A Review - Industrial & Engineering Chemistry Research (ACS Publications) [Internet]. [cited 2018 Jul 23]. Available from: https://pubs.acs.org/doi/abs/10.1021/ie800298z

27. García-Lario AL, Aznar M, Martinez I, Grasa GS, Murillo R. Experimental study of the application of a NiO/NiAl2O4 catalyst and a CaO-based synthetic sorbent on the Sorption Enhanced Reforming process. Int J Hydrog Energy. 2015 Jan 5;40(1):219–32.

28. Pichardo PA, Karagöz S, Tsotsis T, Ciora R, Manousiouthakis VI. Technical economic analysis of an intensified Integrated Gasification Combined Cycle (IGCC) power plant featuring a sequence of membrane reactors. J Membr Sci. 2019 Jun 1;579:266–82.

29. Karagoz S. Multi-Scale Modeling and Simulation of Intensified Reactive-Separation Processes for Hydrogen Production and CO2 Capture via the Water-Gas Shift Reaction (WGSR) [Internet]. UCLA; 2018 [cited 2019 Feb 6]. Available from: https://escholarship.org/uc/item/7161q4tk

30. Karagöz S, da Cruz FE, Tsotsis TT, Manousiouthakis VI. Multi-scale membrane reactor (MR) modeling and simulation for the water gas shift reaction. Chem Eng Process - Process Intensif. 2018 Nov 1;133:245–62.

31. Multi-scale modeling and simulation of a novel membrane reactor (MR)/adsorptive reactor (AR) process - ScienceDirect [Internet]. [cited 2019 Mar 11]. Available from: https://www.sciencedirect.com/science/article/abs/pii/S0255270118313837

32. Holiastos K, Manousiouthakis V. Minimum hot/cold/electric utility cost for heat exchange networks. Comput Chem Eng. 2002 Jan 15;26(1):3–16.

33. Manousiouthakis V, Martin LL. A minimum area (MA) targeting scheme for single component MEN and HEN synthesis. Comput Chem Eng. 2004 Jul;28(8):1237–47.

34. Linnhoff B, Ahmad S. Cost optimum heat exchanger networks—1. Minimum energy and capital using simple models for capital cost. Comput Chem Eng. 1990 Jul 1;14(7):729–50.

35. Hall SG, Ahmad S, Smith R. Capital cost targets for heat exchanger networks comprising mixed materials of construction, pressure ratings and exchanger types. Comput Chem Eng. 1990 Mar;14(3):319–35.

36. Department of Energy/National Energy Technology Laboratory. Quality Guidelines For Energy System Studies – Capital Cost Scaling Methodology. Report No.: DOE/NETL-341/013113.

37. Peters MS, TImmerhaus, Klaus D., West, Ronald Emmett. Plant design and economics for chemical engineers. Vol. 4. New York: McGraw-Hill; 1968.

38. Department of Energy/National Energy Technology Laboratory. Quality Guidelines For Energy System Studies – Performing a Techno-economic Analysis for Power Generation Plants. Report No.: DOE/NETL-2015/1726.

39. Schmidt S, Clayton R. Dynamic Design of a Cryogenic Air Separation Unit. 2013;41.

Chapter 5: Intensified Energetically Enhanced Steam Methane Reforming (IEER) Through the Use of Membrane Reactors

5.1 Abstract

This work focuses on the implementation of membrane reactors (MRs) in the production of hydrogen through steam methane reforming (SMR). A novel equilibrium MR model featuring Gibbs Free Energy Minimization is introduced and applied to the SMR-MR process. In addition, the concept of "energetically enhanced steam methane reforming (EER)," which allows for the use of a hybrid (methane combustion/renewable energy) energy supply in the production of hydrogen, is intensified. The UNISIM software (Honeywell^{TM}) is used to create a range of intensified flowsheets depicting the proposed IEER-MR process as well as two baseline flowsheets depicting "a standard SMR-MR process" and "a fully exothermic EER process." Heat integration studies are carried out on the developed flowsheets, and the baseline designs are compared to the IEER-MR designs to identify energetic intensification.

5.2 Introduction

The concept of process intensification is currently one of the most important trends in chemical engineering. It has been defined as the development of technology and methods that can produce dramatic improvements in chemical processing[1]. These drastic improvements can consist of substantial decrease in equipment volume, energy consumption, or waste formation that can lead to safer, sustainable, and cheaper manufacturing processes[2]. Process intensification (PI) can offer methods of supporting sustainable industrial growth through a variety of tools. Some of these tools include the use of a pinch-like targeting framework that can combine two or more heat sources into a single intensified device aimed at thermal process intensification[3], and the use of the Infinite DimEnsionAl State-space (IDEAS) conceptual framework, which has been applied to topics such as reactive distillation systems[4], and energetically enhanced reforming[5]. Along with these intensification frameworks, is the integration of multi-functional units such as

membrane reactors. Membrane reactor processes can be used to attain PI objectives since they have the ability of simultaneous reaction and separation. The study of membrane reactor processes' contribution in the process intensification field has been vastly researched[6] including the intensification of lactic acid production[7] and biodiesel production[8].

Membrane reactors (MRs) combine reaction and separation in one single unit through the removal of, at minimum, one of the species present. Typically, these types of reactors are used when reactions are limited by thermodynamic equilibrium, since removing at least one of the reacting products through membrane permeation results in an increase in the conversion and yield beyond the limiting equilibrium value[9]. In addition to improving a reaction's yield, MRs can increase the selectivity and yield of enzymatic and catalytic reactions by selectively removing intermediate species that would otherwise deactivate the reaction[9]. MRs have been studied in the production of various materials including biodiesel[10], chitooligosaccharides[11], and hydrogen[12–15]. The production of hydrogen has been a particular area of interest for MRs through steam-methane reforming. Studies have been done on the use of ceramic membrane reactors for converting methane to syngas[13], steam reforming of a hydrocarbon to produce H_2, CO, and CO_2[15], and our team specifically, has researched producing H_2 via the water gas shift (WGS) reaction in the context of the IGCC process for power generation from coal[16]. In this work, the application of MRs to Energetically Enhanced Steam Methane Reforming (EER) is explored.

The definition of an Energetically Enhanced Process (EEP) is as follows: "a process is Energetically Enhanced, compared to its traditional counterpart, if its energy consumption at high temperatures is either reduced or eliminated, even if such reduction necessitates higher energy consumption at lower temperatures[17]." Our team has explored energetic intensification of a network in our previous works[5,18] that detail the energetic intensification of a traditional SMR

process, and quantifies the parametric conditions required for this intensification. Currently, the SMR process remains the most economical process for hydrogen production, and is typically carried out industrially at 1100K as a highly endothermic process[19]. Due to the high temperature heat requirements for reforming to occur, EEP techniques were used to develop a reforming process where the 1100K heat load was substantially reduced to the point of exothermicity[20]. This reduction in heat load was due to the recycling of CO into the reformer, which resulted in an increase in conversion of the exothermic water-gas-shift reaction. As the concentration of CO in the reformer feed was increased, the total endothermic load decreased until it became exothermic. Consequently, for exothermicity to be reached, the amount of CO required in the reformer feed was approximately 15 kmol/hr of CO per 1 kmol/hr of CH_4[20], yielding a high amount of recycle. For this reason, the implementation of MRs into the EER framework was considered for EER intensification because MRs can increase reaction yield, thus decreasing the total plant recycle.

The paper is structured as follows; first, the MR Gibbs Free Energy equilibrium model is presented; second, Honeywell's flowsheet simulator UNISIM is utilized to develop three baseline flowsheets, and three IEER flowsheets; subsequently, heat integration studies are performed and results are presented; finally, the IEER process results are discussed and conclusions are drawn.

5.3 Gibbs Free Energy Minimization Formulation for Membrane Reactors

For the considered MRs implemented into the SMR process, the use of equilibrium reactor models is considered. In particular, a Gibbs free energy minimization problem is formulated to account for species permeation through a membrane. Applying the necessary conditions of optimality to a Gibbs equilibrium formulation for membrane reactors, combined with the

chemical potential's definition, imply the equality of chemical potentials of a species in the phases in which that species is present.

$$\left\{ \begin{array}{l} \pi\left(T,P,\left\{a_i\right\}_{i=1}^{NE}\right) \triangleq \underset{\left\{n_j^{(g)}\right\}_1^{NC},\left\{n_j^{(l)}\right\}_1^{NC},\left\{n_j^{(s)}\right\}_1^{NC}}{\min} \quad \sum_j^{NC} \left[\begin{array}{l} n_j^{(g)}\Delta G_{f_j}^{o(g)}\left(T\right)+n_j^{(l)}\Delta G_{f_j}^{o(l)}\left(T\right) \\ +n_j^{(s)}\Delta G_{f_j}^{o(s)}\left(T\right)+n_j^{(P)}\Delta G_{f_j}^{o(P)}\left(T\right) \\ +RT\left[\begin{array}{l} n_j^{(g)}\ln\left(\dfrac{n_j^{(g)}}{\sum_l^{NC} n_l^{(g)}}P\right)+n_j^{(l)}\ln\left(\dfrac{n_j^{(l)}}{\sum_l^{NC} n_l^{(l)}}\right) \\ +n_j^{(P)}\ln\left(\dfrac{n_j^{(P)}}{\sum_l^{NC} n_l^{(l)}}\right) \end{array} \right] \end{array} \right] \\ s.t. \quad a_i-\sum_k^{NP}\sum_j^{NC}\nu_{ij}n_j^{(k)}=0 \quad \forall i=1,NA \\ n_j^{(g)}\geq 0;\ n_j^{(l)}\geq 0;\ n_j^{(s)}\geq 0 \qquad \forall j=1,NC \end{array} \right\}$$

The indices $i=1,m;\ j=1,n;k=1,NP$ denote the ith atom, jth species, and kth phase respectively, and the variables α, n, T, P, G denote the atomic molar flow rate (moles/s), molar flow rate (moles/s), temperature (K), pressure (bar), and Gibbs free energy (kJ/mol) respectively. The indices NC, NE, NP are the number of components, the number of elements, and the number of phases respectively, and the variable $\nu_{i,j}$ denotes the number of ith type atoms in the jth species' molecule.

For the IEER-MR formulation, the permeate will be denoted as a separate phase in the reactor. Below is the formulation for membrane reactors undergoing the steam-methane

reforming with species: methane, steam, carbon monoxide, carbon dioxide and hydrogen and carbon.

$$\pi\left(T,P,\{a_C,a_H,a_O\}\right)\triangleq \min_{n_{CO},n_{CH_4},n_{H_2O},n_{H_2},n_{CO_2},n_C}$$
$$\left[\begin{array}{l} n_{CO}^{(g)}G_{CO}^{o(g)}(T)+n_{CH_4}^{(g)}G_{CH_4}^{o(g)}(T)+n_{H_2O}^{(g)}G_{H_2O}^{o(g)}(T)+ \\ +n_{H_2}^{(g)}G_{H_2}^{o(g)}(T)+n_{CO_2}^{(g)}G_{CO_2}^{o(g)}(T)+n_C^{(s)}G_C^{o(s)}(T)+ \\ +n_{H_2}^{(p)}G_{H_2}^{o(p)}(T) \\ +RT\left(\begin{array}{l} n_{CO}^{(g)}\ln\left(\frac{n_{CO}^{(g)}}{n_{CO}^{(g)}+n_{CH_4}^{(g)}+n_{H_2O}^{(g)}+n_{H_2}^{(g)}+n_{CO_2}^{(g)}}P\right)+ \\ +n_{CH_4}^{(g)}\ln\left(\frac{n_{CH_4}^{(g)}}{n_{CO}^{(g)}+n_{CH_4}^{(g)}+n_{H_2O}^{(g)}+n_{H_2}^{(g)}+n_{CO_2}^{(g)}}P\right)+ \\ +n_{H_2O}^{(g)}\ln\left(\frac{n_{H_2O}^{(g)}}{n_{CO}^{(g)}+n_{CH_4}^{(g)}+n_{H_2O}^{(g)}+n_{H_2}^{(g)}+n_{CO_2}^{(g)}}P\right)+ \\ +n_{H_2}^{(g)}\ln\left(\frac{n_{H_2}^{(g)}}{n_{CO}^{(g)}+n_{CH_4}^{(g)}+n_{H_2O}^{(g)}+n_{H_2}^{(g)}+n_{CO_2}^{(g)}}P\right)+ \\ +n_{CO_2}^{(g)}\ln\left(\frac{n_{CO_2}^{(g)}}{n_{CO}^{(g)}+n_{CH_4}^{(g)}+n_{H_2O}^{(g)}+n_{H_2}^{(g)}+n_{CO_2}^{(g)}}P\right)+ \\ +n_{H_2}^{(p)}\ln\left(\frac{n_{H_2}^{(p)}}{n_{H_2}^{(p)}}P^p\right) \end{array}\right) \end{array}\right] \Rightarrow$$

$$\begin{array}{ll} s.t. & a_C-\left(n_{CO}^{(g)}+n_{CH_4}^{(g)}+n_{CO_2}^{(g)}+n_C^{(s)}\right)=0 \\ & a_H-\left(4n_{CH_4}^{(g)}+2n_{H_2O}^{(g)}+2n_{H_2}^{(g)}+2n_{H_2}^{(p)}\right)=0 \\ & a_O-\left(n_{CO}^{(g)}+n_{H_2O}^{(g)}+2n_{CO_2}^{(g)}\right)=0 \\ & n_{CO}^{(g)}\geq 0,\ n_{CH_4}^{(g)}\geq 0,\ n_{H_2O}^{(g)}\geq 0,\ n_{H_2}^{(g)}\geq 0,\ n_{CO_2}^{(g)}\geq 0,\ n_C^{(s)}\geq 0,\ n_{H_2}^{(p)}\geq 0 \end{array}$$

The superscripts $g;\ s;\ p$ denote the gas, solid, and permeate phases respectively, and the subscripts $C;H;O;CH_4;H_2O;CO;CO_2;H_2$ denote the carbon, hydrogen and oxygen atoms, and the methane, water, carbon monoxide, carbon dioxide and hydrogen species respectively. The above formulation was used to model the MR reactors, which were implemented in both the baseline SMR-MR process and the IEER-MR processes. Table 5-1 below details the above formulation as applied to a membrane reactor with permeate pressure at 1 bar, retentate pressure

at 40 bar, and temperature at 890K with varying CH_4/CO/H_2O inlets. As the CO conversion increases the heat load of the reactor decreases illustrating the possible energetic enhancement of including CO in the reforming reactor feed.

Table 5-1: *Thermodynamic Gibbs Minimization equilibrium membrane reactor simulations*

MR Inlet (kmol/hr)			**MR Outlet Retentate (P=40 bar) (kmol/hr)**					**MR Outlet Permeate (P=1 bar) (kmol/hr)**	**T=890K**
CH_4	*CO*	*H_2O*	*CH_4*	*CO*	*CO_2*	*H_2O*	*H_2*	*H_2*	*Heat Load (kJ/s)*
1	0	2	0.0033	0.0281	0.9687	0.5346	0.0393	3.9195	52.59
1	0.5	2	0.0406	0.1164	1.3429	0.1977	0.0435	4.1775	46.53
1	1	2	0.1809	0.2644	1.5547	0.1262	0.0545	3.9574	35.66
1	2	2	0.9464	0.7380	2.3156	0.1309	0.1059	2.3703	-19.71
1	6	2	2.0902	1.4722	3.4376	0.1527	0.1661	0.0009	-102.30
1	0	4	0.0009	0.0149	0.9842	2.0167	0.0774	3.9042	52.58
1	0.5	4	0.0024	0.0293	1.4683	1.5340	0.0778	4.3834	47.67
1	1	4	0.0065	0.0561	1.9373	1.0692	0.0787	4.8390	42.74
1	2	4	0.3618	0.5288	3.1094	0.2524	0.1090	4.9148	8.89
1	6	4	1.4955	1.2564	4.2481	0.2474	0.1858	2.5759	-73.23
1	0	6	0.0006	0.0124	0.9869	4.0137	0.1286	3.8565	52.57
1	0.5	6	0.0015	0.0214	1.4771	3.5243	0.1290	4.3438	47.64
1	1	6	0.0022	0.0329	1.9649	3.0373	0.1292	4.8291	42.74
1	2	6	0.0285	0.1643	3.8071	1.2214	0.1339	6.5876	22.75
1	6	6	0.7176	0.9730	5.3095	0.4081	0.1900	5.9668	-35.22
1	0	10	0.0010	0.0112	0.9878	8.0132	0.2311	3.7537	52.54
1	0.5	10	0.0011	0.0179	1.4810	7.5200	0.2313	4.2466	47.63
1	1	10	0.0013	0.0256	1.9731	7.0283	0.2315	4.7376	42.71
1	2	10	0.0051	0.0708	3.9241	5.0811	0.2328	6.6758	23.05
1	6	10	0.0433	0.2682	6.6885	2.3548	0.2399	9.3188	-6.85

5.4 Traditional SMR Baseline Process

A baseline flowsheet is first created on the UniSim (Honeywell Inc. trademark) software, that captures a traditional design of this process (Figure 5-1) with corresponding stream and energy flow tables (Appendix Table 5-3). The Peng Robinson equation of state is used to capture the thermodynamic properties of the gas mixture. CH_4 (1 kmol/hr) and H_2O (2 kmol/hr) enter the

flowsheet at 298K. Subsequently, both are compressed to 5 bar through the use of a compressor and a pump. Prior to entering a reformer with outlet temperature 1100K, the water and carbon dioxide undergo heating. The reformer outlet is subsequently fed into a sequence of high temperature shift (650K outlet temperature), low temperature shift (475K outlet temperature) reactors with cooling in between. The resultant stream is then cooled before undergoing water, carbon dioxide and hydrogen separation all at 313K. The water, unreacted methane, and carbon monoxide are recycled to the reformer, while hydrogen (4 kmol/hr) and carbon dioxide (1 kmol/hr) are the flowsheet products.

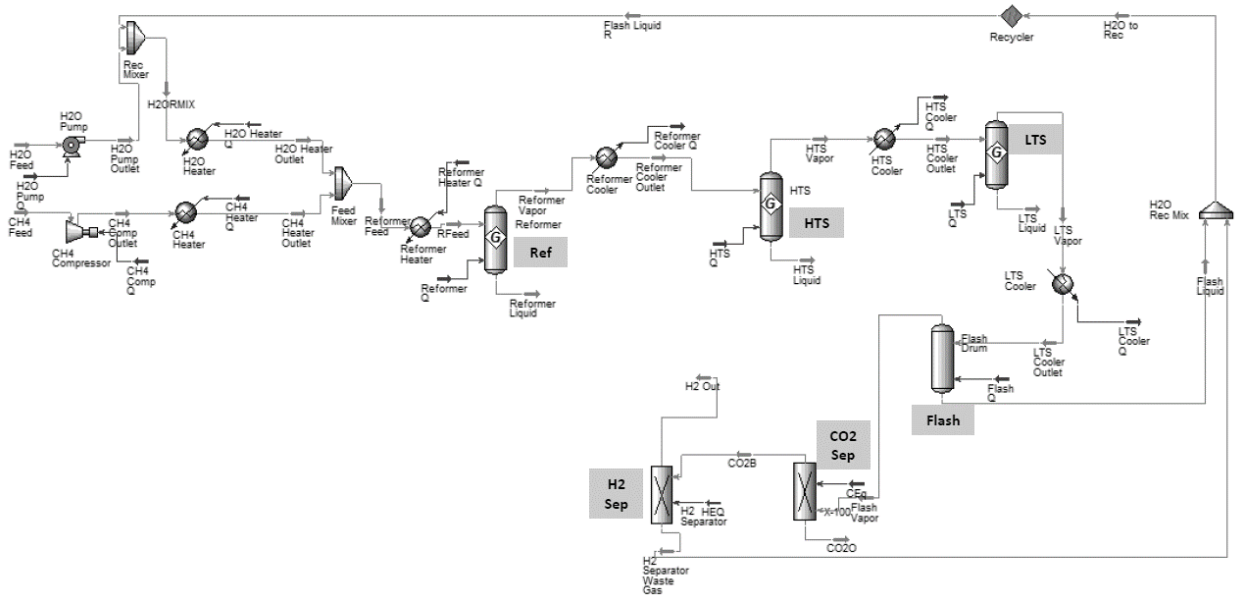

Figure 5-1: *Traditional SMR Baseline Flowsheet*

The work of separation required from the ideal CO_2 and H_2 separators is approximately 2.36 kJ/s and is calculated through the use of the following formula derived in our previous work[5],

$$\dot{W}_{Ideal} = \sum_{i \in S_O} F_i \left(H_i - T_\sigma S_i \right) - \sum_{i \in S_I} F_i \left(H_i - T_\sigma S_i \right)$$

where the variables $\dot{W}_{Ideal}; F; H; S; T_{\sigma}$ are denoted as the ideal work of separation (kJ/s), the mass flow rate (mol/s), the specific enthalpy (kJ/mol), the specific entropy (kJ/mol K), and the temperature of the environment (K) respectively, and the subscripts $S_o; S_i$ denote the outlets and inlets of the separators respectively.

In addition to the work of separation calculations, heat integration studies were carried out using the mathematical formulation developed for minimum hot/cold/electric utility cost problems for heat exchange networks[21]. This globally optimal thermodynamic heat and power integration approach is used to determine the minimum total hot/cold/electric utility cost required in process flowsheets given process streams with known flowsheet inlet and outlet temperatures and flow rates, and utility streams. Below Figures 5-2 – 5-3 demonstrate the heat integration studies carried out for the traditional SMR baseline design, external hot utility loads of 60.7 kJ/s, 5.48 kJ/s, and 4.16 kJ/s are needed at 1200K, 770K and 420K respectively, and an external cold utility load of 3.15 kJ/s is needed at 298K.

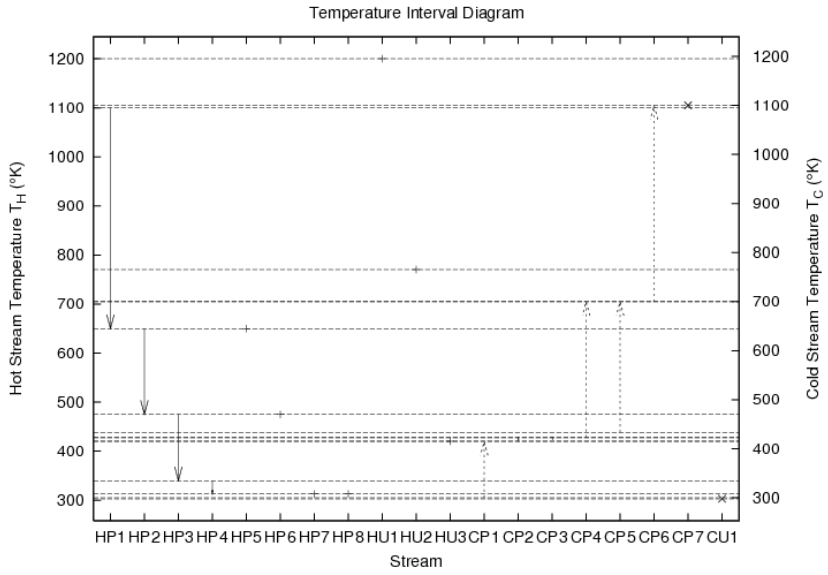

Figure 5-2: *Traditional SMR Baseline flowsheet heat integration temperature interval diagram*

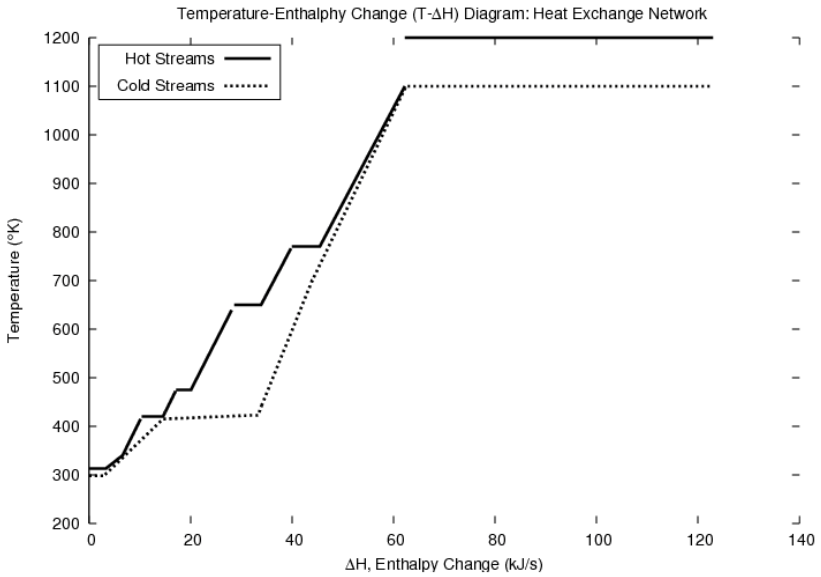

Figure 5-3: *Traditional SMR Baseline flowsheet heat integration temperature-enthalpy change diagram*

5.5 Baseline EER Process

The EER process was first described in a patent[20] where a fully exothermic reforming process was presented. A baseline flowsheet depicting this exothermic process can be found below in Figure 5-4, with corresponding energy and material flow specifications detailed in Appendix Table 5-4.

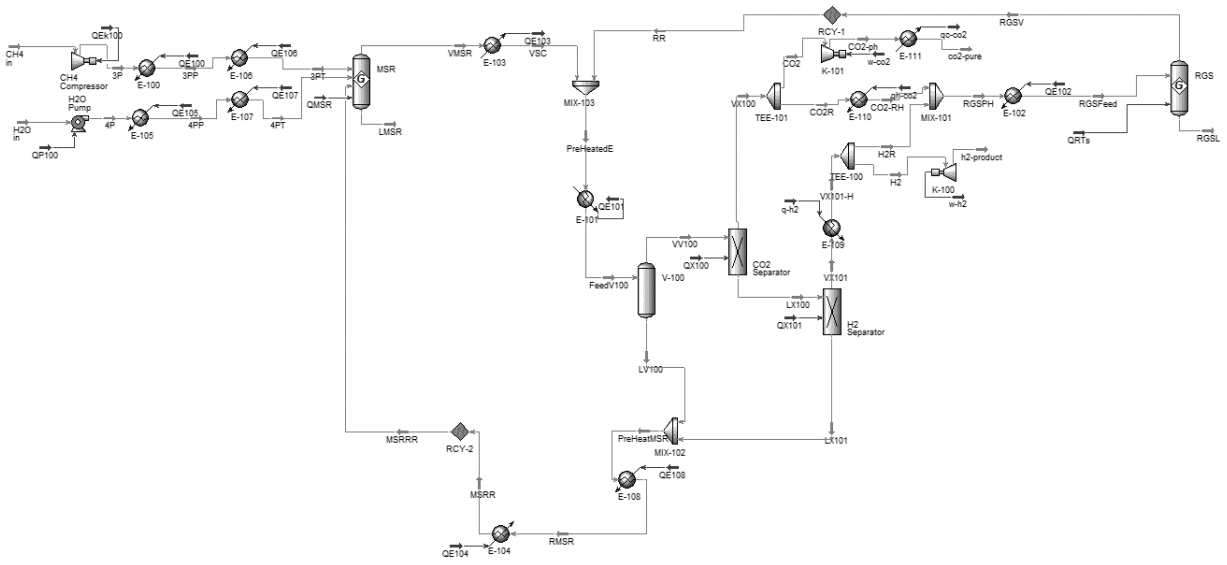

Figure 5-4: *EER Baseline Flowsheet*

The overall inlets of the EER baseline flowsheet are 1 kmol/h of CH_4 and 2 kmol/h of H_2O, which are both compressed/pumped to 5 bar, heated to 1140K, and mixed with a recycled stream of CO and H_2O before the mixture of H_2O/CO/CH_4 is fed into the EER reformer. The total reformer heat load is an exothermic load of -0.853 kJ/s. The outlet is subsequently cooled to 750K and mixed with the outlet of the Reverse Gas Shift (RGS) reactor before undergoing cooling to reach a temperature of 313K. At this point, the stream undergoes a series of separators starting with a water flash separator, followed by a CO_2 separator, and finally an H_2 separator. The water separated through the flash is mixed with the waste stream of the H_2 separator before undergoing heating to 1140K to mix with the inlet CH_4/H_2O streams. The pure CO_2 is split to provide the 1 kmol/hr that is compressed to 40 bar and serves one of the flowsheet's overall outlets; the remaining CO_2 is mixed with pure H_2 from the H_2 separator and the CO_2 separator waste gas is fed into the H_2 separator. The pure H_2 stream is split to provide 4 kmol/h of H_2 that is expanded to 1 bar, which along with the pure CO_2 at 40 bar makes up the flowsheet's overall outlets; the remaining H_2 is mixed with the remaining pure CO_2. This mixture of H_2/CO_2 is

heated to 750K before being fed to the RGS reactor, which has an endothermic heat load of 62.46 kJ/s. The RGS reactor is used to produce the CO required by the flowsheet to reach exothermicity. The work of separation required from the ideal CO_2 and H_2 separators is approximately 46.53 kJ/s. For this specific case 1200K, 900K, 770K, 420K hot utility streams and a 298K cold utility stream were made available. Below Figures 5-5 – 5-6 demonstrate the heat integration studies carried out for the EER baseline design, which determined that the entire flowsheet requires 65.83 kJ/s of 770K hot utility, 127.48 kJ/s of 420K hot utility, and 169.90 kJ/s of 298K cold utility.

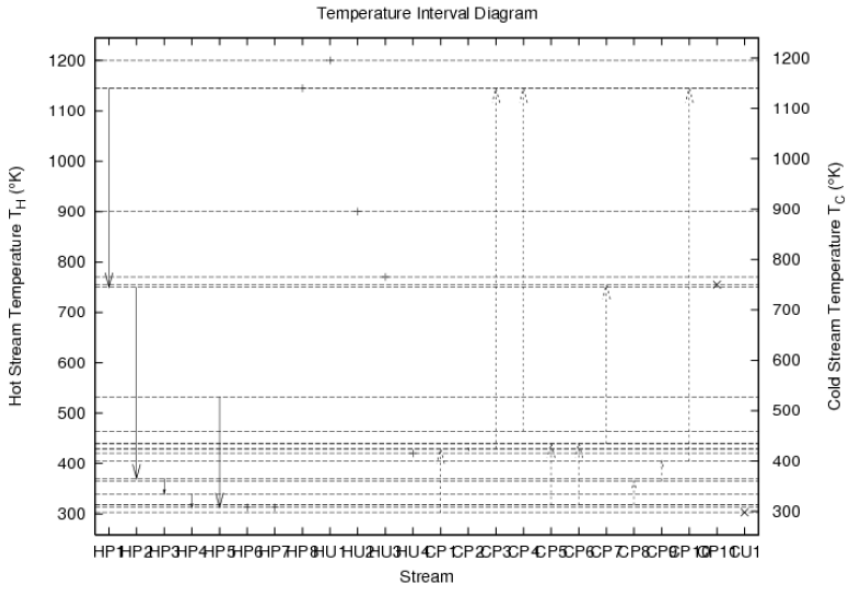

Figure 5-5: *EER Baseline flowsheet heat integration temperature interval diagram*

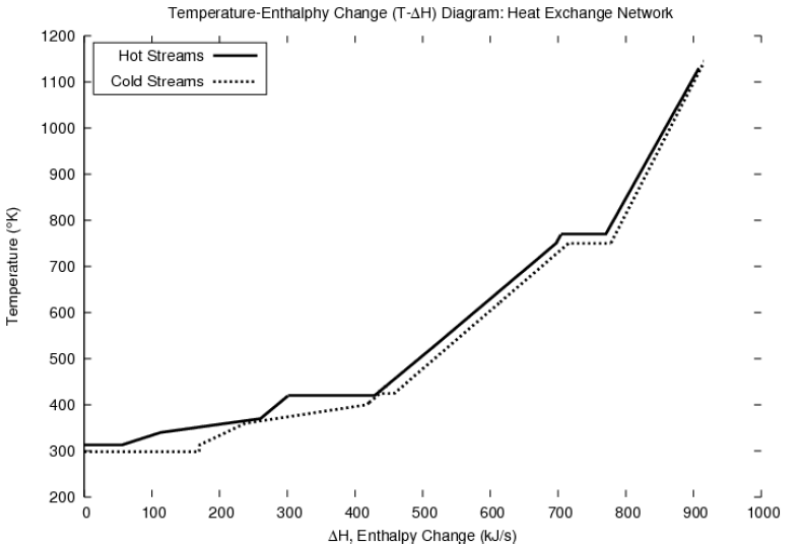

Figure 5-6: *EER Baseline flowsheet heat integration temperature-enthalpy change diagram*

5.6 Baseline SMR-MR Process

A baseline SMR-MR process is developed that has overall flowsheet inlets of 1 kmol/h of CH_4 and 2 kmol/h of H_2O, and overall flowsheet outlets of 4 kmol/h of H_2 and 1 kmol/h of CO_2. The flowsheet is depicted in Figure 5-7 below and material and energy stream details can be found in Appendix Table 5-5. The CH_4/H_2O inlets are compressed/pumped to 40 bar before undergoing heating to reach a temperature of 873K, where it is mixed with a H_2O recycle stream. This CH_4/H_2O mixture is fed to the SMR-MR reactor, which was modeled with Gibbs free energy minimization MR formulation detailed above, and the results of which were implemented in UNISIM through the use of a conversion reactor and separator. The overall heat load of the SMR-MR reactor is 52.5 kJ/s.

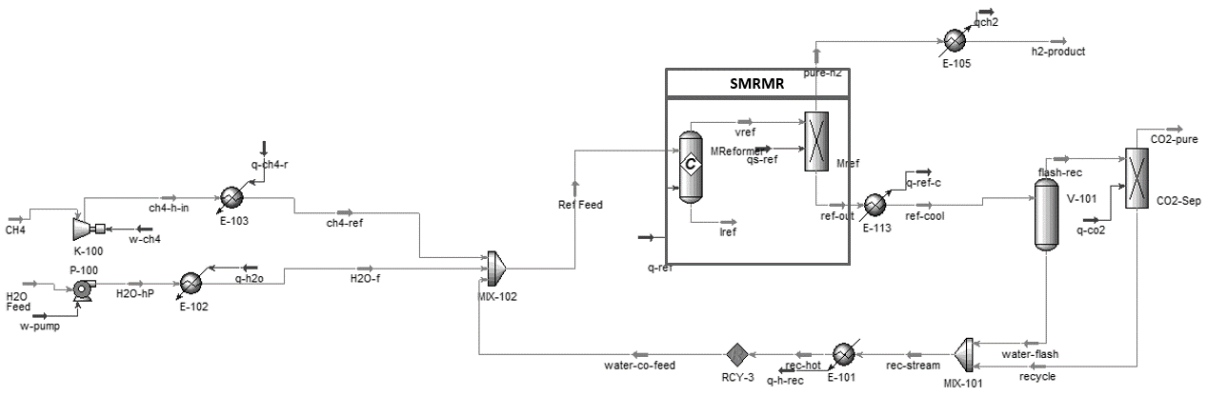

Figure 5-7: *SMR-MR Baseline flowsheet*

The SMR-MR's permeate H_2 outlet is cooled to 313K to serve as one of the flowsheet's overall outlets, while the retentate is cooled to 313K prior to undergoing separation through a series of separators. The cooled retentate is fed into a water flash separator, and then fed to a CO_2 separator, where the pure CO_2 serves as an outlet, while the waste gas is mixed with the water from the flash separator, heated to 873K, and then mixed with the CH_4/H_2O inlet. For this specific case 900K, 770K, 530K, and 420K hot utility streams and a 298K cold utility stream were made available. Below Figures 5-8 – 5-9 demonstrate the heat integration studies carried out for the EER baseline design, which determined that the entire flowsheet requires 52.74 kJ/s of 900K hot utility, 20.72 kJ/s of 530 kJ/s hot utility, and 8.02 kJ/s of 298K cold utility. The total work of separation required from the ideal CO_2 and H2 separators is 0.205 kJ/s.

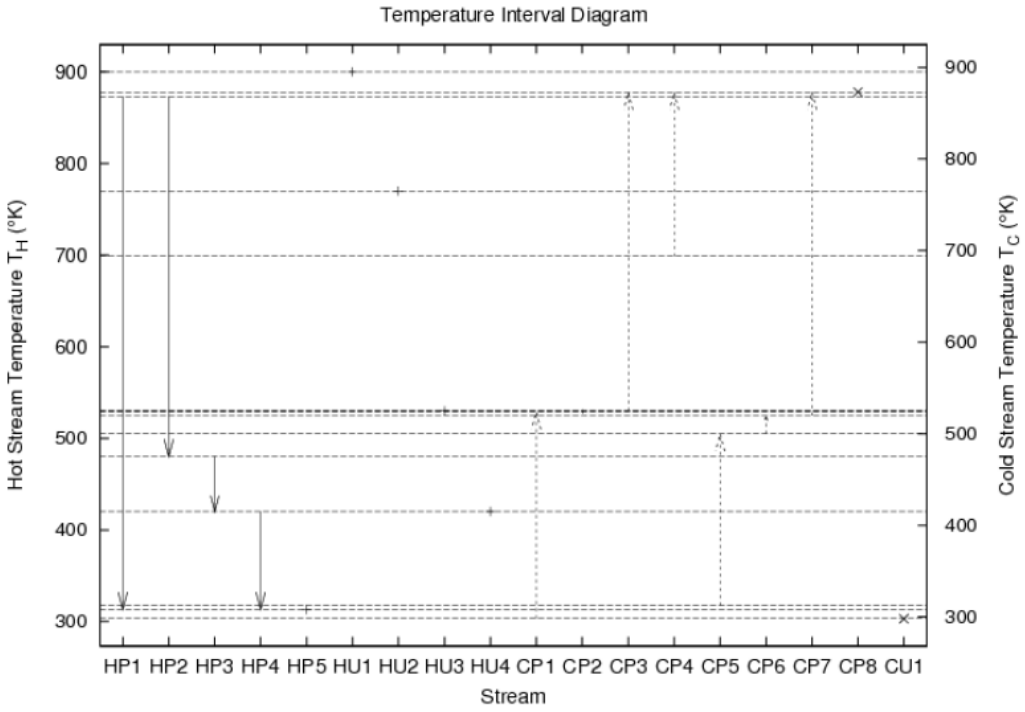

Figure 5-8: *SMR-MR Baseline flowsheet heat integration temperature interval diagram*

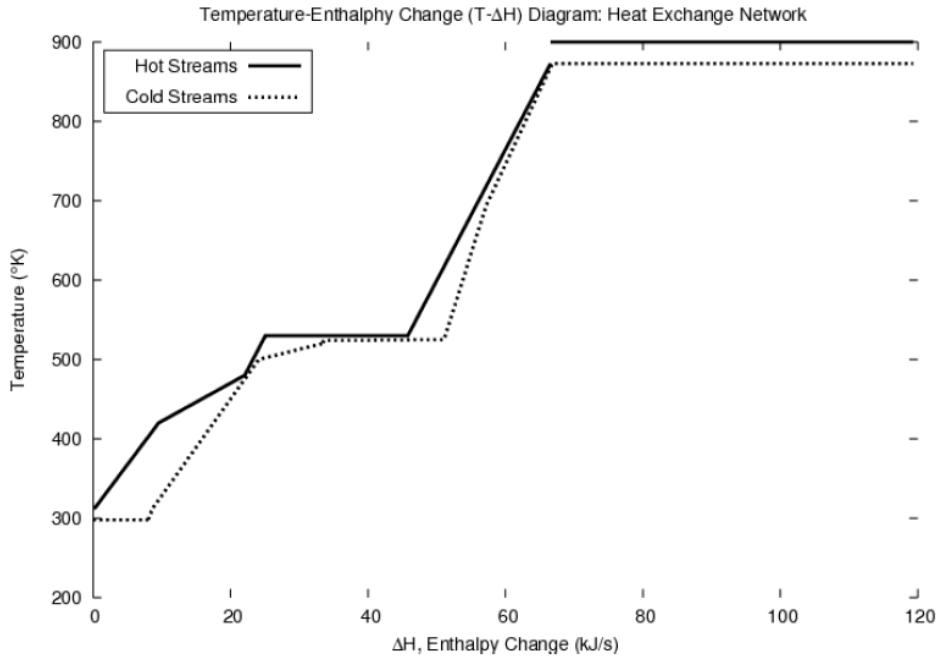

Figure 5-9: *SMR-MR Baseline flowsheet heat integration temperature-enthalpy change diagram*

5.7 IEER Process

The IEER-MR process is displayed below with three different case studies considered. These case studies have a sequence of three reactors including a co-current water-gas-shift MR (WGS-MR), followed by a counter-current WGS-MR, which is then followed by a SMR-MR, whose total heat load ranges from endothermic to exothermic. The co-current WGS-MR has water fed into the permeate side of the membrane so that the permeate and retentate stream flow in the same direction. This allows the total pressure of the permeate and retentate to remain at 40 bar, while still allowing for significant hydrogen permeation. The counter-current WGS-MR has water fed into the permeate side of the membrane so that the permeate and retentate stream flow in opposite directions. The SMR-MR runs with a permeate pressure of 1 bar, while the retentate runs with a pressure of 40 bar, allowing significant hydrogen separation.

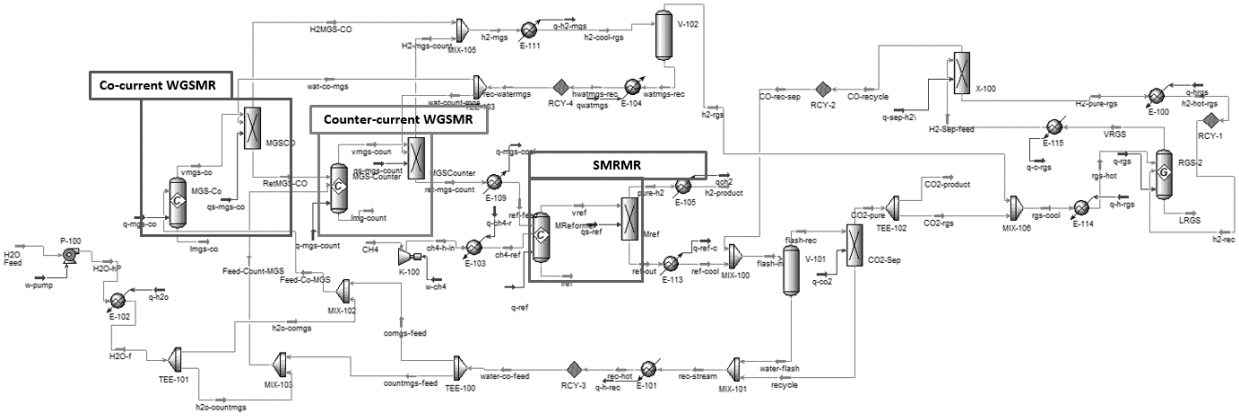

Figure 5-10: *IEER-MR flowsheet*

The overall inlets (1 kmol/h of CH_4 and 2 kmol/h of H_2O) and outlets (4 kmol/h of H_2 and 1 kmol/h of CO_2) of the IEER-MR are the same as the above two baseline designs. Furthermore, all three IEER-MR cases have the same flowsheet processes with differing stream

compositions. The flowsheet's inlets of CH_4/H_2O are compressed/pumped to 40 bar, heated to 878K, and mixed with a CO/H_2O before being fed to the co-current WGS-MR. The co-current WGS-MR's retentate outlet is fed into the counter-current WGS-MR, and the permeate of both WGS-MRs is mixed and subsequently cooled before being fed into a flash separator. The water from the flash separator is heated and recycled back to feed both WGS-MRs' permeate stream as an H_2 flushing mechanism. The retentate stream of the counter-current WGS-MR is then cooled to 873K before it is fed to the SMR-MR. The pure H_2 stream is cooled and serves as a flowsheet product, while the retentate is cooled to 313K before it undergoes a series of separators (water flash followed by CO_2 separator). The pure CO_2 from the separation process is split into two streams, one of which serves as a flowsheet outlet while the other is mixed with the high purity H_2 from the WGS-MR's permeate stream. Subsequently, this CO_2/H_2 mixture is fed into a RGS reactor to produce the CO required by the flowsheet, which is recycled to the aforementioned flash separator. An H_2 separator follows the RGS reactor, and the pure H_2 is recycled back into the RGS to yield a higher CO_2 conversion.

Case 1 of the IEER process has a total feed of 1 kmol/hr CH_4, 4 kmol/hr H_2O and 1 kmol/hr of CO to the membrane reactor sequence, produces a total of 5.2 kmol/hr of H_2 and 2.0 kmol/hr of CO_2, and has a total MR sequence reactor endothermic heat load of 42.16 kJ/s. The details regarding the co-current WGS-MR, counter-current WGS-MR, and SMR-MR can be found in Figure 5-11 below and the flowsheet's material and energy stream details can be found in Appendix Table 5-6.

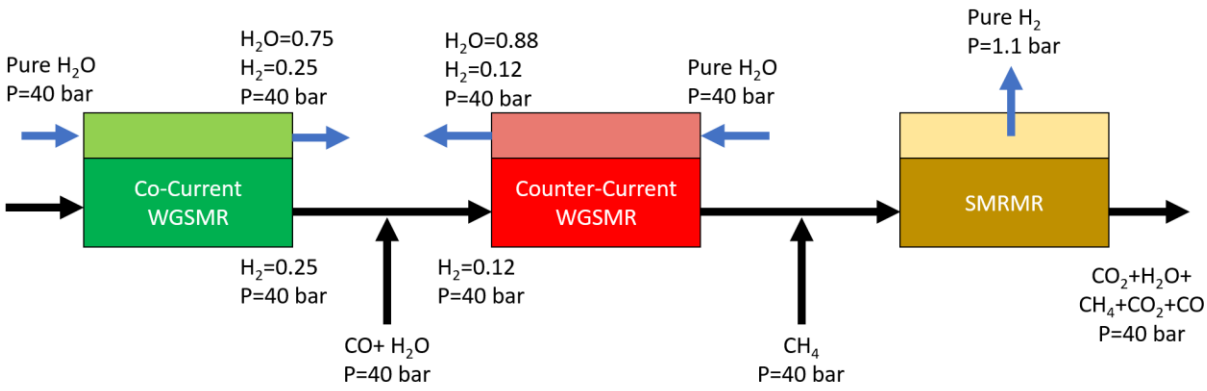

Figure 5-11: *Case study 1 flowsheet details of membrane reactor network*

Heat integration studies were also carried out for Case 1 (Figures 5-12 – 5-13), and the entire flowsheet requires 41.62 kJ/s of 900K hot utility, 8.11 kJ/s of 770K hot utility, 86.08 kJ/s of 530K hot utility, and 53.39 kJ/s of 298K cold utility. In addition, the total work of separation required from the ideal CO2 and H2 separators is 5.14 kJ/s.

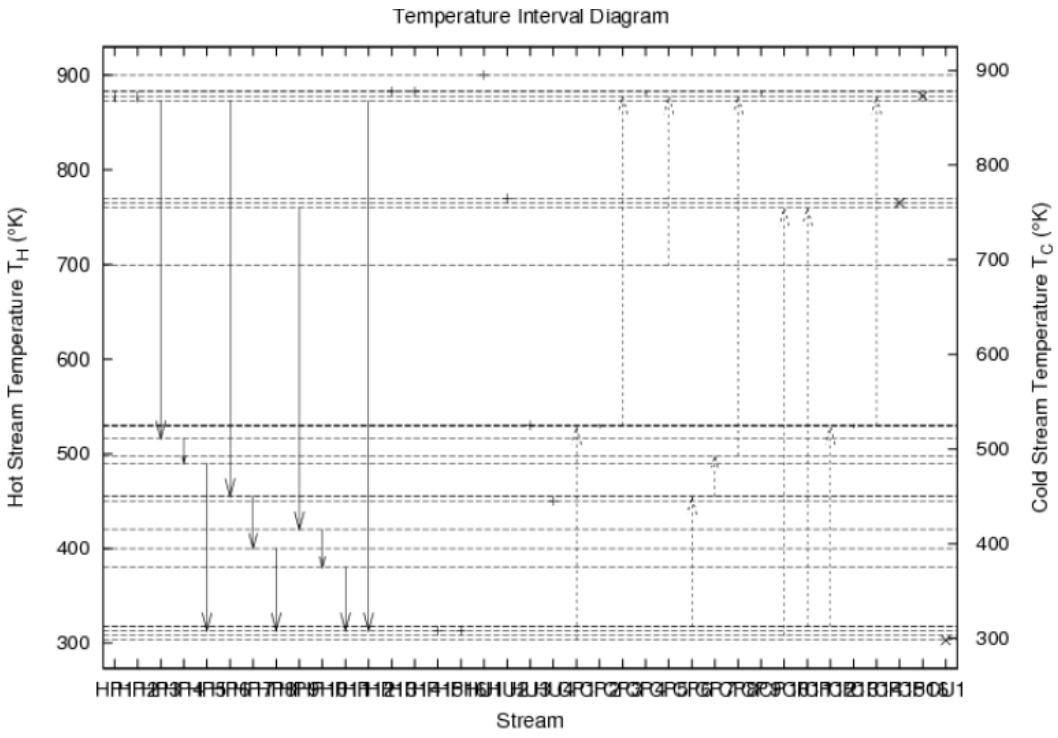

Figure 5-12: *Case 1 IEER-MR flowsheet heat integration temperature interval diagram*

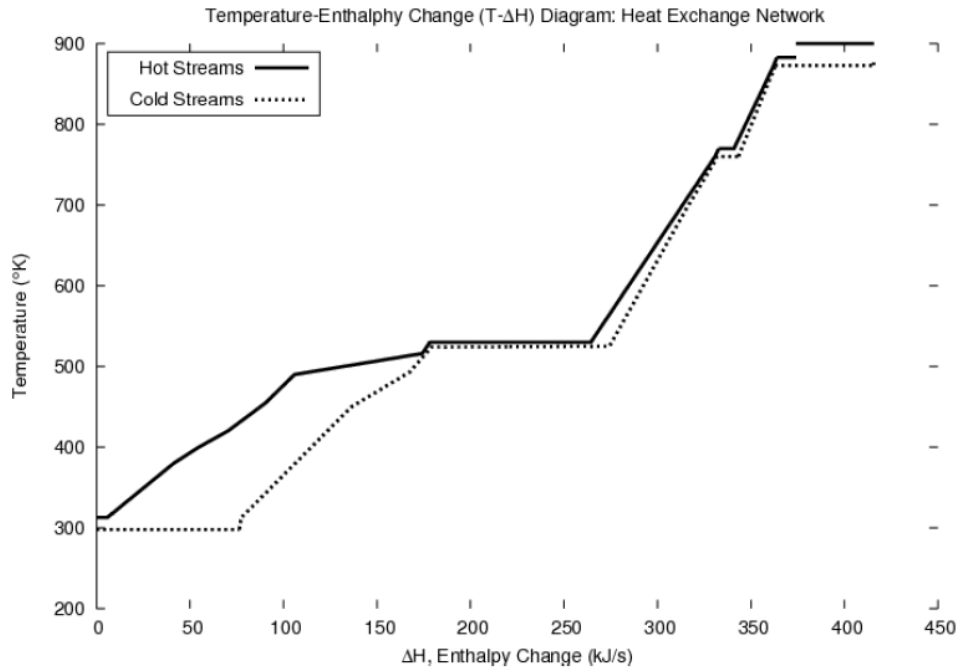

Figure 5-13: *Case 1 IEER-MR flowsheet heat integration temperature-enthalpy change diagram*

Case 2 of the IEER process has a total feed of 1 kmol/hr CH_4, 5 kmol/hr H_2O and 2 kmol/hr of CO to the membrane reactor sequence, produces a total of 6.1 kmol/hr of H_2 and 2.9 kmol/hr of CO_2, and has a total MR sequence reactor endothermic heat load of 33.70 kJ/s. The details regarding the co-current WGS-MR, counter-current WGS-MR, and SMR-MR can be found in Figure 5-14 below and the flowsheet's material and energy stream details can be found in Appendix Table 5-7.

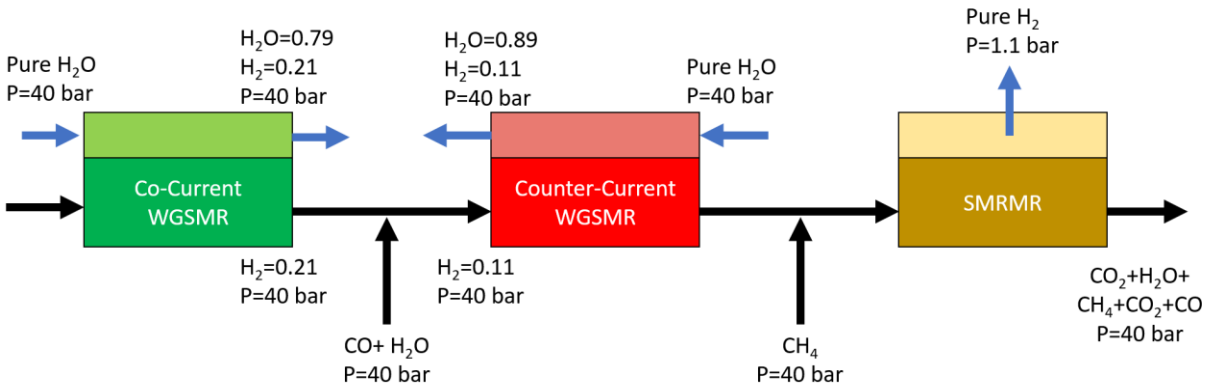

Figure 5-14: *Case study 2 flowsheet details of membrane reactor network*

Heat integration studies were also carried out for Case 2 (Figures 5-15 – 5-16), and the entire flowsheet requires 32.93 kJ/s of 900K hot utility, 19.44 kJ/s of 770K hot utility, 141.0 kJ/s of 530K hot utility, and 138.9 kJ/s of 298K cold utility. In addition, the total work of separation required from the ideal CO2 and H2 separators is 9.07 kJ/s.

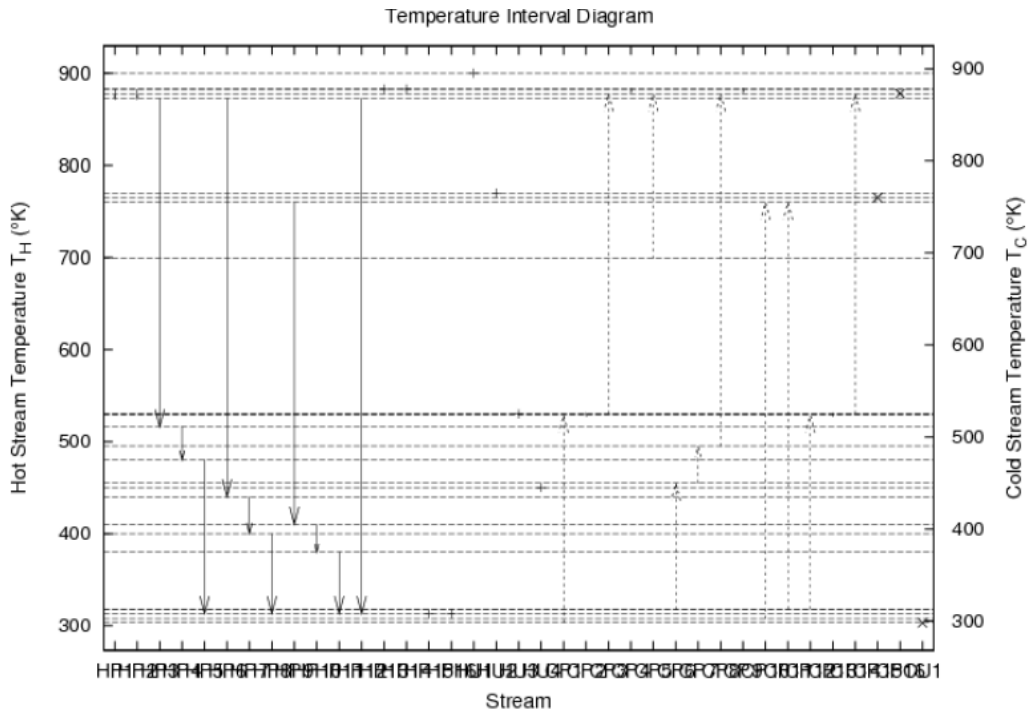

Figure 5-15: *Case 2 IEER-MR flowsheet heat integration temperature interval diagram*

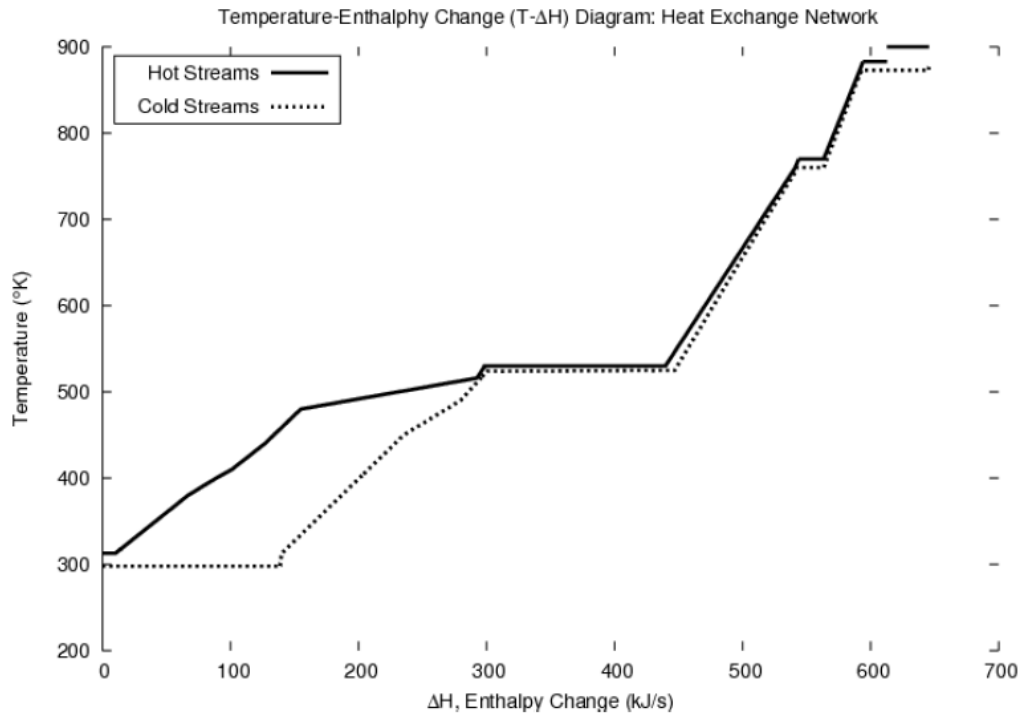

Figure 5-16: *Case 2 IEER-MR flowsheet heat integration temperature-enthalpy change diagram*

Case 3 of the IEER process has a total feed of 1 kmol/hr CH_4, 10.5 kmol/hr H_2O and 5.5 kmol/hr of CO to the membrane reactor sequence, produces a total of 9.6 kmol/hr of H_2 and 6.4 kmol/hr of CO_2, and has a total MR sequence reactor exothermic heat load of -0.08 kJ/s. The details regarding the co-current WGS-MR, counter-current WGS-MR, and SMR-MR can be found in Figure 5-17 below and the flowsheet's material and energy stream details can be found in Appendix Table 5-8.

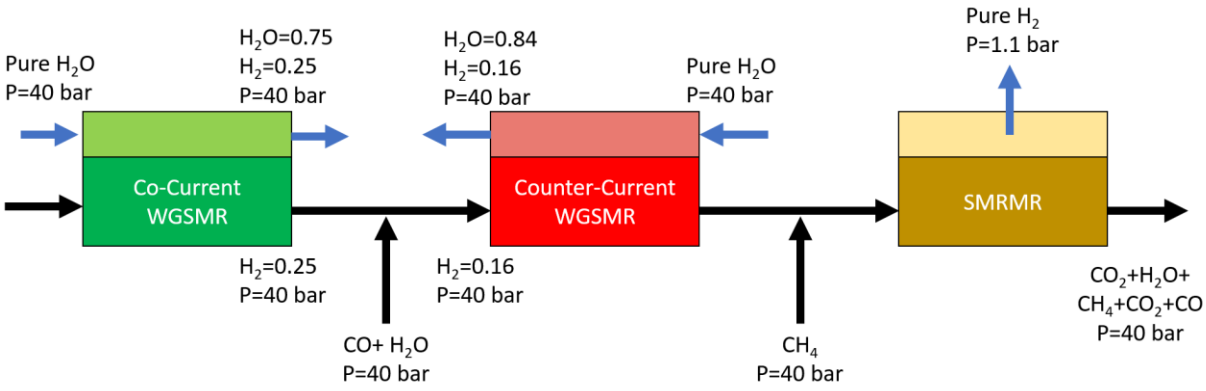

Figure 5-17: *Case study 3 flowsheet details of membrane reactor network*

Heat integration studies were also carried out for Case 3 (Figures 5-18 - 5-19), and the entire flowsheet requires 52.88 kJ/s of 770K hot utility, 248.8 kJ/s of 530K hot utility, and 265.7 kJ/s of 298K cold utility. In addition, the total work of separation required from the ideal CO_2 and H2 separators is 24.65 kJ/s.

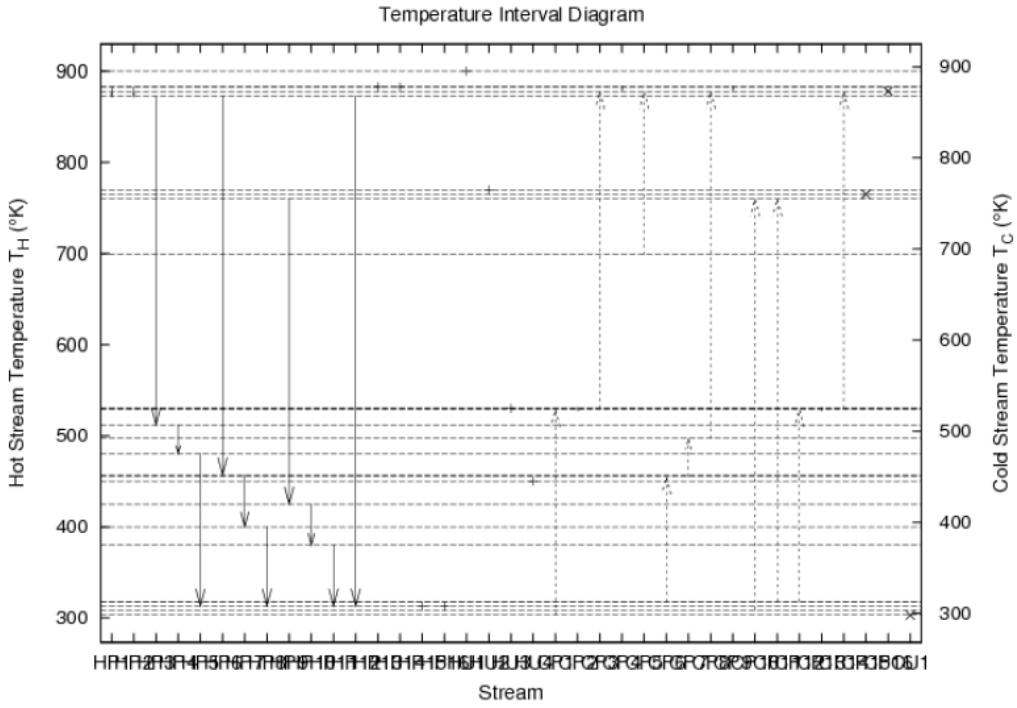

Figure 5-18: *Case 3 IEER-MR flowsheet heat integration temperature interval diagram*

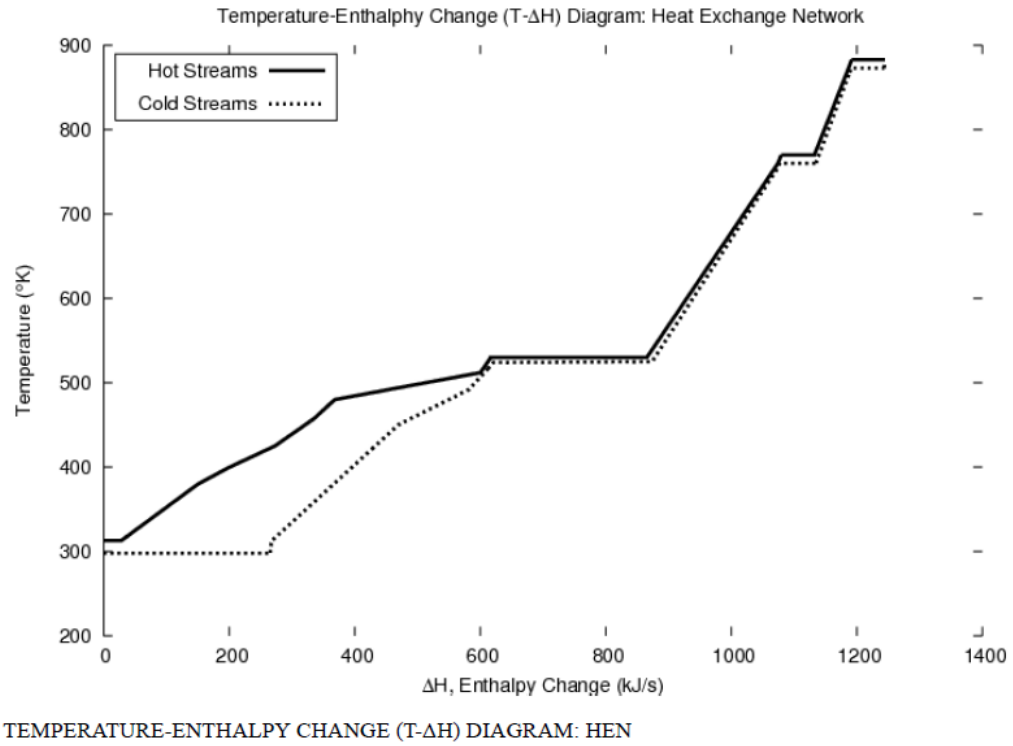

Figure 5-19: *Case 3 IEER-MR flowsheet heat integration temperature-enthalpy change diagram*

5.8 Results and Discussions

Five flowsheets were presented above including two baseline designs and three IEER-MR designs. All case studies consider an external feed of 1 kmol/hr CH_4 and 2 kmol/hr H_2O feed, and produce 4 kmol/hr of H_2 at 1 bar and 1 kmol/hr of CO_2 at 40 bar that leave the flowsheet. A summary table can be found below (Table 5-2) displaying all significant details of the above developed flowsheets.

The traditional SMR baseline has a reactor inlet of 1/0.07/2.25 kmol/hr of $CH_4/H_2O/CO$, operating temperature of 1100K, and endothermic load of 60.70 kJ/s. The EER baseline has a reactor inlet of 1/17.70/14.64 kmol/hr of $CH_4/H_2O/CO$, operating temperature of 1145K, and exothermic load of -0.85 kJ/s. SMR-MR baseline has a reactor inlet of 1/3.1/0 kmol/hr of $CH_4/H_2O/CO$, operating temperature of 873K, and endothermic load of 52.5 kJ/s. Case 1 of the IEER-MR flowsheet has a total inlet to the MR sequence consisting of 1/4/1 kmol/hr of

$CH_4/H_2O/CO$, operating temperature ranging between 883K-873K, and total endothermic load of 42.16 kJ/s. Case 2 of the IEER-MR flowsheet has a total inlet to the MR sequence consisting of 1/5/2 kmol/hr of $CH_4/H_2O/CO$, operating temperature ranging between 883K-873K, and total endothermic load of 33.70 kJ/s. Case 3 of the IEER-MR flowsheet has a total inlet to the MR sequence consisting of 1/10.5/5.5 kmol/hr of $CH_4/H_2O/CO$, operating temperature ranging between 883K-873K, and total exothermic load of 0.08 kJ/s. The IEER cases 1 and 2 deliver approximately 31% and 44% when compared to the traditional SMR baseline, and 20% and 36% decrease in the total MR endothermic heat load when compared to the SMR-MR baseline design respectively, with an increase in total MR flowrate of 2 kmol/hr and 4 kmol/hr respectively, while the total MR heat load of IEER Case 3 is exothermic. The EER baseline design is also exothermic, but requires much higher total inlet flowrates (33.34 kmol/hr) when compared to the intensified exothermic design shown in IEER Case 3 (17 kmol/hr). This represents a 52% reduction in total inlet flowrate to the EER reformer when compared to the IEER-MR sequence. As can be seen by this significant reduction in endothermic heat loads when compared to the traditional SMR and SMR-MR baseline designs, the IEER-MR designs can provide significant energetic intensification. In addition, the significant reduction in total reformer inlet flowrate between the two exothermic cases shows further intensification of the EER process.

It is clear from Table 5-2 that none of the presented MR cases require the 1200K hot utility load, which represents the burning of natural gas used in traditional steam-methane reforming as the energetic source for the SMR reaction. Therefore, all of the presented case studies including the SMR-MR and exothermic baseline designs can utilize concentrated solar power to meet the energetic needs since the highest temperature required for these energetic loads is 900K. According to the National Renewable Energy Laboratory[22], solar towers can currently deliver

temperatures of 835K, and are expected to reach 920K by 2020, which meet the IEER-MR requirements. In addition, the total work of compression for the SMR-MR baseline and the IEER-MR cases are equal (5.07 kJ/s), while the EER baseline has a slightly lower total work of compression (4.22 kJ/s). The EER baseline requires less compression work because the MR flowsheets (SMR-MR and IEER-MR) compress the inlet CH_4 to 40 bar from 1 bar, while the EER baseline only compresses the inlet CH_4 to 5 bar from 1 bar, and the CO_2 product to 40 bar from 5 bar. It should also be noted that the EER baseline expands the H_2 product from 5 bar to 1 bar, which produces 3.88 kJ/s of work. By contrast, the H_2 product of the MR flowsheets are produced through the SMR-MR's permeate, which is at 1 bar. The work required for H_2 separation is 0/19.04/3.30/6.06/16 kJ/s for the SMR-MR baseline/EER Baseline/IEER-MR Case 1/IEER-MR Case 2/IEER-MR Case 3. The SMR-MR baseline does not contain an ideal H_2 separator, since all hydrogen separation is done through the MR, while the IEER-MR cases have an ideal H_2 separator following the RGS reactor. For the EER Baseline, the H_2 separator is the only means of hydrogen separation, and due to the significant amount of CO and H_2O that must be fed into the reformer for exothermicity, the separator feed is larger than that of the IEER-MR cases. Similarly, the work required for CO_2 separation is 0.205/27.49/1.83/3.01/8.64 for the SMR-MR baseline/EER Baseline/IEER-MR Case 1/IEER-MR Case 2/IEER-MR Case 3. The increase in work required for CO_2 separation between the cases is due to the increase in CO and H_2O fed into the EER reformer/IEER-MRs. The total work of separation required by the EER flowsheet is 46.53 kJ/s, while its exothermic counterpart (IEER-MR Case 3) requires 24.64 kJ/s; this represents a 47% decrease in the total work required by the flowsheet. The IEER-MR process was developed to help reduce the significant work of separation and flow recycle

requirements of the novel EER concept. Overall, it reduces both significantly thus making the EER concept more industrially realizable.

5.9 Conclusions

The intensification of the novel energetically enhanced reforming (EER) process through the use of membrane reactors (MRs) was presented and discussed. Two baseline designs depicting the EER process and a standard SMR-MR process were developed and presented along with three novel IEER-MR cases depicting the full range of the IEER-MR concept. It was found that the IEER-MR Case 3 (exothermic case) flowsheet yielded a 47% decrease in the total work of separation required, and a 52% reduction in the total reformer/sequence of MRs inlet feed when compared to the EER baseline. It was also found that the IEER-MR flowsheets had a 20% and 36% reduction in the total MR endothermic heat load for IEER-MR Case 1 and 2 respectively, when compared to the SMR-MR baseline. This was accomplished with only a total MR inlet feed increase of 2 kmol/hr and 4 kmol/hr for IEER-MR Case 1 and 2 respectively. The IEER-MR cases presented intensified both baseline designs energetically through a reduction in heat loads and total work required, while also depicting the full range of the total MR reformer sequence heat loads (highly endothermic to exothermic) realizable through the EER concept

Table 5-2: *Summary table of all case studies*

Metric	Traditional SMR Baseline	EER Baseline	SMR MR Baseline	IEER-MR Case 1	IEER-MR Case 2	IEER-MR Case 3
Overall CH4 inlet (kmol/h)	1	1	1	1	1	1
Overall H2O inlet (kmol/h)	2	2	2	2	2	2
Overall H2 outlet (kmol/h)	4	4	4	4	4	4
Overall CO2 outlet (kmol/h)	1	1	1	1	1	1
HU (1200K) energy consumption (kJ/s)	60.70	0	N/A	N/A	N/A	N/A
HU (900K) energy consumption (kJ/s)	0	0	52.74	41.62	32.93	0
HU (770K) energy consumption (kJ/s)	5.48	65.83	0	8.11	19.44	52.88
HU (530K) energy consumption (kJ/s)	0	N/A	20.72	86.08	141.0	248.8
HU (420K) energy consumption (kJ/s)	4.16	127.48	N/A	N/A	N/A	N/A
CU (298K) energy consumption (kJ/s)	3.15	169.90	8.02	53.39	138.9	265.7
CH_4 mol fed to membranes /SMR reactor (kmol/h)	1	1	1.0	1	1	1
CO mol fed to membranes /SMR reactor (kmol/h)	0.07	14.64	0	1	2	5.5
H_2O mol fed to to membranes /SMR reactor (kmol/h)	2.25	17.70	3.1	4	5	10.5
CO_2 mol from to membranes /SMR reactor (kmol/h)	1	8.69	0	2.0	2.9	6.4
H_2 mol from to membranes /SMR reactor (kmol/h)	4	10.22	4	5.2	6.1	9.6
MR Network/SMR Reactor heat load (kJ/s)	60.47	-0.8529	52.48	42.16	33.70	-0.0809
Total work of compression (kJ/s)	1.46	4.22	5.07	5.07	5.07	5.07
Total work of pumping (kJ/s)	0.005	$5.30*10^{-3}$	0.05	0.05	0.05	0.05
Total work of Turbine (kJ/s)	0	3.88	0	0	0	0
Work for H2 separation (kJ/s) (minimum)	0.53	19.04	0	3.30	6.06	16.0
Work for CO2 separation (kJ/s) (minimum)	1.83	27.49	0.205	1.83	3.01	8.64

5.10 Appendix

Table 5-3: *Traditional SMR Baseline Flowsheet material and energy stream details*

Stream Name	CH4 Feed	CH4 Comp Outlet	CH4 Heater Outlet	H2O Feed	H2O Pump Outlet	H2O Heater Outlet	Reformer Feed	Reformer Vapor	Reformer Liquid	Reformer Cooler Outlet
Vapour Fraction	1.00	1.00	1.00	0.00	0.00	1.00	1.00	1.00	0.00	1.00
Temperature (K)	298	433.6	700	298	298.0	700	699.6	1100	1100	650
Pressure (bar)	1.01	5	5	1.01	5	5	5	5	5	5
Molar Flow (kmol/h)	1.00	1.00	1.00	2.00	2.00	2.40	3.40	5.40	0.00	5.40
Heat Flow (kJ/s)	-20.81	-19.35	-15.62	-159.02	-159.01	-145.35	-160.97	-81.99	0.00	-104.86
Stream Name	**HTS Vapor**	**HTS Liquid**	**HTS Cooler Outlet**	**LTS Vapor**	**LTS Liquid**	**Flash Vapor**	**Flash Liquid**	**H2 Out**	**H2 Separator Waste Gas**	**Flash Liquid R**
Vapour Fraction	1.00	0.00	1.00	1.00	0.00	1.00	0.00	1.00	0.68	0.39
Temperature (K)	650	650.00	475.00	475	475	313	313	313	313	312.99
Pressure (bar)	5	5	5	5	5	5	5	5	5	5
Molar Flow (kmol/h)	5.40	0.00	5.40	5.40	0.00	5.24	0.17	4.00	0.24	0.40
Heat Flow (kJ/s)	-110.13	0.00	-118.66	-121.57	0.00	-117.95	-13.33	0.47	-10.09	-23.41
Stream Name	**H2ORMIX**	**LTS Cooler Outlet**	**H2O to Rec**	**RFeed**	**CO2O**	**CO2B**				
Vapour Fraction	0.07	0.97	0.39	1.00	1.00	1.00				
Temperature (K)	300.4	313.0	313.0	1100	313	313				
Pressure (bar)	5	5	5	5	5	5				
Molar Flow (kmol/h)	2.40	5.40	0.40	3.40	1.00	4.24				
Heat Flow (kJ/s)	-182.43	-131.27	-23.41	-142.46	-109.28	-8.89				
Stream Name	**CH4 Feed**	**CH4 Comp Outlet**	**CH4 Heater Outlet**	**H2O Feed**	**H2O Pump Outlet**	**H2O Heater Outlet**	**Reformer Feed**	**Reformer Vapor**	**Reformer Liquid**	**Reformer Cooler Outlet**
CH4	1.00000	1.00000	1.00000	0.00000	0.00000	0.03730	0.32016	0.01659	0.01659	0.01659
CO	0.00000	0.00000	0.00000	0.00000	0.00000	0.02797	0.01976	0.15116	0.15116	0.15116
CO2	0.00000	0.00000	0.00000	0.00000	0.00000	0.00002	0.00002	0.04636	0.04636	0.04636
H2O	0.00000	0.00000	0.00000	1.00000	1.00000	0.93470	0.66007	0.18435	0.18435	0.18435

H2	0.00000	0.00000	0.00000	0.00000	0.00000	0.00000	0.00000	0.60154	0.60154	0.60154
Stream Name	**HTS Vapor**	**HTS Liquid**	**HTS Cooler Outlet**	**LTS Vapor**	**LTS Liquid**	**Flash Vapor**	**Flash Liquid**	**H2 Out**	**H2 Separator Waste Gas**	**Flash Liquid R**
CH4	0.01659	0.01659	0.01659	0.01659	0.01659	0.01713	0.00000	0.00000	0.38111	0.22219
CO	0.06065	0.06065	0.06065	0.01244	0.01244	0.01284	0.00000	0.00000	0.28580	0.16663
CO2	0.13687	0.13687	0.13687	0.18507	0.18507	0.19101	0.00033	0.00000	0.00000	0.00014
H2O	0.09384	0.09384	0.09384	0.04563	0.04563	0.01497	0.99966	0.00000	0.33309	0.61104
H2	0.69205	0.69205	0.69205	0.74026	0.74026	0.76405	0.00001	1.00000	0.00000	0.00000
Stream Name	**H2ORMIX**	**LTS Cooler Outlet**	**H2O to Rec**	**RFeed**	**CO2O**	**CO2B**				
CH4	0.03730	0.01659	0.22219	0.32016	0.00000	0.02117				
CO	0.02797	0.01244	0.16662	0.01976	0.00000	0.01588				
CO2	0.00002	0.18507	0.00014	0.00002	1.00000	0.00000				
H2O	0.93470	0.04563	0.61104	0.66007	0.00000	0.01850				
H2	0.00000	0.74026	0.00000	0.00000	0.00000	0.94445				
Energy Flow Name	**CH4 Comp Q**	**CH4 Heater Q**	**H2O Pump Q**	**H2O Heater Q**	**Reformer Q**	**Reformer Cooler Q**	**HTS Cooler Q**	**Flash Q**	**HTS Q**	**LTS Q**
Heat Flow (kJ/s)	1.46	3.73	0.01	37.08	60.47	22.87	8.53	0.00	-5.27	-2.91
Energy Flow Name	**LTS Cooler Q**	**Reformer Heater Q**	**HEQ**	**CEq**						
Heat Flow (kJ/s)	9.70	18.51	-0.73	-0.22						

Table 5-4: *EER Baseline Flowsheet material and energy stream details*

Stream Name	**VMSR**	**LMSR**	**FeedV100**	**VV100**	**LV100**	**LX100**	**VX100**	**VX101**	**LX101**	**PreHeatMSR**	**MSRR**	**MSRRR**	**CH4 in**	**H2O in**
Vapour Fraction	1	0	0.8126	1	0	0.9923	1	1	0.9543	0.4986	1	1	1	0
Temperature (K)	1145	1145	313	313	313	313	313	313	313	313	1140	1140	298	298
Pressure (bar)	5	5	5	5	5	5	5	5	5	5	5	5	1	1
Molar Flow (kmol/h)	35.86	0.00	78.57	63.84	14.73	43.04	20.80	26.95	16.10	30.82	30.82	30.86	1.00	2.00
Heat Flow (kJ/s)	-1402.18	0.00	-3959.66	-2793.25	-1166.41	-536.60	-2261.03	3.16	-544.72	-1711.13	-1276.03	-1277.47	-20.81	-159.02
Stream Name	**PreHeatedE**	**H2**	**H2R**	**CO2**	**CO2R**	**RGSPH**	**RGSFeed**	**RGSV**	**RGSL**	**RR**	**3P**	**3PT**	**4P**	**4PT**

Vapour Fraction	1.0000	1	1	1	1.0000	1	1	1	0	1	1	1	0	1.0000
Temperature (K)	750	435.00	435.00	313	313	434.4	750	750	750	750.00	459.2	1140	298	1140
Pressure (bar)	5	5	5	5	5	5	5	5	5	5	5	5	5	5
Molar Flow (kmol/h)	78.57	4.00	22.95	1.00	19.80	42.74	42.74	42.74	0.00	42.71	1.00	1.00	2.00	2.00
Heat Flow (kJ/s)	-3448.89	4.35	24.95	-108.72	-2152.31	-2099.71	-1960.64	-1898.18	0.00	-1895.88	-19.04	-7.25	-159.01	-116.60
Stream Name	**VSC**	**3PP**	**4PP**	**RMSR**	**VX101-H**	**CO2-RH**	**CO2-ph**	**co2-pure**	**h2-product**					
Vapour Fraction	1	1.0000	1	1.0000	1.0000	1.0000	1	1	1					
Temperature (K)	750	700	700	650.00	435.00	435.00	532.2	313	313.1					
Pressure (bar)	5	5	5	5	5	5	40	40	1					
Molar Flow (kmol/h)	35.86	1.00	2.00	30.82	26.95	19.80	1.00	1.00	4.00					
Heat Flow (kJ/s)	-1553.02	-15.62	-126.51	-1429.46	29.30	-2124.67	-106.28	-109.16	0.47					
Stream Name	**VMSR**	**LMSR**	**FeedV100**	**VV100**	**LV100**	**LX100**	**VX100**	**VX101**	**LX101**	**PreHeatMSR**	**MSRR**	**MSRRR**	**CH4 in**	**H2O in**
CH4	0.00074	0.00074	0.00034	0.00041	0.00000	0.00061	0.00000	0.00000	0.00164	0.00086	0.00086	0.00082	1.00000	0.00000
CO	0.24200	0.24200	0.18797	0.23100	0.00000	0.34000	0.00710	0.00000	0.90800	0.47400	0.47400	0.47453	0.00000	0.00000
CO2	0.19983	0.19983	0.26557	0.32671	0.00056	0.00485	0.99290	0.00000	0.01296	0.00704	0.00704	0.00703	0.00000	0.00000
H2O	0.27203	0.27203	0.19967	0.01517	0.99943	0.02250	0.00000	0.00000	0.06018	0.50894	0.50894	0.50881	0.00000	1.00000
H2	0.28494	0.28494	0.34645	0.42637	0.00000	0.63237	0.00000	1.00000	0.01691	0.00883	0.00883	0.00882	0.00000	0.00000
Stream Name	**PreHeatedE**	**H2**	**H2R**	**CO2**	**CO2R**	**RGSPH**	**RGSFeed**	**RGSV**	**RGSL**	**RR**	**3P**	**3PT**	**4P**	**4PT**
CH4	0.00034	0.00000	0.00000	0.00000	0.00000	0.00000	0.00000	0.00000	0.00000	0.00000	1.00000	1.00000	0.00000	0.00000
CO	0.18800	0.00000	0.00000	0.00710	0.00710	0.00329	0.00329	0.14222	0.14222	0.14222	0.00000	0.00000	0.00000	0.00000
CO2	0.26557	0.00000	0.00000	0.99290	0.99290	0.45985	0.45985	0.32093	0.32093	0.32078	0.00000	0.00000	0.00000	0.00000
H2O	0.19967	0.00000	0.00000	0.00000	0.00000	0.00000	0.00000	0.13893	0.13900	0.13900	0.00000	0.00000	1.00000	1.00000
H2	0.34600	1.00000	1.00000	0.00000	0.00000	0.53686	0.53686	0.39800	0.39793	0.39809	0.00000	0.00000	0.00000	0.00000
Stream Name	**VSC**	**3PP**	**4PP**	**RMSR**	**VX101-H**	**CO2-RH**	**CO2-ph**	**co2-pure**	**h2-product**					
CH4	0.00074	1.00000	0.00000	0.00086	0.00000	0.00000	0.00000	0.00000	0.00000					
CO	0.24246	0.00000	0.00000	0.47433	0.00000	0.00710	0.00710	0.00710	0.00000					
CO2	0.19983	0.00000	0.00000	0.00704	0.00000	0.99300	0.99300	0.99300	0.00000					

H2O	0.27203	0.00000	1.00000	0.50894	0.00000	0.00000	0.00000	0.00000	0.00000					
H2	0.28494	0.00000	0.00000	0.00883	1.00000	0.00000	0.00000	0.00000	1.00000					
Energy Flow Name	**QMSR**	**QE101**	**QE104**	**QE102**	**QRTs**	**QE103**	**QEk100**	**QE100**	**QP100**	**QE105**	**QX101**	**QX100**	**QE106**	**QE107**
Heat Flow (kJ/s)	-0.85	510.77	153.43	139.07	62.46	150.84	1.77	3.42	0.01	32.51	-4.96	-4.38	8.37	9.90
Energy Flow Name	**QE108**	**q-h2**	**qh-co2**	**w-co2**	**qc-co2**	**w-h2**								
Heat Flow (kJ/s)	281.67	26.14	27.60	2.45	2.89	3.88								

Table 5-5: *SMR-MR Baseline Flowsheet material and energy stream details*

Stream Name	**vref**	**lref**	**pure-h2**	**ref-out**	**ref-cool**	**flash-rec**	**water-flash**	**CO2-pure**	**recycle**	**rec-stream**
Vapour Fraction	1	0	1	1	0.4966	1	0	1	0.9608	0.07880
Temperature (K)	873	873	873	873	313	313	313	313	313	312.7
Pressure (bar)	40	40	1.1	40	40	40	40	40	40	40
Molar Flow (kmol/h)	6.19	0.00	4.00	2.19	2.19	1.09	1.10	1.00	0.09	1.19
Heat Flow (kJ/s)	-151.78	0.00	18.66	-170.60	-198.00	-110.46	-87.54	-109.71	-0.82	-88.36
Stream Name	**rec-hot**	**water-co-feed**	**H2O Feed**	**H2O-hP**	**H2O-f**	**ch4-h-in**	**ch4-ref**	**h2-product**	**Ref Feed**	**CH4**
Vapour Fraction	1	1	0	0	1	1	1	1	1	1
Temperature (K)	873	873	298	298.3	873	693.8	873	313	870.7	298.00
Pressure (bar)	40	40	1	40	40	40	40	1.1	40	1
Molar Flow (kmol/h)	1.19	1.19	2.00	2.00	2.00	1.00	1.00	4.00	4.19	1.00
Heat Flow (kJ/s)	-68.54	-68.55	-159.02	-158.97	-123.10	-15.75	-12.61	0.47	-204.26	-20.81
Stream Name	**vref**	**lref**	**pure-h2**	**ref-out**	**ref-cool**	**flash-rec**	**water-flash**	**CO2-pure**	**recycle**	**rec-stream**
CH4	3.89E-03	0.0039	0.0000	0.0110	0.0110	0.0222	0.0000	0.0000	0.2800	0.0203
CO	0.0003	0.0003	0.0000	0.0007	0.0007	0.0014	0.0000	0.0000	0.0181	0.0013
CO2	0.1636	0.1630	0.0000	0.4630	0.4630	0.9208	0.0113	1.0000	0.0000	0.0105
H2O	0.1765	0.1710	0.0000	0.4993	0.4993	0.0033	0.9886	0.0000	0.0413	0.9200
H2	0.6558	0.6618	1.0000	0.0260	0.0260	0.0523	0.0000	0.0000	0.6607	0.0479
Stream Name	**rec-hot**	**water-co-feed**	**H2O Feed**	**H2O-hP**	**H2O-f**	**ch4-h-in**	**ch4-ref**	**h2-product**	**Ref Feed**	**CH4**

CH4	2.03E-02	2.06E-02	0.00E+00	0	0.00E+00	1	1	0	0.244665	1
CO	1.31E-03	0.000879	0.00E+00	0	0	0	0	0	0.000249	0
CO2	0.010527	0.010528	0.00E+00	0	0	0	0	0	0.002985	0
H2O	0.920011	9.20E-01	1	1	1.00E+00	0	0	0	7.38E-01	0.00E+00
H2	4.79E-02	4.80E-02	0.00E+00	0	0.00E+00	0	0	1.00E+00	0.013616	0
Energy Flow Name	**q-ref**	**qs-ref**	**q-ref-c**	**q-co2**	**q-h-rec**	**w-pump**	**q-h2o**	**w-ch4**	**q-ch4-r**	**qch2**
Heat Flow (kJ/s)	52.47	-0.17	27.39	-0.07	-19.81	0.05	35.87	5.07	3.14	18.19

Table 5-6: *IEER-MR Case 1 Flowsheet material and energy stream details*

Stream Name	**lmgs-co**	**vmgs-co**	**H2MGS-CO**	**RetMGS-CO**	**vmgs-coun**	**lmg-count**	**H2-mgs-count**	**ret-mgs-count**	**vref**	**ref-feed**	**lref**	**pure-h2**	**ref-out**	**h2-mgs**
Vapour Fraction	0	1	1	1	1	0	1	1	1	1	0	1	1	1
Temperature (K)	883	883	883	883	883	883	883	883	873	873	873	873	873	883
Pressure (bar)	40	40	40	40	40	40	40	40	40	40	40	1.1	40	40
Molar Flow (kmol/h)	0.00	2.52	0.00	2.52	5.22	0.00	9.98	4.19	7.19	4.19	0.00	4.02	3.16	9.99
Heat Flow (kJ/s)	0.00	-136.94	-0.06	-136.94	-284.01	0.00	-544.75	-288.99	-249.73	-289.50	0.00	18.76	-268.64	-544.81
Stream Name	**h2-cool-rgs**	**ref-cool**	**flash-rec**	**water-flash**	**CO2-pure**	**recycle**	**CO2-product**	**CO2-rgs**	**watmgs-rec**	**h2-rgs**	**rgs-cool**	**rgs-hot**	**VRGS**	**LRGS**
Vapour Fraction	0.1037	0.708	1	0	1.0000	0.992	1	1	0	1	1	1	1	0.0000
Temperature (K)	313	313.00	312.6	312.6	313	313	313	313	313	313.00	303	755	760	760
Pressure (bar)	40	40	40	40	40	40	40	40	40	40	40	40	40	40
Molar Flow (kmol/h)	9.99	3.16	4.44	1.98	3.20	1.24	1.00	2.20	8.95	1.04	3.24	3.24	9.00	0.00
Heat Flow (kJ/s)	-708.47	-301.41	-385.47	-157.35	-351.21	-34.60	-109.73	-241.48	-708.44	-0.03	-241.51	-224.71	-191.93	0.00
Stream Name	**H2-Sep-feed**	**h2-rec**	**H2-pure-rgs**	**CO-recycle**	**h2-hot-rgs**	**CO-rec-sep**	**flash-in**	**rec-stream**	**rec-hot**	**water-co-feed**	**comgs-feed**	**countmgs-feed**	**H2O Feed**	**H2O-hP**

Vapour Fraction	0.8843	1.0000	1	0.6754	1.0000	0.6756	0.6915	0.3868	1	1	1	1	0	0
Temperature (K)	313	755	313	313	755	313.00	312.6	312.5	878	878	878	878	298	298.3
Pressure (bar)	40	40	40	40	40	40	40	40	40	40	40	40	1	40
Molar Flow (kmol/h)	9.00	5.76	5.74	3.26	5.74	3.26	6.42	3.22	3.22	3.22	1.52	1.70	2.00	2.00
Heat Flow (kJ/s)	-240.47	21.28	0.68	-241.58	21.20	-241.41	-542.82	-191.95	-150.78	-150.80	-71.18	-79.62	-159.02	-158.97
Stream Name	**H2O-f**	**h2o-comgs**	**h2o-countmgs**	**Feed-Co-MGS**	**Feed-Count-MGS**	**CH4**	**ch4-h-in**	**ch4-ref**	**wat-count-mgs**	**wat-co-mgs**	**rec-watermgs**	**hwatmgs-rec**	**h2-product**	
Vapour Fraction	1	1	1	1	1	1	1	1	1	1	1	1	1	
Temperature (K)	878.00	878.00	878	877.63	877.6	298	693.8	873	873	873	873	873	313	
Pressure (bar)	40	40	40	40	40	1	40	40	40	40	40	40	1.1	
Molar Flow (kmol/h)	2.00	1.00	1.00	2.52	2.70	1.00	1.00	1.00	8.95	0.00	8.95	8.95	4.02	
Heat Flow (kJ/s)	-122.98	-61.49	-61.49	-132.67	-141.11	-20.81	-15.75	-12.61	-550.83	-0.06	-550.89	-550.78	0.47	
Stream Name	**lmgs-co**	**vmgs-co**	**H2MGS-CO**	**RetMGS-CO**	**vmgs-coun**	**lmg-count**	**H2-mgs-count**	**ret-mgs-count**	**vref**	**ref-feed**	**lref**	**pure-h2**	**ref-out**	**h2-mgs**
CH4	0.00382	0.00382	0.00000	0.00382	0.00391	0.00391	0.00000	0.00488	0.00284	0.00488	0.00382	0.00382	0.00000	0.00382
CO	0.02640	0.02640	0.00000	0.02640	0.00451	0.00451	0.00000	0.00562	0.00328	0.00562	0.02640	0.02640	0.00000	0.02640
CO2	0.17928	0.17928	0.00000	0.17930	0.20581	0.20581	0.00000	0.25662	0.28865	0.25662	0.17928	0.17928	0.00000	0.17930
H2O	0.59120	0.59120	0.79866	0.59126	0.55950	0.55950	0.89646	0.69756	0.12803	0.69756	0.59120	0.59120	0.79866	0.59126
H2	0.19933	0.19933	0.20134	0.19926	0.22627	0.22627	0.10354	0.03530	0.57721	0.03530	0.19933	0.19933	0.20134	0.19926
Stream Name	**h2-cool-rgs**	**ref-cool**	**flash-rec**	**water-flash**	**CO2-pure**	**recycle**	**CO2-product**	**CO2-rgs**	**watmgs-rec**	**h2-rgs**	**rgs-cool**	**rgs-hot**	**VRGS**	**LRGS**
CH4	0.00000	0.00645	0.00460	0.00000	0.00000	0.01647	0.00000	0.00000	0.00000	0.00000	0.00000	0.00645	0.00460	0.00000
CO	0.00000	0.00745	0.24300	0.00002	0.00000	0.87202	0.00000	0.00000	0.00000	0.00000	0.00000	0.00745	0.24300	0.00002
CO2	0.00000	0.65585	0.72100	0.00879	1.00000	0.00000	1.00000	1.00000	0.00000	0.00000	0.00000	0.65585	0.72100	0.00879

H2O	0.89644	0.29100	0.00309	0.99119	0.00000	0.01107	0.00000	0.00000	1.00000	0.00213	0.89644	0.29100	0.00309	0.99119
H2	0.10400	0.03930	0.02800	0.00000	0.00000	0.10044	0.00000	0.00000	0.00007	0.99787	0.10400	0.03930	0.02800	0.00000
Stream Name	**H2-Sep-feed**	**h2-rec**	**H2-pure-rgs**	**CO-recycle**	**h2-hot-rgs**	**CO-rec-sep**	**flash-in**	**rec-stream**	**rec-hot**	**water-co-feed**	**comgs-feed**	**countmgs-feed**	**H2O Feed**	**H2O-hP**
CH4	0.00000	0.00000	0.00000	0.00000	0.00000	0.00000	0.00318	0.00634	0.00634	0.00634	0.00000	0.00000	0.00000	0.00000
CO	0.11733	0.00000	0.00000	0.32392	0.00000	0.32442	0.16828	0.33558	0.33558	0.33554	0.11733	0.00000	0.00000	0.32392
CO2	0.12731	0.00000	0.00000	0.35148	0.00000	0.35100	0.50100	0.00540	0.00540	0.00540	0.12731	0.00000	0.00000	0.35148
H2O	0.11757	0.00000	0.00000	0.32460	0.00000	0.32442	0.30791	0.61403	0.61403	0.61407	0.11757	0.00000	0.00000	0.32460
H2	0.63779	1.00000	1.00000	0.00000	1.00000	0.00000	0.01938	0.03865	0.03865	0.03865	0.63779	1.00000	1.00000	0.00000
Stream Name	**H2O-f**	**h2o-comgs**	**h2o-countmgs**	**Feed-Co-MGS**	**Feed-Count-MGS**	**CH4**	**ch4-h-in**	**ch4-ref**	**wat-count-mgs**	**wat-co-mgs**	**rec-watermgs**	**hwatmgs-rec**	**h2-product**	
CH4	0.00000	0.00000	0.00000	0.00382	0.00399	1.00000	1.00000	1.00000	0.00000	0.00000	0.00000	0.00000	0.00000	
CO	0.00000	0.00000	0.00000	0.20238	0.21127	0.00000	0.00000	0.00000	0.00000	0.00000	0.00000	0.00000	0.00000	
CO2	0.00000	0.00000	0.00000	0.00326	0.00340	0.00000	0.00000	0.00000	0.00000	0.00000	0.00000	0.00000	0.00000	
H2O	1.00000	1.00000	1.00000	0.76723	0.75701	0.00000	0.00000	0.00000	0.99993	0.99993	1.00000	1.00000	1.00000	
H2	0.00000	0.00000	0.00000	0.02331	0.02433	0.00000	0.00000	0.00000	0.00007	0.00007	0.00000	0.00000	0.00000	
Energy Flow Name	**q-mgs-co**	**qs-mgs-co**	**q-mgs-count**	**qs-mgs-count**	**q-ref**	**q-mgs-cool**	**qs-ref**	**q-h2-mgs**	**q-ref-c**	**q-co2**	**q-h-rgs**	**q-rgs**	**q-c-rgs**	**q-sep-h2**
Heat Flow (kJ/s)	-4.27	0.00	-5.96	1.10	52.39	0.51	-0.16	163.66	32.77	-0.33	16.80	11.49	48.54	-0.43
Energy Flow Name	**q-hrgs**	**q-h-rec**	**w-pump**	**q-h2o**	**w-ch4**	**q-ch4-r**	**qwatmgs**	**qch2**						
Heat Flow (kJ/s)	20.52	-41.17	0.05	35.99	5.07	3.14	157.67	18.29						

Table 5-7: *IEER-MR Case 2 Flowsheet material and energy stream details*

Stream Name	lmgs-co	vmgs-co	H2MGS-CO	RetMGS-CO	vmgs-coun	lmg-count	H2-mgs-count	ret-mgs-count	vref	ref-feed	lref	pure-h2	ref-out	h2-mgs
Vapour Fraction	0	1	1	1	1	0	1	1	1	1	0	1	1	1
Temperature (K)	883	883	883	883	883	883	883	883	873	873	873	873	873	883
Pressure (bar)	40	40	40	40	40	40	40	40	40	40	40	1.1	40	40
Molar Flow (kmol/h)	0.00	3.31	0.18	3.27	6.97	0.00	16.59	5.11	8.11	5.11	0.00	4.01	4.10	16.77
Heat Flow (kJ/s)	0.00	-172.88	-8.03	-173.08	-367.85	0.00	-896.01	-376.79	-337.68	-377.43	0.00	18.71	-356.55	-904.04
Stream Name	**h2-cool-rgs**	**ref-cool**	**flash-rec**	**water-flash**	**CO2-pure**	**recycle**	**CO2-product**	**CO2-rgs**	**watmgs-rec**	**h2-rgs**	**rgs-cool**	**rgs-hot**	**VRGS**	**LRGS**
Vapour Fraction	0.1134	0.7777	1	0	1.0000	0.9930	1	1	0	1	1	1	1	0.0000
Temperature (K)	313	313.00	312.51	312.5136113	313	313	313	313	313	313.00	302.8	755	760	760
Pressure (bar)	40	40	40	40	40	40	40	40	40	40	40	40	40	40
Molar Flow (kmol/h)	16.77	4.10	6.89	2.82	4.71	2.19	1.00	3.71	14.86	1.90	5.61	5.61	17.61	0.00
Heat Flow (kJ/s)	-1176.74	-396.11	-578.51	-224.29	-516.51	-62.51	-109.73	-406.79	-1176.70	-0.05	-406.84	-377.98	-312.79	0.00
Stream Name	**H2-Sep-feed**	**h2-rec**	**H2-pure-rgs**	**CO-recycle**	**h2-hot-rgs**	**CO-rec-sep**	**flash-in**	**rec-stream**	**rec-hot**	**water-co-feed**	**comgs-feed**	**countmgs-feed**	**H2O Feed**	**H2O-hP**
Vapour Fraction	0.893207781	1.0000	1	0.6595	1.0000	0.6600	0.7094	0.4379	1	1	1	1	0	0
Temperature (K)	313	755	313	313.00	755.00	313.00	312.5	312.5	878	878	878	878.00	298	298.3
Pressure (bar)	40	40	40	40	40	40	40	40	40	40	40	40	1	40
Molar Flow (kmol/h)	17.61	12.00	11.99	5.62	11.99	5.62	9.72	5.01	5.01	5.01	2.31	2.70	2.00	2.00
Heat Flow (kJ/s)	-404.82	44.34	1.41	-407.01	44.30	-406.69	-802.80	-286.80	-225.99	-225.99	-104.20	-121.80	-159.02	-158.97
Stream Name	**H2O-f**	**h2o-comgs**	**h2o-countmgs**	**Feed-Co-MGS**	**Feed-Count-MGS**	**CH4**	**ch4-h-in**	**ch4-ref**	**wat-count-mgs**	**wat-co-mgs**	**rec-watermgs**	**hwatmgs-rec**	**h2-product**	

Vapour Fraction	1	1	1	1	1	1	1	1	1	1	1	1	1	
Temperature (K)	878.00	878.00	878	877.58	877.6	298	693.8	873	873	873	873	873	313	
Pressure (bar)	40	40	40	40	40	1	40	40	40	40	40	40	1.1	
Molar Flow (kmol/h)	2.00	1.00	1.00	3.31	3.70	1.00	1.00	1.00	14.73	0.13	14.87	14.86	4.01	
Heat Flow (kJ/s)	-122.98	-61.49	-61.49	-165.69	-183.29	-20.81	-15.75	-12.61	-906.81	-8.25	-915.06	-914.81	0.47	
Stream Name	**lmgs-co**	**vmgs-co**	**H2MGS-CO**	**RetMGS-CO**	**vmgs-coun**	**lmg-count**	**H2-mgs-count**	**ret-mgs-count**	**vref**	**ref-feed**	**lref**	**pure-h2**	**ref-out**	**h2-mgs**
CH4	0.00502	0.00502	0.00000	0.00509	0.00518	0.00518	0.00000	0.00705	0.00445	0.00705	0.00448	0.00000	0.00880	0.00000
CO	0.04980	0.04980	0.00000	0.05050	0.00751	0.00751	0.00000	0.01020	0.00645	0.01020	0.00650	0.00000	0.01280	0.00000
CO2	0.22674	0.22676	0.00000	0.22971	0.27746	0.27744	0.00000	0.37812	0.36156	0.37812	0.36035	0.00000	0.71537	0.00000
H2O	0.47170	0.47162	0.75932	0.47775	0.41787	0.41795	0.88813	0.56946	0.11235	0.56946	0.10888	0.00000	0.22229	0.88678
H2	0.24673	0.24678	0.24068	0.23698	0.29199	0.29193	0.11187	0.03510	0.51520	0.03510	0.51979	1.00000	0.04080	0.11322
Stream Name	**h2-cool-rgs**	**ref-cool**	**flash-rec**	**water-flash**	**CO2-pure**	**recycle**	**CO2-product**	**CO2-rgs**	**watmgs-rec**	**h2-rgs**	**rgs-cool**	**rgs-hot**	**VRGS**	**LRGS**
CH4	0.00000	0.00880	0.00523	0.00000	0.00000	0.01650	0.00000	0.00000	0.00000	0.00000	0.00000	0.00000	0.00000	0.00000
CO	0.00000	0.01277	0.28500	0.00003	0.00000	0.89741	0.00000	0.00000	0.00000	0.00000	0.00000	0.00000	0.10848	0.10848
CO2	0.00000	0.71537	0.68300	0.00831	1.00000	0.00000	1.00000	1.00000	0.00000	0.00000	0.66100	0.66100	0.10206	0.10206
H2O	0.88678	0.22200	0.00305	0.99167	0.00000	0.00963	0.00000	0.00000	1.00000	0.00213	0.00072	0.00072	0.10871	0.10871
H2	0.11300	0.04080	0.02430	0.00000	0.00000	0.07647	0.00000	0.00000	0.00007	0.99787	0.33828	0.33828	0.68075	0.68075
Stream Name	**H2-Sep-feed**	**h2-rec**	**H2-pure-rgs**	**CO-recycle**	**h2-hot-rgs**	**CO-rec-sep**	**flash-in**	**rec-stream**	**rec-hot**	**water-co-feed**	**comgs-feed**	**countmgs-feed**	**H2O Feed**	**H2O-hP**
CH4	0.00000	0.00000	0.00000	0.00000	0.00000	0.00000	0.00371	0.00720	0.00720	0.00720	0.00720	0.00720	0.00000	0.00000
CO	0.10848	0.00000	0.00000	0.33980	0.00000	0.33998	0.20192	0.39164	0.39164	0.39164	0.39164	0.39164	0.00000	0.00000
CO2	0.10206	0.00000	0.00000	0.31968	0.00000	0.32000	0.48700	0.00468	0.00468	0.00468	0.00468	0.00468	0.00000	0.00000

H2O	0.10871	0.00000	0.00000	0.34052	0.00000	0.33998	0.29032	0.56311	0.56311	0.56311	0.56311	0.56311	1.00000	1.00000
H2	0.68075	1.00000	1.00000	0.00000	1.00000	0.00000	0.01720	0.03337	0.03337	0.03337	0.03337	0.03337	0.00000	0.00000
Stream Name	**H2O-f**	**h2o-comgs**	**h2o-countmgs**	**Feed-Co-MGS**	**Feed-Count-MGS**	**CH4**	**ch4-h-in**	**ch4-ref**	**wat-count-mgs**	**wat-co-mgs**	**rec-watermgs**	**hwatmgs-rec**	**h2-product**	
CH4	0.00000	0.00000	0.00000	0.00502	0.00525	1.00000	1.00000	1.00000	0.00000	0.00000	0.00000	0.00000	0.00000	
CO	0.00000	0.00000	0.00000	0.27331	0.28579	0.00000	0.00000	0.00000	0.00000	0.00000	0.00000	0.00000	0.00000	
CO2	0.00000	0.00000	0.00000	0.00327	0.00342	0.00000	0.00000	0.00000	0.00000	0.00000	0.00000	0.00000	0.00000	
H2O	1.00000	1.00000	1.00000	0.69511	0.68119	0.00000	0.00000	0.00000	0.99993	0.99993	0.99993	0.99993	0.00000	
H2	0.00000	0.00000	0.00000	0.02329	0.02435	0.00000	0.00000	0.00000	0.00007	0.00007	0.00007	0.00007	1.00000	
Energy Flow Name	**q-mgs-co**	**qs-mgs-co**	**q-mgs-count**	**qs-mgs-count**	**q-ref**	**q-mgs-cool**	**qs-ref**	**q-h2-mgs**	**q-ref-c**	**q-co2**	**q-h-rgs**	**q-rgs**	**q-c-rgs**	**q-sep-h2**
Heat Flow (kJ/s)	-7.19	0.02	-11.48	1.85	52.37	0.64	-0.16	272.70	39.56	-0.52	28.86	20.85	92.03	-0.78
Energy Flow Name	**q-hrgs**	**q-h-rec**	**w-pump**	**q-h2o**	**w-ch4**	**q-ch4-r**	**qwatmgs**	**qch2**						
Heat Flow (kJ/s)	42.88	-60.81	0.05	35.99	5.07	3.14	261.88	18.24						

Table 5-8: *IEER-MR Case 3 Flowsheet material and energy stream details*

Stream Name	**lmgs-co**	**vmgs-co**	**H2MGS-CO**	**RetMGS-CO**	**vmgs-coun**	**lmg-count**	**H2-mgs-count**	**ret-mgs-count**	**vref**	**ref-feed**	**lref**	**pure-h2**	**ref-out**	**h2-mgs**
Vapour Fraction	0	1	1	1	1	0	1	1	1	1	0	1	1	1
Temperature (K)	883	883	883	883	883	883	883	883	873	873	873	873	873	883
Pressure (bar)	40	40	40	40	40	40	40	40	40	40	40	1.1	40	40
Molar Flow (kmol/h)	0.00	10.19	2.35	9.59	15.88	0.00	30.06	11.19	14.19	11.19	0.00	4.06	10.13	32.40
Heat Flow (kJ/s)	0.00	-513.61	-104.70	-516.42	-847.99	0.00	-1535.39	-870.20	-831.82	-871.64	0.00	18.91	-850.96	-1640.10

Stream Name	ref-cool	flash-rec	water-flash	CO2-pure	recycle	CO2-product	CO2-rgs	watmgs-rec	h2-rgs	rgs-cool	rgs-hot	VRGS	LRGS	H2-Sep-feed
Vapour Fraction	0.6896	1	0	1	0.9920	1	1	0	1	1	1	1	0	0.8663
Temperature (K)	313	312.77	312.77	313	313	313	313	313	313	303.77	755	760	760	313
Pressure (bar)	40	40	40	40	40	40	40	40	40	40	40	40	40	40
Molar Flow (kmol/h)	10.13	20.44	8.49	14.45	5.99	1.00	13.45	27.11	5.30	18.74	18.74	39.49	0.00	39.49
Heat Flow (kJ/s)	-957.62	-1758.89	-674.52	-1585.19	-175.26	-109.73	-1475.46	-2146.01	-0.14	-1475.60	-1376.70	-1242.14	0.00	-1471.06

Stream Name	H2-pure-rgs	CO-recycle	h2-hot-rgs	CO-rec-sep	flash-in	rec-stream	rec-hot	water-co-feed	comgs-feed	countmgs-feed	H2O Feed	H2O-hP	H2O-f	h2o-comgs
Vapour Fraction	1	0.7155	1	0.7155	0.7065	0.4152	1	1	1	1	0	0	1	1
Temperature (K)	313	313	755	313.00	312.77	312.64	878	878	878	878	298	298.34	878	878
Pressure (bar)	40	40	40	40	40	40	40	40	40	40	1	40	40	40
Molar Flow (kmol/h)	20.69	18.80	20.69	18.80	28.93	14.48	14.48	14.48	9.19	5.29	2.00	2.00	2.00	1.00
Heat Flow (kJ/s)	2.44	-1475.79	76.46	-1475.79	-2433.41	-849.78	-670.00	-669.68	-425.09	-244.59	-159.02	-158.97	-122.98	-61.49

Stream Name	Feed-Co-MGS	Feed-Count-MGS	CH4	ch4-h-in	ch4-ref	wat-count-mgs	wat-co-mgs	rec-watermgs	hwatmgs-rec	h2-product	h2-cool-rgs	h2-rec	h2o-countmgs	
Vapour Fraction	1	1	1	1	1	1	1	1	1	1	0.1634	1	1	
Temperature (K)	877.84	877.76	298	693.80	873	873	873	873	873	313	313	755	878	
Pressure (bar)	40	40	1	40	40	40	40	40	40	1.1	40	40	40	
Molar Flow (kmol/h)	10.19	6.29	1.00	1.00	1.00	25.36	1.75	27.11	27.11	4.06	32.40	20.75	1.00	
Heat Flow (kJ/s)	-486.59	-306.08	-20.81	-15.75	-12.61	-1560.94	-107.77	-1668.71	-1668.40	0.48	-2146.14	76.66	-61.49	

Stream Name	lmgs-co	vmgs-co	H2MGS-CO	RetMGS-CO	vmgs-coun	lmg-count	H2-mgs-count	ret-mgs-count	vref	ref-feed	lref	pure-h2	ref-out	h2-mgs

CH4	0.00332	0.00328	0.00000	0.00348	0.00331	0.00335	0.00000	0.00471	0.00371	0.00471	0.00375	0.00000	0.00520	0.00000
CO	0.07420	0.07330	0.00000	0.07790	0.01150	0.01160	0.00000	0.01630	0.01280	0.01630	0.01300	0.00000	0.01800	0.00000
CO2	0.27622	0.27514	0.00000	0.29227	0.34080	0.34206	0.00000	0.48378	0.45197	0.48378	0.45291	0.00000	0.63287	0.00000
H2O	0.35007	0.35565	0.74606	0.37770	0.32353	0.31819	0.84398	0.45877	0.22077	0.45877	0.21605	0.00000	0.30914	0.83689
H2	0.29621	0.29258	0.25394	0.24864	0.32088	0.32479	0.15602	0.03650	0.31071	0.03650	0.31431	1.00000	0.03480	0.16311
Stream Name	**ref-cool**	**flash-rec**	**water-flash**	**CO2-pure**	**recycle**	**CO2-product**	**CO2-rgs**	**watmgs-rec**	**h2-rgs**	**rgs-cool**	**rgs-hot**	**VRGS**	**LRGS**	**H2-Sep-feed**
CH4	0.00520	0.00258	0.00000	0.00000	0.00879	0.00000	0.00000	0.00000	0.00000	0.00000	0.00000	0.00000	0.00000	0.00000
CO	0.01800	0.27015	0.00002	0.00000	0.92171	0.00000	0.00000	0.00000	0.00000	0.00000	0.00000	0.13520	0.13520	0.13520
CO2	0.63287	0.70691	0.00857	1.00000	0.00000	1.00000	1.00000	0.00000	0.00000	0.71748	0.71748	0.20533	0.20533	0.20533
H2O	0.30914	0.00312	0.99140	0.00000	0.01060	0.00000	0.00000	0.99993	0.00213	0.00060	0.00060	0.13549	0.13549	0.13549
H2	0.03480	0.01730	0.00000	0.00000	0.05890	0.00000	0.00000	0.00007	0.99787	0.28192	0.28192	0.52398	0.52398	0.52398
Stream Name	**H2-pure-rgs**	**CO-recycle**	**h2-hot-rgs**	**CO-rec-sep**	**flash-in**	**rec-stream**	**rec-hot**	**water-co-feed**	**comgs-feed**	**countmgs-feed**	**H2O Feed**	**H2O-hP**	**H2O-f**	**h2o-comgs**
CH4	0.00000	0.00000	0.00000	0.00000	0.00182	0.00363	0.00363	0.00364	0.00364	0.00364	0.00000	0.00000	0.00000	0.00000
CO	0.00000	0.28403	0.00000	0.28403	0.19086	0.38126	0.38126	0.38139	0.38139	0.38139	0.00000	0.00000	0.00000	0.00000
CO2	0.00000	0.43135	0.00000	0.43134	0.50192	0.00503	0.00503	0.00503	0.00503	0.00503	0.00000	0.00000	0.00000	0.00000
H2O	0.00000	0.28463	0.00000	0.28463	0.29321	0.58573	0.58573	0.58559	0.58559	0.58559	1.00000	1.00000	1.00000	1.00000
H2	1.00000	0.00000	1.00000	0.00000	0.01220	0.02435	0.02435	0.02436	0.02436	0.02436	0.00000	0.00000	0.00000	0.00000
Stream Name	**Feed-Co-MGS**	**Feed-Count-MGS**	**CH4**	**ch4-h-in**	**ch4-ref**	**wat-count-mgs**	**wat-co-mgs**	**rec-watermgs**	**hwatmgs-rec**	**h2-product**	**h2-cool-rgs**	**h2-rec**	**h2o-countmgs**	
CH4	0.00328	0.00306	1.00000	1.00000	1.00000	0.00000	0.00000	0.00000	0.00000	0.00000	0.00000	0.00000	0.00000	
CO	0.34396	0.32073	0.00000	0.00000	0.00000	0.00000	0.00000	0.00000	0.00000	0.00000	0.00000	0.00000	0.00000	
CO2	0.00453	0.00423	0.00000	0.00000	0.00000	0.00000	0.00000	0.00000	0.00000	0.00000	0.00000	0.00000	0.00000	

H2O	0.62626	0.65150	0.00000	0.00000	0.00000	0.99993	0.99993	0.99993	0.99993	0.00000	0.83689	0.00000	1.00000	
H2	0.02197	0.02050	0.00000	0.00000	0.00000	0.00007	0.00007	0.00007	0.00007	1.00000	0.16311	1.00000	0.00000	
Energy Flow Name	**q-mgs-co**	**qs-mgs-co**	**q-mgs-count**	**qs-mgs-count**	**q-ref**	**q-mgs-cool**	**qs-ref**	**q-h2-mgs**	**q-ref-c**	**q-co2**	**q-h-rgs**	**q-rgs**	**q-c-rgs**	**q-sep-h2**
Heat Flow (kJ/s)	-27.02	0.25	-25.49	3.33	52.43	1.44	-0.23	506.04	106.66	-1.56	98.90	57.90	228.92	-2.29
Energy Flow Name	**q-hrgs**	**q-h-rec**	**w-pump**	**q-h2o**	**w-ch4**	**q-ch4-r**	**qwatmgs**	**qch2**						
Heat Flow (kJ/s)	74.02	-179.79	0.05	35.99	5.07	3.14	477.61	18.43						

5.11 References

1. Stankiewicz, A. & Moulijn, J. A. Process Intensification. *Ind. Eng. Chem. Res.* **41**, 1920–1924 (2002).

2. Stankiewicz, A. Reactive separations for process intensification: an industrial perspective. *Chem. Eng. Process. Process Intensif.* **42**, 137–144 (2003).

3. Baldea, M. A pinch-like targeting framework for systematic thermal process intensification. *AIChE J.* n/a-n/a doi:10.1002/aic.15971

4. da Cruz, F. E. & Manousiouthakis, V. I. Process intensification of reactive separator networks through the IDEAS conceptual framework. *Comput. Chem. Eng.* **105**, 39–55 (2017).

5. Pichardo, P. & Manousiouthakis, V. I. Infinite DimEnsionAl State-space as a systematic process intensification tool: Energetic intensification of hydrogen production. *Chem. Eng. Res. Des.* **120**, 372–395 (2017).

6. Drioli, E., Stankiewicz, A. I. & Macedonio, F. Membrane engineering in process intensification—An overview. *J. Membr. Sci.* **380**, 1–8 (2011).

7. Pal, P., Sikder, J., Roy, S. & Giorno, L. Process intensification in lactic acid production: A review of membrane based processes. *Chem. Eng. Process. Process Intensif.* **48**, 1549–1559 (2009).

8. Qiu, Z., Zhao, L. & Weatherley, L. Process intensification technologies in continuous biodiesel production. *Chem. Eng. Process. Process Intensif.* **49**, 323–330 (2010).

9. Becker, R. *Computer-Aided Design of Catalysts*. (CRC Press, 1993).

10. Dubé, M. A., Tremblay, A. Y. & Liu, J. Biodiesel production using a membrane reactor. *Bioresour. Technol.* **98**, 639–647 (2007).

11. Jeon, Y.-J. & Kim, S.-K. Production of chitooligosaccharides using an ultrafiltration membrane reactor and their antibacterial activity. *Carbohydr. Polym.* **41**, 133–141 (2000).

12. Uemiya, S., Sato, N., Ando, H., Matsuda, T. & Kikuchi, E. Steam reforming of methane in a hydrogen-permeable membrane reactor. *Appl. Catal.* **67**, 223–230 (1990).

13. Balachandran, U. *et al.* Ceramic membrane reactor for converting methane to syngas. *Catal. Today* **36**, 265–272 (1997).

14. Kikuchi, E. Membrane reactor application to hydrogen production. *Catal. Today* **56**, 97–101 (2000).

15. Minet, R. G. & Tsotsis, T. T. Catalytic ceramic membrane steam/hydrocarbon reformer. (1991).

16. Garshasbi, A. *et al.* Membrane-based reactive separations for process intensification during power generation. *Catal. Today* (2017). doi:10.1016/j.cattod.2017.10.039

17. Natural-Gas-Derived Hydrogen in the Presence of Carbon Fuel Taxes and Concentrated Solar Power - ACS Sustainable Chemistry & Engineering (ACS Publications). Available at: https://pubs.acs.org/doi/abs/10.1021/acssuschemeng.7b02745. (Accessed: 21st February 2019)

18. Pichardo, P. & Manousiouthakis, V. I. On the Intensification of Natural Gas-Based Hydrogen Production Utilizing Hybrid Energy Resources. *Smart Sustain. Manuf. Syst.* **2.2**, 1–24 (2018).

19. National Research Council & National Research Council and National Academy of Engineering. *The Hydrogen Economy: Opportunities, Costs, Barriers, and R&D Needs*. (2004). doi:10.17226/10922

20. Manousiouthakis, V. I., Albassam, A. M. & Conner, J. A. Energetically enhanced reforming process. (2017).

21. Holiastos, K. & Manousiouthakis, V. Minimum hot/cold/electric utility cost for heat exchange networks. *Comput. Chem. Eng.* **26**, 3–16 (2002).

22. Turchi, C. & Mehos, M. Current and future costs for parabolic trough and power tower systems in the US market.